UNIVERSITY of ABERTAY DUNDEE
School of Contemporary Sciences

# Identification and characterization of novel autoregulatory mechanism controlling Ataxia telangiectasia mutated gene expression, protein trafficking and function

**Hilal Shahid Khalil**
**Student I.D: 0605341**

**A Thesis submitted in partial fulfilment of the University of Abertay Dundee for the Degree of Doctor of Philosophy in Medical Biotechnology**

**Principal Supervisor: Professor Nikolai Zhelev**

**Second Supervisor: Professor John Palfreyman**

**March, 2012**
**Dundee, United Kingdom**

# Preface

In the last couple of decades, the scientific breakthroughs and landmarks achieved in life sciences and human health care have been truly remarkable. The mapping of full human genome was completed in 2003, scientists cracked the secret of reprogramming adult skin cells into induced pluripotent stem cells in 2007, we got a step closer to developing vaccine for AIDS in 2011, and the possibility of cure for mitochondrial disease through *in vitro* fertilization in 2012.

While our understanding of molecular mechanisms underlying tumourigenic transformation has also increased immensely, unfortunately, the latest UK statistics of incidences of all types of cancers and mortality rates are still gloomy. Cancer remains the second leading cause of death in UK and incidences for all types of cancers from 1979 to 2008 in Great Britain alone have increased both in males and females. On a positive side, the increasing rate of incidences of cancer is paralleled by our vigour and drive in research towards finding the best anti cancer therapeutic approach.

Scientists have classified cancer as the disease of the cell cycle caused by frequent mutations in cell cycle regulatory machinery and DNA repair enzymes. This definition classifies all the proteins functioning in DNA repair, cell cycle progression, arrest and apoptosis as critical determinants of not only the cancer phenotype, but also of the therapeutic approach that is devised to combat it. We now know that the efficacy of the gold standard treatments of cancer involving chemotherapy and radiotherapy can be further enhanced if it is coupled with careful manipulation of the above mentioned proteins. To this end, inhibition of DNA repair enzymes or those implicated in cell cycle arrest have proven to increase the sensitivity of cancer cells towards these treatment modalities.

Ataxia telangiectasia mutated (ATM) protein kinase was discovered to function at the core of the signalling pathways that connect the cellular DNA repair machinery with the cell cycle and apoptotic signalling. It was discovered that inhibition of ATM under certain conditions could enhance the therapeutic efficacy of genotoxic agents by sensitizing cells. However, all the cancer treatments almost always cause detrimental side effects because of harmful effects on the surrounding normal cells.

Owing to the intricacy and high degree of cross-talk of signalling networks within eukaryotic cells, manipulation of ATM pathway specifically, or of DNA damage response (DDR) pathway in general, is expected to result in wide variety of signalling alteration. Hence, while employing any of DDR manipulation strategies, it is imperative to fully characterise its effects not only in terms of the activity of target molecule, but its spatio-temporal regulation, transcriptional machinery, protein stability, downstream signalling activity and finally on overall cell fate first in normal cells and then correlate those with the responses generated in cancer cells.

My PhD. research commenced with keeping all of the above goals in mind in order to elucidate the critical role of ATM and its regulation and functional characterisation during DDR in normal and cancer cells and to develop or establish a conceptual frame work for the applicability of the novel findings made through this research in medical biotechnological applications. This involved their utility in designing novel cell based kinase assay or biosensor of DNA damage and generation of quantitative data of DDR for the construction of first of its kind of deterministic mathematical model of mammalian signalling pathway in cancer.

# Acknowledgements

First and foremost, I would like to thank with all my heart and soul, my principal supervisor, Professor Nikolai Zhelev. Sir, you have been an amazing mentor, a role model, and above all, an excellent supervisor and friend. All the attributes that I have acquired from you in the past three years, your approach towards science, and your entire philosophy of life has deeply inspired me and are treasure that will remain with me lifelong. Needless to mention that I would not have completed this PhD successfully without your guidance and supervision.

A big thank you to Professor John Palfreyman, my second supervisor. You have helped me tremendously throughout my PhD. Your key scientific discussion, and monthly meetings, your keen interest in my project and your endless notes of appreciation and encouragement have proven vital for the success of this project. You have always helped me not only in my scientific endeavours but also in the administrative issues. Thank you for all that.

Many thanks to Dr. Hemanth Tummala for advising and assisting me throughout my PhD. Your own passion for science, and your aspiration to be the best in your field was a driving force for me too. Your late night, long hours work with me side by side set a terrific example for me. You have been a very sincere friend too.

Special thanks to Dr. Yousef Deeni for all the help, training and support in my first year. I would also like to thank the very hard working technicians, my colleagues, MRes students and the whole team of School of Contemporary Sciences for all your help and support.

I would also like to thank my parents and my brother and sister. You guys have been amazing. You are my main driving force, and the source of my self-belief and motivation. Without your emotional support, I would not have reached this phase in life. I owe my success to you. I hope I have made baba and mama proud!

This PhD. work was made possible because of Northwood Charitable trust, which was the financial sponsor of the project. Many thanks for all your support.

## Abbreviations/Notations/Symbols

| | |
|---|---|
| A-T | Ataxia Telangiectasia |
| ATM | Ataxia Telangiectasia mutated |
| $ATM_{mut}$ | Mutated ATM |
| ATR | Ataxia Telangiectasia mutated and Rad-3 related |
| BLAST | Basic Local Alignment Search Tool |
| BSA | Bovine Serum Albumin |
| BRCA1/2 | Breast cancer type 1/2 susceptibility protein |
| Bp | Bair pairs |
| Chk1 | Checkpoint kinase 1 |
| Chk2 | Checkpoint kinase 2 |
| CHX | Cycloheximide |
| COPI | Coatomer protein I |
| CYT | Cytoplasm |
| DAPI | 4, 6-diamidino-2-phenylindole |
| DDR | DNA damage response |
| Dox | Doxorubicin |
| DNA-PK | DNA dependent protein kinase |
| DSBs | Double stranded DNA breaks |
| E2F1 | E2F Transcription Factor 1 |
| ELISA | Enzyme linked immunosorbent assay |
| ER | Endoplasmic reticulum |
| GFP | Green fluorescent protein |

| | |
|---|---|
| GTPase | Guanosine triphosphate hydrolase |
| GNEF | Guanine nucleotide exchange factor |
| H2AX | Histone 2A variant X |
| γ-H2AX | Phosphorylated H2AX at Serine 139 |
| HPLC | High pressure liquid chromatography |
| HRP | Horse radish peroxidase |
| HRR | Homologous recombination repair |
| IR | Ionizing radiation |
| Kb | Kilo base |
| KU | KU55933 |
| LAR | Luciferase assay reagent |
| LB | Luria Bertani |
| MCS | Multiple cloning site |
| MRN | Mre11-Rade50-Nbs1 protein complex |
| NHEJ | Non-homologous end joining |
| NR | Neutral red |
| NUC | Nuclear fraction |
| OD | Optical density |
| pATM | Phosphorylated ATM Serine-1981 |
| pATR | Phosphorylated ATR Serine- 428 |
| pBRCA1 | Phosphorylated BRCA1 S-1594 |
| PBS | Phosphate buffered saline |
| pChk1 | Phosphorylated Chk1 Serine-296 |
| pChk2 | Phosphorylated Chk2 Threonine-68 |
| PCR | Polymerase chain reaction |
| PFA | Paraformaldehyde |

| | |
|---|---|
| PI3/4K | Phosphotidyle Inositol 3/4 Kinase |
| PIKK | Phosphatidyle Inositol Kinase like kinase |
| PKB | Protein Kinase B |
| Rb | Retinoblastoma |
| RFP | Red fluorescent protein |
| RIPA | Radioimmunoprecipitation assay |
| RAS | Rat sarcoma viral oncogene homolog |
| RPA | Replication protein A |
| RPM | Revolution per minute |
| SAP | Shrimp alkaline phosphatase |
| SDM | Site directed mutagenesis |
| SDS | Sodium dodecyle sulfate |
| SDSPAGE | Sodium dodecyle sulfate polyacrylamide gel electrophoresis |
| SMC1 | Structural maintenance of chromosome protein 1 |
| SOB | Super Optimal broth |
| SSA | Single strand annealing |
| SSB | Single stranded DNA breaks |
| TAE | Tris Acetate EDTA buffer |
| TB | Terrific broth |
| UT | Untreated |
| UTR | Untranslated region |
| UV | Ultraviolet radiation |
| YFP | Yellow fluorescent protein |

## SYNOPSIS

Ataxia-telangiectasia mutated gene product (ATM) is a 350 kDa Serine/Threonine kinase belonging to the family of Phosphatidylinositol-3 kinase like kinases. ATM functions as a key element in DNA Damage Response (DDR), a mechanism that maintains genomic integrity within the cells. ATM is activated after double stranded DNA damage and initiates signalling cascades that determine the process of decision-making of cell fate and involves the participation of multiple proteins. This vital protein acts first by sensing double stranded DNA breaks and second by transducing the signal and activating other downstream proteins of the repair pathway via its kinase function. This provides an important link between signals generated after DNA damage, the cell cycle pathway and apoptotic machinery. This function is crucial for mammalian cells which are constantly challenged by genotoxic agents from a variety of sources and therefore require a robust sensing and repair mechanism to maintain cell vitality. Cells lacking ATM are hypersensitive to cytotoxic insults, particularly genotoxic stress, induced through radiation or radiomimetic drugs.

This thesis describes the discovery and characterisation of novel autoregulatory feedback loops of ATM kinase in human cells. Firstly, I have discovered that inhibition of ATM kinase activity causes induction of ATM protein expression followed by time dependent oscillations. This novel autoregulatory mechanism was demonstrated in cell cycle independent manner and both in the absence and presence of DNA damage. ATM promoter assay revealed that this autoregulation was governed at the transcriptional level. Furthermore, this autoregulatory induction of ATM was also accompanied by a transient upregulation of P53, pATR and E2F1 levels. Elucidation of the underlying trafficking mechanism of ATM during such autoregulation and in DDR also revealed a novel ATM sub-cellular trafficking mechanism which was dependent on its own kinase activity. This trafficking mechanism involved DNA damage induced Golgi to nuclear transport of phosphorylated ATM S-1981 to elicit DDR. This was found to be a conserved pathway required during the initiation of DDR and was demonstrated in multiple cell lines.

Further studies into the sub-cellular transport machinery revealed the involvement of β-COPI coatomer protein in this mechanism of ATM trafficking, which was found to be autoregulated by ATM kinase, and required 387-388 ATM di-Lysine motif.

The discovery of these functionally important autoregulatory mechanisms of ATM were further utilised to develop Luciferase reporter based biosensor of DNA damage and single cell fluorescence based ATM inhibition assay to screen for ATM inhibitors. Finally, following the discovery and characterisation of these functional spatio-temporal autoregulations of ATM, quantitative estimations of the kinetics of signalling cascades initiated by it during DDR and its overall outcome on cellular fate were determined to study ATM pathway systematically for employing a quantitative systems biology approach.

These novel findings have immensely increased our understanding of ATM regulation and function. Elucidation of the mechanisms of novel autoregulations of ATM provide new dimensions through which DDR pathway could be manipulated, and as such could be utilised for achieving targeted cellular sensitivity in therapeutic intervention of cancer.

## Table of Contents

## FIGURES

## Tables

# Chapter One

# General Introduction

With faith, discipline and selfless devotion to duty, there is nothing worthwhile that you cannot achieve.

Muhammad Ali Jinnah, Founder of Pakistan (1876 –1948)

## 1.1 Introduction

For the survival and normal functioning of a cell and ultimately of the whole organism, conservation and protection of the native DNA sequence and structure is necessary. However, our bodies are constantly exposed to diverse types of genotoxic insults from various sources that can damage cellular DNA and threaten the survival. DNA damage can result from exogenous as well as endogenous means. Major exogenous sources include exposure to ionizing radiation (UV, X-rays, gamma rays) and through contact with certain chemical carcinogens. Endogenous means of DNA damage may include generation of reactive oxygen species resulting from metabolic by-products during cellular respiration, mechanical damage to chromosomes e.g. when dicentric or catenated chromosomes are pulled to opposite poles during mitosis, during programmed genomic rearrangements induced by nucleases and defective metabolism of chromosomal ends (Khanna KK et al., 2001). The different sources of DNA damage can cause a wide variety of DNA lesions. E.g. Ionizing radiation can induce single or double stranded DNA breaks (SSBs or DSBs respectively), UV light can cause the formation of pyrimidine dimers or depurination, chemical carcinogens can cause DNA cross links, enzyme-mediated base removal may produce abasic sites, and spontaneous cytosine deamination can result in non-native DNA base, Uracil, (Ross JB., 2006). Additionally, Replication fork arrest caused by SSBs can result in its collapse and creation of DSBs (Shen Z et al., 2007). In most of the instances, generation of DNA lesions cause structural and functional changes in DNA that can accumulate through cell division and in extreme cases, lead to cancer and death. Generation of DSBs is generally regarded as the most toxic of all DNA lesions while its repair, as the most complex process (Valerie K et al., 2003). Errors in the repair of DSBs can result in deletion or insertion mutations, chromosomal translocation, and genomic instability leading to malignancy (Elliot B et al., 2002).

## 1.2 Mechanisms of Eukaryotic DNA repair

In order to maintain genomic integrity, eukaryotic cells have developed intricate DNA damage sensing and repair mechanism that combats the diverse sources of DNA damage and ensures survival. Critical features of this highly robust repair mechanism are the ability to specifically recognize the DNA lesion and efficiently remove it. Additionally, the different repair responses that are generated and the resulting network signalling triggered within the cell not only repairs the DNA lesion, but is also tightly linked with the cellular machinery that governs cell-fate decision e.g. cell cycle arrest to promote survival or apoptosis for programmed cell death. Depending upon the scale and type of DNA damage, different repair responses can be activated with different outcomes for the cell. Fig. 1.1 shows a simplified illustration of different components of the repair pathway and its effects on cell-fate.

There are six damage-type-specific repair mechanisms that are triggered for dealing with different kinds of DNA damage. Table 1 shows the different types of DNA damage and the type-specific DNA repair mechanism that is activated as a result of it.

Table 1.0: Types of DNA damage and the mechanism of its repair.

| **Type of DNA damage** | **Repair mechanism** |
|---|---|
| Methylated ($O^6$ or $N^7$) Guanine | Direct repair |
| Oxidised/Deaminated bases | Base excision repair |
| Bulky DNA lesions, DNA-protein adducts | Nucleotide excision repair |
| Mismatched bases | Mismatch repair |
| Double stranded DNA breaks | Non-homologous end joining |
| Double stranded DNA breaks | Homologous recombination |
| Double stranded DNA breaks | Single strand annealing |

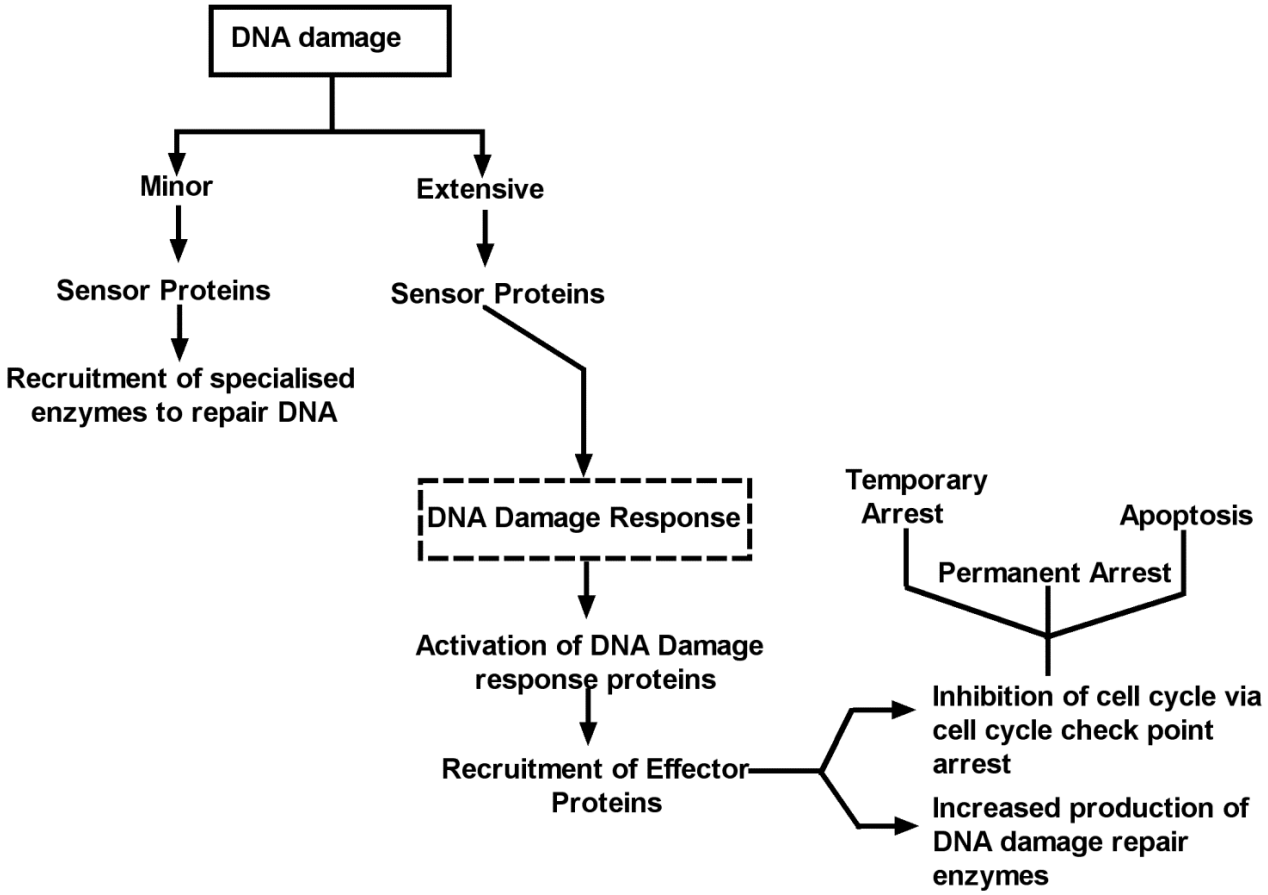


**Figure 1.1: Cellular responses to DNA damage**. Depending upon the scale of DNA damage, one of the two pathways may be activated. If the DNA damage is minor, sensor proteins are activated which recruit specialized DNA repair enzymes to the damaged site and DNA is repaired. However, if the DNA damage is extensive, the DNA Damage Response (DDR) pathway is activated which activates specialized transducer proteins that amplify the damaged signal and activate effector proteins. The effector proteins cause cell cycle arrest and increase in the production of DNA damage repair enzymes. The arrest at the cell cycle checkpoints may result in temporary halting of the cell cycle, a permanent arrest or induction of apoptotic pathways.

Since the current PhD research focuses on regulation and functional elucidation of ATM, a protein kinase involved in DSB repair, DNA repair mechanisms activated only after DSBs, i.e. Non-homologous end joining, Homologous recombination and single strand annealing will be discussed in more detail.

### 1.2.1 Non-homologous end joining (NHEJ)

This mode of DNA repair is often described as error-prone. Double stranded breaks produced by nucleases or after exposure to ionizing radiation (IR) are often repaired by this mechanism (Shen Z et al., 2007). It is thought to be the predominant type of repair mechanism of DSBs in mitotically replicating cells and has been studied in greater detail. The hallmark of NHEJ is its ability to ligate non-ligatable DNA ends.

In this mechanism, after the generation of DSBs, a heterodimeric protein called KU comprising of KU70 and KU80 subunits, binds to the ends of DNA breaks and occupies a region of 16-18bp (Walker JR et al., 2001). This heterodimer next recruits its catalytic subunit called DNA-PKcs to the DNA end which displaces the KU dimer to the inside and binds at the extreme ends of broken DNA (Yoo S et al., 1999). This results in the formation and activation of trimeric DNA-PK holoenzyme, a key kinase in NHEJ repair (Smith GC et al., 1999). Once this kinase is activated, it recruits and phosphorylates key DNA damage repair proteins including WRN, which is a 3' to 5' exonuclease (Karmakar P et al., 2002), and Artemis having specific 5' to 3' exonuclease as well as endonucleolytic activity on 5' and 3' hairpins and overhangs (Ma Y et al., 2002) and Replication protein A (RPA) which binds and subsequently stabilizes single-stranded DNA intermediates formed during DSBs and thus prevents complementary DNA from reannealing (Broderick S et al., 2010).

The exonucleases recruited can digest and process the damaged DNA ends for ligation. Next, DNA-PK phosphorylates XRCC4, a binding partner of DNA ligase IV, which is then recruited to the damaged DNA ends. DNA polymerases POLμ or POLλ are next recruited which fill the DNA gaps produced by DNA damage (Mahajan KN et al., 2002) while XRCC4-Ligase IV complex seals the nicks (Chen L et al., 2000). DNA-PK also autophosphorylates itself which causes its detachment from the DNA lesion (Chan DW et al., 1996). A simplified cartoon version of the entire process of DNA repair mediated by NHEJ is depicted in Fig. 1.2.

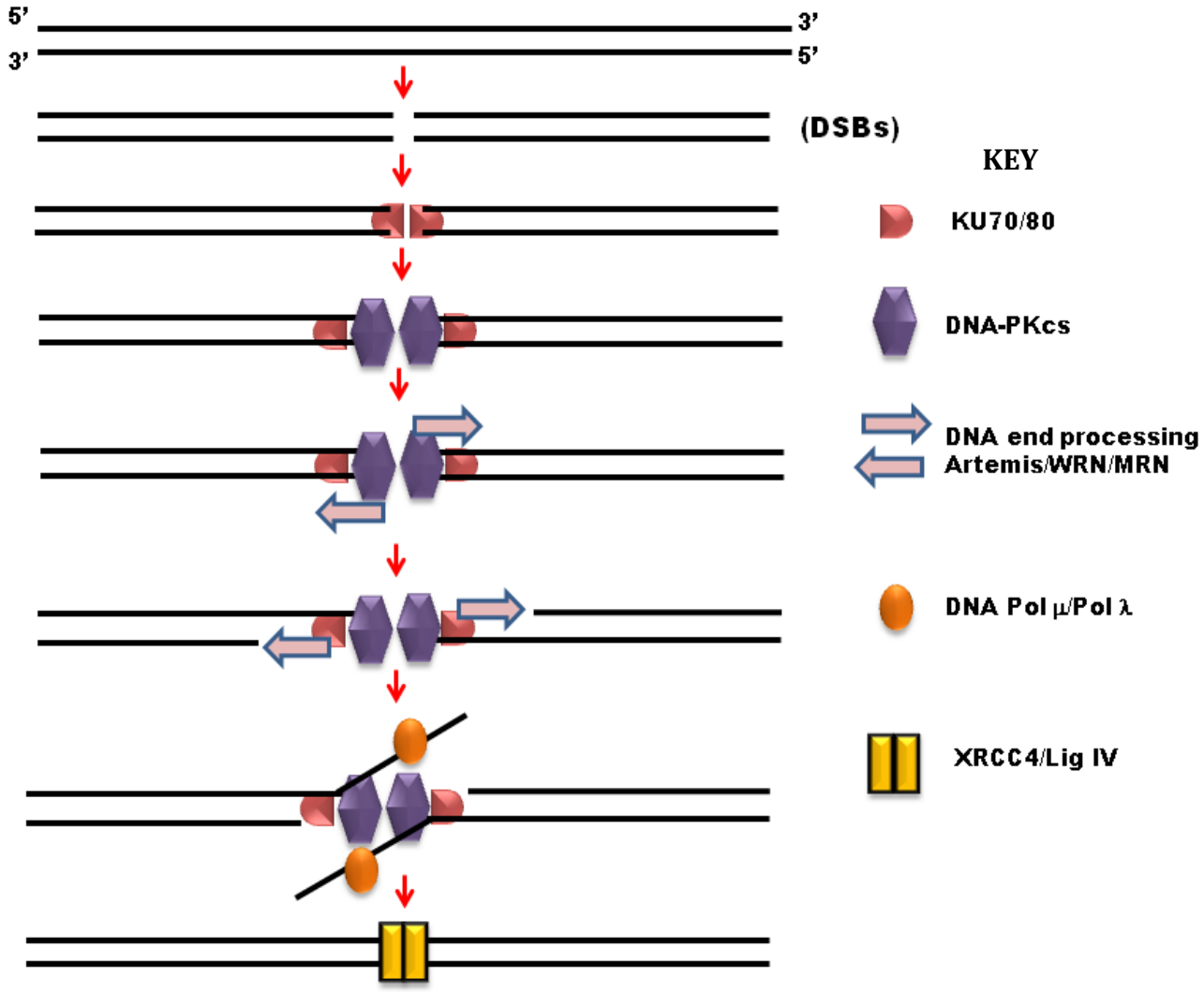


**Figure 1.2: Double stranded DNA repair via Non-homologous end joining (NHEJ).** After DNA undergoes double stranded breaks, it may be repaired in an error prone mechanism via NHEJ. The DNA breaks are first detected by KU subunits which recruit DNA-PK catalytic subunit and assemble DNA-PK holoenzyme. This results in the recruitment of specific endonucleases that carry out DNA ends processing for subsequent ligation, DNA polymerase μ or λ to fill in the gaps and XRCC/LigIV complex to seal the DNA nicks. The Figure is designed on the basis of information from Walker JR et al., 2001, Yoo S et al., 1999 and Ma Y et al., 2002).

### 1.2.2 Homologous Recombination repair (HRR)

This mode of DNA repair is referred to as error-free mechanism. DNA damage caused by either IR or replication fork arrest are primarily repaired by this mechanism. The reason why greater repair accuracy is achieved with this mechanism is because of use of homologous sequences in the genome e.g. sister chromatids, homologous chromosomes or repeated regions, to prime the repair synthesis. For this reason, HRR is most active in late S/G2 phase (Takata M et al., 1998). The fact that HRR can use homologous chromosomes as a template for the resynthesis of damaged DNA can result in loss of heterozygosity, an important feature of HRR repair.

The HRR process is triggered by the generation of DSBs primarily post S-phase. This is followed by extensive 5' to 3' end processing resulting from the activities of the recruited exonucleases i.e. MRE11, present as a complex in MRE11/Rad50/NBS1, collectively called MRN complex (Carney JP et al., 1998) and WRN (Shrivastav M et al., 2007). Additional roles of MRN complex are also presumed to firstly recruit the key protein kinase in DSB repair known as ATM, via its NBS1 subunit, which is known to be a substrate for ATM phosphorylation (Lim DS et al., 2000) and unwind DNA via ATPase activity of its Rad50 subunit (William RS et al., 2007). After the 5' to 3' resection, the exposed single strands recruit RPA protein which coat the resected single stranded DNA and also recruit RAD51 (Golub EI et al., 1998). RAD51 forms nucleoprotein complexes on RPA-coated single stranded DNA to initiate strand exchange, with the help of its five paralogues, RAD51B, C, D, XRCC2 and XRCC3.

The resulting nucleoprotein filament searches the nearby sequences to find a homologous sequence which is later invaded with the help of RAD54, an ATPase related to DNA helicases (Swagemakers SM et al., 1998). This is followed by the recruitment of RAD52 which forms a seven-monomer ring structure at the nucleoprotein filament that can interact with both double and single stranded DNA (Van Dyck E et al., 1999). Additionally, breast cancer susceptibility genes, BRCA1 and BRCA2 are also recruited to the site, which can act as scaffolding proteins and may also interact with RAD51 and RPA (Yang H et al., 2002).

All these initial events result in stand invasion of the DNA overhangs and pairing with homologous sequences. Using this homologous sequence as a DNA template, DNA polymerase starts filling the gaps of the resected 5' to 3' DNA ends of the damaged homologue. At this point, there is a formation of an intermediate DNA structure, called Holliday junction (Duckett DR et al., 1988).

During HRR, this Holliday junction can be resolved either by disengagement of the two pairs of strands resulting in a non-crossing over mode of HRR, or via its endonucleolytic cleavage mediated by resolvases resulting in a cross-over mode (Valerie K et al., 2003). Finally, the DNA ends are ligated. The DNA polymerase and the ligase involved in HRR are as yet unknown. The entire scheme of DNA repair via HRR pathway is illustrated in Fig. 1.3.

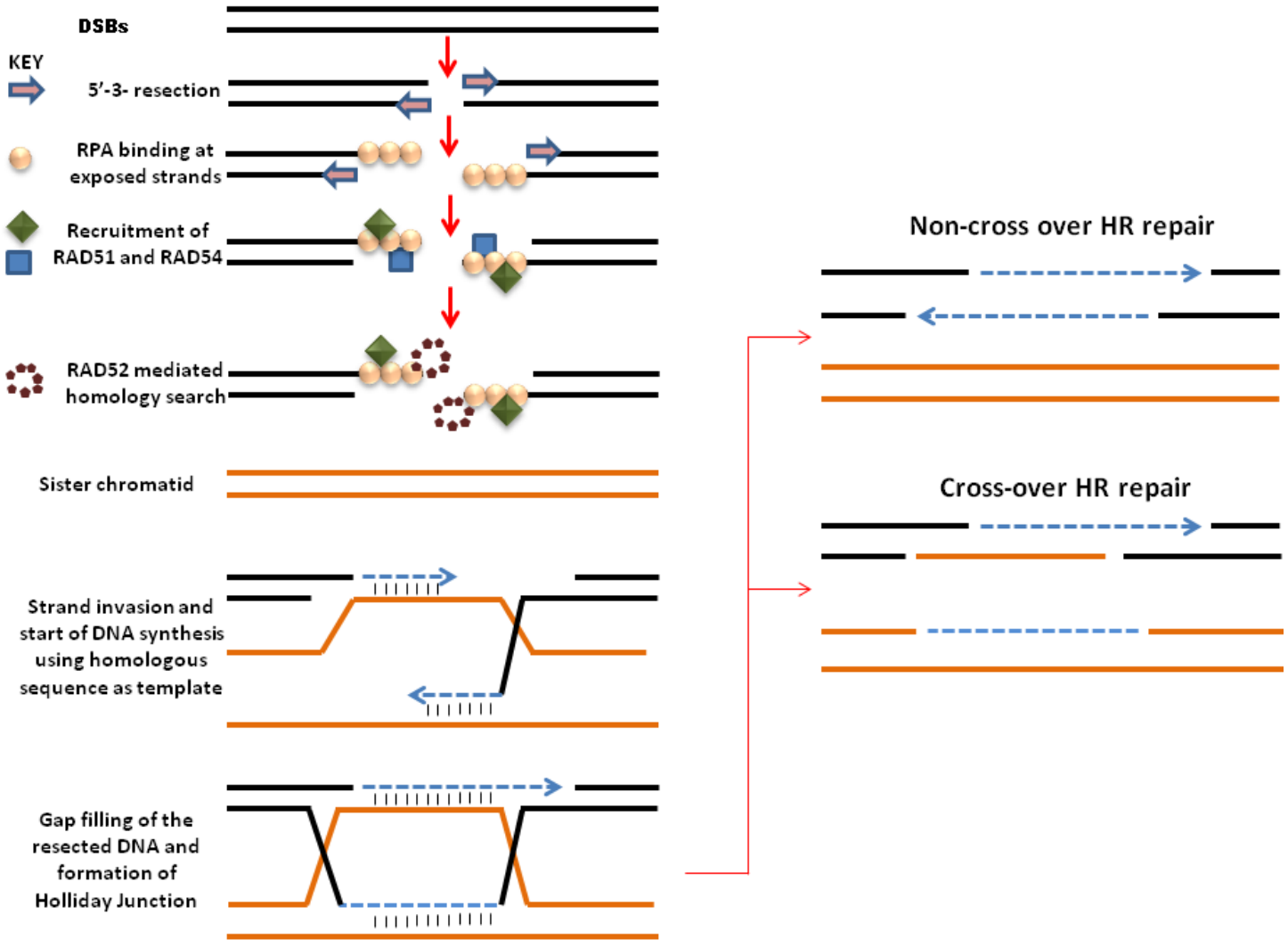


**Figure 1.3: Double DNA break repair via Homologous Recombination (HR).** After DNA undergoes DSBs, it may be repaired via HR. The DNA with DSBs is shown in black, the DNA from sister chromatid or homologous chromosome is shown in orange while the newly synthesised DNA is depicted by dotted blue lines. In this mechanism of error free repair, the DSBs recruit MRN complex, which has exonuclease and ATPase activity via its MRE11 and RAD50 subunits respectively and which may recruit ATM via its NBS1 subunit. Resection of DNA strand results in recruitment of RPA, which further recruit Rad51, its paralogues and Rad54, together forming nucleoprotein complex at the site of damage. Recruitment of Rad52 commences homology search and strand invasion which can result in the formation of D-loop structure. Unknown DNA polymerases extend the resected DNA strands using homologous sequences as template which results in the formation of Holliday junction. The Holliday junction may be resolved either in crossing over or non crossing over fashion and the nicks are sealed by DNA ligases. The figure is designed based on information from Lim DS et al., 2000, William RS et al., 2007, Swagemakers SM et al., 1998 and Duckett DR et al., 1988.

### 1.2.3 Single strand annealing (SSA)

Single strand annealing is a non-conservative process of DNA repair of DSBs. In this process, when DNA breaks are produced, DNA resection takes place most likely by the exonuclease activity of MRN complex. The length of the resected DNA, and hence of the DNA overhangs, depends upon how far up within DNA sequence, homology is found within direct repeats. Once homology with either of the two DNA overhangs is found, strand annealing takes place at those homologous regions, while the rest of the non-homologous sequences are cleaved (Valerie K et al., 2003). Repair via SSA does not require RAD51. However, for the purpose of homology search, heptameric RAD52 ring formation still takes place. ERCC1/XPF nuclease is known to be involved in the endonucleolytic activity (Adair GM et al., 2000). Finally, the gaps are filled with DNA polymerase and followed by ligation of DNA ends. Fig. 1.4 shows the scheme of repair via SSA.

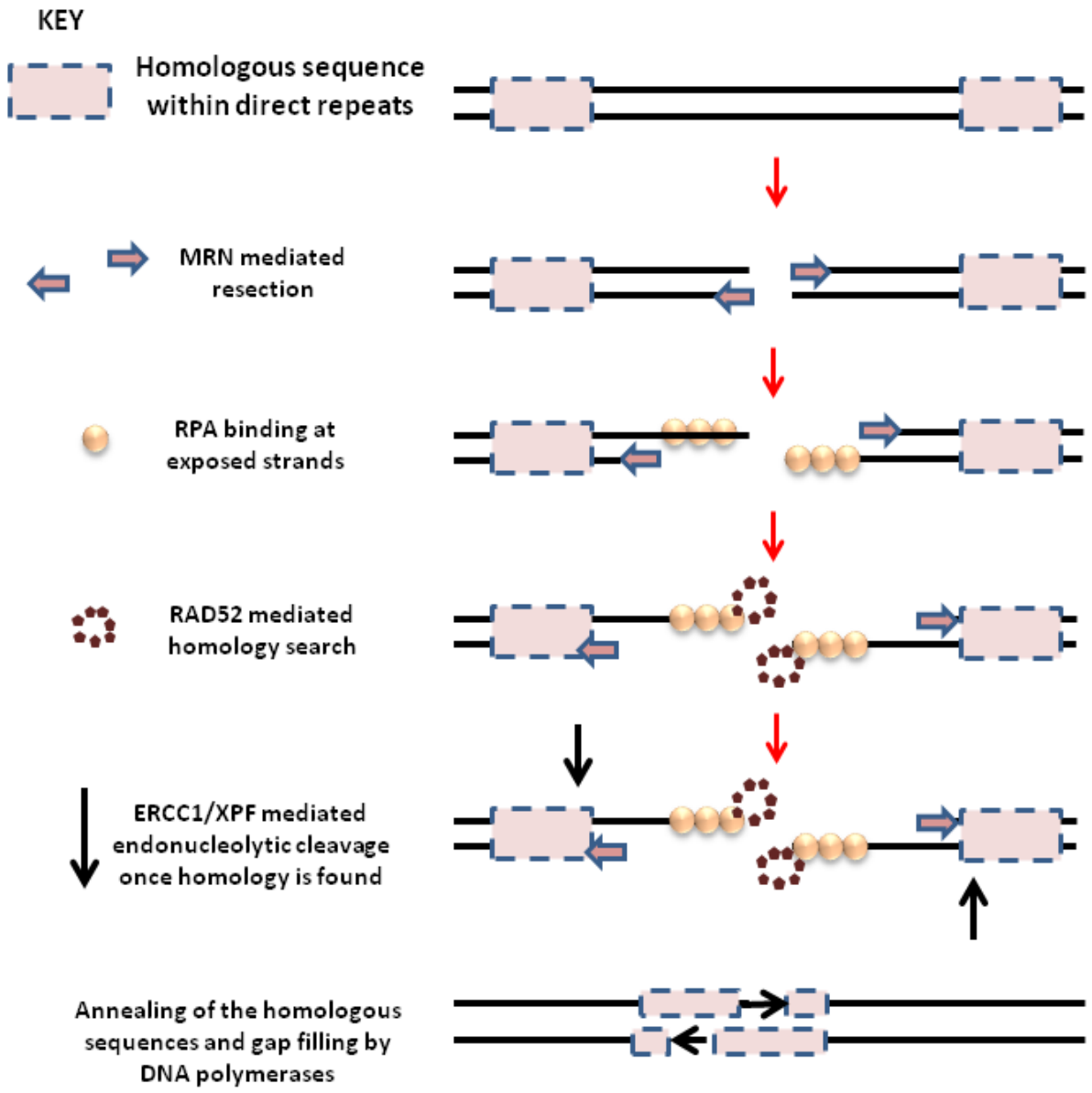


**Figure 1.4: Double DNA break repair via Single Strand Annealing (SSA).** After DNA undergoes DSBs, it may be repaired in a non-conservative mechanism via SSA. MRN mediated resection of damaged DNA ends causes recruitment of RPA, which coat the resulting single strands and recruits Rad52 that commences search for homology sequence in the direct repeats. ERCC1 causes endonucleolytic cleavage following by gap filling and ligation. This mode of repair results in loss of DNA sequence and hence known as non-conservative DNA repair. The Figure is designed based on information from Valerie K et al., 2003 and Adair GM et al., 2000.

As illustrated in Fig. 1.1, cellular responses generated after genotoxic insults not only depend on the type of DNA damage and the associated repair mechanism, but also on the scale or magnitude of a particular damage. Hence, if damage is of a lower scale, DNA damage sensors, e.g. KU subunits, MRN complex or WRN would detect the damage and recruit specialized repair enzymes as mentioned above to efficiently repair the damage. However, if there is an extensive DNA damage, with an impact on the entire cellular physiology, the cellular machinery governing cell-fate decision is mobilized. These signalling responses that are triggered after extensive DNA damage not only activate and recruit repair enzymes, but also give rise to a pathway called DNA damage response (DDR) pathway (Hartwell LH et al., 1989). The most important function of this pathway is to link the signalling generated in response to DNA damage with the cell cycle signalling pathway. Figure 1.5 represents a simple illustration of this link.

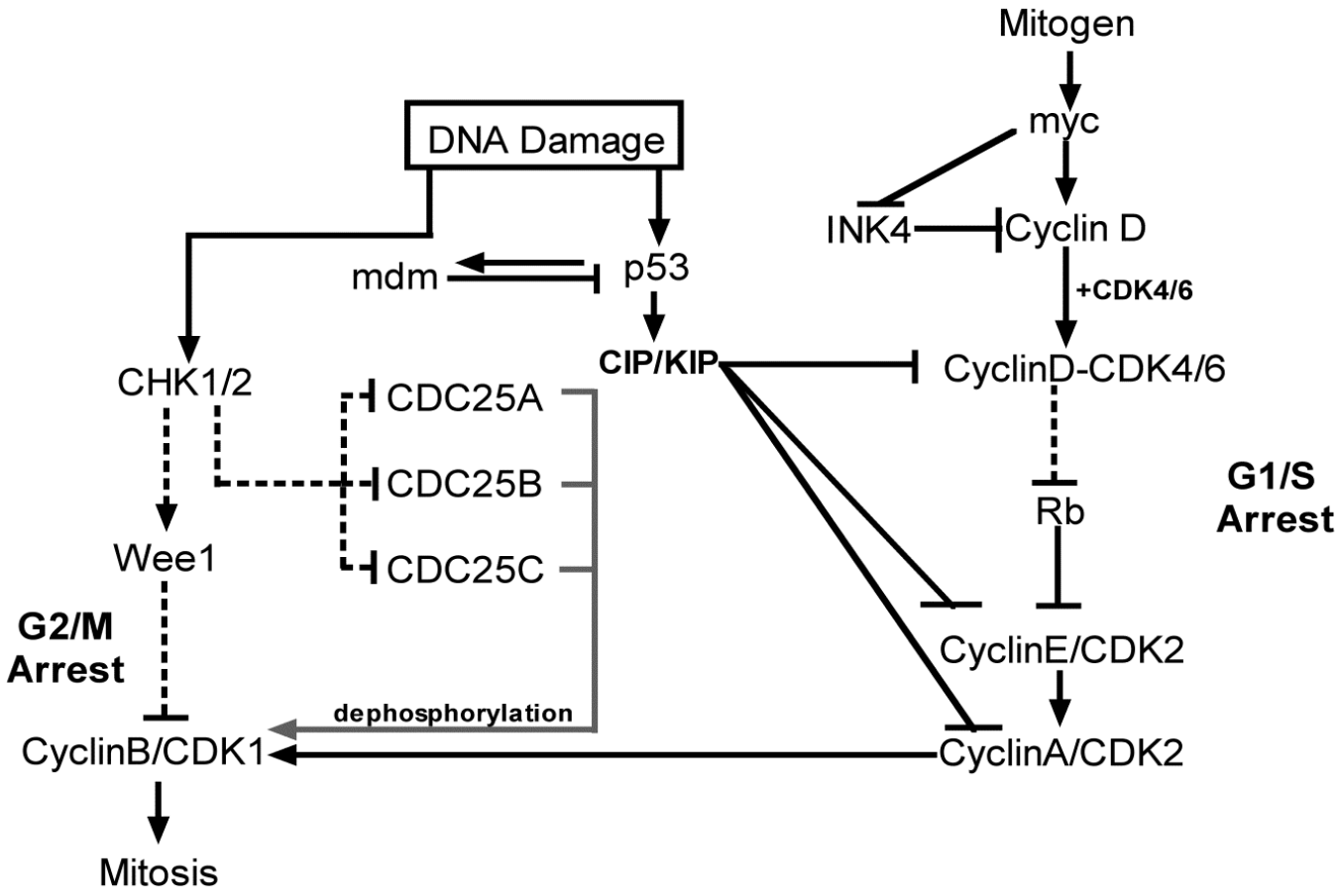


**Figure 1.5: The DNA damage pathway and its crosstalk with the cell cycle.** Lines with arrow heads represent activation while lines with bar heads represent deactivation, dotted lines with arrow heads indicate activation via phosphorylation and dotted lines with bar heads denote phosphorylational inactivation. Grey lines with arrow heads represent dephosphorylation. After DNA damage, P53 and checkpoint kinases Chk1/Chk2 proteins are activated. P53 activation results in concomitant rise in the CIP/KIP proteins, P21 and P27 which inhibit cyclin/CDK complexes, blocking the cell cycle progression which results in G1/S arrest. The activated chk1/chk2 kinases activate Wee1, a protein kinase as well as inhibit the function of Cdc25 group of phosphatases, which normally dephosphorylate and activate cyclin/cdk complexes. The inactivation of cyclinB/CDK1 activity via both phosphorylational inactivation by wee1 as well as inhibition of its activating phosphatases by Chk1/Chk2 result in G2/M arrest. Thus in a normal cell, both G1/S and G2/M checkpoints are functional and may arrest the cell cycle upon DNA damage, to allow time for DNA repair.

## 1.3 Ataxia-telangiectasia mutated (ATM)

The DDR pathway has evolved to be a complex, yet sensitive, highly integrated and interconnected pathway which can trigger cellular responses including DNA repair, cell cycle arrest and apoptosis (Kastan MB et al., 2004). Central to DDR is the Ataxia telangiectasia mutated gene that codes for Ataxia telangiectasia mutated protein (ATM), a 370 kDa Serine/Threonine kinase, functioning as a core component of the DDR signalling pathway (Savitsky K et al., 1995). ATM belongs to phosphatidylinositol-3 kinase like kinase (PIKK) super family of large proteins having phosphatidylinositol-3/4 kinase (PI3K/PI4K) catalytic domain thus functioning as an important kinase in DDR signal transduction. It acts as a sensor of DSBs and through its kinase function, is responsible for the initiation of a signalling cascade by activating other downstream signal transducers and effector proteins of the DDR pathway. These effectors in turn modulate cell cycle progression, recruit DNA repair enzymes and may also trigger apoptosis if the DNA damage is beyond the repair capacity of the cell. Hence, ATM links responses generated by DNA damage with cell cycle progression and apoptotic pathways. This represents a very important function as in conditions of extensive DNA damage, cell cycle must be temporarily halted to allow adequate time for recruitment of DNA repair proteins and the actual repair of DNA. This ensures the integrity of genomic DNA and overall health and survival of dividing cells and prevents partially repaired DNA to pass on to daughter cells. Alternatively, ATM signalling may lead to permanent arrest of cell cycle, or in extreme cases trigger apoptosis (Lee Y et al., 2000).

ATM and other members of the PIKK family are also involved in DNA replication and recombination, and homologous repair during normal meiotic recombination events (Barlow C et al., 1998).

## 1.4 The ATM gene

The ATM gene is located on chromosome 11 (11q22-23) determined via linkage analysis (Gatti RA et al., 1988). It belongs to the class of housekeeping genes (Chen X et al., 1997). The full genomic organization along with intron-exon boundaries was determined by Uziel, T., et. al (1996). ATM gene consists of 66 exons which span around 150 Kb of the whole genomic DNA, with a coding sequence of 9168bp (Prokopcova J et al., 2007). The entire ATM contig shows a low GC content of 38.1% (Platzer M et al., 1997). The first two exons are termed 1a and 1b. The initiation codon lies in exon 4 and the last exon which is 3.8 kb is the largest (Uziel, T et al., 1996). The first 4 exons of the ATM gene, which lie in the 5-UTR have been found to undergo extensive alternative splicing. Apart from that, the 3.6 Kb long 3-UTR, spreading across the last exon, also possesses alternative polyadenylation sites (Uziel, T., et al., 1996). This results in generation of different mRNA transcripts having varying sequences and lengths. It has been suggested that the different UTRs within ATM mRNA transcripts may have important regulatory roles via the formation of different secondary structures and varying number of AUG codons (Savitsky, K., et al., 1997).

Because of the sheer size of the ATM, special cloning and expression vectors were required for its clonal manipulation. The first successful attempt to clone the whole ATM gene dates back to 1995 via positional cloning (Savitsky, K., et al., 1995).

Other attempts to clone either its cDNA fragments coding only the kinase domain of ATM (Ziv Y et al., 1997) or full length ATM (Scot SP et al., 1998) quickly followed. Shortly after the successful cloning of the full length ATM cDNA, several groups developed mouse models of a dysfunctional ATM that helped elucidate different functional aspects of ATM (Elson A et al., 1996, Barlow, C., et al., 1998).

## 1.5 ATM promoter regulation

ATM shares a bi directional promoter with another housekeeping gene called NPAT which lies around 0.55kb upstream of the ATM start codon (Imai T et al., 1996, Imai T et al., 1997). The ATM side of the promoter activity is found to be 3 times stronger than on the NPAT side. This promoter region has been found to be TATA less, has CCAAT boxes and several other important promoter sites including CREB, SP1, AP-2, GCF (Byrd PJ et al., 1996, Gentilini F et al., 2009). For the sequence of ATM promoter and details of its *cis*-regulatory elements, see Appendix-I, A1.1.3.

There is some evidence of the existence of another putative promoter region immediately upstream of the first coding exon which also possesses TATA box (Platzer M., et al., 1997). This may contribute in the basal level expression of the ATM gene. In the past, several researchers including my group have targeted the ATM promoter region to study its activity or elucidate ATM expression patterns (Khalil HS et al., 2011, Craig AL et al., 2010, Gueven N et al., 2006, Gueven, N, et al., 2003, Hirai Y et al., 2001). While ATM is generally regarded as a constitutively expressed gene with no major change in its overall expression, it has been found that the promoter activity is tissue specific, and shows an induction of transcription in certain conditions (Khalil HS et al., 2011, Craig AL et al., 2010).

A higher induction is seen in tissues with lower basal level of ATM and vice versa (Rogatcheva, MB et al., 2007). Moreover, some tissues show higher protein expression without any changes to mRNA levels suggesting a translational control rather than promoter regulation (Fang ZM et al., 2001).

## 1.6 ATM protein: Domains, post-translational modification and expression

ATM is expressed as nuclear 3056 amino acid long Serine/Threonine protein kinase (Chen G et al., 1996, Scot SP et al., 1998). The 3-D crystal structure of this protein is as yet, unknown. However through protein sequence analysis and homology determination, several protein domains have been identified in ATM.

The kinase function of ATM is maintained by 350 residues long, PI3K/PI4K domain spreading between amino acids 2712 to 2962. It also contains a FAT domain (name derived from FRAP, ATM and TRRAP) at region 1960 to 2566 amino acids and a C-terminal FAT domain (FATC domain) between residues 3024 and 3056 (Morgan SE et al., 1997). Apart from that, a leucine zipper motif between residues 1217—1238 (Savitsky K et al., 1995, Morgan SE et al., 1997) and a ten amino acids long, proline rich c-Abl (a tyrosine kinase) interacting region between residues 1373 – 1382 have been identified (Shafman T et al., 1997). Fig. 1.6 shows the domain architecture of ATM protein along with their associated functions.

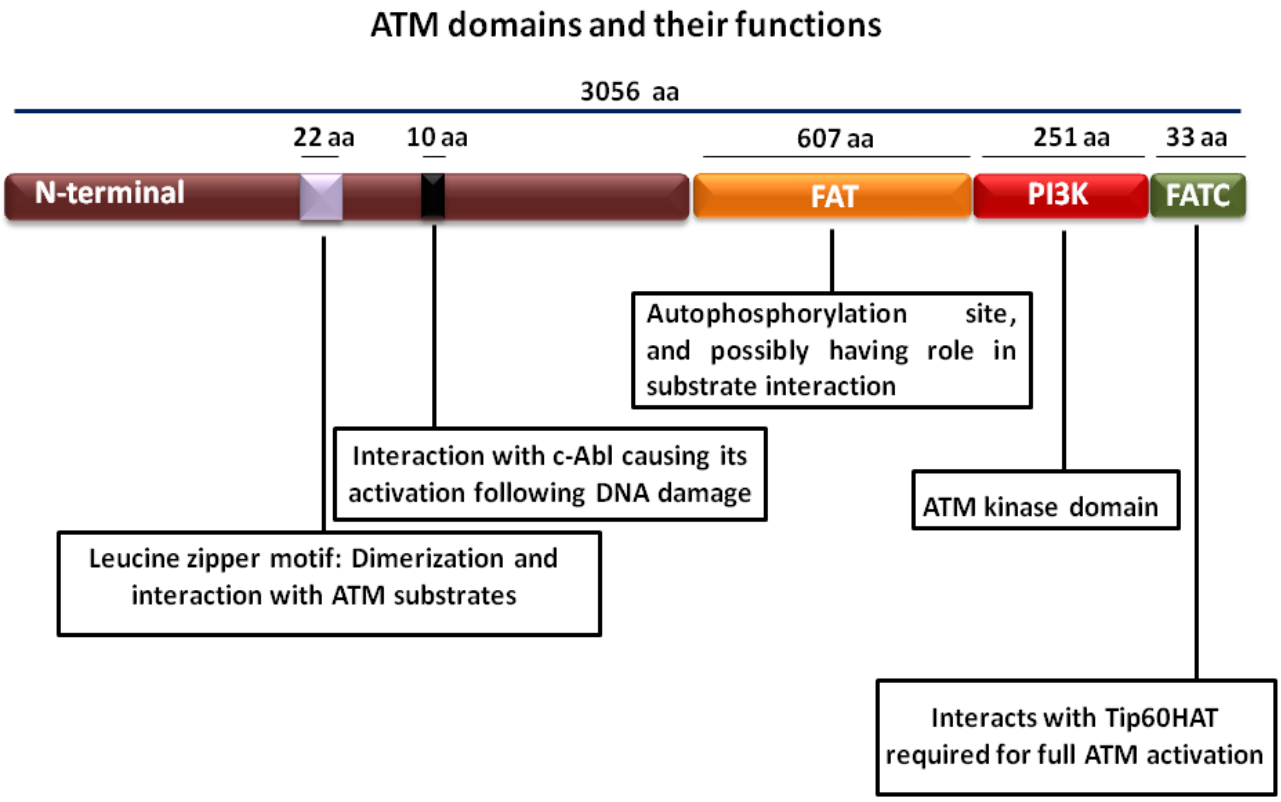


**Figure 1.6: The domain architecture of ATM and the associated functions.** The 3056 amino acid long ATM protein has been shown to have a FAT domain, a kinase domain and FATC domain at the extreme C-terminal. The 251 amino acid long, C-terminal kinase domain of ATM classifies it in the PIKK superfamily of protein kinases. The figure is designed on the basis of data from Morgan SE et al., 1997, Savitsky K et al., 1995 and Shafman T et al., 1997.

ATM is a constitutively expressed protein which is held in an inactive homodimeric or higher order multimeric state. In this form, the kinase domain of one molecule is buried in a region surrounding residue serine 1981 of the partner monomer. Upon genomic insults e.g. exposure to ionizing radiation, the pre existing ATM molecules undergo rapid autophosphorylation at residues Ser367, Ser1893 and Ser1981, the last serine being in the FAT domain (Bakkenist CJ et al., 2003, Kozlov SV et al., 2006). This autophosphorylation results in dimer or oligomer dissociation and the release of kinase active monomers (Bakkenist CJ., et al., 2003). These monomers have exposed N-terminal sequences to bind to their substrates while C-terminal kinase domain for their subsequent phosphorylation. DNA damage induced full activation of ATM also involves acetylation of Lysine 3016 present in the FATC domain by Tip60 histone acetyle transferase (Sun Y et al., 2005 & 2007). The complete list of phosphorylated ATM residues determined so far is given in table 2.0.

Table 2.0: ATM phosphorylational mapping

| **ATM** | | |
|---|---|---|
| **Residue modified** | **Position** | **Reference** |
| Serine | 72 | Matsuoka S et al., 2007 |
| Serine | 85 | Matsuoka S et al., 2007 |
| Serine | 86 | Matsuoka S et al., 2007 |
| Serine | 367 | Kozlov SV et al., 2006 |
| Serine | 373 | Matsuoka S et al., 2007 |
| Serine | 1883 | Oppermann FS et al., 2009 |
| Serine | 1893 | Kozlov SV et al., 2006 |
| Serine | 1981 | Bakkenist, CJ., et al., 2003 |
| Serine | 1985 | Matsuoka S et al., 2007 |
| Serine | 2996 | Daub H et al., 2008 |

In terms of its expression, ATM is regarded as a housekeeping gene with a steady constitutive expression (Gately DP et al., 1998). It is ubiquitous and is expressed in several embryonic and adult tissues (Chen G et al., 1996). However, the overall expression varies from organ to organ. High expression has been observed in developing nervous system (Soares HD et al., 1998, Qi J et al., 2004), spleen, thymus and testis (Chen G et al., 1996, Gueven N et al., 2006). Additionally, higher amounts are also seen in those tissues which undergo frequent proliferation and genetic recombinations to ensure the genomic integrity (Rogatcheva MB et al, 2007, Meyn MS et al., 1999).

ATM, regarded as the caretaker of the genome (Levitt NC, et al., 2002), is also thought to be involved in oxidative stress response (Guo Z et al., 2010), apart from being activated after genomic insults. In keeping with its role as a constitutively expressed gene, ATM protein level is generally believed to remain constant within the cells. It has been reported that ATM does not undergo any change in its total protein levels after DNA damage, with the only change being dimer to monomer transition and activation of its kinase activity (Brown KD et al., 1997, Bakkenist CJ et al., 2003). ATM expression was earlier also reported to remain constant throughout the cell cycle. Furthermore, following genotoxic insults, no major change in its sub-cellular localisation had been observed initially after its discovery (Watters D et al., 1997).

However, few years later, contrary reports emerged demonstrating an alteration in ATM protein expression under certain circumstances accompanied by a corresponding change in ATM activity. In one study, radiation-induced upregulation of ATM *in situ* and in response to mitogens resulting in increased ATM kinase activity was reported (Fukao T et al., 1999). By contrast, epidermal growth factor was reported to down-regulate ATM at the transcriptional level (Gueven N et al., 2001).

In most of these instances, alterations in the amount of ATM protein resulted in variation in its activity, ultimately impacting cellular sensitivity towards genotoxic agents.

Promoter studies of ATM further revealed radiation inducibility (Gueven N et al., 2003) and tissue-dependent variation in expression *in vivo* (Gueven N et al., 2006). Finally, recently, I reported a link between ATM activity and its expression via promoter studies (Khalil HS et al., 2011). All these later discoveries challenged the earlier belief of ATM gene to be a constitutively expressed gene and indicated the presence of additional mechanisms through which ATM expression and activity could be modulated, apart from the mere dimer to monomer transition event.

## 1.7 The ATM signalling pathway and its role in DNA damage response

As mentioned earlier, ATM is present at a nodal point in the DDR pathway, and has the ability to trigger variety of cellular responses including DNA repair, cell cycle arrest and apoptosis in nuclear cells. ATM, as a DSBs sensor, not only ensures upregulation of repair enzymes followed by prompt DNA repair, but also signals to a variety of other key proteins with a consequence on cell-fate. This important link between DNA damage, the cell cycle progression and cellular apoptotic machinery is provided by ATM function and is illustrated in Fig. 1.7.

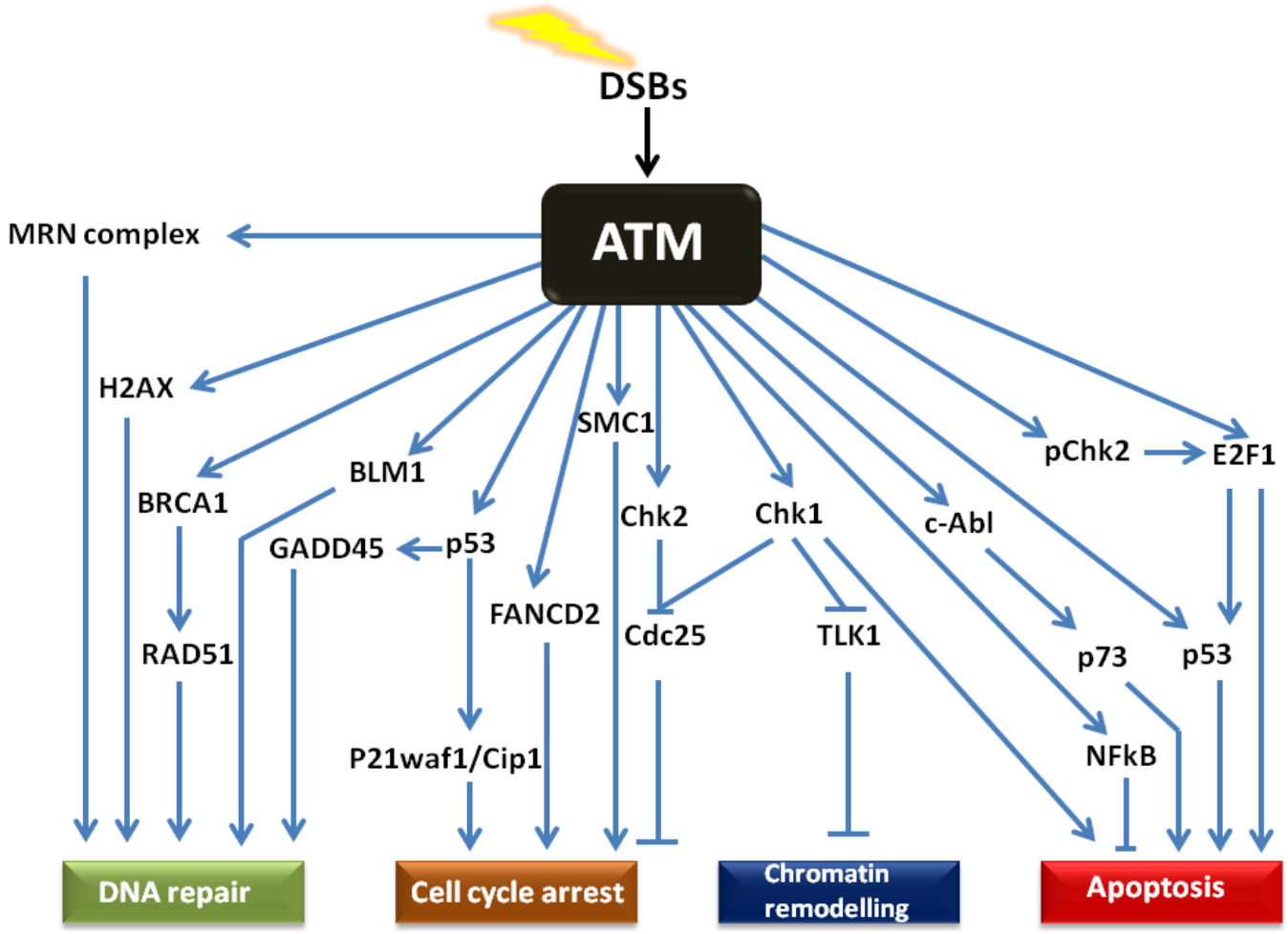


**Figure 1.7: The ATM pathways and their associated consequences on cell-fate.** ATM is present at the core of DNA damage pathway, activated upon DSBs and functions via multiple routes. While great deal of cross-talk exists between individual pathways, its major downstream substrates for DNA repair are MRN complex, BRCA1, RAD51and, P53, for cell cycle arrest are SMC1, CIP/KIP family of proteins via P53 and checkpoint kinases, for chromatic remodelling are Chk1 and for apoptosis are c-Abl, P53, Chk2, E2F1, P73 and NFkB. The figure is designed on the basis of data from Banin S et al., 1998, Chehab NH et al., 2000, Maya R et al., 2001, Xu Y et al., 1996, Westphal CH et al., 1997, Powers JT et al., 2004 and Chong MJ et al., 2000).

Since ATM function is implicated in a number of responses resulting from DNA damage, it needs to interact in a timely manner with a variety of downstream effectors. These interactions induce various signalling functions such as checkpoint arrest with P53, Mdm2 and Chk2 in the G1 (Banin S et al., 1998, Chehab NH et al., 2000, Maya R et al., 2001) damage induced S-phase arrest with NBS1, BRCA1, FancD2 and SMC1 (Lim DS et al., 2000, Taniguchi T et al., 2002, Kim ST et al., 2002, Xu B et al., 2002), G2/M arrest with BRCA1 and hRad17 (Xu B et al., 2001, Bao S et al., 2001) and apoptosis with E2F1, Chk2, P53, P73 and Bax (Xu Y et al., 1996, Westphal CH et al., 1997, Chong MJ et al., 2000, Urist MA et al., 2004, Powers JT et al., 2004). Table 3.0 shows a classification of ATM substrates with respect to their roles in influencing different phases of the cell cycle.

Table 3.0: ATM substrates in different phases of the cell cycle.

| ATM | | | |
|---|---|---|---|
| **G1** | **G1/S** | **S** | **G2/M** |
| P53<br>Mdm2<br>Nbs1 | P53<br>cAbl<br>Rad51 | RPA<br>Chk2<br>FANCD2<br>H2AX<br>BRCA1<br>CtIP<br>MRN | Chk1<br>Chk2<br>Rad17(RFC) |

Table is based on data collected from Xu B et al., 2002, Lim DS et al., 2000, Chehab NH et al., 2000 and Maya R et al., 2001 and Prokopkova J et al., 2006.

Once DNA damage causes DSBs, a change in the higher order of chromatin structure is caused, because of the unwinding and relaxation of the local DNA super-coil. This topological change in DNA results in the exposure of a variant form of histone H2A, called H2AX (Bakkenist CJ et al., 2003). The exposed H2AX is a substrate for ATM and is thought to trigger its activation. Activated ATM and the pre-existing constitutively active ATM phosphorylate H2AX at serine 139, further referred to as γ–H2AX. H2AX is regarded as the earliest substrate of ATM after DSBs and hence γ–H2AX formation represents one of the earliest events after DNA damage (Burma, S., et al., 2001).

γ–H2AX acts as a docking site for variety of other proteins involved in the DNA damage response pathway which in turn recruit additional ATM molecules to amplify its signal and form discrete ATM foci at the broken DNA ends. These proteins include MRN complex (composed of MRE11, RAD50 and NBS1), MDC1, RPA, RAD51, RAD52, RAD54, BRCA1 and BLM1 in the DNA repair component of DDR pathway.

The MRE11 component of the MRN complex executes 3'-5' exonuclease activity, the RAD50 component maintains the broken ends intact and provides ATPase activity, that itself has endonucleolytic activity, while Nbs1 recruits and possibly triggers further activation of ATM molecules (Carney JP et al., 1998) which also undergo acetylation by Tip60 (Sun Y et al., 2007). RPA phosphorylation by ATM is thought to divert its role from DNA replication to repair (Wang H et al., 2001). BRCA1 is an important ATM substrate having multiple functions. It has a role in homologous repair by activating the enzyme Rad51. Its phosphorylation by ATM at residues Ser1423 and Ser1524 triggers its transcriptional activity causing increased transcription of P21 and GADD51, hence having a role in cell cycle arrest as well (Gatei M et al., 2001).

BRCA1 is also thought to act as a scaffolding protein for the multiple protein complexes (Wang Q et al., 2000) that form discrete foci at the broken ends. Finally, ATM kinase activity for some of its substrate itself is dependent on BRCA1 protein (Foray N et al., 2003).

These initial events lead to generation of pool of active ATM molecules that amplify and transduce the signals to its effector molecules that determine the fate of the cell, other than the DNA repair component. ATM links the DNA damage response to cell cycle checkpoint arrest and apoptosis partly via the tumour suppressor protein P53. ATM phosphorylates P53 at serine 15 that causes its increased stability and activation (Banin S., et al., 1998). ATM also contributes in P53 activation via mdm2 phosphorylation at serine 395 that hinders mdm2 interaction with P53 (Maya R et al., 2001). Additionally, ATM phosphorylates both checkpoint kinases Chk1 and Chk2 upon DNA damage (Matsuoka S et al., 2000, Falck J et al., 2001, Gatei M et al., 2003), which in turn phosphorylate P53 on serine 20 and contribute further in its stabilization (Shieh SY et al., 2000). Once P53 is activated, it acts as transcriptional factor for important proteins including inhibitors of cdk-cyclin complexes e.g. the CIP and KIP family of cyclin-cdk inhibitors, P21/waf1 and P27 (Deng C et al., 1997). As shown in Fig. 1.5, these bind and inhibit cycle-cdk complexes, an event which causes cell cycle arrest at G1/S phase. P53 also activates GADD45 via which, it links itself to ATM induced DNA repair. Another downstream target of ATM implicated in S-Phase arrest is Fanconi anemia group D2 protein (FANCD2) phosphorylated at Ser222 via (Taniguchi T et al., 2002). P53 is also responsible for causing apoptosis in ATM dependent manner (Westphal CH et al., 1997).

Apart from the mentioned role of the checkpoint kinases Chk1 and Chk2 in P53 stabilization, these effectors also phosphorylate Cdc25 phosphatases. Chk2 phosphorylates Cdc25A phosphatase at serine 123 which causes its inactivation rendering it unavailable to dephosphorylate and activate cdk-cyclin complexes, which otherwise cause cell cycle progression. This results in checkpoint arrest mainly at the G1/S phase (Falk J et al., 2001). Chk1 regulates the activities of Cdc25B by its phosphorylational inactivation and causes cell cycle arrest mainly in G2/M phase (Kramer A et al., 2004). Furthermore, Chk1 also phosphorylates Cdc25C on serine 216 that serves as a binding site for 14-3-3σ protein, which sequesters it from nucleus (Sanchez Y et al., 1997) rendering it unavailable to dephosphorylate and activate cdk-cyclin complexes important for mitotic entry (Fig. 1.5).

As illustrated in Fig. 1.7, ATM also plays a pivotal role in apoptotic induction both in P53 dependent and independent manner. Firstly, ATM can phosphorylate E2F1 on serine 31, which results in its increased stability and can cause apoptosis in P53 dependent manner (Carcagno AL et al., 2009, Powers JT et al., 2004) as well as in an independent manner (Stiews T et al., 2000). E2F1 can also undergo Chk2 dependent phosphorylation after DNA damage and trigger apoptosis (Stevens C et al., 2003). Additionally, ATM dependent apoptosis can also be induced via Chk1 (Sahu RP et al., 2001).

In a P53 independent mechanism, ATM can phosphorylate and activate c-Abl tyrosine kinase which via P73 dependent mechanism can induce apoptosis following extensive DNA damage (Wang JY et al., 2000). Finally, ATM can also modulate apoptotic pathway following DNA damage, by stabilizing nuclear factor kappaB (NFkb) [reviewed in (Ahmed KM et al., 2007)].

## 1.8 The DDR and protein trafficking

Eukaryotic cellular machinery involves intricate signalling pathways that ensure proper functioning of the cell as a whole and appropriate cross talk between the different components within the cell. It is now clear that many signalling events including DDR involve extensive intracellular protein trafficking mechanisms as well. Protein trafficking thus represents a very important constituent of eukaryotic cellular physiology. This mechanism is not only used to distribute newly synthesised and correctly folded proteins to their final destination, but also to facilitate transport of mature proteins from one sub-cellular compartment to the other for their proper functioning. In terms of DDR signalling, these trafficking events may take place to either provide association of DDR enzymes with their substrates, to sequester a DDR transcription factor from its target promoter, or to prevent/allow complex formation between two proteins which would trigger or alter DDR signalling. Furthermore, within signalling pathways, intracellular protein trafficking events can also not only influence the overall signalling efficiency of a particular pathway, but can cause distinct compartmentalization of a multifunctional protein, a phenomenon that can lead to a bias in its downstream signalling event.

In terms of the role of protein trafficking in cell cycle progression, a typical example is phosphorylation of Cdc25C by checkpoint kinases. Cdc25C phosphorylation at serine 216 by Chk1 creates a binding site for 14-3-3, which mediates its transport to the cytoplasm, sequestering it from its substrate, CyclinB-Cdk1 to prevent cell cycle progression (Sanchez Y et al., 1997). Another example is the controlled nucleo-cytoplasmic shuttling of E2F1 protein that is required for the progression of cell cycle (Ivanova IA et al., 2007).

Illustration of the importance of protein trafficking in the DNA repair component of DDR is provided by BARD1 protein, which is retained in the nucleus by BRCA1 resulting in DNA repair. In the absence of BRCA1, BARD1 is transported to cytoplasm where it triggers apoptotic signalling (Rodriguez JA et al., 2004). Finally, in terms of apoptotic induction, sub-cellular localisation of P53 protein is a key determinant. While in the cytoplasm, it may form complex with antiapoptotic protein Bcl-xL preventing apoptosis, any nuclear P53 induction will trigger apoptotic proteins e.g. PUMA which itself can traffic to cytoplasm, release P53 from the Bcl-xL complex that can trigger mitochondrial membrane permeabilization leading to apoptosis (Chipuk JE et al., 2005). Secondly, while nuclear translocation of P53 triggers its proapoptotic transcriptional function upon treatment with anticancer DNA damaging agents, the same molecule is transported to mitochondria upon treatment with a tumour promoting agent, where it inhibits the activities of tumour suppressor, Manganese superoxide dismutase (Zhao Y et al., 2005).

Important constituents of these intricate intracellular protein trafficking systems are vesicular carriers called coatomer proteins (Palade G., 1975). These coatomer proteins form key structural and functional components of protein traffic. They coordinate, sort and manage the proteins to be transported (hereby termed as cargo proteins) by first recognizing the cargo protein, then forming coated vesicles around them and eventually transporting them to their destination.

The three most extensively studied mammalian vesicular carriers are clathrin coated vesicles, which are involved in endocytic and late secretory pathway, COPI coated vesicles, which function in reverse traffic and early secretory pathway and COPII coated vesicles involved in forward traffic emerging from Endoplasmic reticulum (Beck R et al., 2009, McMohan HT et al., 2004).

These coatomer proteins recognize and bind to specific recognition motifs in their substrates and carry out their transport via a well regulated, energy dependent protein trafficking system.

As the current study discovered the involvement of COPI coated vesicles in ATM protein trafficking, the mechanism of transport mediated by this coatomer protein is illustrated in detail in Figure 1.8. COPI coated vesicles are composed of seven subunits namely α, β, β', γ, δ, ε and ζ (Kuge O et al., 1993). The canonical recognition motif in the substrates of COPI is the dilysine KKXX motif where the X is any of the other amino acids. Di-Arginine RXR motif represents another class of COPI recognizable signal sequences in COPI substrates, which signals their endoplasmic reticulum localisation via retrograde transport (Beck R et al., 2009).

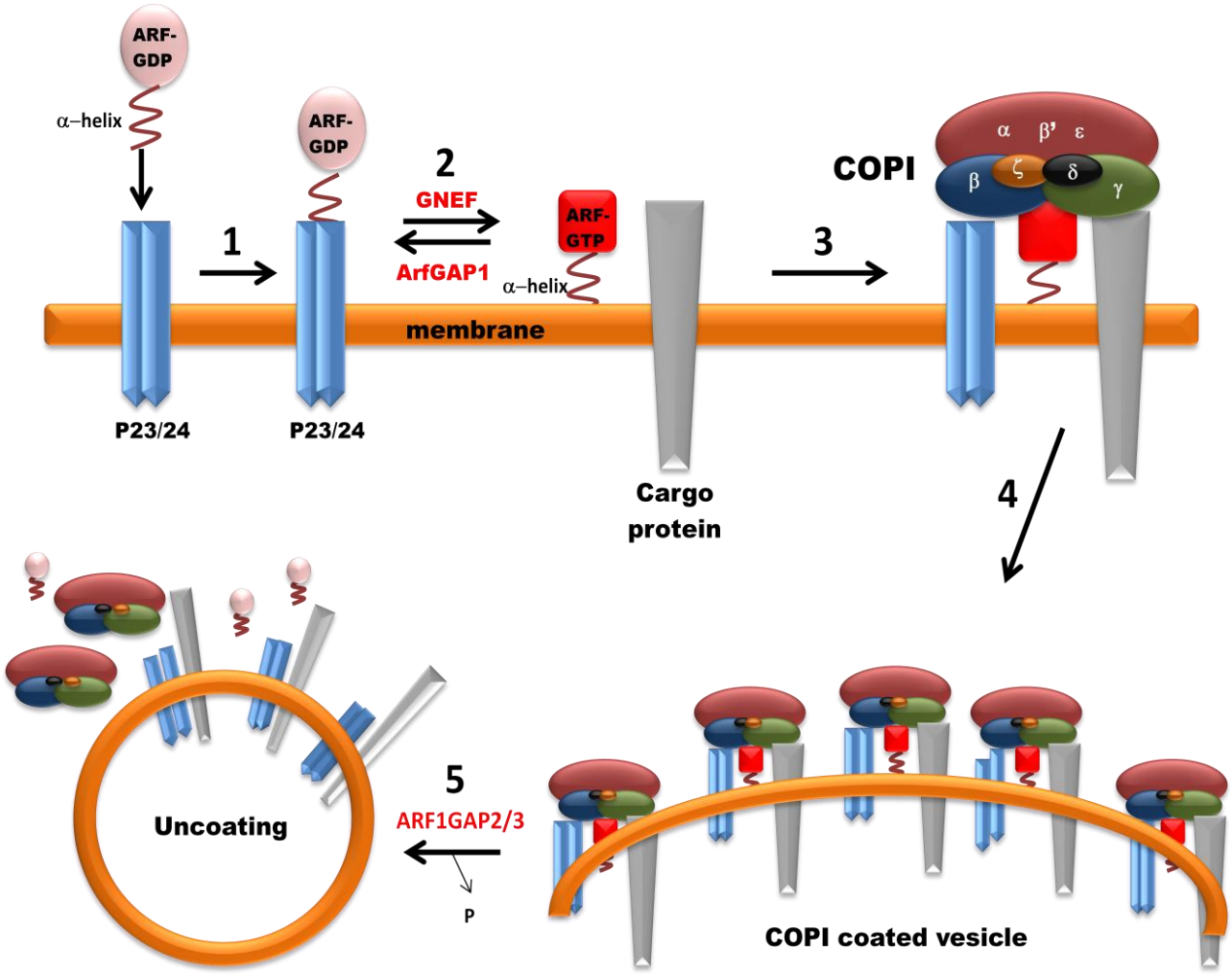


**FIGURE 1.8: COPI mediated protein transport.** (1) ARF1, a small GTPase of the RAS superfamily recognizes 23-24 kDa of type-I transmembrane protein of p24 superfamily. (2) Once anchored, the ARF1 GTPase undergoes exchange of the bound GDP to GTP, a process catalysed by Guanine Nucleotide Exchange Factor (GNEF). This causes conformational change in ARF1 causing exposure of its N-terminal amphipathic alpha helix which causes its anchorage to the membrane. (3) Bound ARF1-GTP complex recruits COPI coatomer protein, composed of seven subunits as indicated. (4) Following COPI recruitment, COPI vesicle formation begins which includes part of the membrane, p23/p24 transmembrane proteins, ARF1-GTP. (5) Once the transport process completes, ARF1GAP2/3, a GTPase activating protein induces hydrolysis of the bound GTP to GDP that brings back ARF1 into its original conformation and the coat sheds. The figure is designed based on information from Palade G., 1975, Kuge O et al., 1993, Beck R et al., 2009 and Bethune J, et al., 2006.

## 1.9 Protein traffic upon DNA damage

There is a vast amount of literature that aims to describe the functioning of DDR pathway from sensing the DNA damage to the recruitment of effector molecules and triggering the cellular machinery involved in cell-fate decision making.

While our understanding of the causes of cellular stresses that lead to DNA damage and their consequences for key events like transcriptional changes, post translational modification and the type of protein repair complexes that are assembled, has improved over the years, there are still gaps in our knowledge of DNA damage induced protein trafficking responses. However, only in the last decade, it has been realised that eukaryotic protein trafficking machinery, apart from facilitating the processing, modification and secretion of nascent proteins, is also actively involved in different regulatory modalities and co-ordination of cell signalling and forms active component of key cellular decision making processes e.g. apoptosis and cell cycle events.

In terms of DNA damage, the most critical function of the protein transport system is to concentrate the repair protein complexes at the site of DNA damage. This is expected to result in the translocation of multitude of proteins to the site of DNA lesion. This is a rapid process as indicated by the fast kinetics of γ–H2AX phosphorylation and the resulting DNA foci formation, estimated to occur within minutes of DNA damage (Paull TT et al., 2000). For this reason, protein trafficking events within the nucleus in response to DNA damage has received greater attention.

P53 is widely characterised to shuttle between nucleus and cytoplasm which is influenced by cell cycle progression and DNA damage (reviewed by Liang SH et al., 2001).

P53 is also known to translocate to mitochondria following radiation or camptothecin treatment, while APE-Ref1 and BAX, after treatment with $H_2O_2$ and etoposide respectively (Marchenko ND et al., 2000, Frossi B et al., 2002, Smaili SS et al., 2001). Other proteins involved in DDR e.g. BRCA1 (Okada S et al., 2003), Chk1 (Enomoto M et al., 2009), Cdc25A (Lopez-Girona A et al., 1999) and BID (Oberkovitz G et al., 2007) show DNA damage induced nuclear export, while still others e.g. Mdmx (Li C et al., 2002) and Optineurin (De Marco N et al., 2006) undergo nuclear import following DNA damage. A vast majority of proteins including the DDR kinases show intranuclear relocalisation upon DNA damage e.g. DNA-PK (Carter T et al., 1990), ATR (Tibbetts RS et al., 2000), Mdm2, (Bernardi R et al., 2004) and p14ARF (Gjerset RA et al., 2006).

The ATM kinase was first regarded as a nuclear protein that was believed to function mainly in the nucleus as a critical DNA damage sensor (Chen G et al., 1996). However, studies regarding its other functions beyond its well characterised role as a nuclear DNA damage sensor kinase were triggered by the increasing understanding of the disease phenotype of Ataxia Telangiectasia (A-T) patients, caused by deleterious mutations in ATM gene (Refer to section 1.10 below). ATM deficiency in patients leads to cancer susceptibility, weak immune system, hypersensitivity to ionizing radiation and sterility while A-T cell lines undergo radio-resistant and damage prone DNA synthesis and abnormality in cell cycle checkpoint arrest (Full details of the A-T disease are given in the following section). While these aberrations can straightforwardly be attributed to the role of ATM in DDR, other neurological disease phenotypes e.g. ataxia, speech defects and abnormal body movements or cellular defects e.g. cytoskeletal abnormalities, plasma membrane defects and high levels of trophic factors requirement for growth cannot all be explained through ATM's role as a nuclear DNA damage sensor.

These initial questions led to key discoveries which supported the role of ATM kinase further than its conventional role in the DDR pathway (Li J et al., 2009, Barlow C et al., 2000, Lim DS et al., 1998, Kuljis RO et al., 1999). Table 10 lists the localisation and associated functions of ATM in different sub-cellular compartments reported so far, apart from its nuclear function.

## 1.10 Ataxia telangiectasia (A-T) disorder and clinical symptoms

The importance of the role of ATM is highlighted by its functional loss in the disease, Ataxia Telangiectasia (A-T) also known as Louis-Barr syndrome. A-T is a rare autosomal recessive multisystem disorder caused by hereditary mutations in the ATM gene. It is the most common recessively inherited type of cerebellar ataxia in small children with a frequency of 1 in 50,000 live births (Swift M et al., 1985).

The disease is characterised by Ataxia, referring to un-coordinated body movements e.g. walking and Telangiectasia which means enlarged blood capillaries that can be seen under the skin. Other characteristic features of A-T include immune deficiency, hypersensitivity to ionizing radiation, and a predisposition to certain cancers (Perlman S et al., 2003). Despite the heterogeneity in the clinical presentation of the A-T syndrome resulting in the initial finding of at least 4 complementation groups (Sonal O et al., 1990), the linkage analysis showed that they all map to the same genomic location on chromosome 11 (11q22.3) containing the *ATM* gene (Getti RA et al., 1988, Chen X et al., 1997).

Heterozygous carriership of ATM seems to be very common in humans, the estimates varying between 1.4 % and 2.2 % of the general population and even more common (up to 12.5 %) in populations with a marked founder effect (Swift M et al., 1990, Gilad S et al., 1996, Su Y et al., 2000). A-T patients from nonconsanguineous families are usually compound heterozygotes. Carriers of defective *ATM* alleles, although generally considered asymptomatic, have been found to have an increased risk of death at any age due to all causes including cancer and ischemic heart disease (Su Y et al., 1996, Thomson D et al., 2005).

### 1.10.1 Neurological features

Most common neurological disorder is progressive cerebellar ataxia which may initially be misdiagnosed as cerebral palsy of the ataxic type. It is apparent as early as the first year of a child. Truncal and gait ataxia are slowly and steadily progressive. This leads to wheelchair confinement in the teenage years. Progression of neurological degeneration continues in the adult life without actual mental retardation. Thus, typical A-T patients are of normal intelligence, although abnormalities in the motor skills make normal learning programs difficult. Abnormalities in the neuronal cells of A-T patients include degeneration of Purkinje cells and thinning of the granule cell layers and some abnormalities in olivary nuclei and medullary tracts (Vineters HV et al., 1985).

### 1.10.2 Telangiectasia

Telangiectasia is the dilation of blood vessels that are visible through the skin. Usually telangiectasia appears 2-4 years of the manifestation of neurological abnormalities, similar to the ataxia, appearance of telangiectasia is progressive as well. First signs of telangiectasia appear mostly in conjunctiva, followed by appearance on ears, over nose and behind the knees. These dilated capillaries are normally not associated with bleeding.

### 1.10.3 Radiosensitivity

Radiosensitivity of A-T patients towards ionizing radiation is understandable owing to the prominent role of ATM in the desensitization towards genotoxic insults. Hence, A-T patients with cancer are extra sensitive to those doses of ionizing radiation, which are otherwise employed for non-A-T cancer patients and this sensitivity is to a life threatening level.

An interesting observation in some A-T patients is the loss of the distal 11q region of the chromosome that harbours key DNA damage response genes including ATM, MRE11, Chk1 and H2AX in several haematological malignancies and solid tumours (Srivastava, N., et al., 2009).

At a cellular level, AT cells, which lack detectable ATM, are unable to detect levels of DNA damage which usually result in activation of the DNA repair machinery, causing sustained DNA damage. Also, they cannot induce cell cycle arrest, resulting in replication of damaged DNA and multiplication of errors until the burden of damage becomes too severe for the genome. In both cases, the cell is directed to a suicide route. Apart from Radiosensitivity, A-T cells have abnormal telomere morphology and genomic instability (Foray N et al., 1997).

### 1.10.4 Cancer predisposition

Cancer predisposition is one of the major complications in A-T with the homozygous A-T patients having a life time risk of 30-40 % (Peterson RD et al., 1992). The correlation between ATM and some forms of cancers have been long established with cancer being the most frequent cause of death of A-T patients.

This link was first observed by Reed, B. et al (1966) who looked at incidences of familial and sporadic cancers in homozygous A-T patients as well as in heterozygous carriers. Numerous statistical studies have been undertaken to form a broader picture to generate a correlation between A-T causing mutations and incidences of different kinds of cancers (Prokopcova J et al., 2007, Mitui M et al., 2009). There are several reports that attempted to demonstrate links between heterozygous and homozygous A-T patients and incidences of familial and sporadic cancers. Such correlations have been found in variety of tumours to different degrees. This degree of correlation is found to be dependent on the type of ATM mutations e.g. missense or nonsense variants and also the nature of mutations (germ line or somatic A-T).

In line with the finding that A-T patients have a weak immune system, the most common malignancy linked with A-T patients is that of immune system (Leukemias and Lymphomas) with the most common being non-Hodgkin's lymphoma (~45%) (Frederick H et al., 1990), followed by acute lymphocytic leukemias (~20%) (Taylor AM., 1992). This link has further been demonstrated by generating knock out mouse models of ATM shown to be highly susceptible to sporadic lymphoid malignancies owing to impairment of the V(D)J recombination in such ATM deficient mouse lymphocytes.The lymphomas in A-T patients tend to be of B-cell origin, whereas the leukemias are usually of T-cell origin. While cancer of the immune system is more common in the early lives of A-T patients (mostly occurring in first 15 years), older A-T patients are at a greater risk of developing a variety of solid tumours including gastric, breast, medulloblastoma and basal cell carcinoma (Meyn, MS., 1999 and Spector BD et al., 1982). Furthermore, the role of heterozygous carriership of defective ATM alleles has been clearly demonstrated in a proportion of familial breast cancer and colorectal cancer cases as well (Prokopcova J et al., 2007, Gao Y et al., 2011).

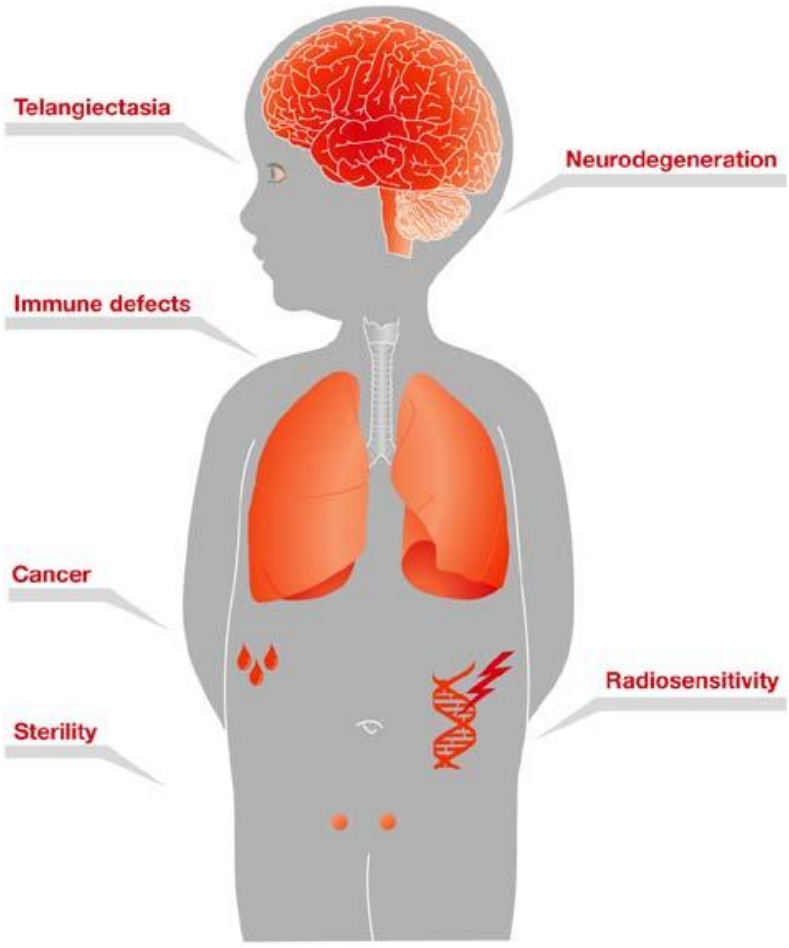


**Figure 1.9: The Ataxia Telangiectasia (AT) disease phenotype.** Early symptoms include progressive cerebral ataxia causing defects in motor skills manifested in early childhood. This is followed by the formation of telangiectasia, immune defects and predisposition to malignancy later in life and sterility in adulthood. Patients show severe radiosensitivity whereby normal doses of chemotherapy, to cure cancer caused by AT disease, to be lethal.
Source: http://traditional4fun.blogspot.com/2008/07/ataxia-telangiectasia-information.html

## 1.11 Targeting ATM pathway for therapeutic intervention in cancer

Decades of research efforts in attempts to elucidate DNA damage response pathways have added significant knowledge to our understanding of the mechanisms involved in DNA damage and repair and induction of apoptosis.

Researchers have identified that cellular sensitivity to genotoxic agents in course of cancer therapy could be achieved by modulating the function of key proteins involved in DNA repair, cell cycle arrest and apoptotic mechanisms. The idea is based on the fact that during genotoxic treatments of chemotherapy and radiotherapy, cells respond by rapidly upregulating expression and activity of DNA repair and cell cycle modulating proteins. The increased activity of these proteins will render such cells resistant to genotoxicity owing to rapid repair of the cytotoxic DNA lesions and thus hinder the cellular sensitivity process and ensure survival. In such circumstances, greater dose of genotoxicity would be required for effective killing of these cells. However, increasing the dosage will have increased cytotoxic effects on the surrounding normal cells and hence cause more side effects of therapy. On the other hand, if the activities of proteins involved in cell cycle arrest and DNA repair are inhibited prior to genotoxic treatment, greater cellular sensitivity towards genotoxic agents during treatment might be achieved. Hence, one important therapeutic strategy for cancer is the identification of important DDR protein inhibitors, which could effectively inhibit the type of DNA repair machinery that is activated and required by cell after a particular genotoxic treatment regimen. Discovery and characterization of such inhibitors not only help to elucidate the functioning of the relevant proteins but can also identify therapeutically relevant targets.

Having established cellular sensitivity strategy towards genotoxic agents, the next key consideration is the specificity of the cytotoxic action towards cancer cells compared to normal cells. Such specificity could be achieved by identifying vital differences between normal and cancer cells and then basing the therapeutic approach on exploiting those differences.

Cancer cells mostly have cell cycle based mutations and DNA repair abnormalities. Such aberrations in vital cellular functions make them more susceptible to chemo and radiotherapies as compared to their normal counterparts. In more than 50% of all cancers, P53 mutations have been found (Vogelstein B et al., 2000). This renders the cancer cell incapable of executing the P53-mediated G1/S cell cycle arrest and the repair of DNA upon genotoxic insults. The only checkpoint that is active in such cancer cells is the G2/M checkpoint, where the damaged cells are still arrested and repaired, enabling them to survive. Therefore, abrogation of this G2/M checkpoint in cancer cells for example via ATM inhibition (ATM → Chk1/Chk2 → Cdc25A/B/C → G2/M arrest link) would disrupt the only functionally available G2/M checkpoint in cancer cells and devoid them of any checkpoint arrest and hence sensitise the cells against genotoxic agents (reviewed by Smith J et al., 2010).

On the other hand, the surrounding normal cells would be less affected by this treatment as they retain a wild type P53 that can still undergo G1/S arrest. This scenario is illustrated in Fig. 1.10. This approach provides an opportunity for targeted cellular sensitivity based on functional inhibition of ATM kinase.

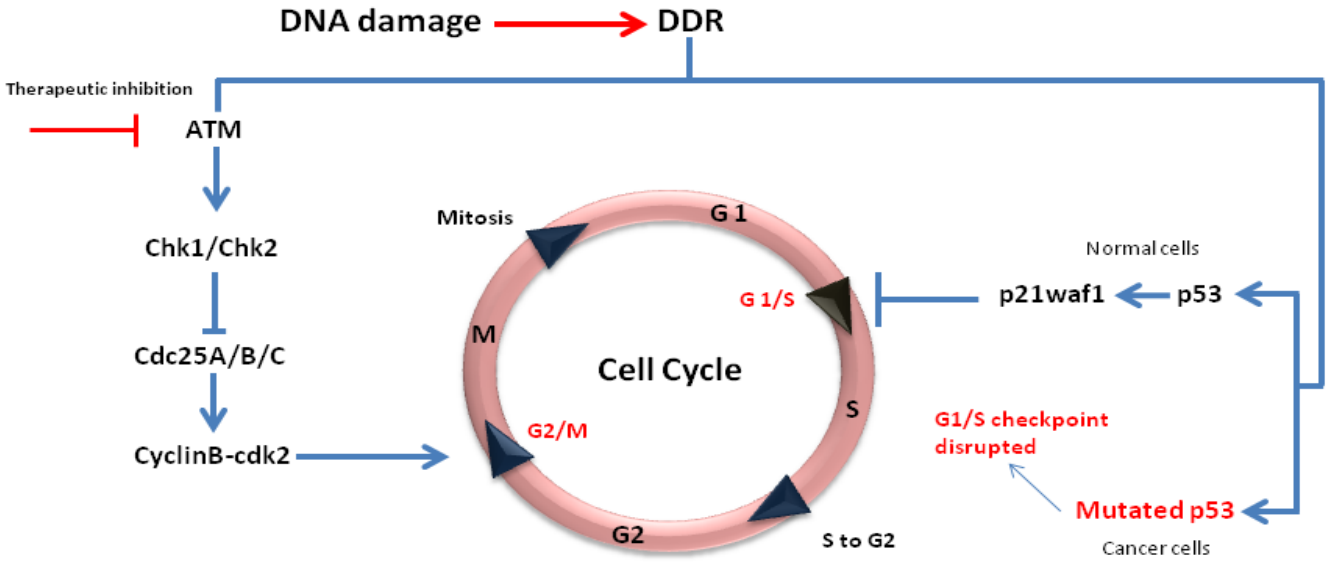


**Figure 1.10: The principle of targeting ATM pathway for achieving cellular sensitivity for therapeutic intervention in cancer.** Lines with arrow heads indicate activation, while lines with bar heads indicate inhibition. Red arrow indicates DNA damage caused by radio or chemotherapy while red line with bar head indicates therapeutic inhibition of ATM. Cancer cells with P53 loss of function mutation have a dysfunctional G1/S checkpoint whereas the G2/M checkpoint may still be functional. When cells are exposed to genotoxic agents, DDR pathway is activated which will cause G1/S arrest via P53 pathway and G2/M arrest via checkpoint kinases Chk1 and Chk2 pathway. Normal cells can be arrest in either of these pathways allowing themselves time for DNA repair. However, cancer cells can only be arrested in G2/M pathway via ATM→Chk1/Chk2 pathway. Disruption of G2/M checkpoint by way of ATM inhibition would result in failure of cancer cell to arrest in any checkpoint causing more sensitivity to genotoxic agents while normal cells with functional P53 would still be arrested and repaired.

In the past, researchers have identified and employed numerous inhibition strategies against DDR proteins in cancer settings and provided proof of principle for DDR inhibition-based targeted cellular sensitivity. Table 4 illustrates recent inhibitors discovered against the prominent proteins in the DDR pathway.

Table 4.0: Different inhibitors that target the major proteins involved in DNA Damage response.

| Target | Compound | Details | Reference |
|---|---|---|---|
| ATM | KU55933 | ATM is a critical kinase of the DNA damage response and acts as a sensor and signal transducer for the damage pathway. KU55933 is the first potent and specific inhibitor of ATM. | Hickson I et al., 2004. |
| ATM | KU60019 | An improved specific ATM kinase inhibitor | Golding SE et al., 2009 |
| ATM | CP466722 | CP466722 is an irreversible and specific inhibitor of ATM | Rainy MD et al., 2008 |
| ATR | NU6027 | A CDK2 and ATR inhibitor | Peasland A et al., 2011 |
| ATM and ATR | CGK73 | ATM and ATR are important DNA damage response kinases that link the response to cell cycle. CP466722 is a potent but reversible inhibitor or both ATR and ATM. | Alao JB et al., 2009 |
| ATM and ATR | Caffeine | ATM and ATR are important DNA damage response kinases that link the response to cell cycle. | Sarkaria JN et al., 1999 |
| DNA-PK | NU7441 | DNA-PK is a DNA dependent kinase identifying double strand breaks activated in non-homologous end joining repair. | Zhao Y et al., 2006 |
| DNA-PK | LY294002 | A general inhibitor of PI3-Kinases used to inhibit DNA-PK activity | Vlahos CJ et al., 1994 |
| ATM and DNA-PK | Wortmannin | A non-specific inhibitor of PI3-Like kinases | Sarkaria JN et al., 1998 |
| Chk1 | AZD7762 | An ATM/ATR dependent kinase with role in S and G2 arrest in response to DNA damage. | Zabludoff SD et al., 2008 |
| Chk1 | PF-00477736 | ATP competitive small molecular inhibitor of Chk1 | Blasina A et al., 2008 |
| Chk2 | C3742 | A potent inhibitor of Chk2 | Arienti KL et al., 2005 |
| Chk1 and Chk2 | UCN-01 | A general protein kinase inhibitor | Koniaras K et al., 2001 |
| Chk1 and Chk2 | XL-844 | An inhibitor of the checkpoint kinases | Riesterer O et al., 2011 |
| $O^6$-alkylguanine-DNA alkyl transferase (AGT) | $O^6$-BG | AGT is a repair factor in the direct repair. $O^6$-BG is the first specific and potent inhibitor of AGT and sensitizes several cancer types to different DNA damaging drugs | Gerson SL., 2004 |
| DNA glycosylases and APE1 | CRT0044876 | DNA glycosylases and endonucleases like APE1 are factors in Base excision repair. This compound is a pseudo substrate, depleting the cell of functional DNA glycosylases. | Madhusudan S et al., 2005 |
| PARP-1 | AZD2281 | Poly-ADP-Ribose polymerase 1is involved in S-phase related DNA repair. | Fong PC et al., 2009 |

In terms of the exploiting DDR pathway for therapeutic intervention, the inhibitors of Poly ADP-ribose polymerase-1 have made the greatest progress and many novel drugs are already in clinical trials (Plummer R et al., 2008).

There are several reports that demonstrate increased cellular sensitivity towards genotoxic agents by way of modulating the ATM signalling pathway through inhibition of ATM kinase specifically. Under genotoxic conditions of chemo or radiotherapy, some tumour cells undergo a premature senescence also called stress-induced senescence (te Poele R et al., 2002). Although this permanent arrest of tumour cells is beneficial and prevents tumour metastasis, such senescent tumour cells resist apoptosis and may re-enter the cell cycle. Crescenzi et al (2008) set out to identify the cellular pathways responsible for the maintenance of such drug induced tumour senescence in breast, lung and colon carcinoma cells and identified the ATM/ATR pathway to be constitutively active in these cells. They successfully used the specific ATM inhibitor KU55933 (Hickson I et al., 2004) and another ATM and ATR inhibitor CGK733 (Alao JB et al., 2009) to block this pathway and demonstrated increased apoptosis in these cell lines. Essentially, while this treatment was cytotoxic to cancer cells, it did not cause apoptosis in the normal senescent human fibroblasts.

Similarly, Morgan SE et al (1997) demonstrated that over-expression of a truncated version of the functionally important leucine zipper domain of the ATM gave rise to a dominant negative ATM mutant in colon cancer cells. They reported that such cells had an increased level of radiosensitivity and chromosomal breakage and an abrogated S-phase checkpoint.

Inhibition of ATM expression, brought about by employing ATM antisense RNA and siRNA mediated gene silencing, represents another strategy adopted by several researchers.

Guha C et al (2000) demonstrated that attenuating ATM levels in human glioblastoma cells, by using antisense RNA against the kinase domain of ATM, increased their radiosensitivity independent of the status of P53. The resulting cells showed higher expression of P53 and P21 proteins, aberrant G2 checkpoint control and increased radiosensitivity after irradiation with a clinically relevant 2 Gy dose. Collis GC et al (2003) in a similar approach assessed the therapeutic potential of siRNA against ATM, ATR and DNA dependent protein kinase for use as radio and chemo sensitizing agent against human prostate cancer cells. This approach reduced the respective protein levels by 90% after 48 hours post treatment, while the sensitivity of the cells to radiation was significantly increased. They also confirmed that such siRNA mediated silencing was a more potent sensitizing agent then some of the inhibitors of these kinases, e.g. wortmannin or LY294002.

Recently, Neijenhuis S et al (2010) reported that lung carcinoma cells expressing an aberrant β-Polymerase, a key enzyme in base excision repair, depend on homologous recombination repair after IR treatment. In such cells, when ATM function was blocked via KU55933 treatment, an increased radiosensitivity was achieved because of failure of cells to repair through HRR.

Truman JP et al (2005) exploited the link between protein kinase C activator, 12-O-tetradecanoylphorbol 12-acetate, termed TPA, and ATM to radiosensitize the otherwise radioresistant human prostate cancer cell line and induce apoptosis. They reported that treatment of cells with TPA increased the levels of an apoptotic inducing regulatory enzyme ceramide synthase (CS) while caused an accompanying decrease in ATM activity, resulting in apoptosis induction after radiation treatment. This group also used antisense ATM oligonucleotides to suppress ATM expression in cancer cells. This resulted in higher levels of CS activation and apoptosis even with low radiation doses of 1Gy in radio resistant prostrate cancer cells.

In another study, Gueven N et al. (2001) established a negative link between EGF and ATM expression and observed that the treatment of human lymphoblasts and fibroblasts with EGF down regulated both ATM and DNA-dependent protein kinases which, in turn, resulted in increased radiosensitization in cells with wild type ATM, while no further radiosensitization was seen in irradiated A-T cells. The group further demonstrated that the reduction of ATM protein levels following EGF treatment resulted from transcriptional suppression of ATM at promoter level.

A-T cells, which are highly chemo- and radiosensitive also have a disrupted NF-kappa B expression. Exploitation of this link between ATM and NF-kappa B pathway regulation (see Fig. 1.7) is an interesting anticancer target and experiments have been performed by using both a dominant negative form of NF kappa B inhibitor, I Kappa B alpha and inhibitors of ATM to disrupt the NF kappa B pathway to achieve chemosensitization and apoptosis of cancer cells (Jung M et al., 2001).

While conceptualization of the ATM inhibition-based anticancer therapeutic approach seems straightforward, there are a number of challenges to overcome. Although, theoretically, such inhibition of ATM function would disable the DDR mediated cell cycle arrest and repair and cause accumulation of DNA damage leading to cell death, there are other similar kinases with overlapping functions with ATM, such as DNA-PK and ATR. Thus, it would require a broad spectrum kinase inhibitor to inhibit all important DDR kinases. On the other hand, a more general inhibitor may have more off target and cytotoxic effects in normal cells, which would lead to increased side effects. Secondly, ATM itself can signal to cause apoptosis via P53 dependent and independent pathways as described earlier, in which case, ATM inhibition may rather desensitise the cells against genotoxic agents and thus defeat the purpose.

Hence, while designing ATM inhibition based strategy for cellular sensitivity against genotoxic agents, it is imperative to consider two vital factors. Firstly, the type of genotoxic agent employed should only trigger a DNA repair response that solely depends on ATM function, thus effective sensitization could be achieved specifically to ATM inhibition after the genotoxic treatment, with no overlapping enzymes activated. This aspect of ATM function is addressed in chapter three of this PhD. Thesis. Secondly and equally vital is to characterise the cellular role of multifunctional ATM kinase (either in DNA repair for cytoprotection or apoptosis) in the context of the experimental setting e.g. dosage and time of treatment of the specific genotoxic agent. Such determination should be done in order to employ ATM inhibition at a precise time point or at a concentration of genotoxic treatment, where ATM is functioning to promote cellular resistance towards cell death and apoptosis. This aspect of ATM function is determined in chapter Six.

## 1.12 Aims and Objectives

The current research work was undertaken for the elucidation and functional characterization of ATM kinase specifically, and mechanism of DDR signalling pathway activation in general. The main aims of the current research study could be categorised in two sections.

One part of the research work was specifically aimed at the determination of ATM kinase function, regulation, trafficking and localisation in cell cycle dependent and independent manner, in normal conditions, upon DNA damage and under ATM kinase inhibited states in normal and cancer cell lines. The effects of these functional features were further aimed to be elaborated in terms of their effects on and consequences for functional partners and substrates of ATM and their overall outcome on cell-fate i.e. cell survival or apoptosis and to identify differences in these responses between normal and cancer cells.

The second part of the research work was aimed at how all the important discoveries made above could either be utilized, or used to establish conceptual framework for development of novel biological tools for their applications in Medical biotechnology.

Research presented in parts of chapters three, four and five have made key functional, regulatory and trafficking discoveries while research work presented in parts of chapters four and six demonstrate the development of key functional applications based on the these discoveries. These involve the development and demonstration of the working principle of novel cell based kinase inhibition assay, biosensor for DNA damage and generation of quantitative data for providing kinetic parameters for the prospective design and construction of deterministic mathematical model of ATM signalling pathway and its associated consequences for cell-fate.

Thus, the overall objective of this PhD. research was firstly to fill the gaps in our existing knowledge and understanding of functional spatio-temporal regulation of ATM in normal human cells, for which, previous literature has contrary reports. Secondly, to determine the effects of this regulation on its downstream substrates and the characterisation of the overall response generated by the cell with differences identified in these responses between normal and cancer cells. Finally, to provide a conceptual framework or working principles for the utilisation and functional applications of these novel findings in medical biotechnology.

# Chapter Two

# Materials and Methods

In all human affairs there are efforts, and there are results, and the strength of effort is the measure of the results.

James Allen, Author and poet (1864 – 1912)

## 2.1 Molecular Biology

### 2.1.1 Agarose gel electrophoresis

Agarose gel electrophoresis was performed for the separation, validation, characterization and purification of DNA following PCR amplifications, restriction digestions, genomic DNA or RNA isolation, estimation of ligation ratios and other clonal manipulations.

Either 0.5% or 1% solution of agarose (Biorad) was made in 1x TAE buffer (Appendix II, A2.1) in a conical flask. The percentage of agarose gel used depended upon the size of DNA (for DNA > 10kb, 0.5 % of agarose was used). Agarose was dissolved in TAE by heating in microwave for 2 minutes (min). Once the agarose was fully dissolved, the solution was cooled to 40 $^{0}$C with the help of tap water. For staining the DNA, Safeview nucleic acid stain (NBS Biologicals) was added at 5µL/100mL of gel. The gel solution was added to the agarose gel electrophoresis tank after assembling it and a comb-plate was inserted in the gel. After the gel solidified, the comb-plate was carefully removed and 1x TAE buffer was added in the gel tank to fully immerse the solidified gel in the buffer. DNA to be analysed was mixed with the DNA loading dye (Qiagen) and carefully loaded in each well. For PCR amplified products, all the content of tube (usually 50µL) were added in each well, for estimation of ligation ratios, or quality of gel purified DNA, 5µL of DNA was used and for restriction screening, 15-20µL of DNA was added. 5µL of DNA ladder (Qiagen) was added in one of the wells to provide reference point for size estimation of the test DNA. The lid of the tank was closed and the attached cables plugged into the power pack. Agarose gels were usually run for 1 hr at 80 volts.

### 2.1.2 Visualization of DNA bands and image capturing

DNA bands within agarose gels were visualized under UV by placing the gels on UV illuminator (UVP upland, USA). To capture the gel images, gels were placed within the Gel documentation machine (Alpha Innotech, USA), and loading the Alphaimager® software. Depending upon the intensity of bands, appropriate exposure time was set (usually between 500-1000 milli seconds) and image captured through the in-build camera. The images were saved in TIFF file format for later analysis.

### 2.1.3 Purification of DNA from agarose gels

In order to purify different DNA molecules from a common mixture (e.g. vector DNA and the insert) or to clean DNA of buffers and salts (e.g. after PCR amplification and restriction digestion), DNA of interest was run on agarose gels and purified from gel using the gel purification kit (Qiagen).

First of all, the gel was placed on UV the illuminator to visualize DNA. Protective equipment (UV face mask, gloves and labcoat) were worn and the UV was turned on. The DNA bands to be purified were carefully cleaved from the gel with the help of scalpel, and straightaway placed in labelled eppendorf tubes. The rest of the protocol was followed according to manufacturer's instructions (Qiagen). Once the DNA was purified, it was run on agarose gel to examine its quality.

### 2.1.4 Restriction digestion of DNA molecules

For clonal manipulation of DNA and to validate the identity of the successfully cloned constructs, restriction digestions using restriction endonucleases were performed according to manufacturer's (Promega) instructions. The final volume of digestion mix was made to 20µL by adding the following:

Sterile, de-ionized water (to the final volume of 20µL).

10x restriction buffer: To final concentration of 1x.

DNA: 1µg (Usual concentration of DNA was maintained at 1µg/µL, hence 1µL used).

The contents were gently mixed by pipetting up and down.

Enzyme-I (between 5-10 units)

Enzyme-II (between 5-10 units)

This restriction digestion mix was incubated for 1 hr at $37^{o}$ in a water bath. For the restriction digestion of PCR amplified products, the DNA was first run on agarose gel in order to gel purify it and then subjected to restriction digestion as above. For cloning purpose, the restriction digestion of plasmid vector was usually followed by SAP mediated (Promega) dephosphorylation of the 5' overhangs. For this, after the completion of the above restriction digestion, the reaction mixture was subjected to $65^{o}$C for 15 min to inactivate restriction enzymes. This was allowed to cook and 1unit of SAP (promega) was added and the mixture incubated for 15 min at 37° C. SAP enzyme was heat inactivated by incubation at $74^{o}$ C for 15 mins.

### 2.1.5 Ligation of DNA molecules

For the ligation of the DNA molecules i.e. the gene of interest or insert and linearized cloning vector, both of these were first run on agarose gel to have an estimate of their relative molar ratios as determined by their relative intensities and size. Based on those intensities, the following ligation ratios were made:

Insert: Vector

3: 1

1:1

1: 3

In these ratios, the volume of the vector was usually maintained constant while that of insert was altered to achieve the above molar ratios. After estimating the volume of vector and insert needed, the following were added in the eppendorf tube in order to make a 10µL ligation reaction:

Insert (volume dependent upon molar ratio)

Vector (volume dependent upon molar ratio)

10x ligation buffer to the final concentration of 1x (Promega)

$T_4$ DNA ligase: 3 weiss units (Promega)

Nuclease free water to final volume of 10µL.

A non-insert control was also used where nuclease free water was added instead of the insert. The above reaction was incubated either at room temperature for 3 hr, or over night at 4 $^{o}$C. For transformation, 5µL of the ligation mixture was usually used.

### 2.1.6 Bacterial transformation

Bacterial transformations were performed to either propagate pre-existing plasmid vectors, in which case, 1µL of vector was used, or for the ligated vectors having inserts, for which, 5µL ligation mix was used. Two types of bacterial transformation techniques were performed in the current research. For both kinds, E. Coli Dh-5α bacterial strain was used.

#### 2.1.6.1 Bacterial transformation by heat shock

In this method, chemo-competent E. Coli cells were employed. For each transformation reaction, 50µL of competent cells were used. First of all, bench surface was swabbed with 70% ethanol and burner was turned on to maintain a sterile environment. Frozen cells maintained at -80°C were taken out and immediately placed on ice. Cells were allowed to thaw slowly on ice and in the meantime, heat block was set to 42°C. After thawing, the chemo competent cells were very gently mixed with the help of pipette and 50µL transferred to a pre-chilled and pre-labelled eppendorf tube. The plasmid vector was next added gently to the tube containing 50µL chemo-competent cells (either 1µL or 5µL of vector added depending upon application) and the tube placed back on ice and allowed to incubate for 30 mins. After incubation, the tube was placed on the heat block maintained at 42°C and heat shock was given for 45 seconds during which, bacterial transformation takes place. The tube was put back on ice for two minutes and then at room temperature.

Pre-heated Terrific Broth (TB, Appendix-II, A2.4) at 37°C was taken out of water bath and 500µL of that was gently added to the transformation tube. The tube was placed in the shaking incubator set at 37°C and allowed to incubate for 90 mins while shaking at 125 revolutions per minute (rpm). In the meantime, LB-agar plates (Appendix-II, A2.21), made with appropriate antibiotic selection (either 50µg/mL kanamycin or 100µg/mL ampicillin) were taken out of fridge, and placed, with lids off, in another incubator set at 37°C.

After the 90 min incubation period, the transformation tube and the LB-agar plates were taken out and placed under the burner. The contents of the transformation tube were carefully transferred on the LB-agar plate and spread evenly with the help of spreader. The plates were taken to incubator maintained at 37°C and placed inverted overnight to allow the transformed bacterial to form colonies.

#### 2.1.6.2 Bacterial transformation by electroporation

Electro-competent Dh-5α cells were used for transformation via electroporation. In this technique, frozen electro-competent cells were taken out of -80°C freezer and placed immediately on ice to allow them to thaw slowly. Depending upon number of transformations, sterile electroporation cuvettes (1mm gap) (molecular bioproducts) were taken out and put on ice. The lab bench was swabbed with 70% ethanol and the burner was turned on. The electro-competent cells were mixed gently and 50µL transferred in a pre-chilled eppendorf tube placed on ice. 1µL of plasmid vector or 5µL of ligation mixture was then transferred to the tube containing the electro-competent cells, mixed very gently and transferred to the pre-chilled electroporation cuvettes. The electroporator (Biorad gene pulser, UK) was turned on and set to 1.8kVolts.

The electroporation cuvettes with the contents were dried with paper towel and placed in the electroporator and pulsed. Electroporation parameters were 1.8volts, 25μF, 200 Ohms. After electroporation, 500μL of pre-warmed TB at 37°C were carefully transferred to the cuvettes, gently mixed and transferred to another eppendorf tube. The tube was placed in the shaking incubator set at 37°C and allowed to incubate for 90 mins while shaking at 125 revolutions per minute (rpm). In the meantime, LB-agar plates (Appendix-II, A2,21), made with appropriate antibiotics were taken out of fridge, and placed, with lids off, in another incubator set at 37°C.

After the 90 min incubation period, the transformation tube and the LB-agar plates were taken out and placed under the burner. The contents of the transformation tube were carefully transferred on the LB-agar plate with antibiotic selection (either 100μg/mL, or Kanamycin 50μg/mL) to allow growth of only transformed bacteria, and spread evenly with the help of spreader. The plates were taken to incubator maintained at 37°C and placed in an inverted position, overnight to allow the transformed bacterial to form colonies.

### 2.1.7 Screening of the transformed bacterial colonies and making glycerol stocks

Following either of the two methods of bacterial transformation, the growth of transformed bacterial colonies on agar plates made with appropriate antibiotics was checked after 16 hr. Using sterile technique, 5mL of pre-warmed (37°C) Luria Bertani medium (LB, Appendix-II, A2.21) was taken in a 15mL centrifuge tube and antibiotics (ampicillin 100μg/mL or kanamycin 50μg/mL, as appropriate) was added into it.

Based on number of colonies in the control plate, colonies from the experimental plates were picked up using a sterile loop and inoculated in each of the 15mL tubes and allowed to grow overnight at 37°C in a shaking incubator at 125rpm. Next day, the tubes with bacterial suspension was taken out, and centrifuged at 5000rpm at 4°C for 15min. The media in the supernatant was discarded and the palette dried on paper towel. After this, to extract the transformed plasmid from bacterial cells, Spin Miniprep kit for plasmid extraction (Qiagen) was used according to the manufacturer's instruction. To screen and verify the cloned insert, restriction digestion were performed using appropriate restriction enzymes (See Appendix-I). After successfully transformed bacterial cultures were identified, glycerol stocks were made in the following way. A 50% filter sterile glycerol solution in LB containing the appropriate antibiotics (ampicillin 100µg/mL, kanamycin 50µg/mL) was made. 400µL of this stock was mixed with 1mL of the successfully transformed bacterial culture, mixed gently and stored in -80°C. Whenever required, these glycerol stocks were streaked on agar plates and grown overnight at 37°C to get colonies of transformed bacteria.

### 2.1.8 Bacterial plasmid extraction:

Once individual colonies of the transformed bacteria appeared on plates with antibiotic selection, they were grown overnight in the presence of the same selection. The cloned plasmid was isolated from transformed bacteria by either micro centrifuge based plasmid Miniprep (Qiagen) or Maxiprep technique (Qiagen). For techniques like propagation and clonal manipulation, plasmid Miniprep was performed. For transfection of mammalian cells, concentrated and high quality DNA preparations were used with plasmid maxiprep technique. Typical concentration of 1mg/mL DNA was achieved by plasmid maxiprep technique (Qiagen).

In this technique, the glycerol stock of successfully transformed bacteria were taken out of -80°C freezer and inoculated in 100mL of LB with antibiotics in a 500mL conical flask and grown overnight. Next day, the bacterial culture was transferred to individual 50mL centrifuge tubes, and centrifuged at 5000rpm at 4°C for 15mins. The supernatant was discarded and palette dried on paper towel. To extract the plasmid, further procedure was followed according to manufacturer's (Qiagen) instructions.

### 2.1.9 Preparation of chemo-competent cells

Chemo-competent cells were made based on the methodology of Hanahan (Hanahan D et al., 1991). All the steps were performed using sterile techniques.

First of all, a previously frozen stock of Dh-5α was taken out from -80°C freezer and streaked on LB-agar media plate and incubated overnight at 37°C. Next day, a single colony was picked up and inoculated in 5ml of super optimal broth (SOB, Appendix-II, A2.18) media. This was allowed to grow overnight at 37°C. Next day, 100ml of SOB media was taken in a 500mL conical flask and 1mL of sterile 1M $MgCl_2$ and 1mL of sterile $MgSO_4$ were added. To this mixture, 2mL of the overnight culture was added and placed in a shaking incubator set at 37°C. The culture was allowed to grow with periodically measuring its optical density (OD) at 600nm. Once the OD reached the value of 0.5 at 600nm, the growth was stopped and the culture transferred using sterile technique to sterile 50mL tubes and placed on ice for 15min. All further steps were performed in either cold room or on ice as much as possible. The 50mL tubes containing the culture were centrifuged at 3000 rpm at 4°C for 15min. The supernatant was carefully discarded by inverting the tubes and drying them on paper towel to remove all traces of media.

To each tube, 16mL of RF1 media (Appendix-II, A2.19) was added and the palette was gently resuspended. The tubes were incubated on ice for 20min. Cells were centrifuged again at 3000rpm at 4°C for 15min. The supernatant was again discarded and the tubes dried on paper towel. To the palette, 2.5mL of RF2 (Appendix-II, A2.20) was added and cells were gently resuspended. Tubes were incubated on ice for 20min. From this suspension, 100µL was added in each pre-chilled eppendorf tube and snap frozen in liquid nitrogen and stored at -80°C.

### 2.1.10 Preparation of Electro-competent cells

All the steps were performed using sterile techniques. Previous frozen stock of electro-competent cells stored at -80°C was taken out and streaked on LB-Agar (Appendix-II, A2.21) plate and placed in incubator at 37°C overnight. Next day, 5mL of TB (Appendix-II, A2.4) was taken in a 50mL centrifuge tube and a single colony from the plate was inoculated and allowed to grow overnight in a shaking incubator maintained at 37°C. Next day, 500mL of TB was taken in a 1 litre conical flask and 2.5mL of the overnight culture was inoculated in it. This was allowed to grow in a shaking incubator at 37°C until the OD at 600nm reached 0.5. At this point, all the culture was aliquoted in individual 50mL centrifuge tubes and placed on ice. From this point onwards, all further steps were performed in either cold room or on ice as much as possible. The tubes were centrifuged at 3000rpm at 4°C for 15min. The supernatant was gently discarded and the tubes inverted on paper towel to remove all traces of media. The palette containing the cells was gently resuspended in 5mL of sterile ice cold water. Centrifugation was repeated as above and the supernatant discarded again. In the similar way, the palette was washed twice in ice cold sterile water.

After the third wash, the palette was gently resuspended in 2.5mL of 10% glycerol solution in ice cold sterile water and incubated on ice for 20min. Pre-chilled eppendorf tubes were taken and 100µL of the cell suspension was added and snap frozen on liquid nitrogen. The frozen cells were stored at -80°C until further use.

### 2.1.11 Isolation of genomic DNA

For the isolation of genomic DNA, buccal swabs were used following the Buccal swab spin® protocol (Qiagen). The buccal swabs were collected by swabbing the inside of the cheek 6 times with a cotton swab (Whatman bioscience).

The cotton head was ejected in the eppendorf tube and allowed to air dry for at least 2 hr. Following this, the manufacturer's instructions were followed to isolate total genomic DNA. The quality of the isolated DNA was examined by running 10µL of the final DNA solution on 1% agarose gel (Appendix-I, A1.1.1). For further applications, genomic DNA was also quantified using spectrophotometric technique (Appendix-I, A1.1.2).

### 2.1.12 PCR amplification

Two kinds of PCR techniques were performed in this study. One was the conventional PCR amplification technique for the amplification and clonal manipulation of DNA using a template DNA either from bacterial Miniprep extraction or genomic DNA extracted from buccal swabs. The second type was colony PCR. In this technique, the bacterial colony used as a source of template DNA used to screen for positive clones for gene of interest. Details about all the PCR reactions performed, DNA templates used, primer sequences and PCR conditions are listed individually for each experiment in Appendix-I.

PCR reaction mix was made on ice in PCR tubes (Fisher scientific) using commercially available PCR reagents (Promega). Typically, each PCR reaction volume was 50µL. The following were added:

GoTaq® flexi buffer (5x).....10µL

$MgCl_2$ (25mM).....2.5µL (final concentration 1.25mM)

Forward primer (10µM stocks).....1µL (final concentration 0.2µM)

Reverse primer (10µM stocks).....1µL (final concentration 0.2µM)

dNTP mix (10mM each).....1µL (final concentration 0.2mM of each)

DNA template.....0.25µg

GoTaq® DNA polymerase.....1.5 units

Nuclease free water.....To 50µL.

Colony PCR reactions were performed to screen for successful clones by using the bacterial cells directly as a source of template DNA and examining the presence of gene of interest using primers specific for that gene. After the appearance of colonies following overnight growth of transformed cells, individual colonies were picked with the help of pipette tips and introduced in PCR tubes containing 5µL water. The same tips were also streaked individually from each colony on another plate in order to preserve the clone. From that 5µL cell suspension, 1µL was used as a DNA template in PCR mix. The total volume of PCR mix was set to 25µL in the following way:

GoTaq® flexi buffer (5x).....5µL

$MgCl_2$ (25mM).....1.25µL (final concentration 1.25mM)

Forward primer (10µM stocks).....0.5µL (final concentration 0.2µM)

Reverse primer (10µM stocks).....0.5µL (final concentration 0.2µM)

dNTP mix (10mM each).....0.5µL (final concentration 0.2mM of each)

DNA template.....1µL of the resuspended colony

GoTaq® DNA polymerase.....1 unit

Nuclease free water.....To 25µL.

After the PCR reactions were completed, the whole reaction mixes were run on 0.5 or 1% agarose gels using appropriate DNA ladders for analysis and subsequent applications.

**2.1.13 Site directed mutagenesis (SDM)**

Site directed mutagenesis of N-terminally tagged YFP-ATM was performed by using commercially available kit (QuikChange II XL Site-Directed Mutagenesis Kit, Stratagene), using primer sequences as listed in Appenix-I section A1.2.6. The SDM reagents were prepared on ice in a 50µL total SDM reaction in the following way:

Reaction buffer (10x).....10µL

DNA template.....10ng

Forward primer (5µM stocks).....1µL (final concentration 100nM)

Reverse primer (5μM stocks).....1μL (final concentration 100nM)

dNTP mix (10mM each).....1μL

QuickSolution.....3μL

*PfuUltra* HF DNA polymerase.....2.5 units

Nuclease free water.....To 50μL.

The SDM reaction mix was put in PCR machine and subjected PCR using cycling conditions as listed in Appendix-I, section A1.2.7. Once the cycle was completed, the tubes were allowed to cool to 37°C. Next, the SDM reaction mix was subjected to Dpn I digestion by adding10 units of Dpn I restriction endonuclease, pipetting the mixture, spinning down, and incubating at 37°C for 1 hr. Dpn I digestion degraded the parental (non-mutated DNA).

To transform the mutated and Dpn I digested SDM mixture, chemo-competent cells from the SDM kit (strategene), previously stored at -80°C were used. Cells were thawed on ice and gently swirled, and 45μL transferred into pre-chilled eppendorf tubes. 2μL of β-marcaptoethanol provided with the kit was introduced in the eppendorf tubes, and incubated on ice for 10 min with gentle mixing after each 2min. After that, 2μL of Dpn I digested SDM mixture was added to the tube containing cells and incubated for 30min on ice. A heat shock of 42°C for 30 seconds was given to the tubes and replaced into the ice for further 2min. 500μL of pre-heated SOB media (A2.18) was then added to the tubes and gently mixed and incubated at 37°C with gentle shaking for 1 hr. The incubated transformation mixture was then plated on agar plates with the antibiotic selection and incubated at 37°C overnight. During SDM reactions, appropriate control reactions were also performed as instructed by the manufacturers (Stratagene). For all the additional data of clonal manipulation and creation of successful YFP-$ATM_{mut}$ construct, see Appendix-I, section A1.2

**2.1.14 RNA extraction:**

Total RNA was extracted from HaCat cells for the generation of cDNA library as a source of template for ATM amplification for subsequent use in ATM cloning. Throughout this procedure, aseptic techniques were followed to minimize ribonucleases and dust contamination. The following procedure was followed:

Hacat cells were grown using appropriate media (table 5.0) in 250-300ml tissue culture flasks until fully confluent. Flasks were taken to the tissue culture hood, media was discarded and cells washed once with sterile PBS (Gibco).

After that, PBS was removed and 2ml of 0.5% trypsin (Gibco) was added in flask, and incubated at 37°C for 5 min. After the cells detached, as observed under light microscope, 5ml of media (with the serum added) was introduced in the flask and the cells resuspended in it to inactivate trypsin and form a uniform suspension. Cells were next counted using haemocytometer (2.2.3) and 1 x $10^7$ cells were transferred into sterile centrifuge tube placed in the tissue culture hood. The tube was centrifuged at 1000rpm for 15 min, taken back into the hood and the supernatant discarded. The palette was loosened by flicking the bottom of the tube and 600µL of lysis buffer (RNeasy Kit, Qiagen) was added and the tube vortexed thoroughly. After this, the cell suspension was homogenized using sterile syringe fitted with blunt end, 18-guage 0.9mm diameter needle (Fisher scientific, UK) 5-8 times. After homogenization, further procedure was followed using manufacturer's instructions (RNeasy kit, Qiagen).

To examine the integrity and quality of extracted RNA, 10µL of the extraction was run on 1% agarose gel in a gel tank previously washed with 10% SDS and autoclaved to remove residual ribonucleases. The resulting two bands (corresponding to 28S and 18S subunits of ribosomal RNA) ensured the integrity of the RNA isolated (Appendix-I, A1.2.1).

### 2.1.15 RNA quantification and determination of purity

Once the RNA was purified and checked for its integrity by running it on agarose gel, it was quantified using spectrophotometric technique. First of all, RNA dilution buffer (10mM Tris.Cl, pH 7) was taken in a sterile cuvette and placed in the spectrophotometer. The wavelength was adjusted to 260 and the buffer was used to blank the spectrophotometer. Next, 10µL of RNA was diluted in 490µL of RNA dilution buffer in a cuvette and its absorbance was measured at A260nm. Each reading was taken 3 times and their means calculated. The RNA was quantified by the following formula:

$$A_{260} \times \text{Dilution factor (50)} \times 44 = x\ \mu g\ /mL$$

To determine the purity, a ratio of the Absorbance at 260 and 280 ($A_{260}/A_{280}$) was calculated after diluting RNA in 10mM Tris·Cl, pH 7.5. An absorbance ratio of around 2 was considered to indicate good quality RNA. For data obtained for RNA extracted from HaCat cells, see Appendix-I, section A1.2.2

**2.1.16 cDNA synthesis**

After the integrity and quality of the total RNA isolated was examined, cDNA synthesis reaction was performed. This was done by using a commercially available kit for cDNA synthesis (Affinity Script Multiple Temperature cDNA synthesis kit, Agilent Technologies) in the following way:

Total RNA used.....1.5µL (This volume corresponded to 1µg of total RNA)

Ribonuclease free water.....to total volume of 15.7µL

Oligo(dT) primers.....1µL (This volume corresponded to 0.5µg of primers)

The reaction mixture was mixed gently with the help of pipette and incubated at 65°C for 5 minutes. After this, the reaction mixture was kept at room temperature for 15 minutes to allow the primers to anneal. Next, the following were added to the reaction mixture to the final volume of 20µL:

2.0 µl of 10× AffinityScript RT Buffer

0.8 µl of dNTP mix (25mM each dNTP, hence final concentration of 0.25mM each dNTP)

0.5 µl of RNase Block Ribonuclease Inhibitor (40 U/µl)

1 µl of AffinityScript Multiple Temperature RT

The reaction mixture was next incubated at 42°C for 5 minutes followed by incubation at 55°C for 1 hour. Finally, the reaction tube was incubated at 70°C for 15 minutes.

### 2.1.17 DNA quantification

The DNA was quantified using spectrophotometric method. First of all, 500µL of distilled water was taken in a cuvette and placed in the spectrophotometer. The wavelength was adjusted to 260 and the water was used to blank the spectrophotometer. Next, 10µL of DNA was diluted in 490µL of distilled water in a cuvette and its absorbance was measured at A260nm. Each reading was taken 3 times and their means calculated. The DNA was quantified by the following formula:

$$A_{260} \times \text{Dilution factor (50)} \times 50 = x\ \mu g\ /mL$$

To determine the purity of DNA, a ratio of the Absorbance at 260 and 280 ($A_{260}/A_{280}$) was calculated after diluting DNA in 10mM Tris·Cl, pH 7.5. An absorbance ratio of around 2 was considered to indicate good quality DNA. For data obtained for DNA extracted from buccal swabs, see Appendix-I, section A1.1.2.

## 2.2 Mammalian tissue culture:

### 2.2.1 Cell lines:

Table 5: The type of cell lines used, their source and the media.

| **Cell line** | **Type** | **Source** | **Nature** | **Media** (Invitrogen) |
|---|---|---|---|---|
| HaCat | Immortalized keratinocytes | Human | Normal | DMEM |
| MCF10A | Breast Epithelial cell line | Human | Normal | DMEM |
| MCF7 | Breast epithelial cell line | Human | Breast cancer | DMEM |
| MDAMB-231 | Breast epithelial cell line | Human | Breast cancer | DMEM/F12 (1:1) |

For all the cell lines listed, the media was supplemented with filter sterilized 10% foetal bovine serum (FBS), 2mM glutamine, 1mM sodium pyruvate, 100µg/mL streptomycin and 100U/mL penicillin all purchased from Invitrogen UK. Cells were maintained at 37% in a tissue culture incubator with an atmosphere containing 5% $CO_2$.

### 2.2.2 Sub-culturing the Human cells

Sub-culturing of human cells used in this study was performed regularly to ensure their survival, regular supply for the study and maintain proper growth conditions.

Sub-culturing was routinely done with cells that reached 80-90% confluence either in flask or tissue culture plates. All the procedure was done using sterile techniques performed in a sterile tissue culture hood. The text below describes the sub-culturing procedure followed for cells grown in 250-300mL flask (T75) in the following manner:

The media, buffers and trypsin were placed in water bath at 37°C at least 30 min prior to sub-culturing the cells. Tissue culture lab coat and gloves were worn. The gloves were sprayed with 70% ethanol. The laminar flow in the hood was turned and the working surface of tissue culture hood was swabbed with 70% ethanol. Any apparatus, media, trypsin and buffers taken inside the hood was first swabbed by 70% ethanol except for tissue culture flasks and plates. The tissue culture flask needed to be sub-cultured (>80% cell confluence) was taken out of incubator, observed under microscope and placed into the hood. With the help of aspirator attached to the suction pump, the old medium was removed from flask. 4mL of PBS (Invitrogen) was added to the cells and the flask gently swirled to wash away the old media and dead cells. PBS was aspirated out. 1mL of pre-warmed 0.25% trypsin (Invitrogen) was gently added on top of cells with the help of serological pipette, and the flask swirled to ensure spreading of trypsin on the entire surface area of flask. The flask was taken into tissue culture incubator maintained at $37^{o}$C with 5% $CO_2$ atmosphere and incubated for 5 min (or until the cells were detached as observed under light microscope). After the cells detached, 4mL of pre-warmed cell culture media (Table 5) was added to the flask to stop further action of trypsin and dilute the cells. With the help of serological pipette, the cell suspension was mixed thoroughly by pipetting up and down to ensure total detachment and to break any cell clumps formed. After this, the number of cells in the suspension was determined (2.2.3) and either seeded into other flasks for propagation and cell culture maintenance, or cryo-frozen for future use (2.2.4). For seeding the cells for different experiments, in other flasks and plates, specific number of cells was used as listed in Table 6.

Table 6: The type of tissue culture flasks and plates employed, specific to experimental type with the number of cells seeded and amount of growth media used in the current research study.

| Flasks or plates | Number of cells seeded | Growth media (mL) | Experiment type |
|---|---|---|---|
| 96-well | $2.5 \times 10^3$ | 0.2 | Cytotoxicity assays (NR uptake) and ELISA |
| 24-well | $5 \times 10^4$ | 0.5 | Promoter transfection for luciferase assay |
| 12-well | $1 \times 10^5$ | 1 | Immunofluorescence studies: For drug treatments of cells grown on Poly-L lysine coated coverslips |
| 60mm | $8 \times 10^5$ | 3 | For liposome mediated cell transfections. |
| 100mm | $2 \times 10^6$ | 10 | Electroporation, Western blotting by harvesting protein lysates of cells treated with different drugs. |
| $25cm^2$ flask | $7 \times 10^5$ | 5 | For cell propagation and maintenance |
| 75 $cm^2$ flask | $2 \times 10^6$ | 12 | For cell propagation, maintenance and freeze storage for future use. |

### 2.2.3 Cell counting

In the current study, human cells were routinely counted for different experiments via counting chamber method. In this method, first of all, the counting chamber and the cover-slip used were cleaned with the help of lens paper and put under light microscope. The cover-slip was placed on top of the gridded area. The grid in the counting chamber was composed of squares of different areas. The cells to be counted were first trypsinized and then diluted in cell culture media (section, 2.2.2).

With the help of micro-pipette, 50µL of cell suspension was taken from the flask and put underneath the cover-slip over the counting chamber where the cell suspension spreads quickly. The cells were counted in ten 0.04mm$^2$ squares in the grid. Then, the number of cells per µL was calculated with the following formula:

Number of cells counted in ten 0.04 mm$^2$ squares = 50 cells (supposed)

Total area in which 50 cells counted = (10 x 0.04) = 0.4 mm$^2$

Total volume = 0.4 mm$^2$ x 0.1 (height of chamber) = 0.04mm$^3$

So, 50 cells in 0.04mm$^3$.

*1 mm$^3$ = 1µL*, hence, .04 mm$^3$ = 0.04µL

If 0.04µL has 50 cells, 1µL has = 50 x 1µL ÷ 0.04µL = 1250 cells.

Hence, 1µL has 1250 cells.

### 2.2.4 Cryofreezing surplus cells and reviving frozen cells

Surplus cells were routinely cryo-frozen for future use. After the cell were trypsinized from a T75 flask (section 2.2.2**)**, 5ml of cell media was added to stop the action of trypsin, and the cell suspension was mixed thoroughly with the help of serological pipette attached to the pipette buoy. The cell suspension was transferred to sterile 15ml centrifuge tube, capped tightly and taken to the centrifuge machine set at 37°C. The cell suspension was centrifuged at 1000rpm for 15 minutes to palette the cells. In the meantime, sterile cryotubes (Thermoscientific) were labelled with cell details and passage number. After centrifugation, the tube was taken back to the hood, supernatant was discarded and the cell palette was gently resuspended in 1ml of freezing media (Appendix-II, A2.22).

The cell suspension in freezing media was carefully transferred to cryotubes, capped properly and immediately taken for storage in -80°C freezer.

When previously frozen cells were needed, the media was first warmed in the water bath at 37°C. 10ml of media was transferred to T75 flask. The cryotube with frozen cells was taken out and immediately put in the water bath at 37°C. As soon as the frozen mixture was thawed (usually after 2min), the cryotube was taken to the tissue culture hood, and with the help of pipette, very gently transferred into the T75 flask with the media. After 16-24 hours, old media was replaced by new media to replenish the nutrients and boost cell growth.

After every 3-4 days, cell media was usually changed by first aspirating the old media, washing the cells with warm PBS, and transferring fresh media into the flask.

### 2.2.5 Cell treatments with drugs

The drugs used in the current research work involved DNA damaging agents, ATM kinase inhibitor and protein synthesis inhibitor. Stock solutions of these drugs were made and stored as instructed by their manufacturers (Appendix-II, A2.27). Working concentrations were achieved by diluting the stock in the media used and were based on prior literature. Table 7 shows the drugs used, their storage and working concentrations and their manufacturers.

Table 7**:** Drugs used in the study, their storage conditions, concentration and their manufacturers.

| **Drug** | **Agent** | **Storage stock** | **Treatment concentration** | **Manufacturer** |
|---|---|---|---|---|
| Doxorubicin | DNA damaging agent | 1mM made with water, stored at 4C° protected from light | 0.1nM to7μM | Sigma-Aldrich |
| Cisplatin | DNA damaging agent | 1mM made with water, stored at 4C° protected from light | 4.8μM | Sigma-Aldrich |
| Hydroxyurea | DNA damaging agent | 1M made with water, stored at 4C° | 1mM | Sigma-Aldrich |
| Bleomycin | DNA damaging agent | 1M made with water, stored at 4C° | 5μM | Sigma-Aldrich |
| KU55933 | ATM kinase inhibitor | 10mM made with DMSO, stored at -20C protected from light | 10μM | Calbiochem |
| Cycloheximide | Protein synthesis inhibitor | 50mM made with water, stored 4°C protected from light. | 50μM | Sigma-Aldrich |

Prior to treatment with these drugs, cells to be treated were taken out of the incubator, old media removed and pre-warmed PBS added. Pre-warmed media was then transferred to falcon tubes (BD bioscience) in the tissue culture hood and the required amount of drug was added to achieve the working concentrations as set out in table 7. The PBS over the cells was taken out and the media with the drug carefully added. The amount of media added was dependent upon the type of tissue culture vial in which the cells were grown (Table 6).

### 2.2.6 Human cell transfection

Human cell transfections were carried out either by liposome mediated gene transfer via the use of commercially available transfection reagent (DNAfectin 2100, NBS biological), or by the use of electroporator (EasyJect, UK). Apart from transfections aimed at performing Dual-Luciferase based promoter assay, all the other transfections were performed on the cells first seeded on poly-L lysine coated coverslips which were placed in the tissue culture dishes. The number of cover-slips placed in the tissue culture dish depended upon the number and type of subsequent drug treatments. The methodologies of both of these techniques are described below.

#### 2.2.6.1 Lipofection

Lipofection was typically carried out in 60mm plate format, apart from experiments involving Dual Luciferase assay, where 24-well plates were used (for transfection details of Dual luciferase assay in 24-well plates, see section 2.3.9). 16-24 hours prior to transfection, cells were seeded at a density of $8 \times 10^5$ in normal cell culture media (section 2.2.1). Usually four cover-slips per 60mm dish were placed. Next day, the dishes were taken out (with 70-90% confluent cells) and put in the tissue culture hood and old media was removed. Cells were washed once with warm PBS and 3mL of pre-warmed serum free and antibiotic free media (Opti-MEM®, Invitrogen) was added per plate and put back in the incubator. Next was to prepare the transfection complexes for subsequent transfection in the following way:

i) 5µg DNA was diluted in 500µL serum and antibiotic free media in an eppendorf tube labelled tube A.

ii) 5µL transfection reagent was slowly added to 500µL of serum and antibiotic free media in another eppendorf tube labelled tube B.

iii) Both tubes were allowed to stand for 5 min.

iv) The contents of tube A were gently mixed with the contents of tube B in another eppendorf tube labelled tube C.

v) Tube C was incubated at room temperature (inside tissue culture hood) for 30 min to form the complex.

vi) 2.4mL of serum free and antibiotic free media was added to a 15mL falcon tube, and the contents of tube C were gently introduced in it. The total volume in this falcon tube now was 3.4mL and was called the transfection media.

vii) The cells to be transfected were taken out of tissue culture hood, old (serum free, antibiotic free) media was aspirated and the 3.4mL of transfection media was added on top of these cells gently.

viii) The plate was placed back in the tissue culture hood and allowed to incubate for 5 hr.

ix) After 5 hr, the transfection media was removed and pre-warmed normal cell culture media was added to the cells. Cells were allowed to grow for 16-24 hours. For transfections involving YFP-ATM or YFP-$ATM_{mut}$, cells were allowed to grow for 48 hours before further studies.

### 2.2.6.2 Electroporation

To perform transfections via electroporation, the electroporation parameters were first optimized to achieve optimum transfection in difficult to transfect, HaCat cell line. The data for determining optimum electroporation parameters is given in Appendix-I, section A1.5. For transfection of cells via Electroporation, 16-24 hr prior to transfection, 2 x $10^6$ cells were seeded in 100mm tissue culture plate. Next day, the tissue culture plate was taken out of incubator (cells around 70-90% confluent), and old media aspirated. Cells were washed once with warm PBS and 1mL of pre-warmed 0.25% trypsin was added and plate incubated for 5 min (or until the cells detached) in the tissue culture incubator. After this, 5mL of pre-warmed cell culture media was added to trypsinized cells to stop the action of trypsin. Cells were pipetted up and down few times and the cell suspension was transferred to sterile 15mL centrifuge tube and capped tightly. The tube with cell suspension was taken out of the tissue culture hood and centrifuged at 1000rpm, 37°C for 10 min. After that, tube was taken out and placed back in tissue culture hood, supernatant discarded and cell palette gently resuspended in 2mL serum free and antibiotic free media (opti-MEM®, Invitrogen). Cells were centrifuged again as described above, supernatant discarded and cell palette resuspended again in 2mL of opti-MEM®. Centrifugation step was performed again and finally the cell palette was resuspended in 0.5mL of opti-MEM®. At this point, the cells were counted with the help of counting chamber (section 2.2.3) and suspension containing 2 x $10^6$ cells was transferred to another eppendorf tube. In this tube, opti-MEM® was added to the final volume of 0.5mL. Next, sterile 4mm electroporation cuvettes (molecular bioproducts) were taken and 0.5mL of cell suspension (2 x $10^6$ cells) was transferred into it.

10µg of DNA to be transfected was directly added to the electroporation cuvette and gently mixed with the help of micropipette. The cuvettes were capped tightly and placed in the electroporator (Easyject, Equibio, UK).

The electroporation program was set at 400V, 125µF and the cells were given the electric pulse. The electroporated cells were immediately taken back to the tissue culture hood and with the help of micropipette, added on top of poly-L lysine coated coverslips placed in a new 100mm tissue culture dish. A total of 10 coverslips were usually placed per 100mm dish. Finally, 9.5mL of pre-warmed cell culture media was introduced in the tissue culture plate and the cells allowed to grow for 16-24 hours. For transfections involving YFP-ATM or YFP-$ATM_{mut}$, cells were allowed to grow for 48 hours before further studies.

## 2.3 Biochemistry

### 2.3.1 Antibodies and the detection systems used in the study:

The different primary antibodies employed in the current study are listed in table 8 below.

Table 8: Primary antibodies used in the study.

| **Antibody** | **Isotype** | **Catalogue number** | **Company** |
|---|---|---|---|
| ATM | Rabbit | Ab17993 | Abcam |
| pATM S-1981 | Rabbit | Ab81292 | Abcam |
| P53 | Mouse | Ab26 | Abcam |
| pP53 S-15 | Mouse | 9947 | Cell signaling |
| pATR | Rabbit | 9947 | Cell signaling |
| Chk2 | Rabbit | 8108 | Abcam |
| pChk2 T-68 | Rabbit | 9947 | Cell signaling |
| E2F1 | Mouse | Ab103 | Abcam |
| pE2F1 S-31 | Rabbit | - | Agilent technology |
| γH2AX | Rabbit | 9947 | Cell signaling |
| Rb (Rb1 1f8) | Mouse | 24 | Abcam |
| Actin | Rabbit | 1801 | Abcam |
| GFP | Rabbit | 290 | Abcam |

To study different DDR and cell cycle proteins listed in table 8, this research employed different biochemical detection systems as a requirement of the employed biochemical techniques. Table 9 provides the list based on different secondary antibody detection systems used, its dilution, the name of the technique employed, and the manufacturer.

Table 9: The different secondary antibody detection systems employed in the study

| **Biochemical technique** | **Secondary antibody used** | **Dilution** | **Detection method** | **Company** |
|---|---|---|---|---|
| Western blotting | Biotin-conjugated | 1 in 2000 | Streptavidin based fluorescence detection | Invitrogen |
| ELISA | HRP conjugated | 1 in1000 | Amplex® Red fluorescence detection | Invitrogen |
| Immunofluorescence | Fluorophore conjugated | 1 in 500 | Fluorescence microscopy | Invitrogen |

### 2.3.2 Protein extraction

For Western blot analysis of different proteins, total protein content was extracted from cells grown in 100mm tissue culture plates at 90% confluency ($1 \times 10^7$ cells) during treatment and protein extraction. The entire extraction process was done on ice as much as possible and cells were never allowed to dry.

Tissue culture plates with cells were taken out of tissue culture incubator and placed on ice. The old media was discarded from the plates and cells were washed three times with 5mL of ice cold PBS. After the third wash, 495µL of ice cold PBS was taken in an eppendorf tube, and 5µL of 100x protease and phosphatase inhibitor cocktail (Pierce Biotechnology) added to it and mixed. The PBS with the inhibitors added was transferred to the tissue culture plate.

With the help of a tissue culture cell scraper, cell monolayer was scrapped off by gently tilting the plate, and scrapping off cells to the bottom. The complete monolayer was scrapped off to produce a cell suspension. This suspension was transferred to a pre-chilled eppendorf tube and centrifuged at 800rpm for 5 min at 4°C to collect the cells in the palette. In the meantime, 1mL of RIPA lysis and extraction buffer (Thermo Scientific, UK) was taken in another tube and 10µL of the protease and phosphatase inhibitor cocktail (Pierce Biotechnology) was added into it and placed on ice. After the centrifugation step, the tube with the cell palette and a supernatant was taken out and its supernatant discarded. The cell palette was then resuspended in 200µL of RIPA lysis buffer (now with inhibitors added) and thoroughly mixed with the help of micropipette. The cell lysate was also subjected vortex for 3 min, followed by centrifugation at 10,000 rpm for 15 min at 4°C. After centrifugation, the cell lysate was placed back on ice, and 150µL of supernatant (extracted protein) was transferred into a pre-chilled and labelled eppendorf tubes. This protein lysate was either further processed or quantified or stored in -80°C for future use.

### 2.3.3 Preparation of cytoplasmic and nuclear fractions

To prepare nuclear and cytoplasmic fractions, cells were first lysed in ice-cold hypotonic buffer (Appendix-II, A2.23), centrifuged and the resulting supernatant (cytosolic fraction) was immediately analyzed or stored at -80°C until use.

To obtain nuclear fractions, the pellet was briefly washed thrice in ice-cold hypotonic buffer (Appendix-II, A2.23), followed by incubation in hypertonic buffer (Appendix-II, A2.24) for 30 min at 4°C, and centrifugation (13,000 x g, 5 min, 4°C). The supernatant (nuclear fraction) was immediately analyzed or stored at -80°C until use.

Subsequently all protein extracts were quantified using the Bradford reagent (Sigma-Aldrich, UK) against BSA as a standard. For verification of the sub-cellular fractions, Immunoblotting was performed using antibodies against nuclear and cytoplasmic marker proteins (Appendix-I, A1.8).

### 2.3.4 Quantification of extracted protein

Protein quantification of the extracted proteins was performed with the help of Bradford assay by using Bradford assay reagent (Pierce Biotechnology) in 96 well-plate format. Before performing the assay for the extracted protein lysates, a standard curve was established with a protein with known concentration (Appendix-I, A1.7).

The protein lysates prepared were taken out of -80°C freezer and allowed to thaw on ice. The tubes were centrifuged at 10,000rpm for 5min at 4°C. In the meantime, the working stock of Bradford reagent (Sigma-Aldrich, UK) was prepared by mixing 1 part in 4 parts of distilled water. After the centrifugation step, 20µL of each protein was transferred in triplicates to each well of the 96-well plate and mixed with 180µL of the Bradford reagent per protein sample. The protein lysate and the Bradford reagent mix was allowed to incubate at room temperature for 5-10 min. Next, the 96-well plate was placed in a spectrophotometer (Thermospectronic, USA) and its reading at 595nm was recorded. Mean of the readings from three wells for each protein sample were taken and quantified by plotting it on the standard curve obtained by performing Bradford assay with a known standard protein (Appendix-I, Fig. A1.19).

Once the concentration of each protein sample was determined, they were all mixed with SDS protein sample buffer (Nupage® LDS sample buffer, Invitrogen) to the final concentration of 1mg/mL. Sample reducing agent (Nupage®Sample reducing agent, Invitrogen, UK) was added to 1x to the protein lysate and stored at -20°C until further use (section 2.3.5).

### 2.3.5 Processing of proteins for Immunoblotting

The quantified proteins (1mg/mL) mixed and stored in SDS-sample buffer were taken out of -20°C freezer and allowed to thaw at room temperature. The samples were then placed on a thermo mixer, heated for 15min at 95°C while shaking. After heating the samples, they were centrifuged at 15000rpm for 15min. 20µL (20µg) of the supernatant of the centrifuged samples were usually loaded (unless otherwise stated) in the SDS-PAGE gels (Novex® Nupage, Invitrogen) for further analysis. Any new protein samples processed for western blot were first run on SDS-PAGE gel and stained with coomassie blue protein stain for the detection of DNA contamination before carrying out western blotting (Data not shown). If the protein samples were found to have DNA contamination, an additional protein sonication step (2 cycles for 10 seconds at 50% pulse) was performed before heating the samples.

### 2.3.6 Immunoblotting

Proteins processed for immunoblotting were first subjected to SDS-PAGE by running the samples on precast gels (Novex® Nupage, Invitrogen) using commercially available SDS-PAGE apparatus (XCell SureLock Mini-Cell system, Invitrogen, UK), transferring them to nitrocellular membrane (Bio-Rad Hybond ECL, UK) and processing and visualizing proteins by fluorescence based detection system (WesternDot™ 625 Western detection kit, Invitrogen UK).

For the blotting of ATM, pATM S 1981 and pATR S 428, 4-12% gradient, pre-cast gels were used while for all the other proteins, 12% gels were used. Also, unless otherwise stated in figure legends, 20µg of protein was loaded per well of these gels. Since the fluorescence based WesternDot™ 625 Western detection system was introduced for the first time in my lab, before proceeding with immunoblotting using this system, it was imperative to first optimize different conditions using this method. The process optimization data is provided in Appendix-I, section A1.4.

Two pre-cast gels (Novex® Nupage, Invitrogen) were used within the SDS-PAGE apparatus (Novex® Nupage, Invitrogen). The gel apparatus was assembled and two pre-cast gels were installed. The inserted comb plates in the gels were carefully removed and the wells gently washed with distilled water. SDS-PAGE running buffer (Appendix-II, A2.12) was poured in the inner chamber until the wells were submerged and in the outer chamber until the whole base was submerged. In the first well of each gel, 15µL of pre-stained protein standard (Invitrogen) was loaded followed by loading the samples. The lid of the gel apparatus was fitted at its position and the cables were connected to the power pack. Gels were run at 150V for 1 hr or until the dye in the protein standard and samples, providing a measure of migration, reached the bottom of gel. After the run was complete, the lid of the gel tank was taken off, and the gel plates carefully taken out. The gel was very carefully taken out of the plates and immediately put in the gel trays and given a wash in the transfer buffer (Appendix-II, A2.13) to remove SDS and excess buffer. While the gels still in transfer buffer, sponge pads and filter papers of the right size were soaked in transfer buffer and placed in the protein blotting apparatus (XCell SureLock Mini-Cell system, Invitrogen, UK).

The gel was next taken out of the gel tray and very carefully placed in the blotting apparatus over two sponge pads and two layers of filter paper. Nitrocellulose membrane (Bio-Rad Hybond ECL, UK) was next cut out at exactly the size of the gel and filter papers, soaked in transfer buffer and placed carefully on top the gel. Two layers of filter papers were again placed on top of the nitrocellulose membrane followed by placing two sponge pads. Next, the western blot protein transfer module (XCell SureLock Mini-Cell system, Invitrogen, UK) was assembled by sandwiching the gel and nitrocellulose membrane in the transfer apparatus and placing it in the gel tank. In the whole assembly process, care was taken not to allow any air bubble formation. The inner chamber with the gel and nitrocellulose membrane was filled completely with transfer buffer, while the outer chamber was partially filled. The lid was placed tightly over the gel tank, the cables connected to the power pack and the proteins transferred at 50V for 1.5 hr.

After the transfer was completed, the protein transfer module was disassembled and the nitrocellulose membrane transferred to the gel tray with the help of forceps. The nitrocellulose membrane was washed gently with distilled water to wash away transfer buffer and any gel residues. The membrane was examined visually for proper transfer of proteins by looking at the transfer efficiency of pre-stained protein standard. To better examine the transfer efficiency and band separation, the nitrocellulose membrane was also stained with Ponceau stain (Ponceau S solution, Sigma-Aldrich UK).

Next, to prevent non-specific reactivity, the membrane was blocked with BSA based blocking buffer (Appendix-II, A2.15) for 2 hr at room temperature with mild shaking. In the meanwhile, primary antibodies were diluted in antibody blocking buffer according to manufacturer's instructions, typically at 1 in 1000 dilution in 8mL of blocking buffer.

The blocking buffer was discarded off the membrane and primary antibody was added. Primary antibody incubation was performed at 4°C overnight with gentle shaking. Next morning, the membrane was further incubated for 1 hr with primary antibody at room temperature.

The membrane was washed three times with washing buffer (Appendix-II, A2.14), each wash for 5 min with gentle shaking. In the last washing step, 1 in 2000 dilution of Biotin-conjugated anti mouse or anti goat secondary antibody (WesternDot™ 625 Western detection kit, Invitrogen UK) was made in washing buffer. The washing buffer in the last washing step was discarded from the membrane and the diluted biotin-conjugated secondary antibody was added. The membrane was incubated for 2 hr at room temperature with mild shaking. After incubation with secondary antibody, the membrane was washed three times with washing buffer for 5 min each with gentle shaking. In the last washing step, streptavidin reagent (WesternDot™ 625 Western detection kit, Invitrogen UK) was taken out of fridge and diluted in 8mL of blocking buffer at 1 in 2000 dilution. The washing buffer was discarded and streptavidin solution added to the membrane. The membrane was incubated for 1 hr at room temperature. After incubation with streptavidin, the membrane was gently washed once with distilled water and taken straightaway to the gel documentation machine for the visualization of bands. Alphaimager® software was used to capture the images with the attached camera. The images were saved in TIFF file format for later analysis typically involving the calculation of relative abundance via Integrated optical densitometry analysis (section, 2.4.2) of each protein in different conditions relative to that in the untreated state.

To establish a loading control, the same blot was stripped off from previous antibodies by incubating the membrane with stripping buffer (Appendix-II, A2.28) for one hour and reprobing with b-Actin antibody.

### 2.3.7 Cell survival assay by Neutral red uptake

Cell cytotoxicity assays were performed after different treatments to measure the degree of cell survival via Neutral red uptake assay (Repetto G et al., 2008). This assay required the preparation of NR medium and NR desorb reagent which are described in Appendix-II, sections A2.25 & A2.26, followed by spectrophotometry at 540± 10nm.

This assay was performed in 96 well plates. Cells were first seeded at a density of 2.5 x $10^3$ and allowed to grow for 24 hr. Some wells were left without cells as negative controls. After incubation, cells were either left untreated or treated with different agents for a set period of time as described in respective figure legends. Each treatment was done in quadruplets. After the treatments were completed, the plate was paced in the tissue culture incubator, and each well washed three times with 250 µL of warm PBS. Next, 250µL of NR-medium (Appendix-II, A2.25) was added per well and the plate was incubated in tissue culture incubator for 5 hr. During this period, all the viable and healthy cells take up the NR dye leaving the dead or dying cells unstained. After incubation, the plate was taken out to the lab bench, the NR medium was removed, and the cells were washed three times with 250µL of PBS. After the final wash, the plate was inverted on paper towel to remove all traces of PBS. Next, 100 mL of NR desorb reagent was added to the cells per well, the plate was taken to the dark room, and shaken for 30 min at 50rpm followed by keeping the plate still for 5 min.

The plate was taken to the 96-well plate reader (Modulus Template, Turner biosystem) and its absorption was measured at 540nm. The means of the values acquired from the quadruplets of each treatment were recorded. All the mean values were normalized to the mean value of untreated cells and expressed as % cell death using the following formula:

$$100 - \left\{ \frac{Abs_{540} \text{ of treated sample}}{Abs_{540} \text{ of Untreated sample}} \right\} x\ 100$$

### 2.3.8 Enzyme-Linked ImmunoSorbent Assay (ELISA)

ELISA was performed in 96-well plates using Amplex® Red detection system (Invitrogen, UK) for the analysis of DDR and cell cycle protein after different drug treatments. Cells were seeded at a density of 2.5 x $10^3$ and allowed to grow for 24 hr. Some wells were left without cells as negative controls. After that, cells were either left without treatment to provide untreated controls or treated with different agents for a set period of time as described in respective figure legends. Each treatment was done in quadruplets. After the treatments were completed, plates were taken out of the incubator. Old media was aspirated out and cells were washed with 250µL of PBS three times. Cell fixation was carried out by incubating cells with 150µL of 3% PFA (Appendix-II, A2.3) for 30 min. PFA was taken out and cells were washed again three times with 250µl of ice cold PBS.

Next, cells were permeabilized by adding 150µL of permeabilization buffer (Appendix-II, A2.5) for 10min, washed thrice with 250µL ice cold PBS, and quenched with 150µL of quenching buffer (Appendix-II, A2.6) for 5 min. After quenching, the quenching buffer was aspirated, cells washed thrice with ice cold PBS, and blocked with 250µL of blocking buffer (Appendix-II, A2.7) for 1 hr. In the meantime, the primary antibodies used for ELISA were diluted 1 in 500 in ELISA blocking buffer. After blocking, the blocking buffer was aspirated out and 100µL of diluted primary antibody was added in each well. In some wells, only blocking buffer was added as no primary controls. After 2 hr of incubation at room temperature, the primary antibody was taken out and wells were washed thrice with 250µL of ELISA washing buffer (Appendix-II, A2.16).

The type of secondary antibody employed for ELISA was horseradish peroxidise conjugated secondary antibody diluted 1 in 1000 in washing buffer. 100µL of this antibody was added in each well including in the no primary control wells and plate incubated for 2 hr. In the meanwhile, Amplex® Red reagent was made (Appendix-II, A2.29) and 100µL of that was added in each well for 30 min in dark. The plate was placed in the 96-well plate fluorescence reader (Modulus template®, Turner Biosystem) and fluorescence intensities in each well were measured using excitation/emission of 570/585 nm. These fluorescence intensities indicated the relative abundance of each protein after a given treatment. The means of the fluorescence values acquired from the quadruplets of each treatment were taken, with each experiment performed on three independent occasions. The mean values were normalized to the mean value of untreated control for that protein and expressed as 1.

### *2.3.9 Dual Luciferase reporter based ATM promoter assay.*

The Dual Luciferase reporter assay (Promega) provides for a quantitative basis of gene expression from potential promoter sequences. It is based on luciferase activity measured from two different sources of Luciferase. One is the firefly (*Photinus pyralis*) luciferase whose gene is driven by the test sequence, and the other is renilla (*Renilla reniformis*) luciferase (pRL-CMV), which is transfected simultaneously and provides for estimation of transfection efficiency. The signal output from the dual luciferase reporters can be distinguished as they have different enzyme structures and substrate requirements.

The luciferase reporter assay works on the following principle: The test sequence, whose transcriptional potential is required to be quantified, is cloned upstream of the Luc gene, which codes for enzyme Luciferase in a vector called PGL3-basic (Promega). The Luc gene is otherwise promoter-less in PGL3-basic vector and hence does not express. If the test sequence has transcriptional potential, it will drive the Luc gene expression and code for luciferase enzyme. The amount of luciferase enzyme expressed, which is indicative of the signal or strength from the upstream test promoter, is measured by adding its substrate Luciferin, whose product emits light which is captured and quantified.

This mechanism establishes a means by which the promoter signal is measured and compared between different experimental conditions.

The light measurement emitted is then normalized to that of Renilla luciferase to account for differences in transfection efficiencies. The luciferase reaction is given in the following equation:

$$Luciferin + O_2 + ATP \rightarrow Oxyluciferin + CO_2 + AMP + ppi + LIGHT$$

For the generation of this assay, ATM promoter sequence was first isolated from whole human genome by PCR amplification using primers specific to ATM promoter region, which also incorporated specific restriction sites for clonal manipulation (for cloning data of ATM promoter including primer sequences and PCR conditions, see Appendix-I, A1.1). This sequence was then cloned into a luciferase reporter vector, PGL3 basic (Promega) to create luciferase reporter gene under the control of ATM promoter (ATMpr/PGL3), (Full details in materials and methods and Appendix-I). The creation and working principle of ATMpr/PGL3 based ATM promoter assay is demonstrated in Fig. 2.1.

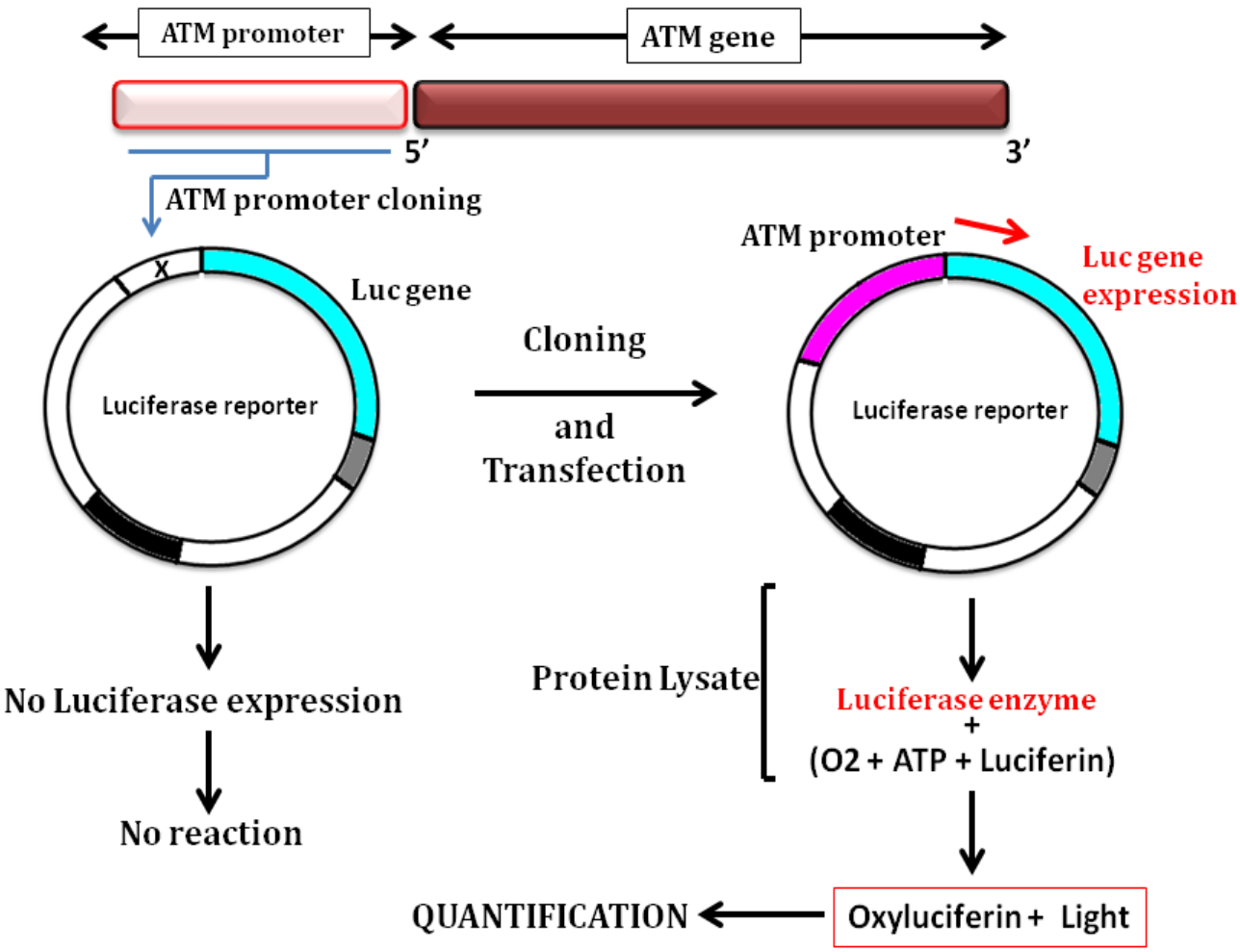


**Figure 2.1: The working principle of Luciferase reporter based ATM promoter assay.** The ATM promoter sequence was cloned upstream of Luc gene (Appendix-I), within PGL3-basic vector (promega), which is otherwise promoterless and does not express. After sequence confirmation, the promoter construct was transfected into human cells where the promoter drove the expression of Luc gene into Luciferase enzyme, whose degree of expression was dependent upon the strength of promoter under test conditions. The expression level of luciferase enzyme was quantified by adding its substrate whose product emitted luminescence which was measured. The measure of luminescence under different test conditions provided quantitative estimations of promoter activity in that condition.

To perform Dual-Luciferase based ATM promoter assay, the ATM promoter region (Bryde PJ et al., 1996) was first amplified from the human genomic DNA using promoter specific primers, cloned into the luciferase reporter vector, PGL-3 basic, and transfected into human epithelial cell line, MCF10A (For all the data of ATM promoter cloning, see Appendix-I, section A1.1). Transfection of the ATM promoter reporter vector was carried out using Lipofection (DNAfectin, NBs Biologicals, UK) and the vector pRL-CMV was used as an internal control for transfection efficiency. Each transfection for a particular experiment was performed in triplicates. Lipofection was carried out in 24-well format by first seeding the cells at a density of 5 x $10^4$ 24 hr prior to transfection. At the time of transfection, the cells were 70-90% confluent.

Old media was removed and cells were gently rinsed with 1mL of pre-warmed PBS. 0.5mL of serum free and antibiotic free media (Opti-MEM®, Invitrogen, UK) was added per well and plate placed back in the incubator. For transfection, the DNA to be transfected i.e. ATMpr/PGL3, the empty PGL3 basic vector and the internal control vector (pRL-CMV) and the transfection reagent (DNAfectin, NBs Biologicals, UK) were taken out and placed in the hood. For each well, 0.5µg of DNA to be transfected (either ATMpr/PGL3 or empty PGL3 basic vector) and 0.1µg of pRL-CMV were mixed together with 25µL of serum free and antibiotic free media Opti-MEM®. Next, 1µL of the transfection reagent was mixed with 25µL of Opti-MEM® in a separate eppendorf tube. The tubes were incubated for 5 min and their contents mixed together and further incubated for 20 min to allow the DNA complex to form.

After the incubation, 0.4mL of Opti-MEM® was added to the tube containing the DNA complex and gently mixed together. The contents of this tube were added in each well and the plate incubated for 5 hours for transfection to take place. After incubation, the old media was removed and 0.5mL of pre-warmed cell culture media was added and plates incubated for at least 16 hr before further experiments and analysis.

After 16-24 hr of transfection, the old media was discarded, cells rinsed once with pre-warmed PBS and treatments with the required drug solutions in media (Table 7) performed. On the day of performing the luciferase assay, 1x passive cell lysis buffer (Dual Luciferase assay kit, Promega, UK) was prepared (Appendix-II, A2.10). The 24-well plate was taken out of incubator, old media discarded, each well gently rinsed with 0.5mL of PBS, and 125µL of the 1x passive lysis buffer added in each well. The plates were placed on shaker and gently rocked (50rpm) for 30 min to form the cellular protein lysates. In the meantime, the Luciferase assay reagent (LAR-II, Promega) was reconstituted (Appendix-II, A2.9) and by means of multi channel pipette for faster and accurate pipetting, 50µL of this reconstituted reagent was added per well of black bottom, opaque 96-well plate (Sigma-Aldrich). The LAR-II reagent provided substrate of luciferase activity generating a stabilized luminescent signal with the addition of the cell lysate.

Next, 20 µL of the cell lysates from each transfection (done in triplicates) were transferred (in quadruplets) to each well of the 96-well plate with the added LAR-II reagent with the help of multi-channel pipette. Hence, four independent readings were taken in 96-well plate for each transfection done in triplicates. After the addition of cell lysate, the plate was immediately placed in the 96-well Luminometer (Modulus template® Turner biosystems) for measuring the luminescence.

Dual luciferase assay program was set up with 2 second of pre-measurement delay followed by measuring luminescence via the in-built luminescence filter at 0.5 second measurement period per well. After the reading, plate was taken out and 50µL of the reconstituted Stop and Glo® (Appendix-II, A2.11) was added per well using multi channel pipette. The addition of the second reagent stopped the luminescence generated by Firefly luciferase (sourced from ATMpr/PGL3) and provided substrate for Renilla luciferase (sourced from pRL-CMV). The plate was returned to the luminometer and another reading was taken as above. The first reading (After LAR-II addition) was normalized to the second reading (after Stop and Glo® addition). The means of the luminescence signals acquired from the quadruplet treatments were taken, with each transfection done in triplicates. The mean values were normalized to the mean value of untreated controls for that experiment and expressed as 1.

### 2.3.10 Immunocytochemistry

Immunostaining of protein of interest was performed on both un-transfected as well as transfected cells expressing a fluorescently tagged gene of interest. In this procedure, cells were seeded (Table 6) on Poly-L lysine coated cover-slips (Appendix-II, A2.2) placed in 12-well tissue culture plates and grown until at 70-90% confluency.

If immunostaining was performed on cells to be transfected as well, cells were first seeded on Poly-L lysine coated cover-slips placed in 60mm tissue culture plates (Table 6), grown until 70-90% confluency, transfected and then individual cover-slips with the transfected cells transferred each to 12-well plates for subsequent treatments.

After the respective experimental treatments were performed on cover-slips placed in 12-well plate, old media was removed and cells were gently rinsed with 1mL of PBS three times.

The PBS was aspirated and 1mL of 3% PFA (Appendix-II, A2.3) was added to each well and incubated at room temperature for 30 min to fix the cells. PFA was taken out and cells were washed three times with 1mL ice cold PBS. Next, cells were permeabilized by adding 1mL of permeabilization buffer (Appendix-II, A2.5) for 10min, washed thrice with 1mL ice cold PBS, and quenched with 1mL of quenching buffer (Appendix-II, A2.6) for 5 min. After quenching, the quenching buffer was aspirated, cells washed thrice with ice cold PBS, and 1mL of the blocking buffer (Appendix-II, A2.7) added for 1 hr.

In the meantime, depending upon number of cover-slips, primary antibodies were diluted 1 in 500 in blocking buffer. 100µL of diluted primary antibody was used per cover-slip by spreading paraffin film straight on the lab bench and transferring 100µL of primary antibody as single drops. After blocking, the blocking buffer was aspirated out and each cover-slip was taken out carefully using forceps, and directly placed on top of the 100µL primary antibody (cell surface down) over the paraffin film. Cover-slips were allowed to incubate with primary antibodies for 2 hr. After primary antibody treatment, each cover-slip was transferred back to 12-well plates with cell surface up. 1mL of ice-cold PBS was introduced in each well to wash the cells, plates gently rocked for 5min and the PBS aspirated out. The washing step was performed thrice. During the final wash, 1 in 500 dilution of fluorophore conjugated secondary antibody (Alexa fluor 488 or 568, Invitrogen, UK) was made in the blocking buffer, paraffin film laid evenly on lab bench, and 100µL of it per cover-slip transferred as single drops. After the final wash, each cover-slip was taken out from wells using forceps, excess PBS dried out using paper towel and directly placed on top of 100µL secondary antibody with the cells facing down.

The secondary antibody dilution was performed in dark for 1 hr. After 1 hr of secondary antibody incubation, each cover-slip was transferred to 12-well plate, and washed 3 times with 1mL of PBS for 5 min with gentle shaking. During the last wash, microscope slides were taken and labelled. On each slide, a drop of mounting media with pre-added DAPI (Vector Laboratories UK) was introduced. The cover-slips were taken out from each well, excess PBS dried with paper towel and placed with cell face down over the mounting media. To seal the slides, a clear nail polish (Boots, UK) was used. The slides were transferred to fridge to dry for 30 min and analysed through fluorescence microscopy.

## 2.4 Bioinformatics and computational programs

### 2.4.1 Primer design and analysis

All the primer sequences designed in the current research (Appendix-I) were first analysed under different criteria before ordering. Primer analysis was performed using the primer analysis software, Oligo-Analyzer (Integrated DNA technologies, UK). First of all, it was made sure that the primer sequence designed had a length between 20-40bp, had a minimum GC content of 50%, and that the forward and reverse primers did not have self complementation. Once, this was established, it was made sure that the primer sequences were specific for the gene of interest by carrying out BLAST analysis (http://blast.ncbi.nlm.nih.gov/Blast.cgi).

Further analysis were performed using the Oligo- Analyzer web resource (http://eu.idtdna.com/analyzer/applications/oligoanalyzer/) which determined its melting temperature, complementary sequence, hair pin formation, and possible self dimers.

Fig. 2.1 shows a screen shot of the Bioinformatic analysis of the designed primer using the Oligo-Analyzer web tool. After the primers were found correct under all the set criteria, they were ordered (Integrated DNA technologies, UK) with PAGE purification. Once the primers arrived in lyophilized form, the primer vials were centrifuged at full speed for 3 min, and resuspended in Nuclease free water (Invitrogen) to make a stock of 100µM. 10µL aliquots of 10µM final stocks were made and stored at -20°C until used.

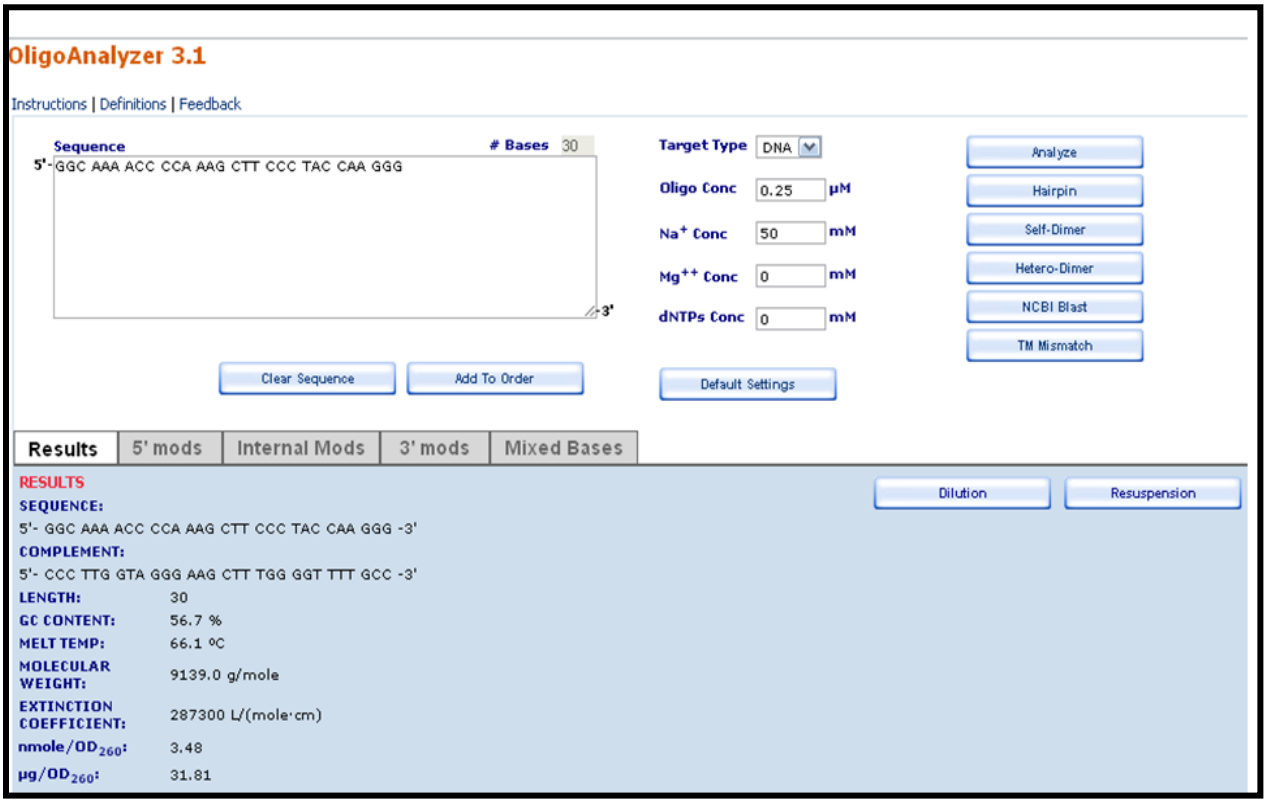


**Figure 2.2: Screen shot of the output window of primer analysis via bioinformatic web resource.** (http://eu.idtdna.com/analyzer/applications/oligoanalyzer/).

### 2.4.2 Relative integrated optical densitometry analysis of immunoblotting signals

Quantitative analysis of raw immunoblots to give a measure of relative abundance of each protein was performed. This was done by first capturing the images in high resolution TIFF format using a charge-coupled device camera (AxioCam MRc, Carl Zeiss), and then calculating integrated optical density of protein bands via Gelpro analysis software (Gelpro Software, USA).

First of all, the Gelpro Analyzer (Version 3.1) software was initiated and the TIFF file of the captured immunoblot was retrieved. The LANES AND BANDS option was clicked and EXTRACT INTENSITY checkbox was checked. This loaded the image from where lanes and bands could be defined. The lane option was selected by clicking "1-D GEL → SHOW TOOL BAR →LANES AND BANDS" and all the lanes were defined in the image. The breadth of each lane, depending upon well size of the gel could be altered at this point. Next, within the "lanes and bands" panel, the band option was selected and the bands whose intensities to be calculated were defined. In each lane, multiple bands could be selected. To show the peaks of each band detected corresponding to its intensity, the option, "1-D GEL → SHOW GRAPH" was selected. This shows the area of the peak representing the intensity calculated within the band defined in a single lane numbered 1 to n depending upon number of lanes. The base of the peak could be defined and altered slightly to cover the whole band area within the blot image. To subtract the background intensity, the background area has to be defined in the blot image. To do this, "1-D GEL → SHOW TOOL BAR → BACKGROUND → ADD LINE" was selected and the background area in between different lanes was defined. To subtract the background intensity from the intensities of bands, "1-D GEL → SHOW GRAPH → BASELINE" was selected and the options "FROM IMAGE" and "PROFILE MINUS BACKGROUND" was checked.

After the lanes were selected, bands were identified and defined and the background subtracted, the Integrated optical densitometry (IOD) analysis were initiated by selecting "1-D GEL → SHOW TOOL BAR → MASS/IOD option. At this point, normalization of the bands could be established in a number of ways. The intensity of each band within a lane could be expressed as a function of intensity of another band in the same lane e.g. to normalize to b-actin bands or the intensity of same bands in all the lanes could be normalized to the intensity of the same band in lane 1.

For example, when normalizing to untreated samples usually loaded in lane 1. This option could be selected from the "Mass/IOD" option which opens up another window in which "Options" is clicked and required normalization choice made. In the Mass/IOD panel, the "IOD" option is selected, which displays IOD calculated from each band as a function of that of band in lane 1. The option "Relative abundance" normalizes the IOD values to a value of that of the control band expressed as 1. These values can directly be exported to Excel files by option "FILE → EXPORT TO → DDE EXCEL". Figure 2.2 shows the screen shot of Gelpro Anayzer 3.1 with its different functions.

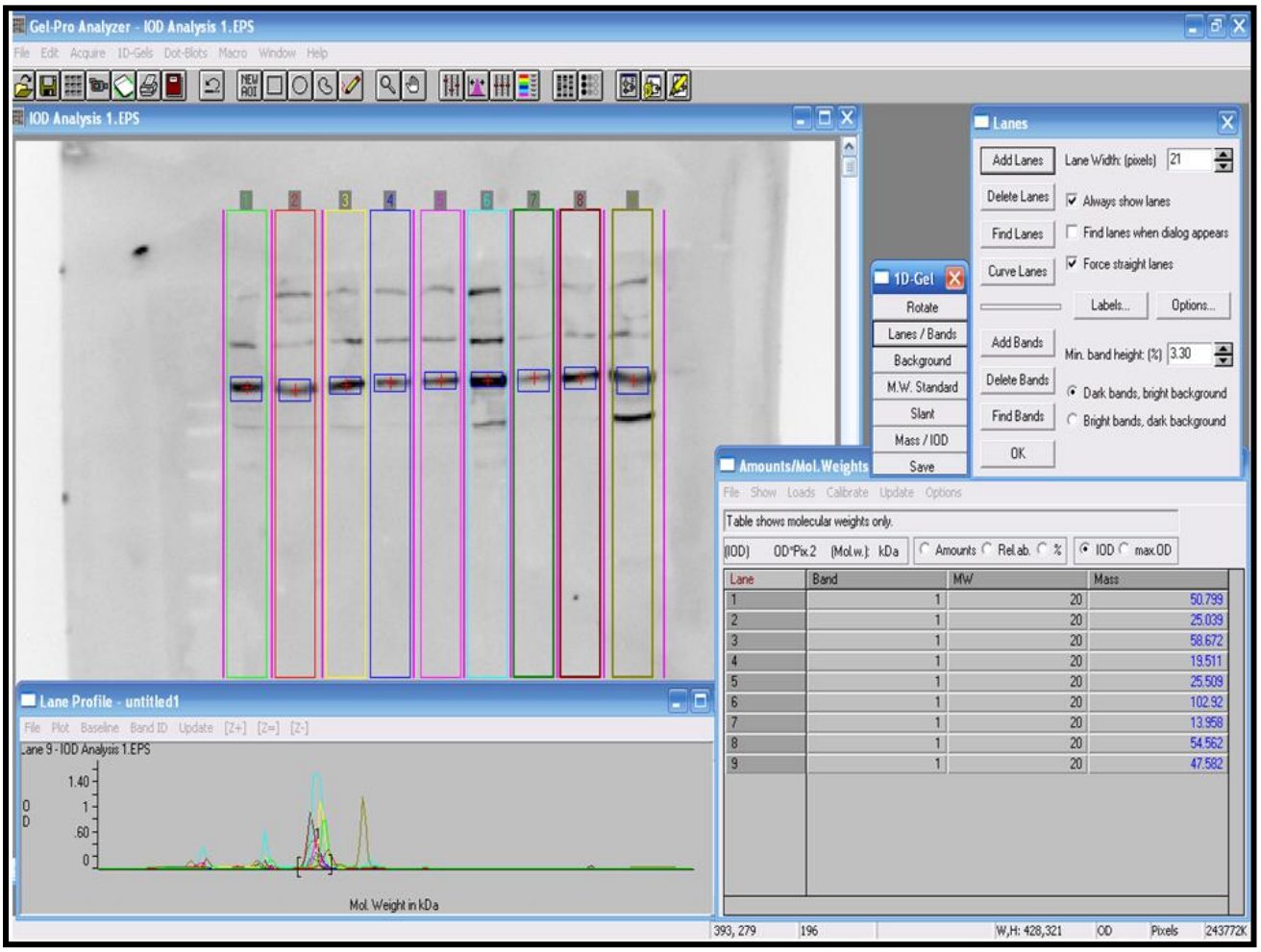


**Figure 2.3: Screen shot of the different windows of Gelpro Immunoblot analysis software used for the semi quantitative measurement of proteins signals.**

A part from the mentioned resources, other Bioinformatic tools were routinely used in the current study. These comprised of Biological data retrieval and genome browser softwares e.g. Ensembl (http://www.ensembl.org/index.html), EMBL (http://www.ebi.ac.uk/embl/), NCBI (http://www.ncbi.nlm.nih.gov/), Sequence analysis softwares e.g. Expasy server tools (http://expasy.org/), DNA complementing-reversing software (http://www.bioinformatics.org/sms/rev_comp.html), Restriction site analysis e.g. NebcutterV2.0 (http://tools.neb.com/NEBcutter2/), and similarity and homology searches e.g. BLAST, phi psi BLAST, BLASTN (http://blast.ncbi.nlm.nih.gov/Blast.cgi).

### 2.4.3 Measurement of Fluorescence intensities

The current research involved measurements of fluorescence intensities to give a quantitative estimate of protein abundance after different experimental treatments. To achieve this, an image analysis software, ImageJ, version 1.44p (http://imagej.nih.gov/ij/) was used. First of all, ImageJ was initiated and the images captured during fluorescence microscopy in high resolution TIFF file format were loaded into the software. Different features of this resource could be used to achieve different visual effects from its option "Process" in the main control panel. For intensity quantification, after the image was loaded, the option "ANALYZE" was clicked which opens up a drop down menu. From this menu, set measurements was selected which opens up a new window where different measurement parameters could be defined by checking each option. For intensity quantification, the options AREA, INTEGRATED DENSITY and STANDARD DEVIATION were selected. A screen shot of the ImageJ software with loaded cellular images is shown in Fig. 2.3. At this point, the quantification of relative intensities was measured in the following two ways:

i) For the quantification of fluorescence intensity of immunostained slides following immunocytochemistry protocols (Fig. 3.10), images were first captured under relevant channels with 10x objective and at 8 different fields of view within a single experimental sample performed in triplicates. Each field of view was set to have at least 50 cells. Similarly, images of the corresponding DAPI stained nuclei within the same fields of view were also captured using DAPI channel. Next, the imageJ software was initiated, the image of the immunostained slide for a particular protein was loaded and the measurement options were selected as mentioned above. To measure intensity, the option "ANALYZE →MEASURE" was clicked which opened up a new window showing the intensity values of the immunostained protein.

Using this technique, fluorescence intensity from the whole field of view of an immunostained slide was calculated. In the same manner, intensities were calculated for all 8 fields of views of the triplicates of same experimental sample and their mean taken. Next, the intensity values of the same fields of views of cells captured with DAPI channel were calculated, their mean taken and used to normalize the corresponding fluorescence intensity values of the immunostained protein. Once this normalization was done, the values of each sample were then further normalized to the value of untreated sample which was expressed as 1.

ii) For the quantification of fluorescence intensity of the expressed fluorescently tagged proteins, the transfections were first done in triplicates and the images of cells expressing the fluorescent tag were captured with 100x objective. Intensities were measured from at least ten cells per transfection and their mean taken. To do this, the imageJ software was initiated as mentioned above, and the images showing the transfected cell captured with the green fluorescence channel, red fluorescent channel and the DAPI stained nucleus were loaded. The ImageJ "FREE HAND TOOL" was selected to define a region of interest within the loaded image, i.e. single cell expressing fluorescent tag. First, the intensity of green fluorescence was measured via "ANALYZE →MEASURE" option. Next, the intensity of red fluorescence from the same cell was measured in a similar manner. From the same image, intensity from an identical area in the background was measured and subtracted from the intensity values of the fluorescent tags. Finally, in the DAPI image, using the "FREE HAND TOOL", the DAPI stained nucleus of the same cell was defined as region of interest, its intensity calculated.

The background of an identical area was subtracted, and the resulting value used to normalize the fluorescence values of each of the expressed fluorescent tags of the experimental samples (Fig. 4.12). Finally, mean values were taken for each experimental sample and the mean value of the green fluorescent tag in the untreated control, set to 1, was used to normalize all the other fluorescence values of samples after different treatment.

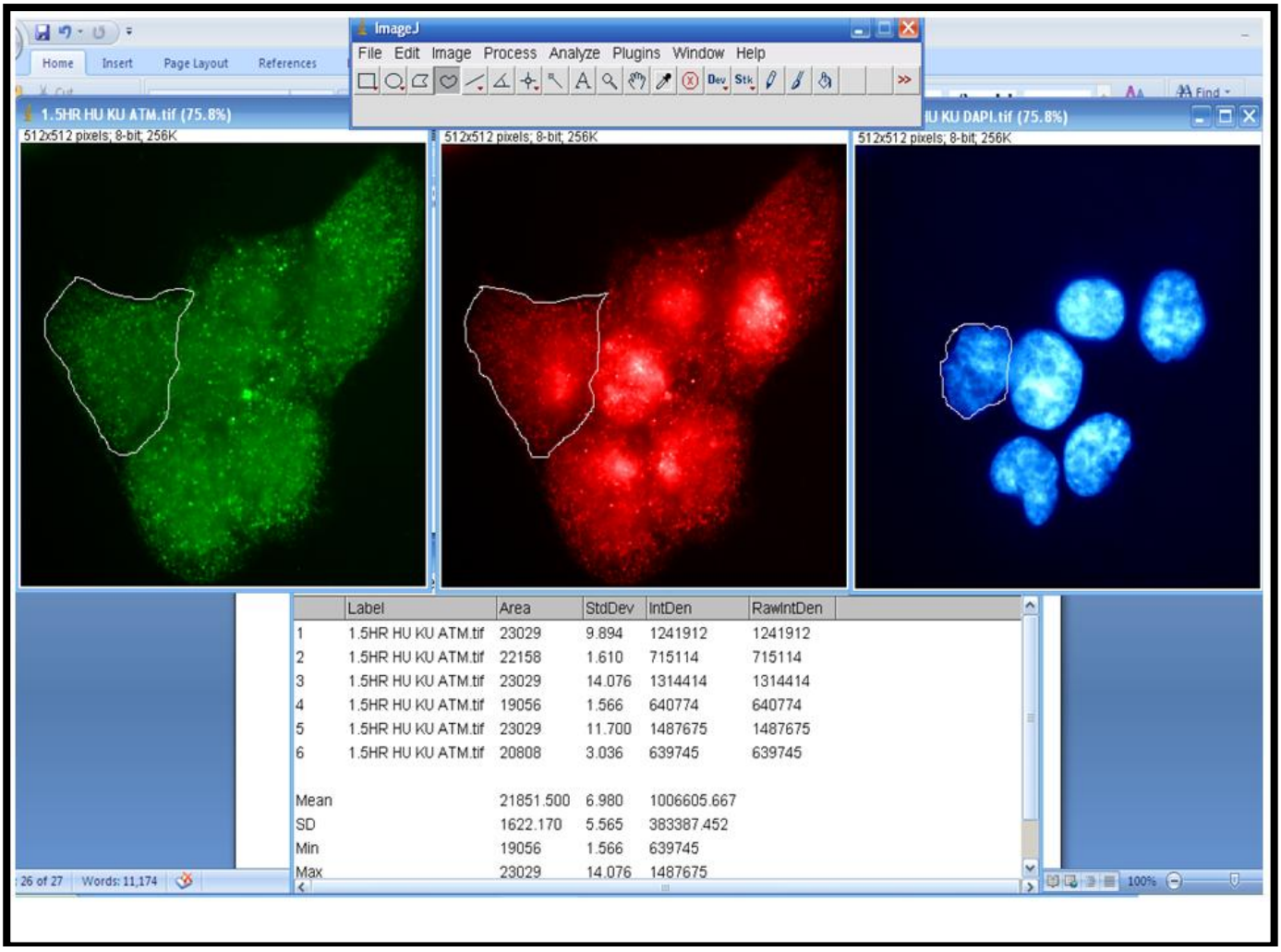


**Figure 2.4:** Screen shot of ImageJ image analysis software for the quantitative fluorescence intensity measurement of different proteins studied in the current research. (http://imagej.nih.gov/ij/).

### 2.4.4 High Pressure Liquid Chromatography (HPLC)

HPLC (Dionex, UK) was performed to study the degree of stability of important drugs used in the current study within the cell culture media. Since some of the drugs were employed for extended periods of time (up to 24 hr) it was imperative to first assess their stability in the cell culture media.

First of all, two buffers named Buffer A and Buffer B were made for HPLC in a chemical fume hood. Buffer A was made up of 0.1% of Trifluoroacetic acid in distilled water (Hydrophilic buffer). Buffer B was made up of Acetonitrile with 0.1% Trifluoroacetic acid (Hydrophobic buffer). The bottles with the buffers were placed next to HPLC equipment and their tubes connected to the pumps. The HPLC equipment was turned on and its software, Chromeleon® initiated. The first step was to wash the HPLC column with the buffers to remove any residual hydrophilic or hydrophobic compounds left over from previous uses. To do this, a panel was selected with templates for manual control of the pumps via:

FILE →DIONEX TEMPLATES → PANELS → DIONEX LC →OBJECT OF TYPE → CONTROL PANEL → DIONEX PUMP PDA 3D AUTOSAMPLER.

Next, this template was connected to the pumps via PUMPS → CONTROL → CONNECT TO TIME BASE → ABERTAY-1 and then CONTROL → ACQUISITION ON. A data acquisition window will be shown. To show the signals, right click on this window, SIGNALS → CHOOSE and the wavelengths at which signals were to be acquired were chosen. Using the manual control of the injectors, Buffer A was set to be injected in the column at 0.1mL/min for 12 hr followed by buffer B for 12 hr. This washed all the hydrophilic and hydrophobic compounds from the column.

Next day, drug solutions were made in the cell culture media (Serum and antibiotic added DMEM) at a concentration used in experiments.

The drug media was transferred to special HPLC autosampler vials (Thermo scientific, UK) and placed in the automated loading tray in the HPLC machine. Next, a pumping program was made consisting of commands for relative pumping from the two buffers through a 0.5 hr interval, usually starting with pumping 100% Buffer A, followed by a gradient consisting of 100% A to 100% B (0% A), followed by another gradient consisting of 100% buffer B to 100% buffer A. This ensured that all the contents within the loaded samples were released from the column in a single pumping program. Depending upon the number of time points through which the stability of a drug was measured, a sequence of pumping programs was made with different intervals in between.

The required number of sequences, known as a batch was started by clicking START. The automated function collected samples from the vials to start HPLC. To view signals, the acquisition was turned on from the desired template as mentioned above. After all the sequences in a batch were executed, the data of the HPLC peaks were analysed. To identify the peak in a give graph corresponding to the drug, the graphical data from the media only and the drug only was compared with the data obtained from vial having media plus drug at a first time point by selecting these sequences →RIGHT CLICK → COMPARE. The additional peak in the drug plus media sample as compared to the media only was identified to be that of drug. The area under the curve (AUC) of the peak corresponding to the drug was determined by right clicking on that peak. Similarly, the AUC of the drug specific peak was measured at all the time points and plotted against time to determine the drug stability (Appendix-I, A1.6).

# Chapter Three

# Cell cycle dependent ATM expression, activity and localisation: Responses generated by DSB inducing agents and ATM kinase inhibition and its impact on DDR signalling pathway in normal Human epithelial cell line

A man should look for what is, and not for what he thinks should be.

Albert Einstein (1879 – 18 April 1955).

## 3.1 Abstract

*Ataxia-telangiectasia mutated (ATM) protein is a Serine/Threonine kinase which initiates signalling mechanism that can modulate the progression of cell cycle upon treatment with different growth factors or induce DDR following double stranded DNA damage. There are contrary reports of the outcome of different growth factors or DNA damage on expression levels of ATM itself or the resulting signalling pathway downstream of ATM. In this section, I have investigated the effects of serum stimulation and the progression of cell cycle on ATM protein expression and its overall consequence for its downstream substrates in human epithelial cell line, MCF10A. Furthermore, I examined the activation of DDR signalling pathway in response to DNA damage by examining the degree of ATM activation during time-dependent treatment with genotoxic agents and the effects of its activity on phospho-induction of its downstream substrates. Serum stimulation of synchronized cells caused induction of total ATM which was also reflected in its phosphorylated levels and underwent time dependent alterations as synchronized cells progressed through the cell cycle. These alterations in protein levels also correlated with the induction of ATM substrates at the same time points. While activation of ATM upon DNA damage did not cause significant change in its protein levels, pATM, P53 and E2F1 levels were rapidly induced but with different kinetics. Double fluorescent immunolocalisation studies performed by immunolabelling ATM, pATM and its substrates not only revealed these protein inductions at single cell level, but also determined their co-localisation and sub-cellular compartments where these inductions took place. Finally, with the use of variety of genotoxic agents, the dependence of the resulting DDR specifically on ATM activity was determined. While Dox induced DDR was completely dependent on ATM, DDR signal transduction resulting from other genotoxic agents was influenced to ATM inhibition to varying degrees, demonstrating an overlapping role of other DDR kinases in such treatments. These studies emphasised the importance of characterising the requirement of ATM expression and activity within DDR signalling pathway before cell sensitisation to genotoxic agents based on inhibition of ATM activity alone could be actualised.*

## 3.2 Introduction

In the past decade, our struggle to find the best therapeutic approach for cancer treatment has witnessed a paradigm shift, from the use of more conventional empirical approach involving general chemotherapy and surgical excisions to a more targeted approach. More precise strategies involve the identification of specific molecular targets that are believed to be of biological significance in terms of their role in DNA damage repair, cell cycle regulation and apoptosis induction in both normal and cancerous states. A prerequisite of molecularly targeted, DDR inhibition based anti cancer approach, in addition to identifying signaling targets, is a detailed and complete understanding of the underlying mechanisms governing those targets, first in the normal cells followed by their extrapolation or exploitation in cancer setting. These include elucidation of regulatory pathways, expression and localisational patterns and the resulting activities of target proteins and their downstream substrates under normal physiological conditions, upon DNA damage, and also the responses generated during their inhibition.

I have previously reported a link between ATM activity and its expression via promoter studies (Khalil HS et al., 2011) in normal as well as cancer cells. Nevertheless, there are still gaps in our understanding of the exact molecular mechanisms that lead from sensing the DNA damage to the regulation, localisation and activation of the ATM molecule and its effect on downstream substrates. Before these regulatory mechanisms could be exploited in cancer therapy, it is vital to elucidate these in normal cells. In this section of my research, I studied the regulation and sub-cellular localisation of ATM in early phases of cell cycle and its kinase activation upon different extents of damage through radiomimetic drugs.

Furthermore, I examined the effects of this activation on phospho induction and localisation of downstream signalling molecules in a time dependant manner in human epithelial cell line MCF10A. Additionally, to determine the dependence of DDR specifically on ATM kinase activity, I employed small molecular inhibitor of ATM kinase, followed by treatments with different genotoxic agents, and studied the resulting substrate induction in this human epithelial cell line.

## 3.3 Results

### *3.3.1 ATM expression and signalling activity is induced upon serum stimulation and through the cell cycle and causes time dependent phospho induction of its substrates during DDR signalling pathway.*

Previous studies have shown that ATM is involved in the regulation of cell cycle progression by phosphorylation of variety of substrates including P53, Chk2 and E2F1 (Banin S. et al., 1998; Lin WC et al., 2001; Powers JT et al., 2004). However, its own regulation during cell cycle and the effects of such regulation on its downstream substrates is not fully elucidated.

First I studied the level of total ATM, phosphorylated ATM, and the phosphorylation of its key substrates P53, Chk2 and E2F1 through the early phases (G1 to S phase) of cell cycle in human epithelial cell line. For this, cells were grown until 70% confluent and serum starved for 48 hours to synchronize them in G1 phase. Serum was added back and cells were allowed to grow for different time points and their protein lysates collected and processed for immuno blotting to analyse the degree of abundance and activity of the above mentioned proteins (Fig. 3.1) as described in materials and methods. Signals obtained from immunoblotting were also subjected to integrated optical densitometry analysis to carry out comparative studies of relative abundance of each protein as shown in Fig. 3.2a-d.

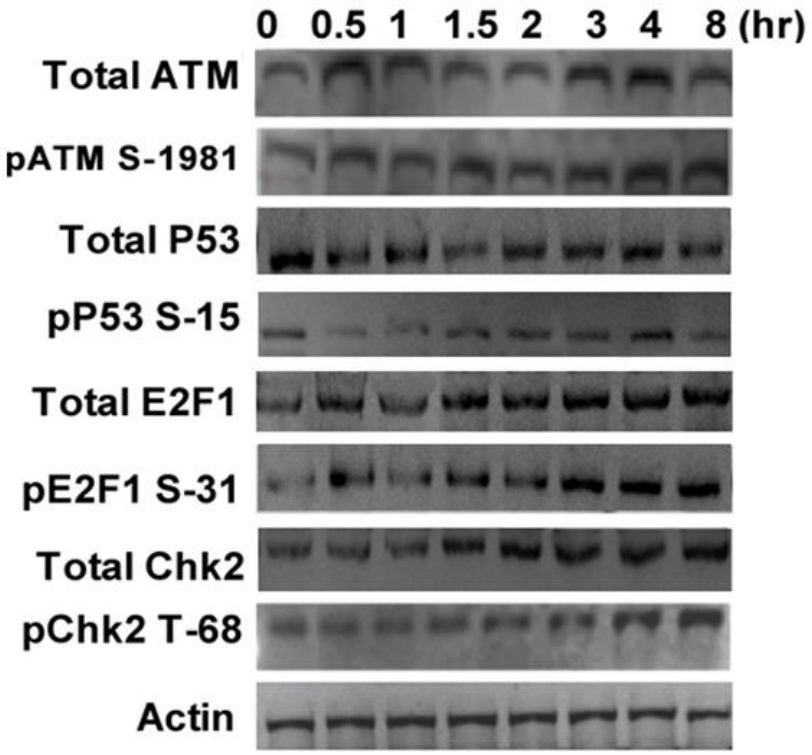


**Figure 3.1: Levels of DNA damage response proteins change during progression of the cell cycle following serum stimulation.** MCF10A cells were seeded in 100mm tissue culture plates at a density of 2 x $10^6$ cells and grown until 70% confluent. Cells were serum starved for 48 hrs by incubating them in serum free media to synchronize them in G1 phase. Serum was added back and synchronized cells allowed to grow for different time points as indicated and cell lysates harvested and processed for immunoblotting for total ATM, pATM S-1981, total P53, pP53 S-15, total E2F1, pE2F1 S-31, and total Chk2 and pChk2 T-68. 20µg of protein was loaded in each well of SDS PAGE gels. For loading control, Actin antibody was also included.

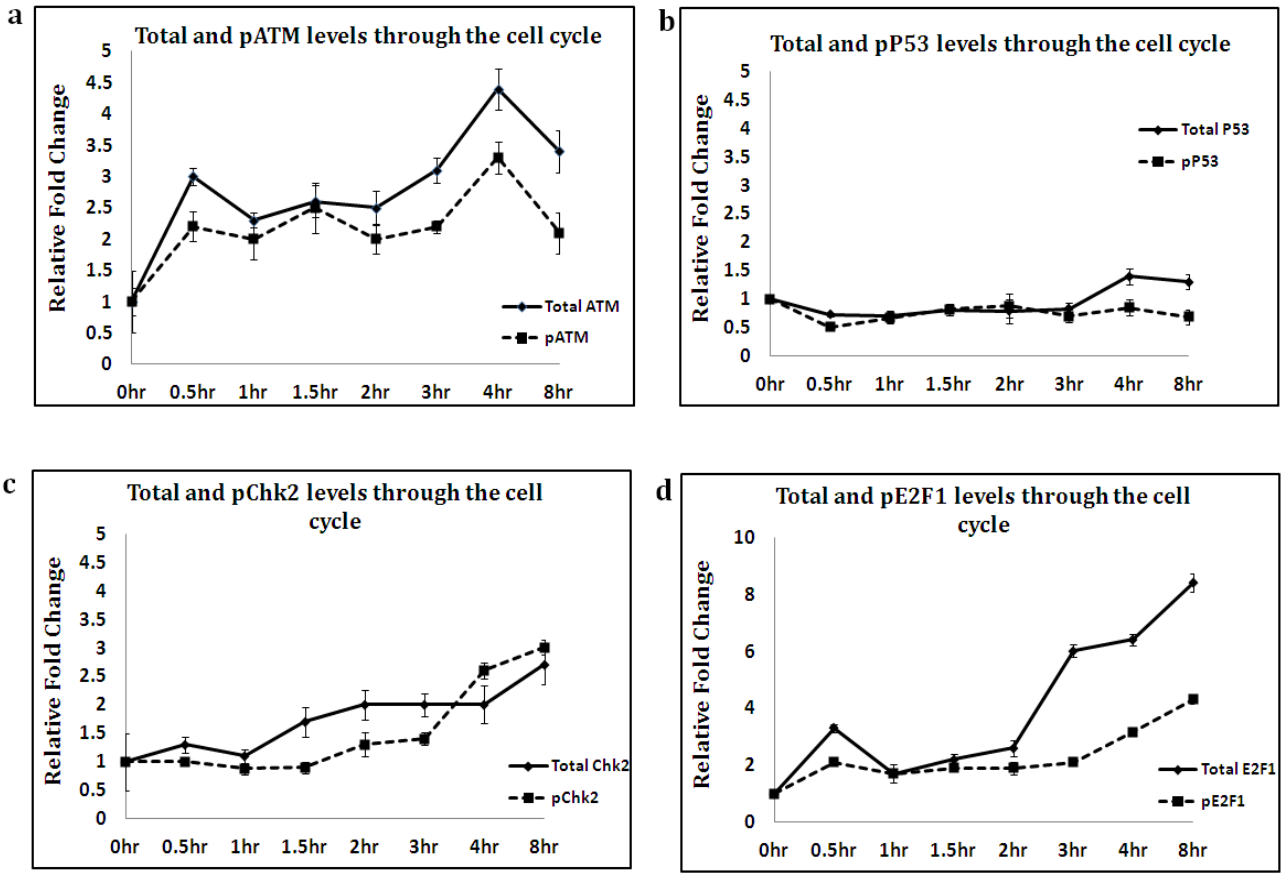


**Figure 3.2: Integrated Optical Densitometry analysis of Immunoblotting results of DDR proteins and their phosphorylated forms during cell cycle progression.** The immunoblotting results in Fig. 3.1 were subjected to semi quantitative analysis by using integrated optical densitometry of immunoblot signal via Gelpro software. Data presented in all panels are the mean with standard error (bars) of n=3 independent experiments normalised to the untreated controls (0 hr time point) expressed as 1. **(a)**, **(b)**, **(c)**, and **(d)** show the analysis for total and phosphorylated forms of ATM, P53, Chk2 and E2F1 respectively.

Immunoblotting of these key DDR proteins revealed that as compared to untreated cells (0 hr), serum stimulation resulted in induction in the levels of both total and phospho ATM serine 1981 (pATM) at 0.5 hour (hr) post serum addition. This serum stimulated upregulation was generally maintained with a further increase at 4 hr time point in the cell cycle while overall showing no major change (Fig. 3.1 & Fig. 3.2a). Consistent with ATM and pATM, both P53 and phospho P53 serine 15 (pP53) also showed an overall increase at 4 hr time point (Fig. 3.1 & 3.2b). While total and phospho Chk2 Threonine 68 (pChk2) levels generally remained unchanged for the first three time points, showed induction at 2 hr and again underwent upregulation of pChk2 at 4 hr post serum addition with highest levels at 8 hr time point (Fig. 3.1 & 3.2c). Both total and phospho E2F1 Serine 31 (pE2F1) also showed induction following serum stimulation consistent with ATM. Moreover, E2F1 underwent further significant changes during the progression of cell cycle, rising after 2 hr post serum addition and maximum at 8 hr with >8 fold increase as determined by integrated optical densitometry analysis of its immunoblot signal (Fig. 3.1 and 3.2d). The observed induction in the levels of these proteins at different time points may indicate a requirement for cell cycle progression. E.g. upregulation of E2F1 (~4 hrs after serum addition) is associated with reduction in cyclin D through G1/S transition to allow cell cycle to progress (Watanabe G et al., 1998).

Next, to determine whether the DDR pathway is active in MCF10A cell line, DNA double strand break inducing agent, Doxorubicin (Dox) was employed to induce DNA damage in the cells synchronized at the same time points and the resulting kinetics of the activation of DDR pathway were studied. This was done by examining total ATM levels and the induction of pATM, total P53 and pP53, total E2F1 and pE2F1 and total Chk2 and pChk2 under DNA damaging conditions of 0.5μM Dox in a time dependent manner through Western blot analysis (Fig. 3.3 & 3.4a-d).

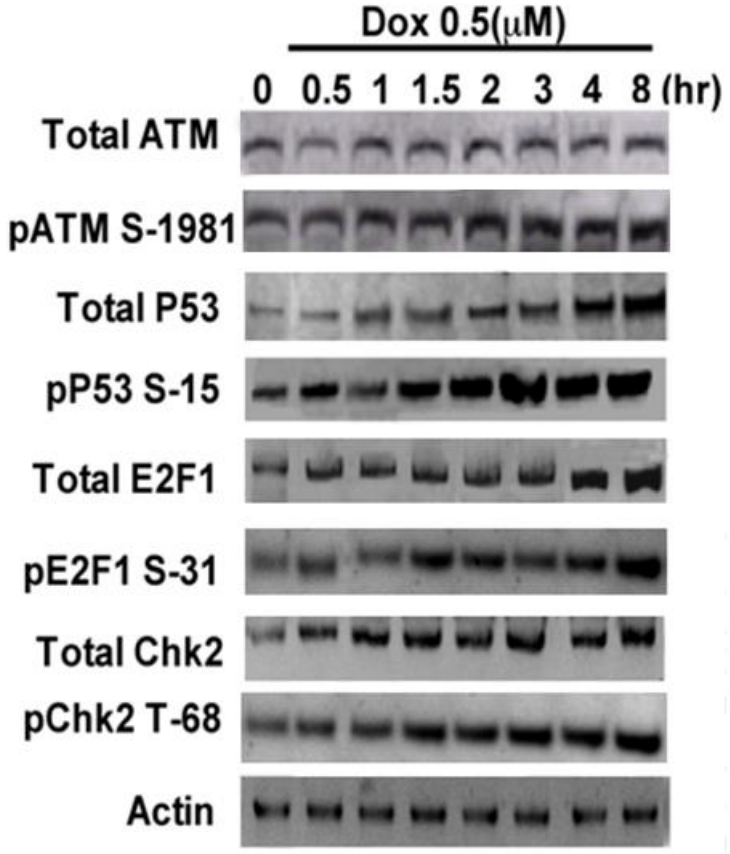


**Figure 3.3: DDR pathway is active in MCF10 human epithelial cell line**. MCF10A cells were seeded in 100mm tissue culture plates at a density of 2 x $10^6$ cells and grown until 70% confluent. Cells were serum starved for 48 hrs by incubating them in serum free media to synchronize them in G1 phase. Serum was added back and synchronized cells were either left untreated, or exposed to 0.5μM Dox for the indicated time points and cell lysates harvested and processed for immunoblotting for total ATM, pATM S-1981, total P53, pP53 S-15, total E2F1, pE2F1 S-31, and total Chk2 and pChk2 T-68. 20μg of protein lysates were loaded in each well of SDS PAGE gels. For loading control, actin antibody was also included.

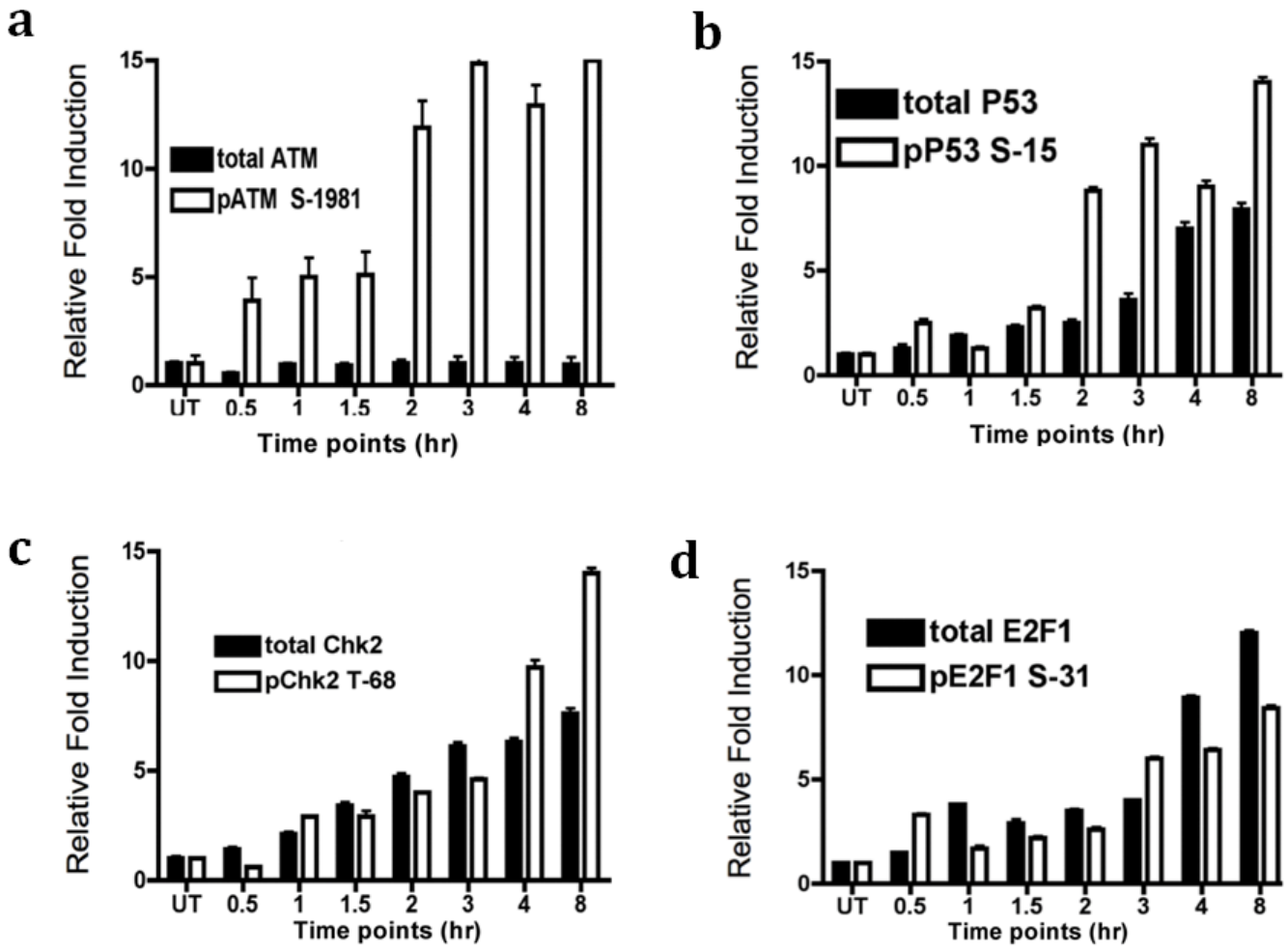


**Figure 3.4: Integrated Optical Densitometry analysis of immunoblotting results of DDR proteins and their phosphorylated forms during DDR activation.** The immunoblotting results in figure 3.3 were subjected to semi quantitative analysis by using integrated optical densitometry of immunoblot signal via Gelpro software. Data presented in all panels are the mean with standard error (bars) of n=3 independent experiments normalised to the untreated controls (UT) expressed as 1. **(a)**, **(b)**, **(c),** and **(d)** show the analysis for total and phosphorylated forms of ATM, P53, Chk2 and E2F1 respectively.

Analysis of the immunoblotting showed that while no major change was observed in the levels of total ATM after DNA damage (compare Fig. 3.1 and 3.3), pATM levels showed induction starting at 0.5 hr of Dox treatment. Increasing the DNA damage by extending Dox treatment to 1 and 1.5 hr caused a further increase in pATM levels at a steady rate. Extending the Dox treatment to 2 hr caused a major induction in its levels causing ~ 2-fold increase as compared to the previous time point as determined by integrated densitometry analysis of the immunoblot signal (Figure 3.4a). This induction increased slightly further and was maintained up to the 8 hr time point (Fig. 3.3 & 3.4a). Similarly, ATM substrates, P53, Chk2 and E2F1 and their phosphorylated forms showed a time dependent induction after Dox treatment but with different kinetics demonstrating a functional DDR pathway in MCF10A cell line (Fig. 3.3 & 3.4b-d).

### *3.3.2 Double immunolabelling of ATM and its substrates during DDR following double stranded DNA damage reveals time dependent nuclear induction of pATM and p53.*

I next set out to determine whether the induction of these DDR proteins observed during cell cycle progression and under DNA damage in Fig 3.1 and Fig. 3.3 also caused any localisational changes and whether the observed induction in those experiments took place in particular sub-cellular compartments. To determine this, MCF10A cells were grown on poly-L lysine coated cover slips and serum starved for 48 hours to synchronize them in G1 phase. Serum was added back and cells were allowed to grow for different time points as indicated after which, treatments were stopped and cells were fixed for double immunocytochemical studies to examine the intra cellular induction and localisational changes in ATM, pATM, pP53 and E2F1 as the cells progressed through the cell cycle (Fig. 3.5).

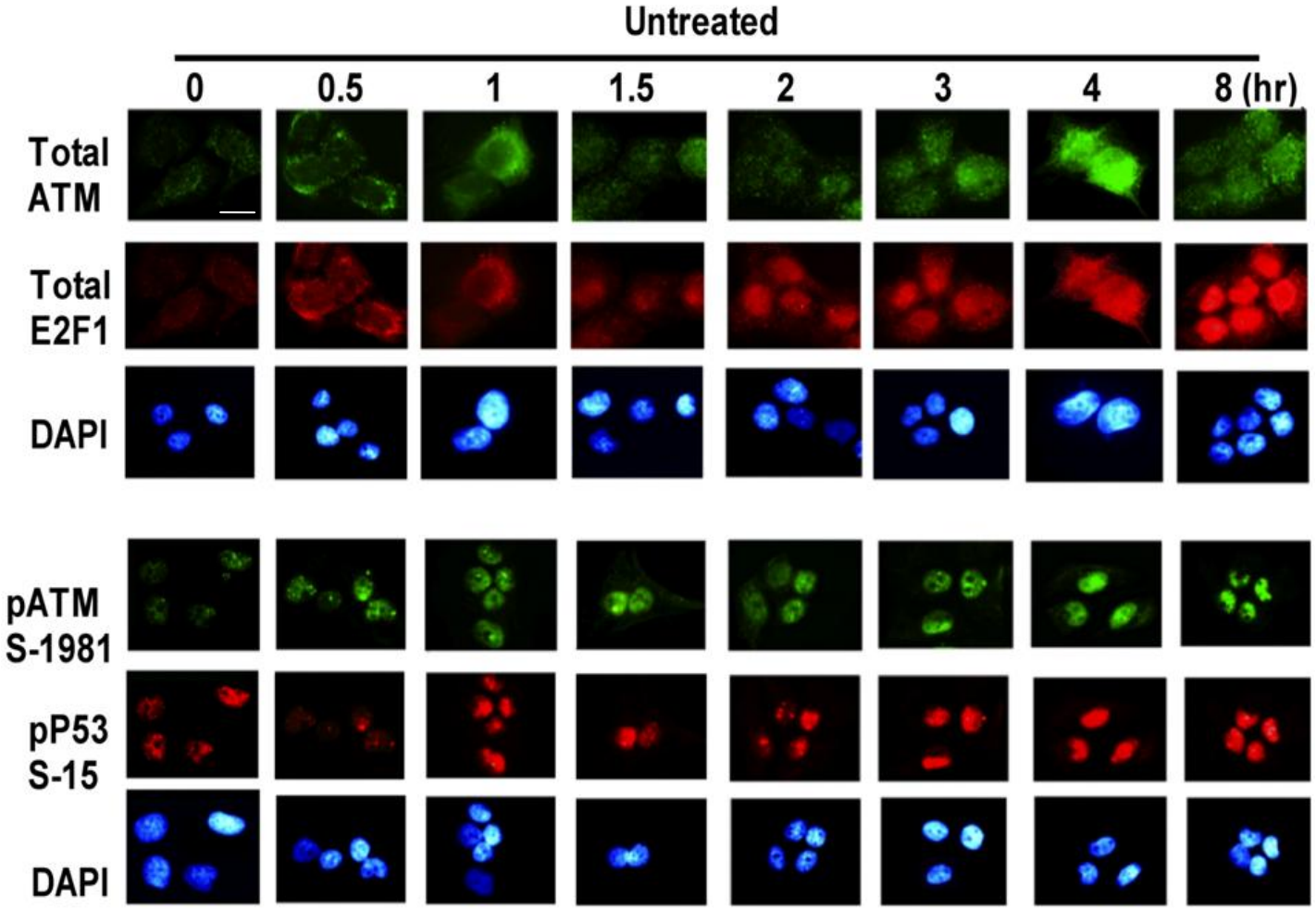
Untreated
0
0.5
1
1.5
2
3
4
8 (hr)
Total ATM
Total E2F1
DAPI
pATM S-1981
pP53 S-15
DAPI

**Figure 3.5: pATM and pP53 undergo nuclear upregulation while E2F1 shows mostly nuclear but some cytoplasmic upregulation during cell cycle progression.** MCF10 cells were seeded on poly L lysine coated coverslips placed in 12-well plates at a density of 1 x $10^5$ cells per well and grown until 70% confluent. Cells were serum starved for 48 hrs by incubating them in serum free media to synchronize them in G1 phase. Serum was added back and synchronized cells allowed to grow for different time points as indicated and processed for Immunocytochemical studies by using antibodies against Total and pATM, E2F1 and pP53. For total and pATM, immunostaining was performed by using Alexa fluor 488® conjugated secondary antibody while total E2F1 and pP53 immunostaining was performed by using Alexa fluor 568® conjugated secondary antibody. Nuclear reference was provided by DAPI staining. These are representative images taken in different fields of view under 100x objective. Scale bar represents 10μm.

In terms of localisation, it was found that ATM and its phosphorylated form were mostly present in the nucleus, consistent with the previous reports (Gately DP et al., 1998) and no significant change in their intracellular localisation was observed through the cell cycle. However, in addition to their nuclear localisation, some cytoplasmic staining of ATM and pATM were also observed at the peri nuclear region. For ATM, this cytoplasmic staining was most prominent in the serum starved state and at 0.5 and 1 hr time point after serum release (Fig. 3.5). In terms of levels of expression, the nuclear ATM was greatly reduced in serum-starved cells and recovered within the nucleus after serum addition in a time-dependent manner. Hence, the changes that we observed in the levels of total and phospho ATM through the cell cycle in western blots (Fig.3.1 & 3.2a) appeared to have taken place in the nuclear compartments of these proteins as revealed by their immunolabelling (Fig. 3.5).

pP53 was observed to have mostly nuclear localisation at all time points (compare pP53 immunostaining with the corresponding DAPI stained nuclei) and appeared to co-localize with pATM (revealed by double immunostaining) suggesting that in the absence of DNA damage, P53 may be maintained in phosphorylated state by ATM (Fig. 3.5). Also, apart from pP53 levels at 0.5 hr of serum stimulation, its immunostaining intensity at all the other time points correlated well with those of ATM and pATM. E2F family of transcription factors are known to be mostly nuclear with some reports suggesting cell cycle dependant localisation and continuous shuttling between nucleus and cytoplasm (Ivanova IA et al., 2007). It is evident that the release of cells from the quiescent state (Time 0) with the addition of growth factors resulted in a sharp rise in both the nuclear and cytoplasmic E2F1 levels starting at 0.5 hr time point of serum addition and continuing further. This correlated well with the previous immunoblotting results for E2F1 (Fig. 3.1).

While the nuclear fraction of E2F1 increased to a greater extent as compared to cytoplasmic, both of these sub-cellular compartments showed induction in E2F1 relative to serum starved state. Hence, the E2F1 induction observed in western blot results (Fig. 3.1) was contributed by both nuclear and cytoplasmic increase.

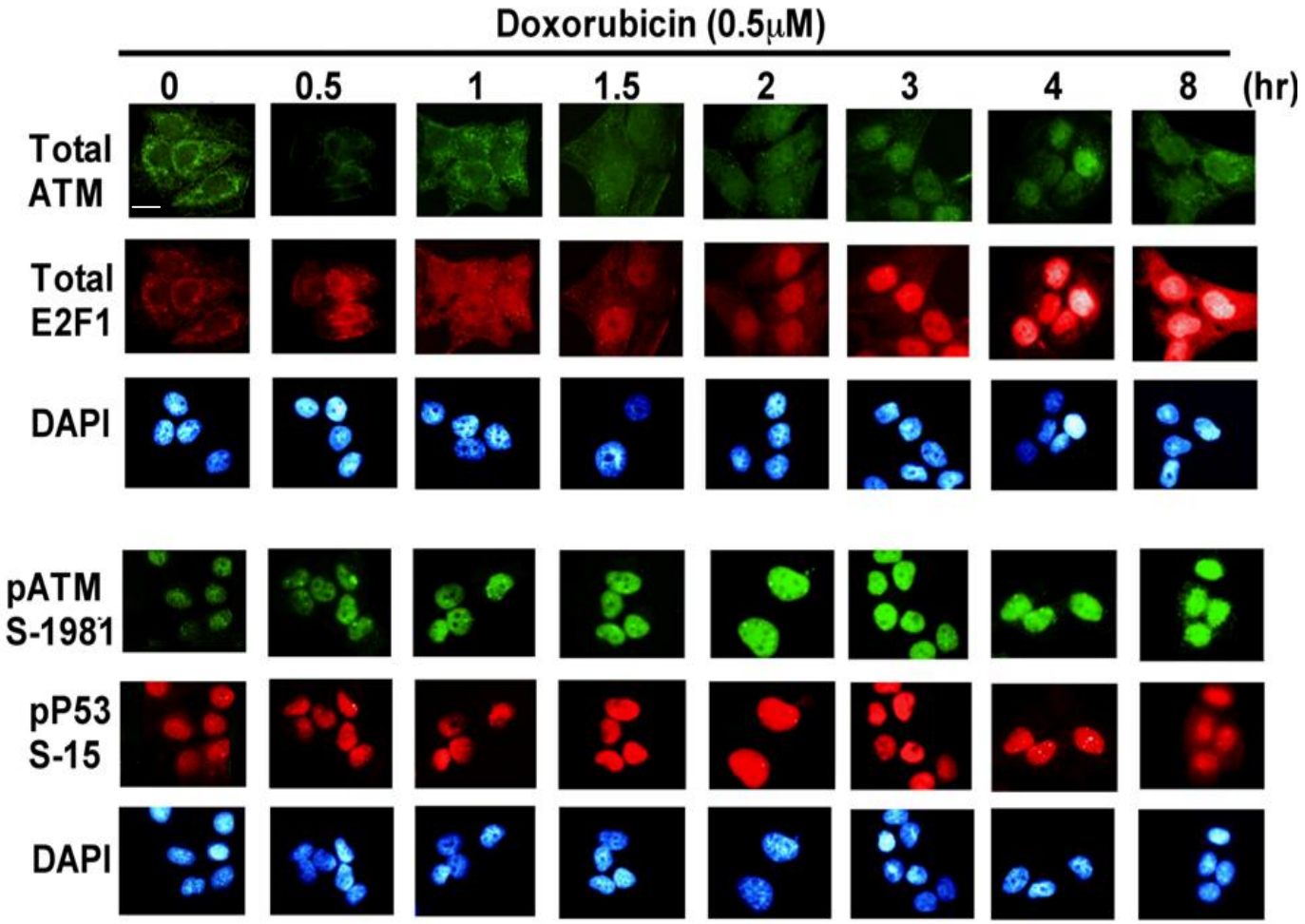
Doxorubicin (0.5μM)
0
0.5
1
1.5
2
3
4
8
(hr)
Total ATM
Total E2F1
DAPI
pATM S-1981
pP53 S-15
DAPI

**Figure 3.6: DNA damage causes rapid nuclear induction of pATM S-15, pP53 S-15 and E2F1 levels with almost no change in total ATM expression**. MCF10 cells were seeded on poly L lysine coated coverslips placed in 12-well plates at a density of 1 x $10^5$ cells per well and grown until 70% confluent. Cells were serum starved for 48hrs by incubating them in serum free media to synchronize them in G1 phase. Serum was added back and synchronized cells were either left untreated, or treated with 0.5μM Dox for different time points as indicated and processed for Immunocytochemical studies by using antibodies against Total and pATM, E2F1 and pP53. For total and pATM, immunostaining was performed by using Alexa fluor 488® conjugated secondary antibody while total E2F1 and pP53 immunostaining was performed by using Alexa fluor 568® conjugated secondary antibody. Nuclear reference was provided by DAPI staining. These are representative images taken in different fields of view under 100x objective. Scale bar represents 10μm.

Total ATM expression and localisation in DNA damaging conditions of 0.5μM Dox for different time periods (Fig. 3.6) exhibited no significant change when compared to the immunostaining pattern through the cell cycle in the untreated controls (Fig. 3.5). The rise in the nuclear ATM post 1.5 hr time point in the untreated controls also remained consistent after DNA damage. However, addition of Dox seemed to result in disappearance of the perinuclear ATM at later time points (compare Fig. 3.6 0 hr time point with 1.5 hr time point). pATM levels not only increased as expected at 0.5 hr of Dox treatment, but this increase was also accompanied by its disappearance from extra nuclear regions. Furthermore, pATM induction correlated with that of pP53. A remarkable increase in nuclear E2F1 levels was observed (compare its immunostaining with the corresponding DAPI stained nuclei) most prominent at and post 3 hr time point of Dox treatment. These inductions not only demonstrated and confirmed the immunoblotting results at cellular level, but also revealed the sub-cellular compartments where the inductions took place and provided co-localisational analysis of the different immunostained proteins of DDR and furthermore demonstrated a functional DDR pathway in this cell line.

### *3.3.3 Doxorubicin-induced DDR pathway primarily depends on ATM in MCF10 cell line.*

To establish the direct role of ATM in the Dox-induced DDR signalling observed in the previous figures, synchronized MCF10A cells were exposed to 0.5μM Dox, which according to Figures 3.2-3.6 should induce DDR. However on this instance, the cells were also exposed to 10μM of the specific small molecular inhibitor of ATM kinase, KU55933 (KU) (Hickson I et al., 2004) for the same time points and protein lysates collected and prepared for immunoblotting.

As evident in figure 3.7, with the treatment of 10μM ATM kinase inhibitor alone or with the addition of Dox, the phosphorylated levels of ATM were completely abrogated at most of the time points as compared to either untreated controls or only Dox treated cells. Phosphorylational stabilisation and activation of P53 is regarded as a key event in the initiation of DDR pathway. Since, it is activated by both ATM (Banin S et al., 1998) and Chk2 (Shieh SY et al., 2000), which itself is a substrate of ATM (Falck J et al., 2001), both of these substrates were also included in the study to asses activation of DDR pathway during ATM inhibited state for up to 8 hr of genotoxic treatment. It was found that the phosphorylated forms of both of these ATM downstream targets dropped below the threshold level (untreated controls), indicating their dependence on ATM not only during DDR signalling following DNA damage, but also under non-DNA damaging (untreated) conditions (Fig. 3.7).

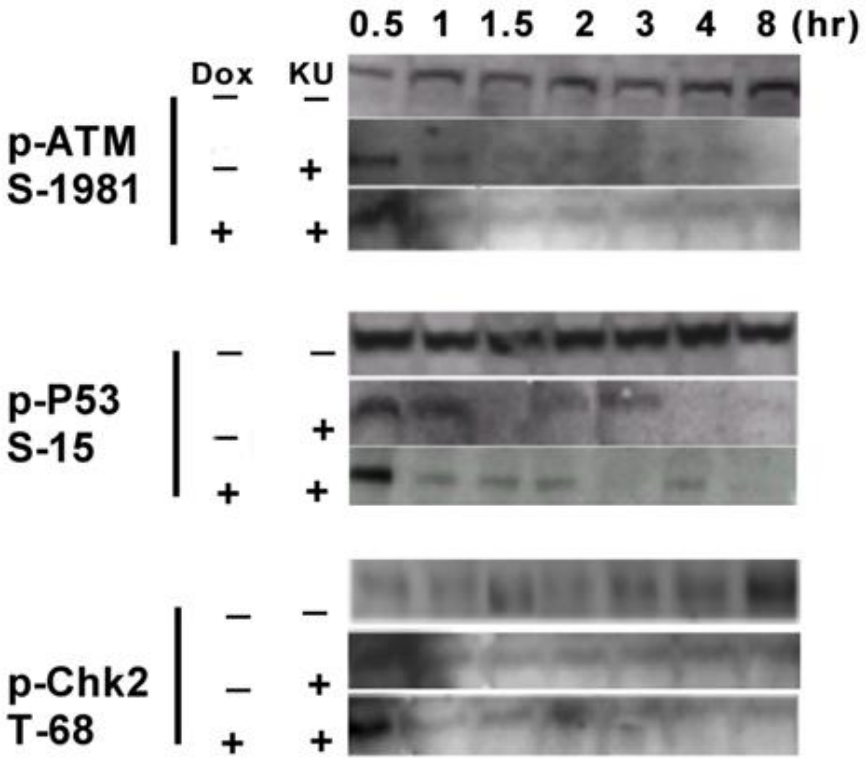


**Figure 3.7: Doxorubicin induced phospho induction of DDR proteins is completely abrogated after treatment with ATM kinase inhibitor.** MCF10A cells were seeded in 100mm tissue culture plates at a density of 2 x $10^6$ cells and grown until 70% confluent. Cells were serum starved for 48 hrs by incubating them in serum free media to synchronize them in G1 phase. Serum was added back and synchronized cells were either left untreated, or treated with 10μM Ku alone, or with the addition of 0.5μM Dox for the indicated time points and cell lysates harvested and processed for immunoblotting for pATM S-1981, pP53 S-15 and pChk2 T-68. 20μg of protein lysates were loaded in each well of SDS PAGE gels.

To demonstrate these western blot results at cellular level, double immunocytochemical labelling of pATM and pP53 were performed on cells grown on coverslips, and treated as above. It was found that nuclear immunostaining of pATM and pP53 quantitatively decreased with the addition of KU with Dox, starting at 0.5 hr treatment and minimum at 8 hr of treatment (Fig. 3.8).

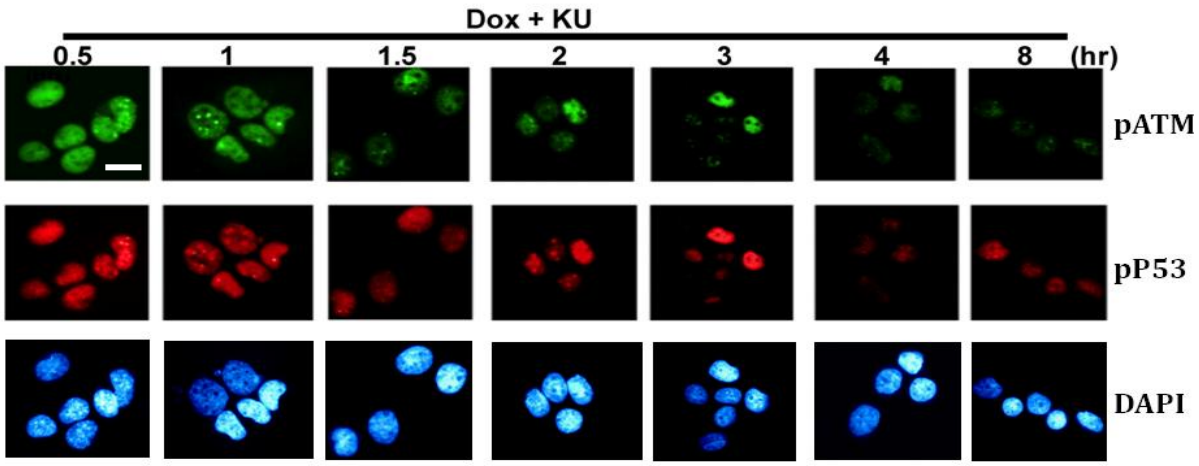


**Figure 3.8: ATM inhibition causes depletion of immunofluorescence signal of nuclear phospho ATM S-1981 and phospho P53 S-15 after doubles stranded DNA damage.** MCF10 cells were seeded on poly L lysine coated coverslips placed in 12-well plate at a density of 1 x $10^5$ cells per well and grown until 70% confluent. Cells were serum starved for 48hrs by incubating them in serum free media to synchronize them in G1 phase. Serum was added back and synchronized cells were treated with 0.5µM Dox and 10µM of ATM kinase inhibitor KU for different time points as indicated and processed for Immunocytochemical studies by using antibodies against pATM S-1981 and pP53 S-15. For pATM, immunostaining was performed by using Alexa fluor 488® conjugated secondary antibody while for pP53, immunostaining was performed by using Alexa fluor 568® conjugated secondary antibody. Nuclear reference was provided by DAPI staining. These are representative images taken in different fields of view under 100x objective. Scare bar represents 10µm.

Altogether, these results demonstrate that the DDR signalling pathway, in context of P53 (functioning at the nodal point of DDR) and Chk2 (key mediator of cell cycle arrest as well as apoptosis) activation after DSB inducing agent doxorubicin, solely depends on ATM kinase activity, at least for up to 8 hrs of genotoxic stress in MCF10A cell line.

### *3.3.4 DDR pathways induced by Bleomycin, Cisplatin and Hydroxyurea do not solely depend on ATM activity.*

In order to determine the kinetics of DDR activation following time dependent treatments with genotoxic agents other than Doxorubicin, MCF10A cells were treated with 5μM Bleomycin (Sun Y et al., 2005), 4.8μM Cisplatin (Jamieson ER et al., 1999) and 1mM Hydroxyurea (Cortez D., 2003) for 0.5, 1, 1.5 and 2 hours. For determining the role of ATM kinase activity in this DDR induction, KU treatment was also performed along with the genotoxic agents to inhibit ATM activity. The resulting DDR activation with and without ATM inhibition was studied by examining pP53 levels following each treatment.

Immunocytochemical study of the cells grown on coverslips (Fig. 3.9a) as well as western blotting (data not shown) was performed for determining pP53 levels. For immunolabelling of pP53, Alexa fluor 568 conjugated secondary antibody was used (red fluorescence) after using pP53 S-15 primary antibody and the resulting immunofluorescence intensities were measured and normalized to the untreated controls (Fig. 3.9b) as described in materials and methods.

All the treatments resulted in pP53 induction which generally showed time dependent increase. While Dox induced pP53 levels were completely abrogated with KU treatment (Fig. 3.7 & 3.8), in case of the other chemo agents, addition of KU did not effectively reduce pP53 levels.

These results demonstrated ATM independent mechanism for DDR induction after treatments with these agents (3.9a & b). Secondly, while KU addition caused a change in the kinetics of pP53 induction, most notably at earlier time points, at 2 hr post-treatment of DNA damaging agents plus KU, the resulting pP53 level was almost comparable to that of the drug only treatment (without KU) (Fig. 3.9) demonstrating only a partial sensitivity of DDR induction towards ATM kinase inhibition.

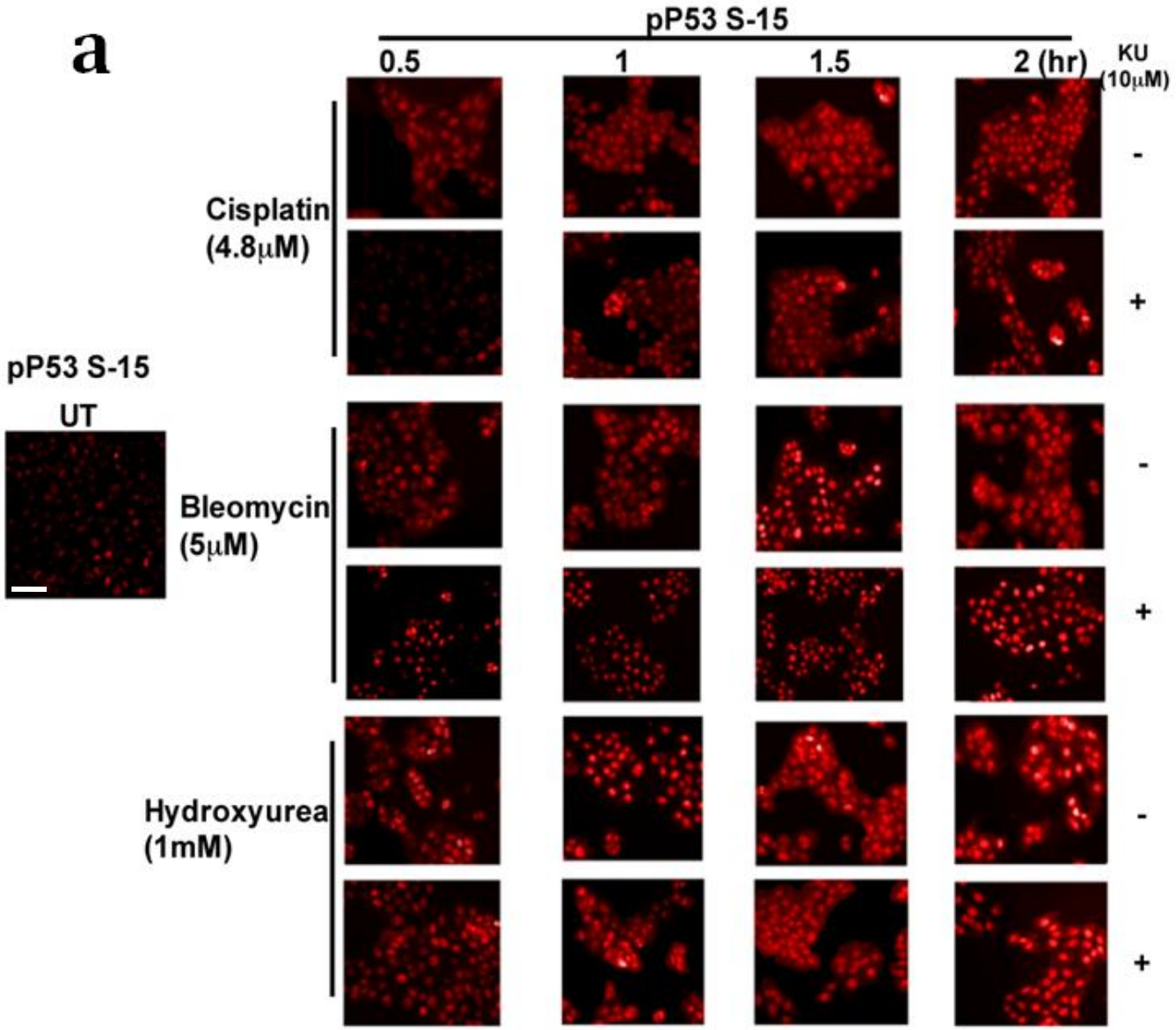
a
pP53 S-15
0.5
1
1.5
2 (hr)
KU (10μM)
Cisplatin (4.8μM)
-
+
pP53 S-15
UT
Bleomycin (5μM)
-
+
Hydroxyurea (1mM)
-
+

**b**

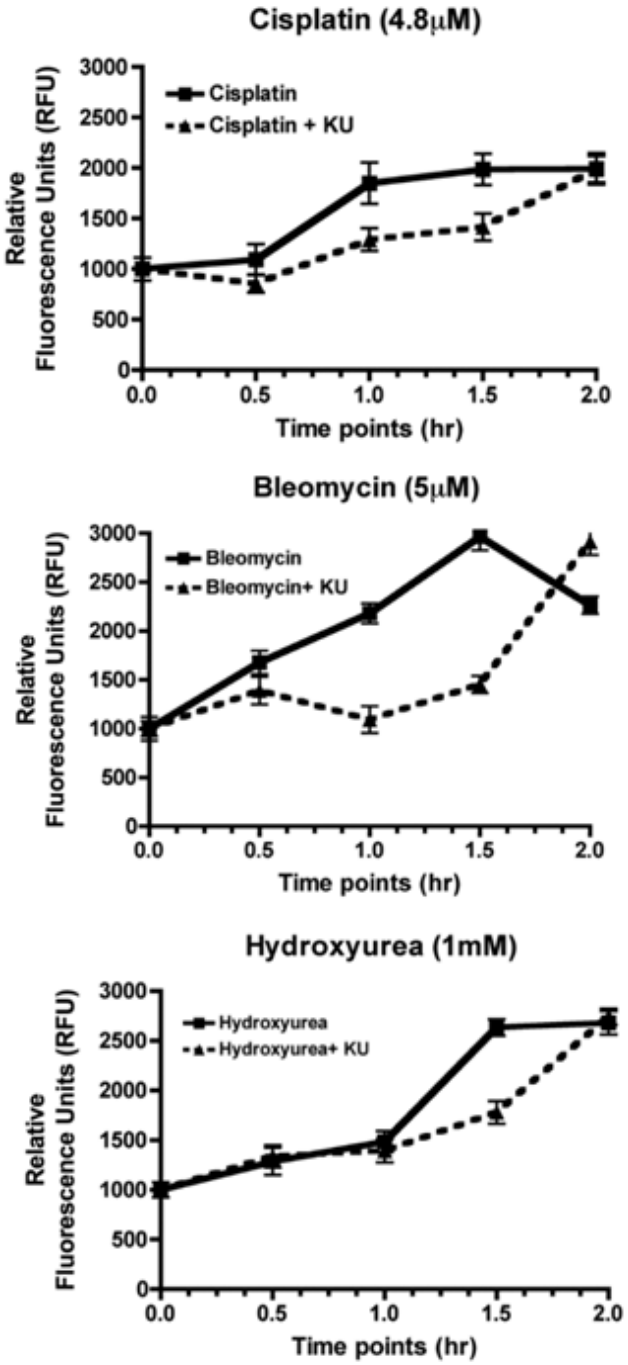
Cisplatin (4.8μM)
Cisplatin
Cisplatin + KU
Relative Fluorescence Units (RFU)
Time points (hr)
Bleomycin (5μM)
Bleomycin
Bleomycin+ KU
Relative Fluorescence Units (RFU)
Time points (hr)
Hydroxyurea (1mM)
Hydroxyurea
Hydroxyurea+ KU
Relative Fluorescence Units (RFU)
Time points (hr)

**Figure 3.9: DDR induced by other forms of DNA damage shows different degree of ATM dependence. (a)** MCF10 cells were seeded on poly L lysine coated coverslips placed in 12-well plate at a density of 1 x $10^5$ cells per well and grown until 70% confluent. Cells were serum starved for 48 hrs by incubating them in serum free media to synchronize them in G1 phase. Serum was added back and synchronized cells were either left untreated (UT), or treated with 4.8μM Cispatin, or 5μM Bleomycin or 1mM Hydroxyurea alone, or each with the addition of 10μM KU for 0.5, 1, 1.5 and 2 hr. Immunostaining was performed by using pP53 S-15 primary antibody and Alexa fluor 568® conjugated secondary antibody. These are representative images taken in different fields of view under 10x objective. Scale bar represents 100μm. **(b)** Graph representing fluorescence intensity measurements of phospho P53 S-15 immunofluorescence signal as generated by immunostaining in (a). The values are based on mean fluorescence intensities in 8 fields of views of each cover slip with minimum of 50 cells, captured with 10x objective with each treatment done in triplicates. All the fluorescence values were normalized to the fluorescence value of DAPI stain of the same image and further normalized to the untreated controls (UT).

## 3.4 Key findings and their significance

In the current study, it was found that ATM protein level underwent an induction following serum stimulation and a further increase at 4 hr post serum addition and that this alteration in protein level also had an impact on its signalling activity as determined by pATM levels, and the levels of its substrates E2F1 and pChk2 at the same time points. On the contrary, protein levels of P53 and pP53 underwent a transient reduction at 0.5 hr of serum stimulation but recovery to normal levels at later time points and again induction at 4 hr post serum induction consistent with ATM. At further time points post serum stimulation, minor protein changes in total ATM and pATM were found to occur mostly in the nuclear fraction. Importantly, it was found that damage induced by Dox primarily required a function of ATM kinase for DDR activation, in terms of pATM, pP53 and pChk2 signalling, at all the time points tested, whereas, DDR induced by other genotoxic agents did not require functional ATM kinase.

Determining cell cycle dependent changes in ATM and its downstream substrates is important in terms of timing the therapeutic inhibition regimes targeting ATM activity. Avoiding the inhibition regimes at time points where ATM activity is naturally high in the cell cycle can help reduce the concentration of inhibitors required and hence prevent off target effects of the inhibitor at higher concentrations. Also, the fact that Bleomycin, Hydroxyurea and Cisplatin induced DDR pathway was only partially sensitive to ATM inhibition, recovering fully at 2 hr time point, suggests that employing ATM inhibitors in combination with these drugs for achieving cellular sensitivity to genotoxic agents may be ineffective, as ATM independent mode of DDR pathway and P53 phosphorylation was resulted with such treatments.

# Chapter Four

# Inhibition of ATM kinase causes transient induction of its transcription and increase in its activity via a novel autoregulatory mechanism: Towards developing a novel cell-based ATM Kinase assay

Nothing is too wonderful to be true if it be consistent with the laws of nature.

Michael Faraday, Chemist and Physicist (1791 – 1867).

## 4.1 Abstract

*Increase in our understanding of the different signalling components involved in and responsible for DDR activation, and their associated mechanisms that govern cell-fate decisions have helped tremendously in conceptualising novel anti cancer strategies. While increased sensitivity of cancer cells towards genotoxic agents by way of inhibiting DDR proteins have been demonstrated in some instances, its complete molecular signalling outcome, impact on surrounding normal cells, and its off target effects are largely unknown. In this section of current research, I have discovered a new mechanism of ATM regulation independent of cell cycle. I have demonstrated that inhibition of ATM kinase activity causes induction of ATM protein followed by oscillation. This discovery of kinase dependent alteration in its own protein expression thus established a novel autoregulatory mechanism of ATM. This autoregulation was demonstrated in cell cycle independent manner and both in the absence and presence of DNA damage. Protein stability studies showed that upregulation of protein expression following kinase inhibition did not result from alteration of ATM half life. Studies of ATM promoter regulation in MCF10A cells further demonstrated that this autoregulatory expression mechanism was governed at the transcriptional level. Furthermore, this induction of ATM was also accompanied by a transient upregulation of P53, pATR and E2F1 levels. These new findings were finally utilised to develop luciferase reporter based biosensor of DNA damage based on ATM activity and fluorescence based ATM inhibition assay for its prospective utilisation in screening for ATM inhibitors. Since ATM inhibition is believed to sensitise cancer cells to genotoxic agents, this novel insight into the mechanism of ATM regulation is critical to consider while designing more precise strategies for modulation of ATM activity in cancer therapy.*

## 4.2 Introduction

In chapter three, it was demonstrated that ATM protein level fluctuates slightly during cell cycle progression and this variation in expression is also reflected in its activity downstream. In contrast, no significant change in its protein level was found after DNA damage at any time up to 8 hours. However, there was a rapid and time dependent rise in pATM S-1981 and other substrates of ATM following time dependent genotoxic treatment. Having established serum stimulation and cell cycle dependent regulation of ATM and its substrates, in this section, I wanted to research the regulatory consequences for ATM and its key DDR substrates following inhibition of ATM kinase activity.

As mentioned earlier, the importance of DDR pathway in influencing cellular responses to DNA damage and controlling cell-fate decision has increased significantly in the last decade. It is now known that modulation of DDR pathway generally, or ATM activity specifically can alter cellular sensitivity to genotoxic agents (Bolderson E et al., 2009). Careful manipulation of ATM activity provides for opportunity to achieve targeted cellular sensitivity. To this end, a variety of DDR inhibition strategies had been devised and tested (see table 4) with varying outcomes. Owing to the intricacy and high degree of cross-talk of signalling networks within eukaryotic cells, manipulation of DDR activity via small molecular inhibitors is expected to result in wide variety of signalling alteration. Hence, while employing any of DDR inhibitors, it is imperative to fully characterise its effects not only in terms of the activity of target molecule, but also on its transcriptional machinery, protein stability and finally downstream signalling.

Hence, in this section of research, I set out to investigate the effects of ATM kinase inhibition on its expression and localisation in order to characterise the role of its activity in monitoring its own protein levels as well as those of its substrates and in modulating transcription. Since chapter 3 demonstrated cell cycle dependent changes in level of ATM protein, non-synchronous cells were used in this section to rule out any cell cycle dependent modulation of ATM and study only the effects caused by ATM kinase inhibition.

## 4.3 Results

### *4.3.1 ATM protein levels are rapidly upregulated after inhibition of its kinase activity.*

In order to study effects of ATM kinase inhibition on its expression in a time dependent manner and to determine whether protein levels of total ATM are influenced by its own kinase activity, small molecular inhibitor of ATM, KU55933 was employed. Since previous chapter identified cell cycle dependent changes in ATM expression levels (section 3.3.1), to avoid such regulatory influence caused by cell cycle progression, this study was undertaken independent of cell cycle to study the regulatory effect on and consequences for total ATM levels caused only by inhibition of its kinase activity. To this end, unsynchronized MCF-10A were grown until 80% confluent and exposed to 10μM KU alone, or with addition of 0.5μMDox, this time to examine regulatory effects of these treatments on protein levels of total ATM. Protein lysates were collected at 0.5, 1, 1.5, 2, 3, 4 and 8 hours post treatment and processed for western blot analysis. The reason for using 10μM KU was based on the finding that this concentration efficiently blocked ATM kinase activity (Chapter 3 and Hickson I et al., 2004).

A striking finding was that the protein levels of total ATM showed rapid induction at 0.5 hr of KU treatment. Continuing the KU treatment further caused oscillation in total ATM levels between different time points (Fig. 4.1a). IOD analysis revealed that this rapid upregulation of ATM at 0.5 hr of KU treatment was 3 fold ($p<0.001$) as compared to the untreated controls (Fig. 4.1b). Furthermore, this transient upregulation and oscillation of ATM upon its kinase inhibition was also found to take place under DNA damage as well, as co-treatment with Dox along with KU still resulted in significant protein induction ($p<0.01$) (Fig. 4.1a & b).

This experiment revealed for the first time that ATM protein levels are influenced by its own kinase activity. Hence, this experiment not only discovered as yet unknown autoregulatory mechanism of ATM regulation, but the fact that inhibition of the kinase caused a rise in total ATM levels also demonstrated a negative feed-back mechanism of this autoregulation, independent of cell cycle. Additionally, while this novel mechanism also appeared to occur under DNA damaging conditions, it was found to be less pronounced under DNA damage (Fig. 4.1).

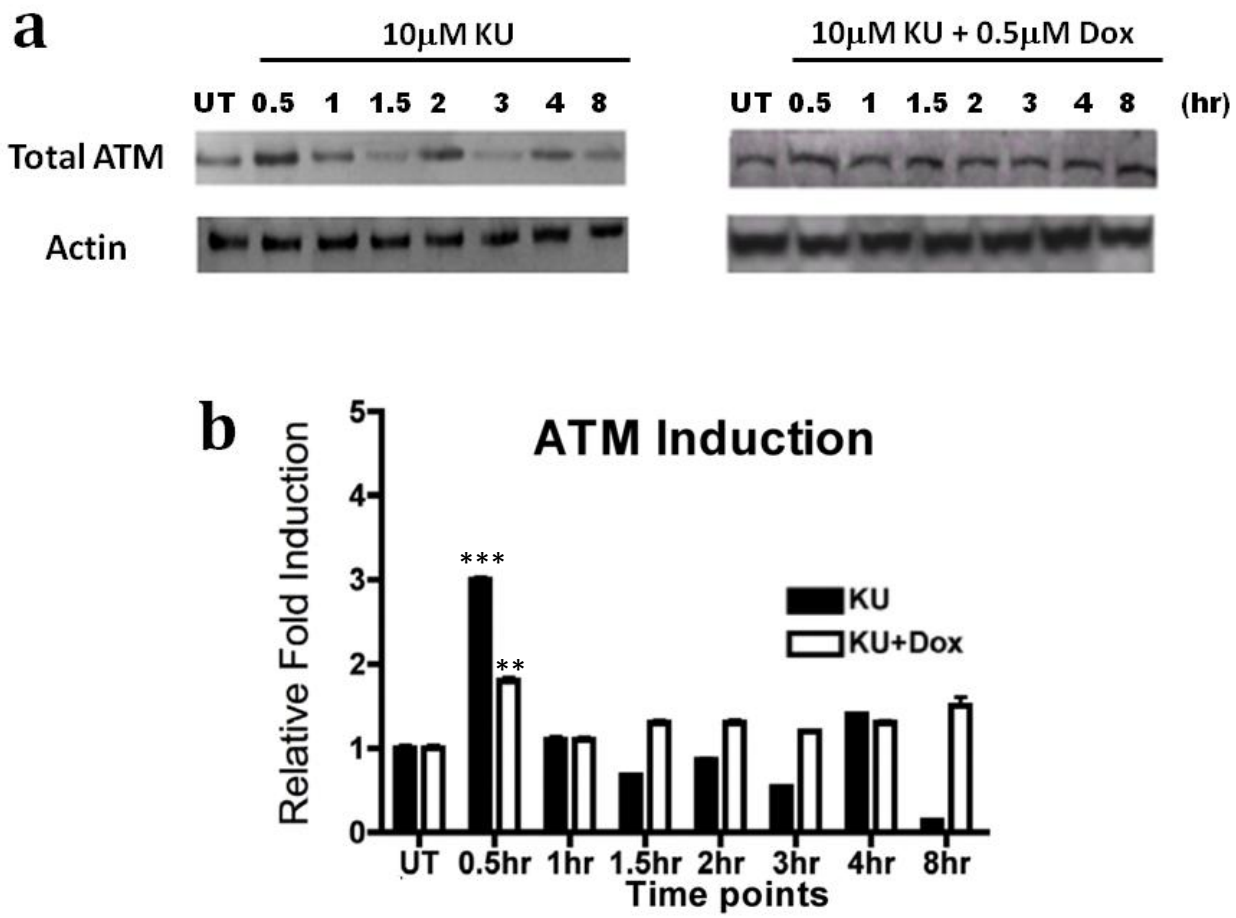


**Figure 4.1: Inhibition of ATM kinase causes a rapid transient up regulation followed by oscillation of total ATM protein levels.** MCF10A cells were seeded in 100mm tissue culture plates at a density of 2 x $10^6$ cells and grown until 80% confluent. Unsynchronized cells were either left untreated (UT) or treated with 10μM ATM kinase inhibitor, KU alone, or with the addition of 0.5μM Dox. Cell lysates were harvested at different time points of treatment as indicated and processed for immunoblotting for total ATM. 20μg of protein lysates were loaded in each well of SDS PAGE gels. **(a)** Immunoblotting result showing a transient induction in total ATM level at 0.5 hr of ATM kinase inhibition followed by oscillation in its levels. **(b)** Semi quantitative analysis of the Immunoblotting result in (a) by using integrated optical densitometry via Gelpro software. Data presented in all panels are the mean with standard error (bars) of n=3 independent experiments normalised to the untreated controls (UT) expressed as 1. For loading control, immunoblotting with Actin antibody was also performed.

To examine this induction at cellular level and to study its sub-cellular localisation, immunofluorescence studies were carried out on MCF10A cells by immunostaining total ATM levels in cells either left untreated, or treated for 0.5, 1, 1.5 and 2 hours with either 10μM KU alone, or KU plus 0.5μM Dox.

Figure 4.2 revealed that this KU induced upregulation was noticeable at cellular level as well and confirmed that both nuclear and cytoplasmic ATM exhibited a rise at this time point as compared to their untreated control counterparts.

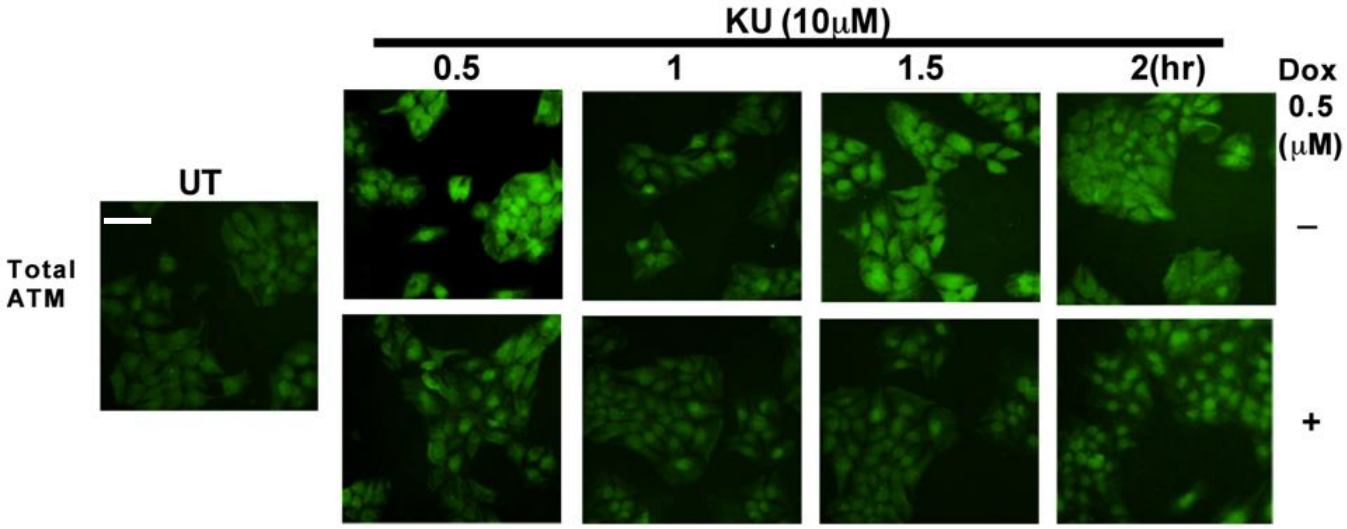


**4.2: ATM kinase inhibition induced upregulation of total ATM is evident at cellular level.** MCF10 cells were seeded on poly L lysine coated coverslips placed in 12-well plate at a density of 1 x $10^5$ cells per well and grown until 70% confluent. Cells were either left untreated (UT), or exposed to 10μM ATM kinase inhibitor KU alone, or with the addition of 0.5μM Dox for the indicated time points. Immunostaining was performed by using total ATM primary antibody with Alexa fluor 488® conjugated secondary antibody. These are representative images taken in different fields of view under 40x objective. Scale bar represents 40μm

### *4.3.2 Induction and oscillation in ATM protein expression following the inhibition of its kinase activity influence downstream ATM signalling.*

In order to further study whether KU induced ATM induction followed by oscillation has an impact on ATM signalling, downstream substrates of ATM as well as its functional partner pATR were also include in the experiment to examine their protein levels through immunoblotting after ATM kinase inhibition.

It is noteworthy to mention here that the previous results in figure 3.7 of chapter three demonstrated abrogation of pATM induction after KU alone and KU plus Dox treatment. However, in the same figure, pATM levels had shown a transient increase in signal at 0.5 hr post treatment with KU and KU plus Dox treatment and abrogation at later time points. This was also consistent for pP53 and pCHK2 at the same time point (Fig. 3.7) which interestingly coincided with the observed KU induced ATM upregulation observed here in Fig. 4.1. To study whether this upregulation of ATM substrates following KU treatment was cell cycle independent, and to rule out effects caused by serum stimulation, unsynchronized MCF10A cells were grown until 80% confluent, treated with 10μM KU alone or with the addition of Dox and cell lysates collected at the same time points as before and processed for western blot analysis. Strikingly, immunoblotting of these protein lysates (30μg) followed by IOD analysis revealed that pATM (> 2 fold) as well as total P53, total E2F1 and pATR showed an induction at 0.5 hr time point after either KU treatment (pATM 2-fold, $p<0.01$; P53 3-fold, $p<0.001$; E2F1 2-fold, $p<0.01$, pATR 1.7-fold) or KU with the addition of Dox (pATM >2fold, $p<0.01$; P53 >2-fold, $p<0.001$; E2F1 > 3-fold, $p<0.01$; pATR > 2-fold $p<0.01$), as compared to the untreated controls (Fig. 4.3a & b).

In cases of pATM and total P53, a part from induction at 0.5 hr time point of KU or KU plus Dox treatment, all the other time points showed lower protein levels than those of untreated controls.

The E2F1 signal, which also showed an initial transient induction at 0.5 hr time point of KU alone or KU plus Dox treatment, on the contrary, continued to increase after 2 hr of KU and Dox treatment demonstrating an ATM independent increase after Dox addition at later time points (Fig. 4.3a & b).

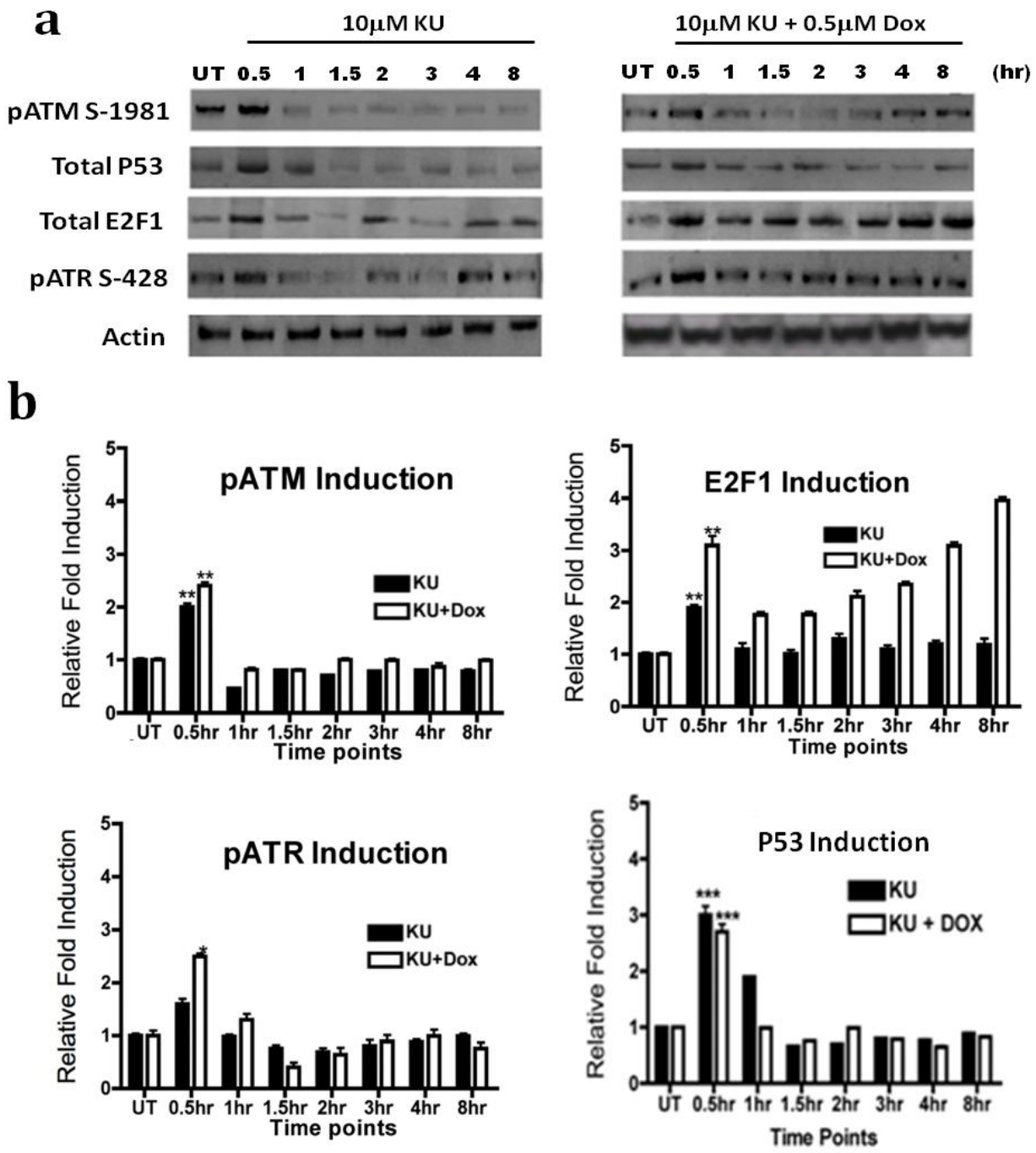


**Figure 4.3: Upregulation of ATM following ATM kinase inhibition is also accompanied by transient induction of pATM, pATR and its substrates P53 and E2F1.** MCF10A cells were seeded in 100mm tissue culture plates at a density of 2 x $10^6$ cells and grown until 80% confluent. Cells were either left untreated (UT), or exposed to 10μM of ATM kinase inhibitor KU alone or with the addition of 0.5μM Dox. Cell lysates were harvested at different time points of treatment as indicated and processed for immunoblotting for pATM S-1981, total P53, total E2F1, and pATR S-428. 30μg of protein lysates were loaded in each well of SDS PAGE gels. For loading control, Actin antibody was also included. **(a)** Immunoblotting result showing induction of pATM, pATR, P53 and E2F1 at 0.5 hr of either KU alone or KU and Dox treatment. **(b)** Semi quantitative analysis of the Immunoblotting result in (a) by using integrated optical densitometry via Gelpro software. Data presented in all panels are the mean with standard error (bars) of n=3 independent experiments normalised to the untreated controls (UT) expressed as 1.

In order to further characterise this KU induced upregulation at a cellular level, immunofluorescence examination of MCF10A cells, grown on coverslips until 70% confluent, were performed and cells were either left untreated, or treated for 0.5, 1, 1.5 and 2 hours with 10μM KU alone, or with the addition of 0.5μM Dox. After treatment, immunostaining of pATM as well as E2F1 (as it showed the highest induction at 0.5 hr with KU plus Dox) was carried out to examine their protein levels. Immunocytochemical studies revealed that the KU induced upregulation of pATM and E2F1 could be demonstrated at cellular level as well (Fig. 4.4). Furthermore and interestingly, at 0.5 hr of KU alone or KU and Dox treatment, there was a very noticeable upregulation only in the nuclear compartment of E2F1 (Fig. 4.4, E2F1 panel). Additionally, there was a reduction in E2F1 level at 1 and 1.5 hr treatment followed by a rise at 2 hr post treatment in KU and Dox treated cells fitting well with the western blot result in Fig. 4.3. However, in KU only treatment, a sustained lower level after the initial spike at 0.5 hr time point was seen.

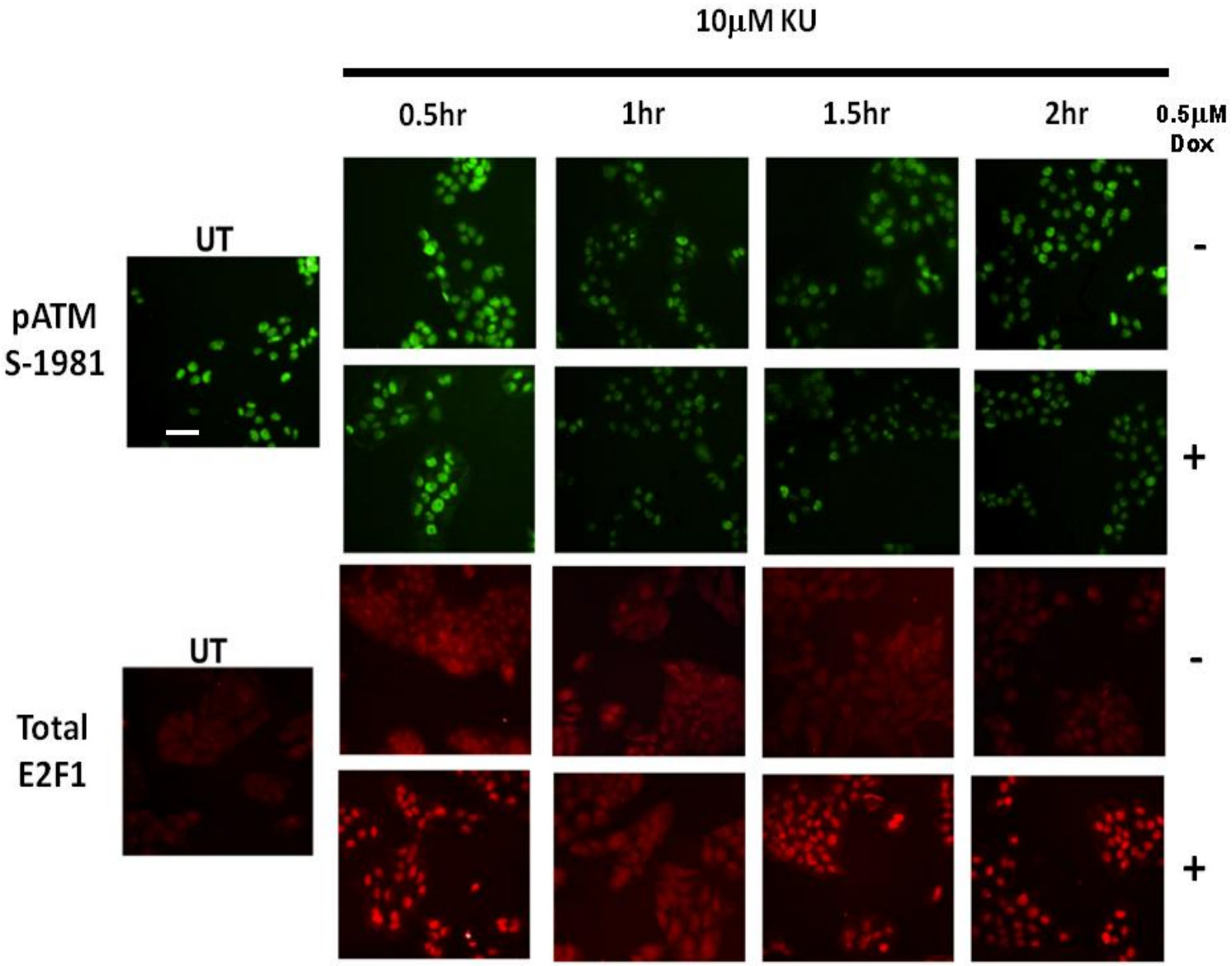


**Figure 4.4: ATM kinase inhibition induced upregulation of E2F1 and pATM is evident at cellular level.** MCF10 cells were seeded on poly L lysine coated coverslips placed in 12-well plate at a density of 1 x $10^5$ cells per well and grown until 70% confluent. Cells were either left untreated (UT) or exposed to 10μM ATM kinase inhibitor KU alone, or with the addition of 0.5μM Dox for the indicated time points. Immunostaining was performed by using pATM S-1981 primary antibody with Alexa fluor 488® conjugated secondary antibody and E2F1 primary antibody with Alexa fluor 568® conjugated secondary antibody. These are representative images taken in different fields of view under 40x objective. Scale bar represents 40μm.

In order to confirm the nuclear upregulation of E2F1 observed in Fig. 4.4 following KU or KU plus Dox treatment, MCF10A cells grown in 10 cm tissue culture plates were treated in the same manner as above and the protein lysates were prepared as nuclear (Nuc) and cytoplasmic (Cyt) fractions. The quality of these fractions was determined by slot blotting for specific nuclear and cytoplasmic protein markers (Appendix-I, section A1.8). Western blotting results of these sub-cellular protein lysates confirmed a distinct nuclear upregulation of E2F1 and pATM at 0.5 hr time point (Fig. 4.5) with the levels at other time points also consistent with those seen in Fig. 4.3 and 4.4.

To rule out the possibility of KU inducing direct DNA damage and thus resulting in the observed pATM, pATR and E2F1 upregulation, cells were treated with the same concentration of KU for different time points and blotted for γH2AX (a biomarker of DNA damage). It was confirmed that KU treatment alone did not cause any DNA damage (Figure 4.6).

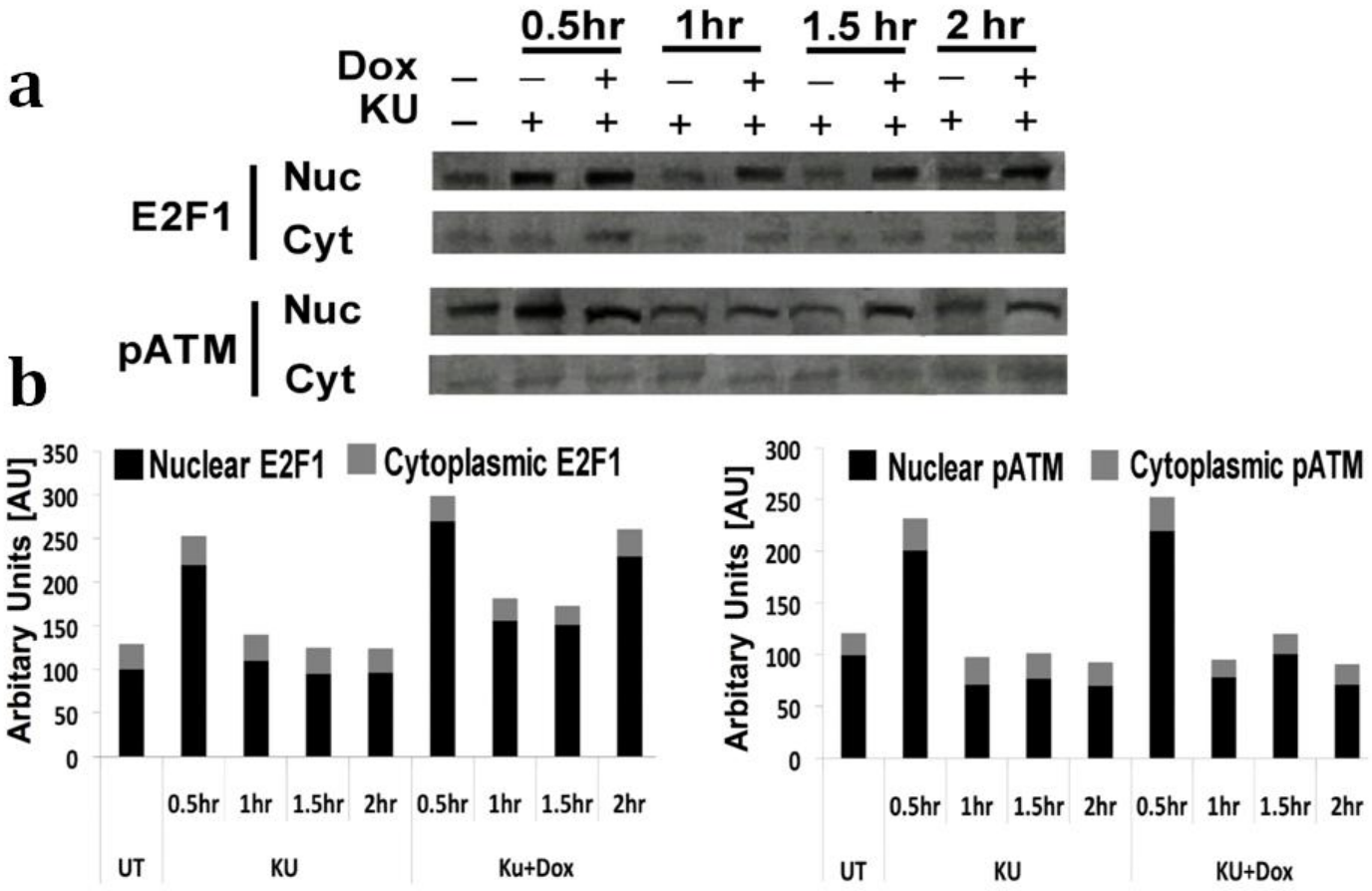


**Figure 4.5: ATM kinase inhibition causes nuclear upregulation of E2F1.** MCF10A cells were seeded in 100mm tissue culture plates at a density of 2 x $10^6$ cells and grown until 80% confluent. Cells were either left untreated (UT), or exposed to 10μM of ATM kinase inhibitor KU alone or with the addition of 0.5μM Dox. Cell lysates were harvested at different time points of treatment as indicated and their nuclear (Nuc) and cytoplasmic (Cyt) protein fractions were prepared as described in materials and methods section and blotted for pATM S-1981 and total E2F1. 30μg of protein was loaded in each well of SDS PAGE gel. The quality of sub-cellular fractions were determined by blotting for Rb (Nuclear protein) and Actin (Cytoplasmic protein) shown in Appendix-I, section A1.8. **(a)** Immunoblotting result showing nuclear induction of E2F1 and pATM following ATM kinase inhibition. **(b)** Semi quantitative analysis of the Immunoblotting result in (a) by using integrated optical densitometry via Gelpro software. Data presented in all panels are the mean with standard error (bars) of n=3 independent experiments normalised to the untreated controls (UT) expressed as 1.

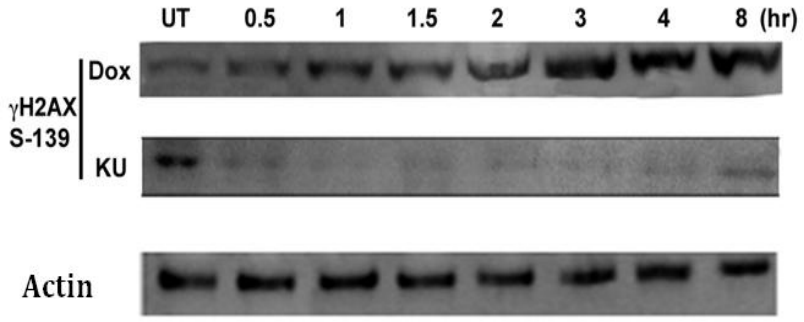


**Figure 4.6: KU induced upregulation of DDR protein is not caused by DNA damage.** MCF10A cells were seeded in 100mm tissue culture plates at a density of 2 x $10^6$ cells and grown until 80% confluent. Cells were either left untreated (UT), or exposed to 10μM of ATM kinase inhibitor KU 0.5μM Dox. Cell lysates were harvested at different time points of treatment as indicated and processed for immunoblotting for γ-H2AX to determine DNA damage. 30μg of protein lysates were loaded in each well of SDS PAGE gels. For loading control, immunoblotting with Actin antibody was also performed.

Taken together, these results demonstrated that KU induced upregulation of ATM protein caused a concomitant increase in pATM levels and this upregulation was also accompanied by a rise in P53, pATR and nuclear E2F1 levels, while KU treatment alone did not cause any DNA damage.

### *4.3.3 Upregulation of ATM protein following the inhibition of its kinase activity does not result from alteration in ATM protein stability.*

Next, I set out to determine the source of this KU induced ATM oscillation following upregulation. One reason for this could be through alteration in protein stability or degradation pathways. To find this, MCF10A cells were grown up to 80 % confluence and chased in presence of 50μM Cycloheximide, an inhibitor of protein synthesis machinery. Following this, cells were either left untreated or further treated with 0.5μM Dox, to study if ATM activation following DNA damage also stabilises ATM, or with 10μM KU to determine if the observed protein induction results from changes in protein half life. Protein lysates were collected after 0.5, 2, 4, 6 and 8 hours of treatment and subjected to immunoblotting.

It was revealed that neither DNA damage nor KU treatment resulted in any variation in protein stability of ATM as determined by the immunoblotting signals, which underwent reduction through time at the same rate as cycloheximide treatment alone revealed by IOD analysis (Fig. 4.6). This confirmed that the induction of ATM protein (Fig. 4.1) is not caused by protein stability changes and may be regulated through transcriptional machinery governing the expression of ATM gene.

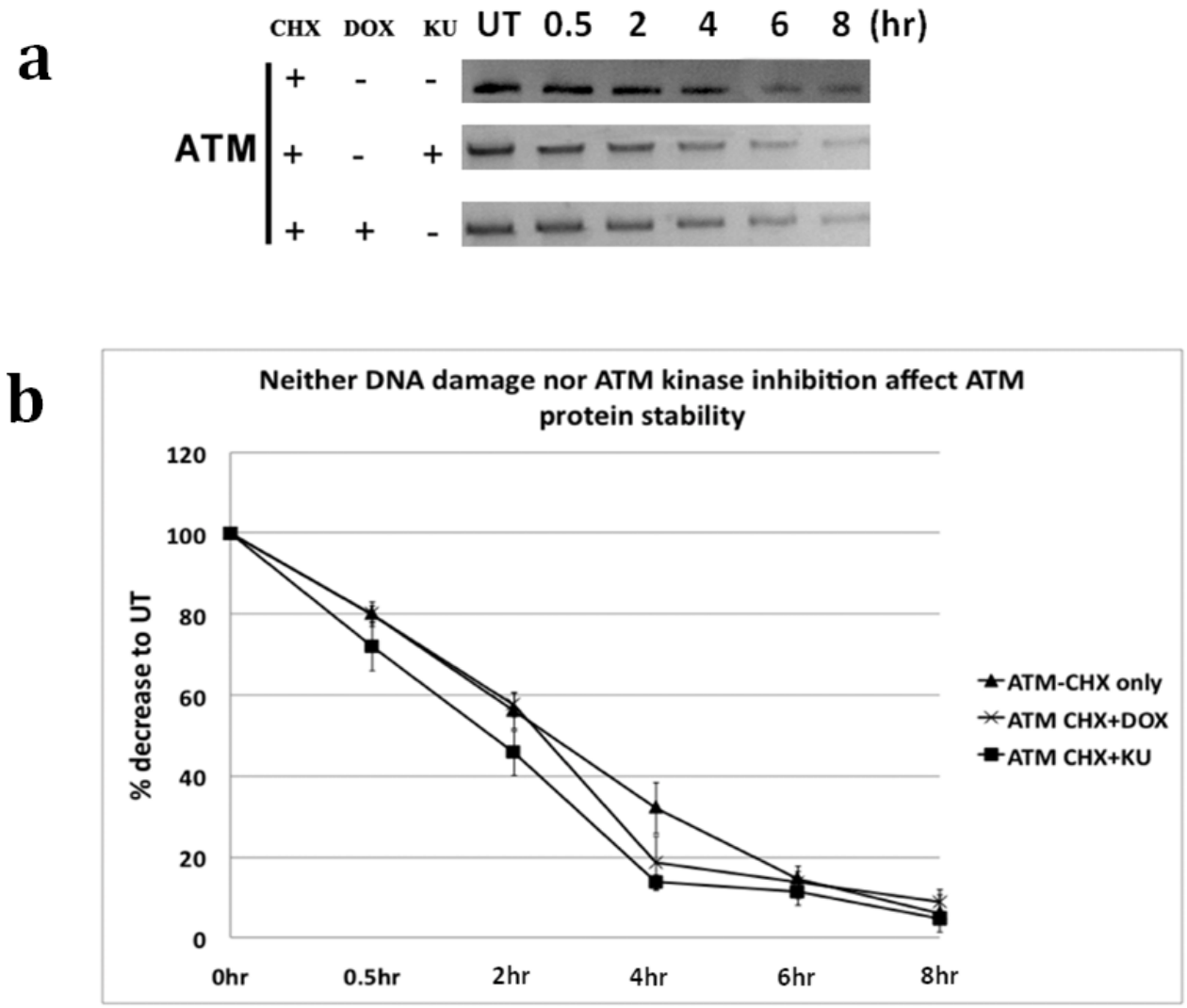


**Figure 4.7: ATM protein stability does not change after treatment with its Kinase inhibitor or DNA damaging agent.** MCF10A cells were seeded in 100mm plates at a density of 2 x $10^6$ cells and grown until 80% confluent and treated with either 100μM cycloheximide or 100μM cycloheximide followed by treatment with either 10μM KU or 0.5μM Dox for different time periods as indicated. Cycloheximide treatment was always 1 hr prior to other treatments. Cells lysates were harvested and processed for immunoblotted for Total ATM. **(a)** Immunoblotting of total ATM after CHX treatment shows similar rates of protein reduction after no treatment, 10μM KU or 0.5μM Dox demonstrating no alteration in protein stability after these treatments. **(b)** Semi quantitative analysis of the Immunoblotting result in (a) by using integrated optical densitometry via Gelpro software. Data presented in all panels are the mean with standard error (bars) of n=3 independent experiments normalised to the untreated controls (UT) expressed as 100%.

### *4.3.4 ATM protein induction and oscillation after inhibition of its kinase activity results from alteration in its transcriptional regulation suggestive of an autoregulatory feedback loop via promoter regulation.*

In the past, several researchers have suggested a transcriptional mode of ATM regulation apart from its phosphorylational autoregulation (Clyde RG et al., 2009, Gueven N et al., 2003 & 2006, Khalil HS et al., 2011 & 2012, Savitsky, K., et al., 1997). In the previous sections, I demonstrated a novel autoregulatory feature of ATM expression at the protein level which did not seem to result from alteration in protein stability. Hence, this mechanism suggested transcriptional regulation of ATM. If indeed this oscillation resulted from its transcriptional regulation, this could possibly mean that ATM promoter may be governing these alterations and as such, an ATM promoter assay would be ideal strategy to answer this and elucidate fully the source of this mechanism.

Hence, in order to confirm transcriptional regulation of ATM, I carried out promoter studies of ATM gene by cloning the ATM promoter and designing luciferase based as well as fluorescence based ATM promoter assays. The promoter region of ATM was based on Byrd PJ et al., 1996. The sequence of the ATM promoter and its *cis*-regulatory elements are listed in Appendix-I (A1.1.3).

These reporter assays were generated, transfected into MCF10A cells, treated with different experimental conditions and further processed based on the type of reporter assay. Output signals of promoter activity were recorded which indicated relative rates of transcription from the promoter and hence established a quantitative basis of analysis of ATM gene expression. This allowed me to characterise the transcriptional regulation of ATM under different conditions and most importantly, under kinase inhibited state to determine the basis for oscillatory behaviour of ATM protein after 0.5 hr KU treatment.

#### *4.3.4.1. Constitutive ATM promoter activity.*

For Dual luciferase reporter assay, first of all, MCF10A cells grown in 24-well plates were transfected with either empty PGL3 vector, or PLG3 vector containing ATM promoter cloned upstream of Luc gene (ATMpr/PGL3). In both the cases, co-transfection with pRL-CMV vector was carried out as an internal control. 18 hr after transfection, dual luciferase reporter assay was performed as in materials and methods and readings were recorded in the luminometer (Modulus template® Turner Biosystem). Normalizations were performed first by the values of internal control pRL-CMV, and then to that of empty PGL3 vector. Figure 4.8 shows the constitutive activity of ATMpr/PGL3 in respect to empty vector and demonstrates its working order.

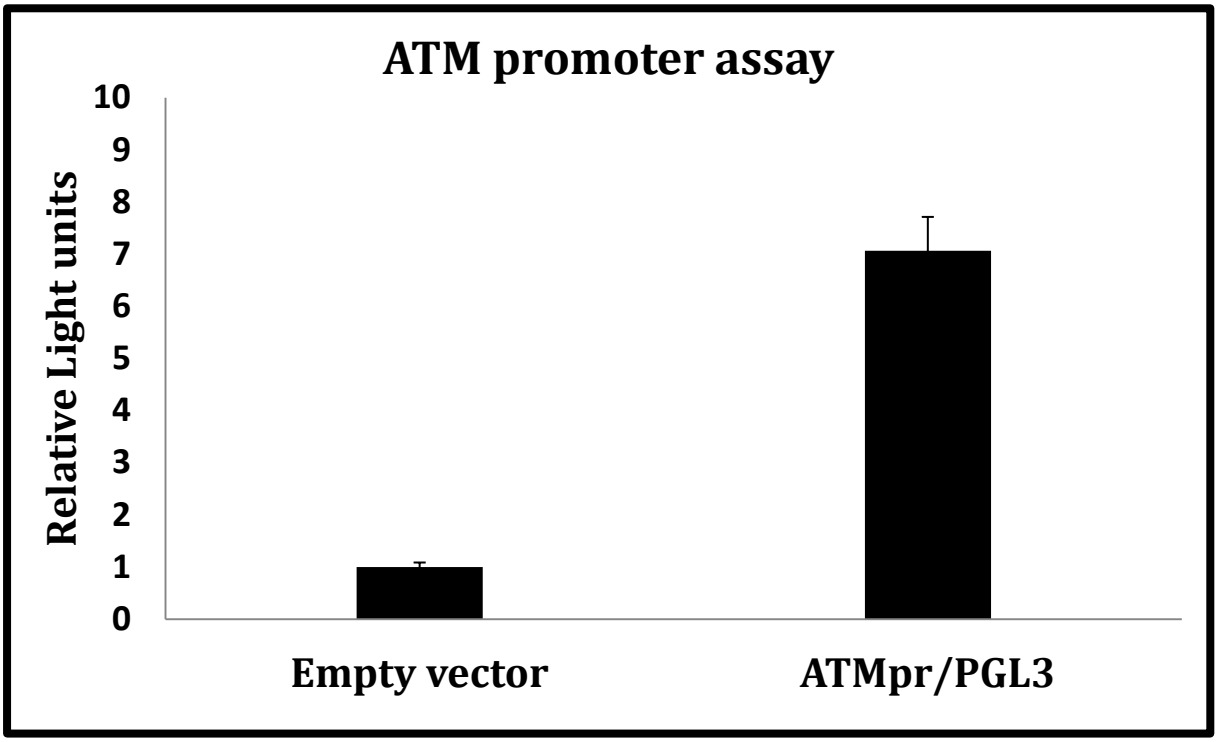


**Figure 4.8: Constitutive ATM promoter activity based on Luciferase reporter assay.** MCF10 cell line was seeded in 24 well plates at a density of 5 x $10^4$ and allowed to grow until 70% confluent. Cells were either transfected with 0.5µg of empty PGL3 basic vector (promega) or 0.5µg of ATMpr/PGL3 using 0.1µg of pRL-CMV (Renilla Luciferase) as an internal transfection efficiency control as described in materials and methods. After 16 hrs of transfection, protein lysates were prepared and transferred in quadruplets to 96 well opaque plates to measure Luciferase activity in luminometer (Modulus template® Turner biosystems) using Dual luciferase reporter assay kit (Promega). Data are the means and standard error (bars) of n=3 independent transfections, for which, each reading was taken in quadruplets. Mean luminescence values were first normalized to the values of Renilla luciferase and then to empty vector expressed as 1.

***4.3.4.2: DNA damage does not cause induction of ATM transcription.***

Since previous literature has mixed reports regarding the transcriptional regulation of ATM upon DNA damage (Brown KD et al., 1997, Hirai Y et al., 2001), I next set out to determine whether activation of DDR signalling upon treatments with DNA damaging agents, apart from causing post transcriptional modification (autophosphorylation) of ATM, also causes any change in ATM transcription in MCF10A cell line. To determine this, cells were transfected with ATMpr/PGL3 reporter and treated with 0.5μM Dox, or 4.8μM Cisplatin or 5μM bleomycin or 1mM hydroxyurea. Treatments were done for 1 hr and luciferase assay was performed as mentioned in materials and methods.

It was found that treatment with these agents for 1 hr did not cause any significant change in ATM transcription (Fig. 4.9) in the cultured MCF10A cells. Hence, it was concluded that the activation of ATM after multiple genotoxic treatments is not accompanied by a rise in ATM transcription (Fig. 4.9).

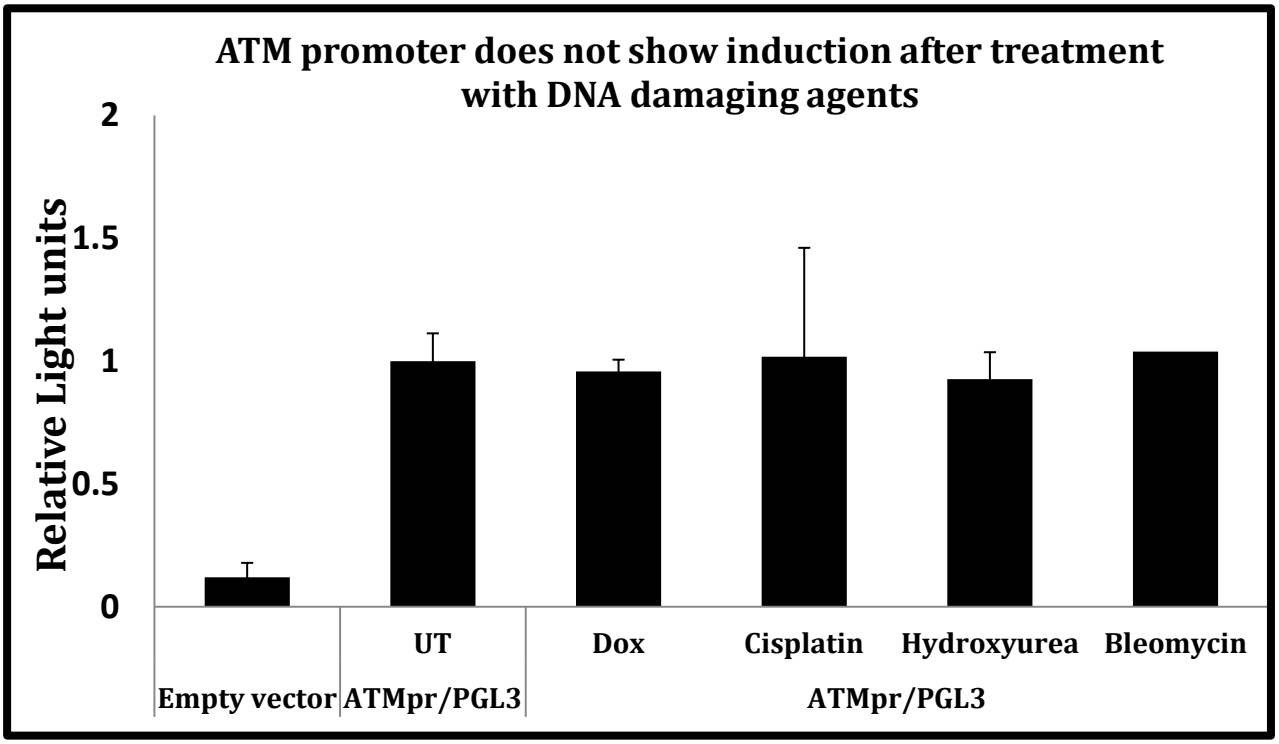


**Figure 4.9: DNA damage does not cause induction of ATM transcription.** MCF10 cell line was seeded in 24 well plates at a density of 5 x $10^4$ and allowed to grow until 70% confluent. Cells were either transfected with 0.5µg of empty PGL3 basic vector (promega) or 0.5µg of ATMpr/PGL3 using 0.1µg of pRL-CMV (Renilla Luciferase) as an internal transfection efficiency control as described in materials and methods. After 16 hrs of transfection, cells were either left untreated, or treated with 0.5µM Dox, or 4.8µM Cisplatin, or 1mM Hydroxyurea or 5µM Bleomycin for 1 hr. After treatments, protein lysates were prepared and transferred in quadruplets to 96 well opaque plates to measure Luciferase activity in luminometer (Modulus template® Turner biosystems) using Dual luciferase reporter assay kit (Promega). Data are the means and standard error (bars) of n=3 independent transfections, for which, each reading was taken in quadruplets. Mean luminescence values were first normalized to the values of Renilla luciferase and then to untreated ATMpr/PGL3 (UT) expressed as 1.

### *4.3.4.3: Luciferase based ATM promoter assay reveals that ATM induction and oscillation after its kinase inhibition is governed at transcriptional level.*

To answer the important question of whether the KU induced upregulation of ATM followed by oscillation is a mechanism caused at the transcriptional level governed through promoter activity, MCF10A cells were transfected either with empty vector or with ATMpr/PGL3 reporter construct and exposed to ATM inhibitor to test this. Treatment was performed in a time course manner with 10μM KU for 0.25, 0.5, 1, 1.5, 2, 3, 4 and 8 hour time points and the resulting promoter responses were quantified by performing dual luciferase assay as mentioned in materials and methods. A striking finding was that after KU treatment, >4 fold induction ($P<0.001$) was observed in the promoter signal at 0.25 hr post treatment (Fig. 4.10). Furthermore, it was observed that after the initial spike at 0.25 hr, the promoter signal showed an oscillatory pattern, reminiscent of the oscillations observed in protein levels of ATM after KU treatment (Fig. 4.1). A part from the initial induction, the values of this oscillation were fluctuating around those of the untreated controls (Fig. 4.10).

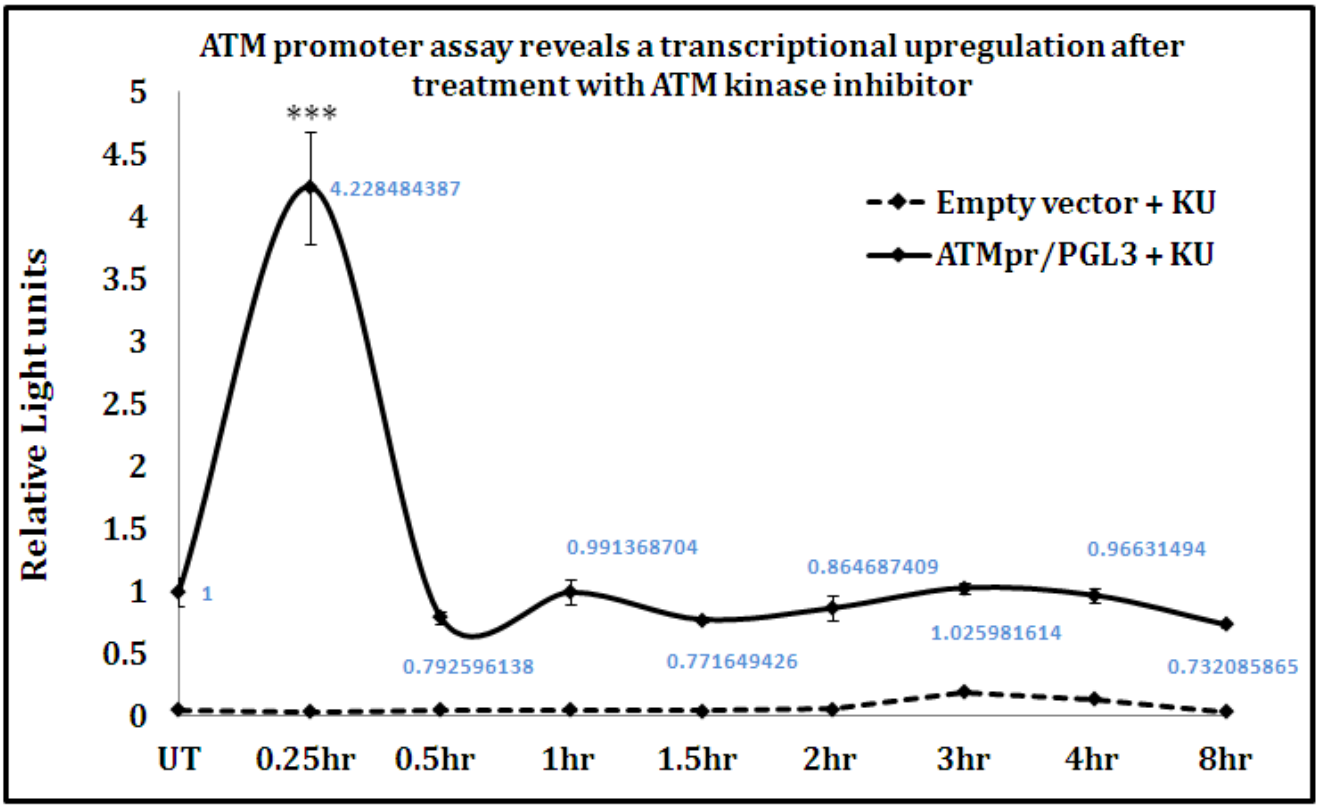


**Figure 4.11: ATM kinase inhibition causes upregulation followed by oscillation of ATM transcription.** MCF10 cell line was seeded in 24 well plates at a density of 5 x $10^4$ and allowed to grow until 70% confluent. Cells were either transfected with 0.5µg of empty PGL3 basic vector (promega) or 0.5µg of ATMpr/PGL3 using 0.1µg of pRL-CMV (Renilla Luciferase) as an internal transfection efficiency control as described in materials and methods. After 16 hrs of transfection, cells were either left untreated, or treated with 10µM KU for the indicated time points. After treatments, protein lysates were prepared and transferred in quadruplets to 96 well opaque plates to measure Luciferase activity in luminometer (Modulus template® Turner biosystems) using Dual luciferase reporter assay kit (Promega). Data are the means and standard error (bars) of n=3 independent transfections, for which, each reading was taken in quadruplets. Mean luminescence values were first normalized to the values of Renilla luciferase and then to untreated ATMpr/PGL3 (UT) expressed as 1 with statistical significance calculated according to the scale (* P<0.05, **P<0.01, ***P<0.001).

Treatment with 0.5μM Dox plus KU also resulted in up to 2 fold induction of promoter signal ($P<0.01$). Furthermore, while treatment with Dox alone did not cause any major transcriptional perturbation, at 0.25 hr time point, the promoter signal showed a slight reduction. Hence it appears that while ATM inhibition causes a rise it its expression, its activation on the contrary caused a slight reduction (Fig. 4.11).

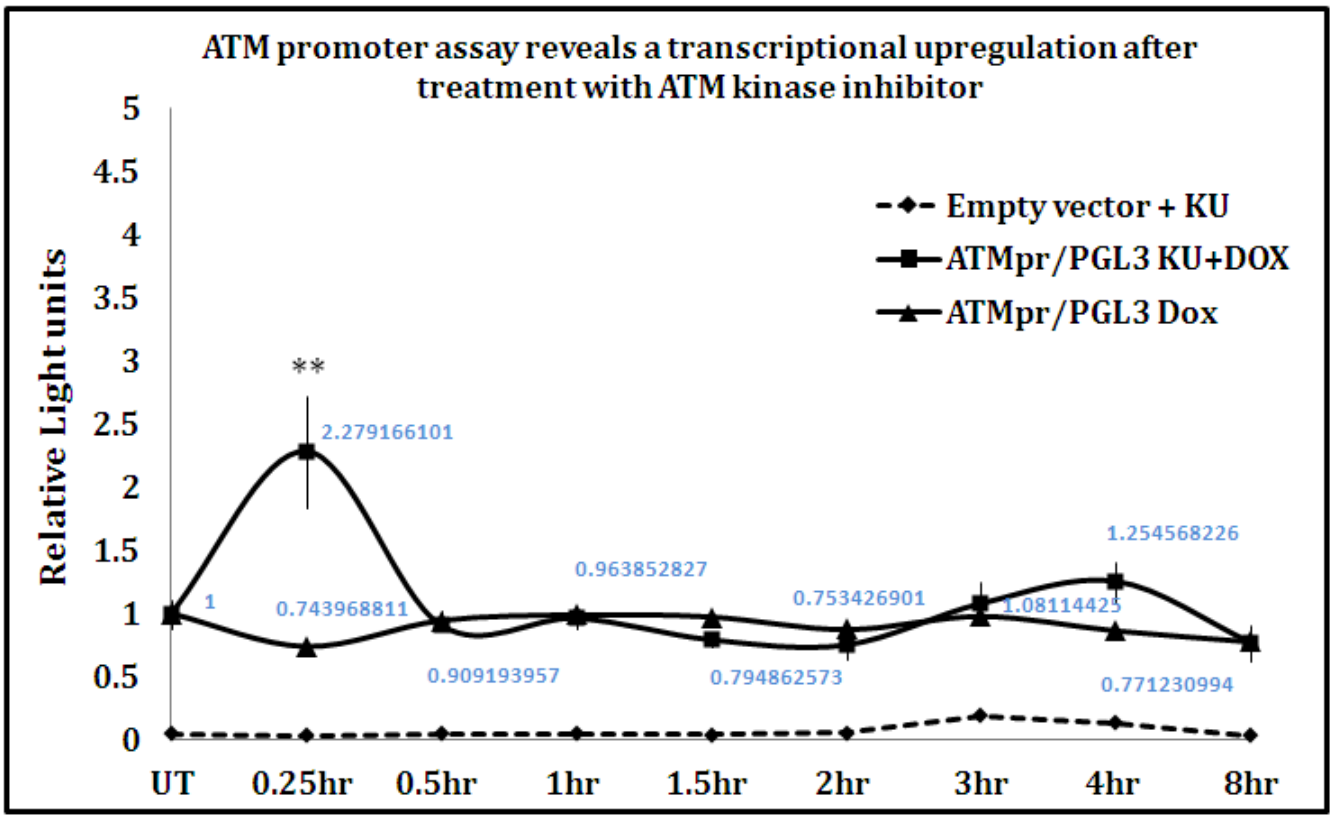


**Figure 4.11: ATM kinase inhibition causes upregulation of ATM transcription during DNA damage.** MCF10 cell line was seeded in 24 well plates at a density of 5 x $10^4$ and allowed to grow until 70% confluent. Cells were either transfected with 0.5µg of empty PGL3 basic vector (Promega) or 0.5µg of ATMpr/PGL3 using 0.1µg of pRL-CMV (Renilla Luciferase) as an internal transfection efficiency control as described in materials and methods. After 16 hrs of transfection, cells were either left untreated, or treated with 10µM KU and 0.5µM Dox for the indicated time points. After treatments, protein lysates were prepared and transferred in quadruplets to 96 well opaque plates to measure Luciferase activity in luminometer (Modulus template® Turner biosystems) using Dual luciferase reporter assay kit (Promega). Data are the means and standard error (bars) of n=3 independent transfections, for which, each reading was taken in quadruplets. Mean luminescence values were first normalized to the values of Renilla luciferase and then to untreated ATMpr/PGL3 (UT) expressed as 1 with statistical significance calculated according to the scale (* P<0.05, **P<0.01, ***P<0.001).

These experiments not only confirmed a transcriptional mechanism of the novel ATM autoregulation, but also provided the basis for developing a cell-based ATM kinase inhibition assay. According to these results, any successful inhibitor of ATM would give rise to a transient spike in ATM transcription. If that transcriptional induction could be detected and quantified, as illustrated in these experiments, a library of potential ATM inhibitory compounds could be screened. Any compound giving rise to the characteristic spike in ATM transcription could be a potential ATM inhibitor and qualified for further analysis. On the other hand, ATM activation induced by DNA damage caused a slight and rapid down-regulation of ATM transcription supporting the value of this assay to be employed as a biosensor of DNA damage, where a decreased signal at precise time point indicates DNA damage.

#### *4.3.4.4 Cell based Fluorescent reporter assay of ATM activity.*

After the successful illustration of this novel autoregulatory mode of ATM regulation at a transcriptional level, I further set out to utilize this mechanism for creating a novel cell-based ATM kinase assay that could be used to assay ATM inhibitors or act as a biosensor of DNA damage. In order to develop this assay, P-Timer1 fluorescent reporter vector (Clonetech) was used. The P-Timer1 fluorescent reporter uses a mutant form of Ds Red fluorophore having two amino acid substitutions, as a result of which, this fluorophore has unique spectral properties. Once the fluorophore is expressed by a test promoter, it emits green fluorescence, but as the protein matures, it incurs some conformational changes shifting its emission to longer wavelength and emits red fluorescence (Terskikh A et al., 2000).

I cloned the promoter region of ATM as used in the Luciferase assay in P-Timer1 (ATMpr/PTimer, see Appendix-I section A1.1 for clonal data) with of the following objectives:

**i)** To test if transcriptional induction of ATM promoter after ATM kinase inhibition can give rise to increased cellular fluorescence observable under microscope.

**ii)** To examine the induction followed by rapid reduction of transcription by means of time dependent spectral changes of fluorescence whereby a higher green fluorescence would indicate an ongoing transcription while reduction in green and concomitant increase in red fluorescence would indicate a halt in the transcription.

**iii)** To demonstrate this autoregulatory mechanism of ATM at single cell level and hence provide grounds for its potential for use in a cell based reporter assay for ATM kinase inhibition or as a biosensor of DNA damage.

Hence, this fluorophore, expressed under the control of ATM promoter was tested for the efficiency, timing and characterization of promoter activity after KU treatment. MCF10A cells were seeded on poly-L lysine coated cover-slips placed in 60mm tissue culture plates and grown until 70% confluent. The cells were transfected with ATMpr/P-Timer reporter. After 24 hr of transfection, cells were treated with 10μM KU for 0.5, 2 and 4 hr, after which, the cover-slips with cells were further processed as mentioned in materials and methods and observed under microscope for the measurement of relative fluorescence. Both the green and the red fluorescence intensities of ATMpr/PTimer expressing cells were measured with ImageJ software (see materials and methods).

In an untreated state, the green and red fluorescence had similar level of expression and hence comparable intensities, and as such giving rise to yellow staining pattern following superimposition of the two images (Fig. 4.12a).

It was found that after 0.5 hr of KU addition, an almost 4 fold increase ($p<0.001$) in green fluorescence occurred. The red fluorescence on the other hand, was still moderate at about half the fluorescence of green at that time point, but greater than its fluorescence in the untreated sample, suggesting a recent induction in transcription in ATMpr/PTimer1 expressing cells (Fig. 4.12 a & b). At a further time point of 2 hr, there was an increased red fluorescence signal and a reduced green fluorescence, suggesting a halt in transcription and the pre-existing green fluorophore maturing into red (Fig. 4.12). After that, at 4 hr time point, the green fluorescent signal appeared to have recovered to a higher intensity which equalled that of the red, suggesting a steady state expression (Fig. 4.12).

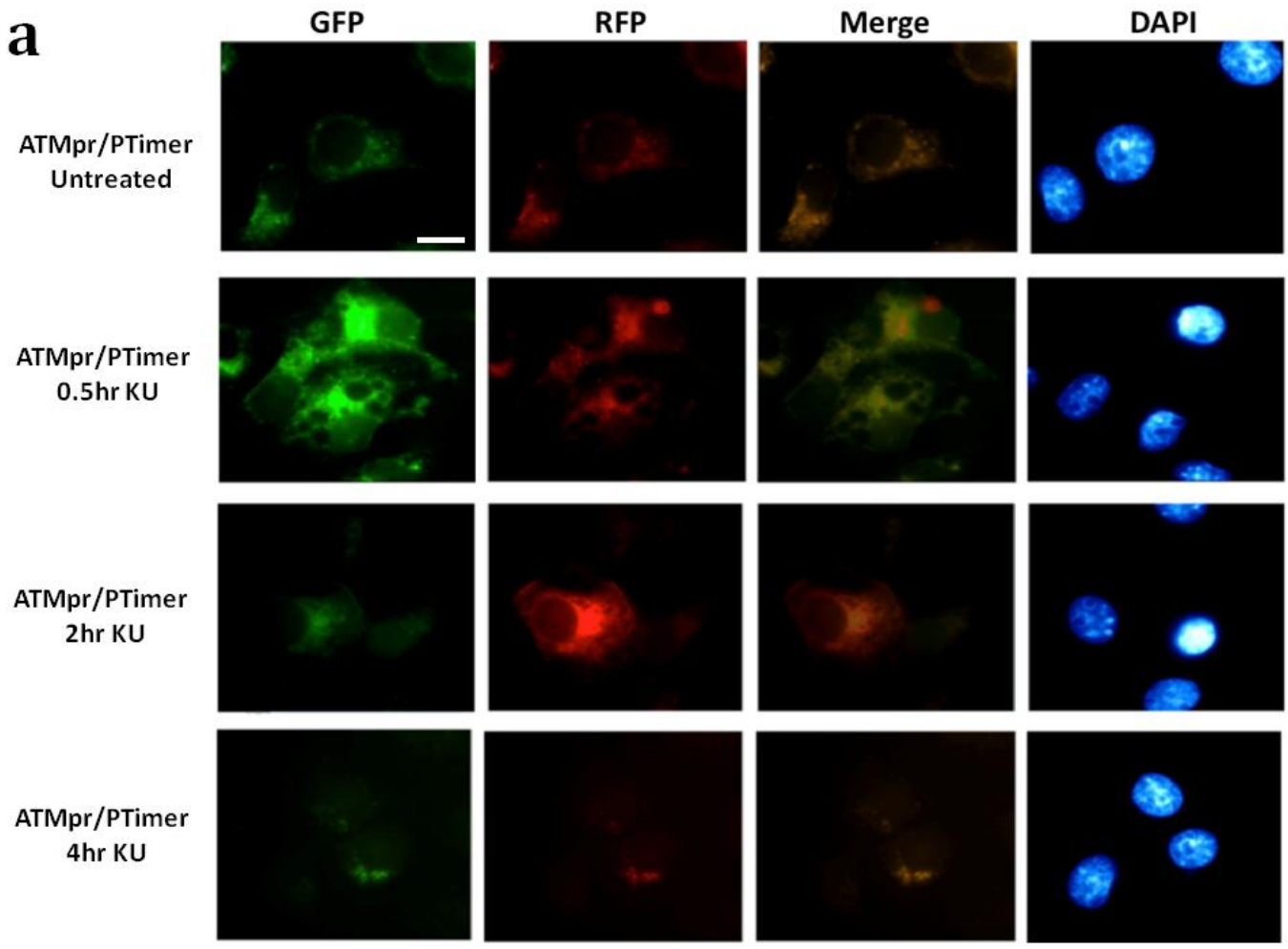
a
GFP
RFP
Merge
DAPI
ATMpr/PTimer
Untreated
ATMpr/PTimer
0.5hr KU
ATMpr/PTimer
2hr KU
ATMpr/PTimer
4hr KU

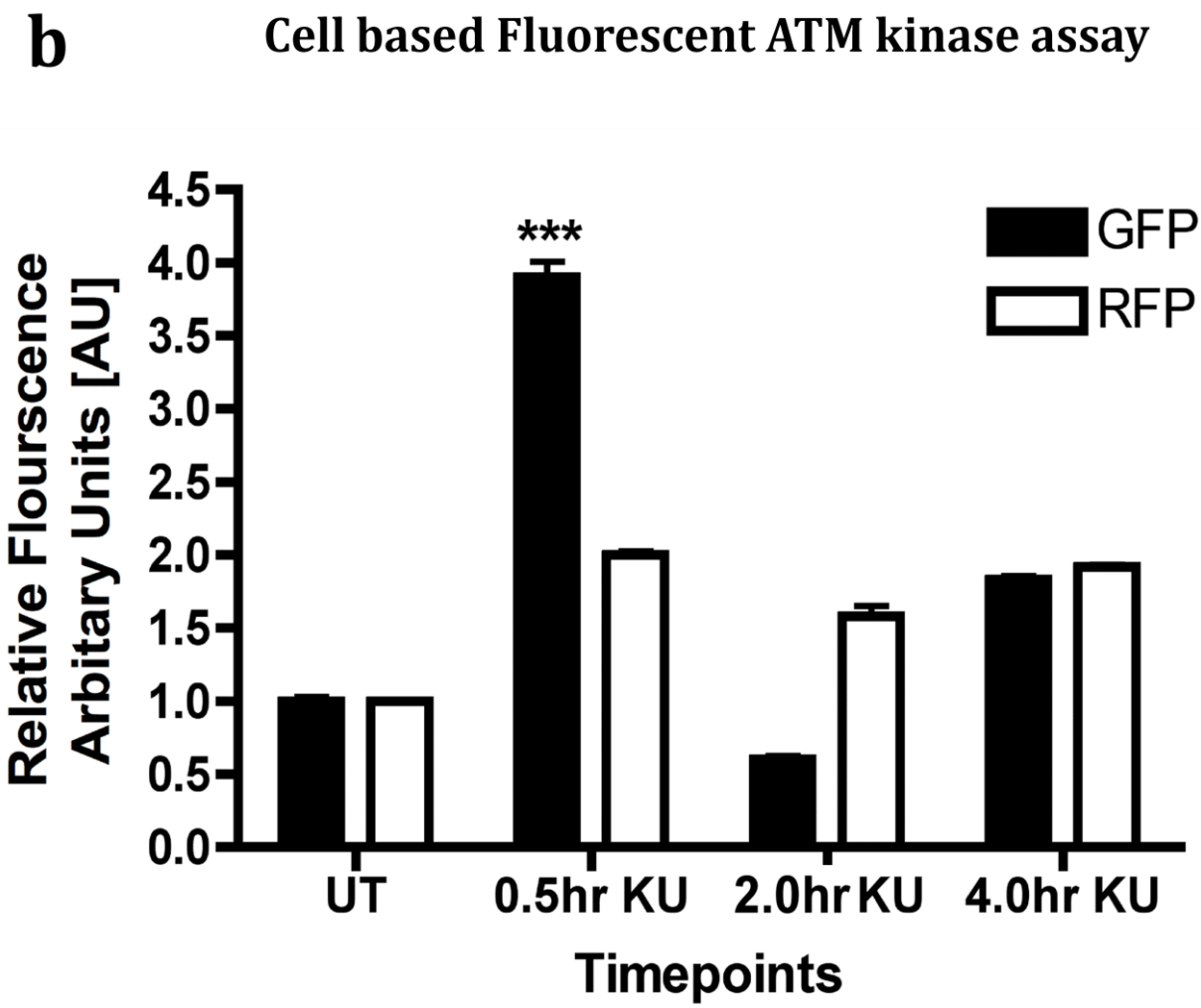


**Figure 4.12: Timing Fluorescent reporter assay of ATM activity.** MCF10 cell line was seeded on Poly L lysine coated coverslips placed in 24 well plates at a density of 1 x $10^5$ and allowed to grow until 70% confluent. Cells were next transfected with ATMpr/Ptimer fluorescent reporter constructs as described in materials and methods. After 24 hrs of transfection, cells were either left untreated, or treated with 10μM KU for the indicated time points. After treatments, cover slips with the cells were further processed for microscopic examination. For nuclear reference, DAPI staining was also performed. These are representative images taken with 100x objectives. **(a)** Expression of ATM promoter driven timing fluorescent reporter showing induction in fluorescence at 0.5 hr of KU treatment. Scale bar represents 10μm**. (b)** Bar chart showing intensity measurements of green (black bars) or red (white bars) fluorescence signal generated in cells expressing ATMpr/Ptimer. The values are based on mean fluorescence intensities from n=3 independent transfections with measurement from at least 10 cells per treatment. Mean values were normalized to the mean fluorescence value of untreated controls (UT) set to 1. The significance calculated according to the scale (* P<0.05, **P<0.01, ***P<0.001).

The overall pattern of ATMpr oscillation after KU treatment was consistent in both types of promoter reporter assays (Fig.4.10 & 4.12), and with the previous western blot results (Fig. 4.1a). Hence it is concluded that the KU-induced upregulation of ATM after inhibition of its kinase activity can be demonstrated at single cell level, and provides its feasibility of use as a novel reporter assay for ATM kinase inhibition as illustrated in Fig. 4.13.

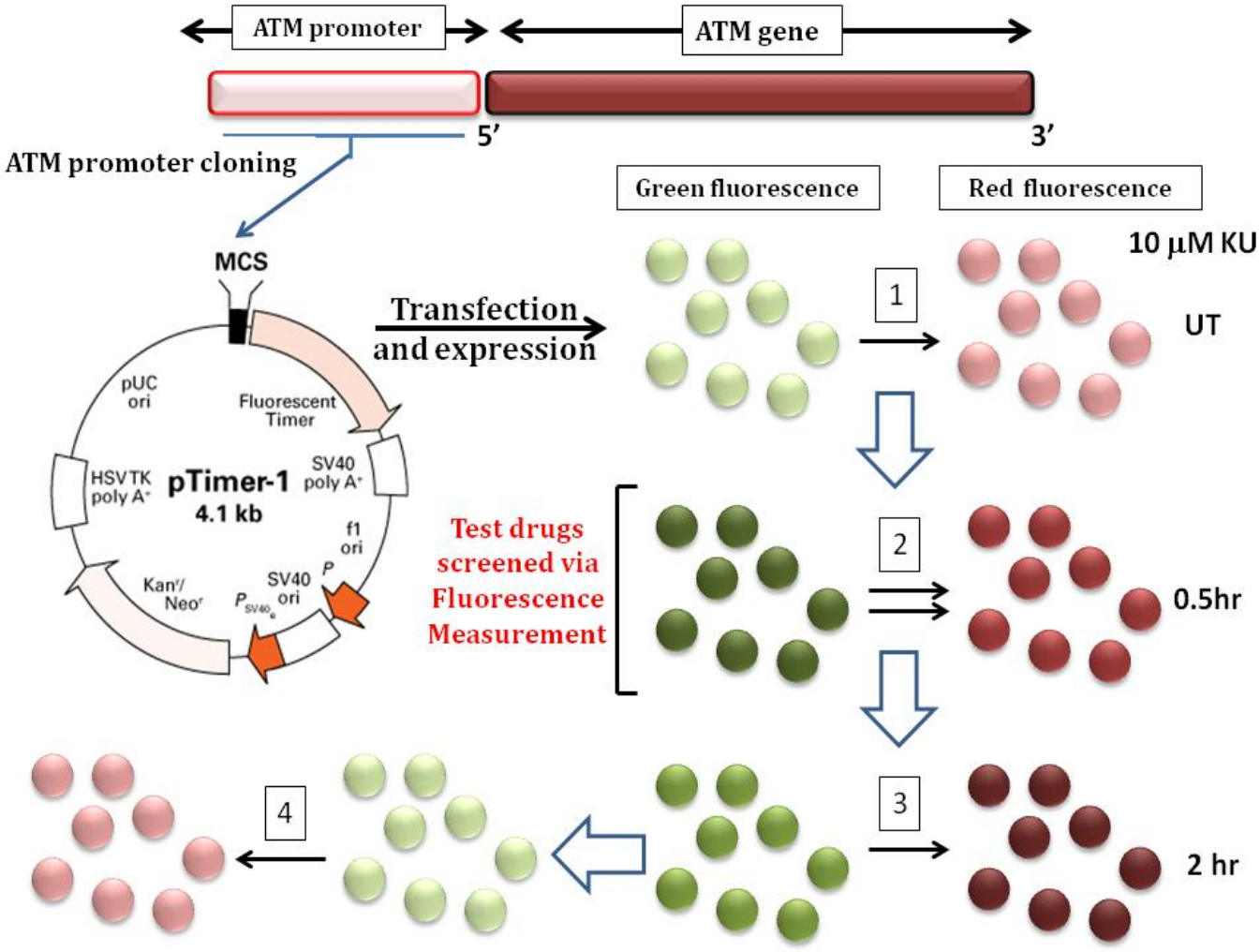


**Figure 4.13: The principle of working of novel cell based fluorescent biosensor of ATM inhibition and activity.** Promoter region of ATM was cloned upstream of timing fluorescent gene in pTimer-1 vector to drive the expression of the timing fluorescent gene. (1) Under normal conditions when ATM is constitutively active, there will be steady expression from the promoter, giving rise to green fluorescence and its steady rate of conversion into red fluorescence, the intensities of both of which were found comparable. (2) Different drugs, either genotoxic agents or candidate ATM kinase inhibitors could be tested at this point. Successful inhibition of ATM, achieved by novel inhibitors, would give rise to the transient upregulation of promoter activity of ATM that would in turn cause induction in green fluorescence. The transient spike in green fluorescence would thus inform of ATM inhibition. (3) At a later time point, the up regulated green fluorescent protein would mature into red fluorescent protein giving rise to an increased red fluorescence. (4) After the initial perturbation, both the ATM promoter will resume the steady state expression of green fluorescence and its steady rate of maturation into red fluorescence. At step (2), if instead DNA damaging agents that activate ATM are employed, the green fluorescence would undergo a reduction owing to a transient down regulation of ATM promoter activity. This would also result in lowering of red fluorescence at a later time point. Thus this assay can potentially be employed as a biosensor of DNA damage as well as a reporter for ATM kinase inhibition.

### 4.4 Key findings and their significance

This section of research discovered a novel ATM autoregulatory behaviour. This study demonstrated that inhibition of the ATM kinase activity leads to upregulation of the ATM protein, giving rise to a temporary peak in its activity accompanied by induction of P53, pATR and E2F1. While inhibitors of DDR proteins are employed to disrupt the G2/M checkpoint arrest after genotoxic treatments, this temporary increase in DDR activity after ATM inhibition is important to consider as it may hinder the therapeutic effect of G2/M checkpoint abrogation, providing an opportunity to repair the DNA in human cells. A luciferase reporter assay of the promoter of ATM not only established a transcriptional basis for this change but also demonstrated the precise timing of this upregulation followed by oscillation in the ATM levels after its inhibition. A fluorescence reporter assay was also developed in this section of study (Fig. 4.12 & 4.13). The working principle of this fluorescence assay was based on the following observations and hypotheses based on those observations:

- ATM kinase inhibition results in rapid induction of its promoter activity.

- ATM kinase activation (through Dox induced DNA damage) results in a slight down regulation of its promoter activity.

- Hence, the promoter activity (transcription) of ATM seems to be influenced/linked with its kinase activity.

- This relationship between kinase activity of ATM and its promoter signal seems negative and could be utilized to screen for inhibitors of ATM kinase whereby, successful inhibition of this kinase by potential candidates would give rise to the temporary spike in promoter signal, which could be measured (Fig. 4.10 & 4.12)

- This relationship, on the other hand, could also be utilized to monitor ATM activation or in other words, as a biosensor of DNA damage, since DNA damage-induced ATM activation caused a slight reduction in its promoter signal as compared to the signal in its constitutively active state (Compare UT and 0.25 hour time points of Dox treatment in Fig. 4.11, representing constitutive and induced ATM activity).

The particular oscillation pattern seen in western blots (Fig. 4.1a) might differ in its timing and regulation in different types of cancers. However, the novel information in this study could be used to time the chemotherapy or radiotherapy treatments to precise time points after ATM inhibition, when the ATM levels are at their lowest hence allowing a better therapeutic intervention.

# Chapter Five

# A novel autoregulatory trafficking mechanism of ATM involves β-COPI mediated Golgi to nuclear transport of pATM S-1981 during initiation of DDR signalling

The more I learn, the more I learn how little I know

Socrates, Philosopher (469 BC– 399 BC).

## 5.1 Abstract

*While there is vast amount of literature that addresses signalling mechanism leading from sensing the DNA damage up to either its repair, or induction of apoptosis, the underlying trafficking events and their associated mechanism for important DDR proteins have not been elucidated to an equally comprehensive level. In this section of the current research, I have demonstrated that in normal human keratinocytes, pATM is localised in Golgi and rapidly undergoes DNA damage induced Golgi export contributing to its concomitant nuclear accumulation. This trafficking mechanism was also found to be conserved in cancer cell lines. Importantly, the Golgi export of pATM and its subsequent nuclear accumulation were abrogated following inhibition of ATM kinase activity. This led to the identification of its kinase dependent autoregulatory role in trafficking during DDR. Furthermore, such inhibition also caused disruption of its co-localisation with β-COPI, coatomer protein involved in Golgi export. Since β-COPI recognizes its substrates via a di-Lysine recognition motif, mutation of an N-terminal di-Lysine motif $^{387}$-KK-$^{388}$ within ATM amino acid sequence to di-Alanine was performed, which caused permanent Golgi retention of ATM and failure to undergo Golgi export or nuclear accumulation following DNA damage. Hence, this section of research has discovered a new aspect of ATM regulation, which involves an autoregulatory ATM kinase dependent Golgi export of pATM mediated by β-COPI during DDR. This function of β-COPI in ATM traffic classifies it as a central component in DDR signalling pathway. The elucidation of this autoregulatory trafficking event of ATM following double stranded DNA damage represents an additional mechanism of ATM regulation and provides another dimension through which DDR could be manipulated to achieve cellular sensitivity to genotoxic agents.*

## 5.2 Introduction

Increasing appreciation of ATM function in cellular physiology in the past couple of decades has also resulted in an equally increasing knowledge about its localisation at a variety of other different cellular components. Table 10 summarises the diverse localisational differences of ATM within the cell and the associated function other than its function as a DDR kinase in the nucleus.

Table 10**:** Extra-nuclear ATM localisation and the associated function in different cells:

| **Cell type** | **Cellular compartment** | **Associated function** | **Reference** |
|---|---|---|---|
| Fibroblasts | Cytoplasmic vesicles | Found to exist in microsomes. Supported a more general role of ATM in cell signalling. | Watters D et al., 1997 |
| 293T cells | Cytoplasmic vesicles | Co-localisation with β-adaptin and as such may have role in intracellular protein traffic mechanisms. | Lim DS et al., 1998 |
| Human perkinje cells | Cytoplasm | May implicate the role of ATM in neurological homeostasis and thus explain the neurodegenerative phenotype of A-T patients | Oka A et al., 1998 |
| Cerebellocortical neurons | Endosomes | May have neuronal cell specific role as there was higher localisation in the endosomes of granule cell neurons than perkinje cells. | Kuljis RO et al., 1999 |
| Human fibroblasts | Peroxisomes | Co-localisation with catalase enzyme and as such may modulate its activity. In A-T fibroblasts, increased catalase activity was found. | Watters D et al., 1999. |
| Murine Perkinje cells and dorsal root ganglion | Cytoplasm | May be required to prevent lysosomal accumulation and have a role in maintaining normal cytoplasmic organelle function. | Barlow C et al., 2000. |
| MCF7 | Plasma membrane | Co-localisation with Casein kinase-2 interacting protein-1 which functions in muscle differentiation and regulation of actin cytoskeleton. | Zhang L et al., 2006. |
| Neuro-2a | Cytoplasm | Forms complex with two synaptic vesicle proteins VAMP2 and synapsin-I and modulate synaptic function. | Li J et al., 2009 |

It is imperative that such differential localisation of the same molecule in different cellular compartments involves rigorous protein trafficking events. The fact that ATM has been shown to interact with karyopherins (Young DB et al., 2005), found to co-localise with β-adaptin (Lim DS et al., 19), is recruited from nucleus to the plasma membrane (Zhang L et al., 2006) and the recent discovery of sequential localisation of pATM in Golgi apparatus and nucleus in normal human primary keratinocytes as well as in squamous cell carcinoma cell lines after UV treatment (Ismail F et al., 2011) also supports the idea that ATM undergoes extensive protein trafficking.

In this section of the current research, I set out to determine whether the activation of ATM following double stranded DNA damage or the inhibition of its kinase activity involves any cellular localisational changes in DDR proteins in general, or ATM in specific, especially the cytoplasmic ATM. Further to this end, to get deeper insights of the protein traffic machinery involved in ATM transport, and also to study ATM regulation in terms of modulation of its transport mechanism under normal conditions and DNA damaging states, I carried out fluorescent tagging, fluorescent immunolocalisation study and subsequent imaging analysis of ATM, sub-cellular organelles and core protein transport vehicles involved in protein traffic. The following results section illustrate the key findings.

## 5.3 Results

### 5.3.1 *ATM is present in the nucleus and at perinuclear region in untreated immortalized human keratinocytes whereas DNA damage causes no change in nuclear while disappearance of ATM from the perinuclear region.*

Previous results in the current research (Section 3.3.2 and Fig. 3.5) commented on some aspects of ATM localisation and revealed distinct cellular distribution of ATM through the cell cycle. In order to get deeper insights and determine cytoplasmic ATM localisation within untreated immortalized human keratinocytes (HaCat cells), and to further our knowledge in terms of ATM trafficking mechanism and transport between cytoplasm and nucleus after double stranded DNA damage, as a starting point, immunolabelling of total ATM was performed. To induce DNA damage, cells were treated with 0.5μM Dox for 0.5, 2 and 4 hr. For visualization of nuclei, DAPI staining was also performed.

It was observed that in untreated HaCat cells, ATM was mostly nuclear, as evident by merging the image with the DAPI stained image of the same cell, but with some localisation in the cytoplasm where it appeared to form punctations (Fig. 5.1). Interestingly, there was a distinct ATM localisation at the perinuclear region as well in the untreated state in HaCat cells, reminiscent of what was observed for MCF10 cells (Compare Fig. 3.3 and 5.1). Double stranded DNA damage caused the appearance of nuclear foci, the frequency of which roughly correlated with the time of treatment. The formation of nuclear foci confirmed an active DDR pathway in this cell line. Furthermore, DNA damage did not cause any appreciable change in the level of nuclear ATM at any time point of Dox treatment.

However, a striking finding was the disappearance or redistribution of the perinuclearly localised ATM after DNA damage. This redistribution of perinuclear ATM was evident at first time point of 0.5 hr treatment and continued further till 4 hr of Dox treatment (Fig. 5.1). It is noteworthy to mention that such localisational changes in ATM following DNA damage were also observed in Fig. 3.6 in MCF10A cell line.

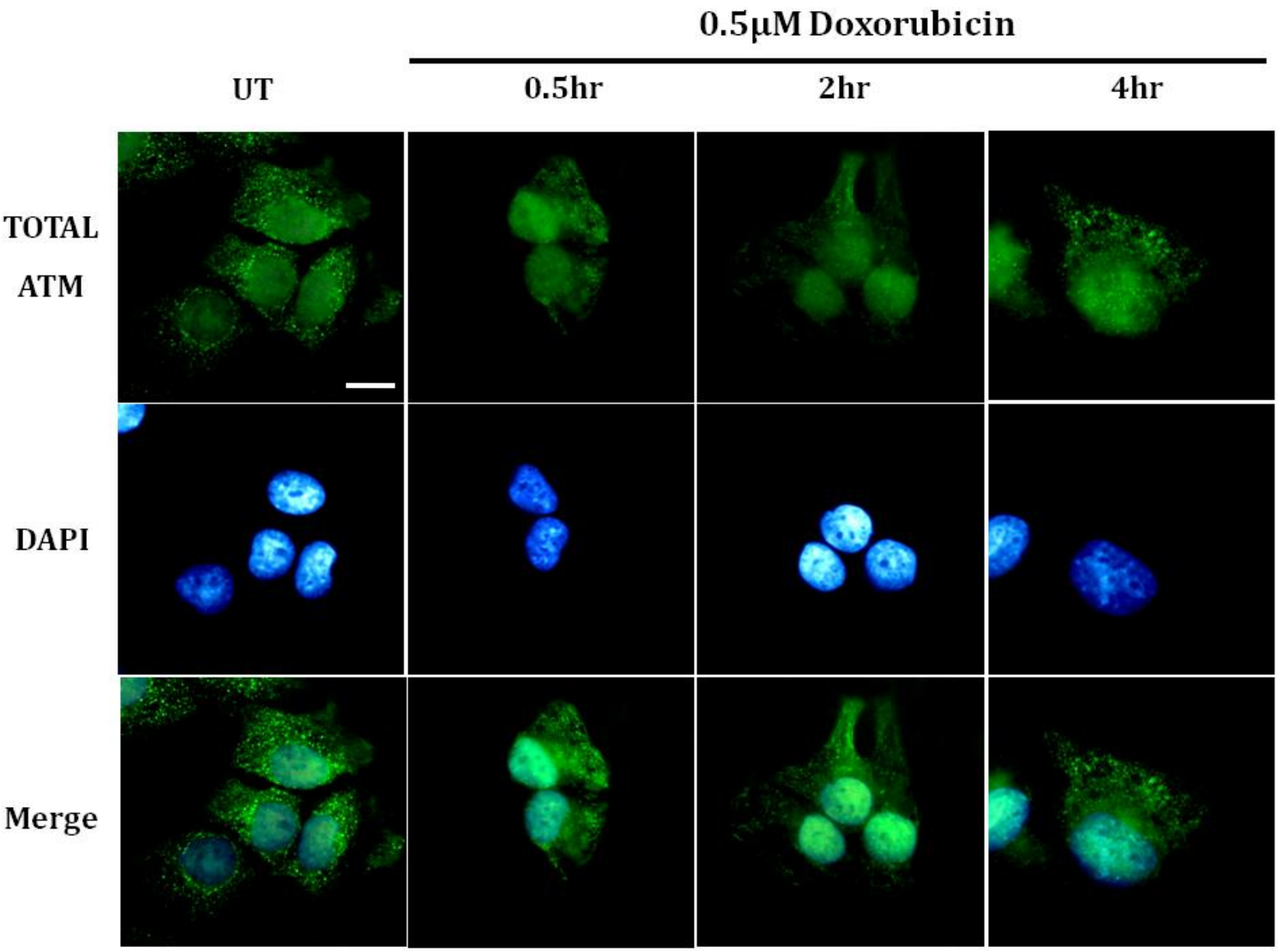
0.5μM Doxorubicin
UT
0.5hr
2hr
4hr
TOTAL ATM
DAPI
Merge

**Figure 5.1: Double stranded DNA damage causes disappearance of ATM from the perinuclear region, distinct nuclear foci while no change in its nuclear levels in HaCat cells.** HaCat cells were seeded on Poly L lysine coated coverslips and grown until 70% confluent and treated as indicated. Immunostaining was performed with total ATM antibody using Alexa fluor 488 conjugated secondary antibody. White arrows point towards perinuclear ATM. Red arrows indicate the presence of DNA damage induced nuclear foci. Nuclear reference is provided by merging of the DAPI stained nuclei of same cells. In the untreated state in HaCat cells, total ATM was mostly nuclear, with some localised at the perinuclear region. 0.5μM Dox treatment for 0.5, 2 or 4hr caused no major change in the nuclear fraction of ATM, however causing redistribution and disappearance of the perinuclearly localised total ATM and the appearance of distinct nuclear foci indicative of activation of ATM dependent DDR in HaCat cells. These are representative images taken in different fields of views under 100x objective. Scale bar represents 10μm.

### 5.3.2 *Phosphorylated ATM at Serine-1981 (pATM) is mostly localized at the perinuclear region in HaCat cells whereas DNA damage causes disappearance of pATM from the perinuclear region with a concomitant time dependent increase in its nuclear accumulation.*

To study the localisation of pATM, the same treatments were repeated but this time using pATM Serine 1981 (pATM) antibody and Alexa fluor 568 conjugated secondary antibody for carrying out its fluorescent immunolocalisation studies. In the untreated cells, while there was presence of some nuclear staining for pATM, it was mostly localized at the perinuclear region. Interestingly however, at 0.5 hr of 0.5µM Dox treatment, there was disappearance of pATM from the perinuclear region with an accompanying and very noticeable increase in the nuclear pATM as confirmed by merging the image with DAPI stained image of the same cell. This nuclear increase of pATM continued further at 2 and 4 hr time points with a continued absence from the perinuclear region (Fig. 5.2). The disappearance of pATM from the perinuclear region after double stranded DNA damage was consistent with the results obtained for total ATM (Fig. 5.1). Hence, while levels of total ATM are unaltered after DNA damage, pATM levels showed a time dependent increase while both total and phosphorylated forms showed discontinuation of their localisation at the perinuclear region after genotoxic treatment. It appeared that the perinuclear pATM in the untreated cells underwent translocation into the nucleus after Dox treatment resulting in an overall increase in the nuclear pATM. Further protein transport studies were undertaken in the following sections to support this and get deeper insight of pATM transport.

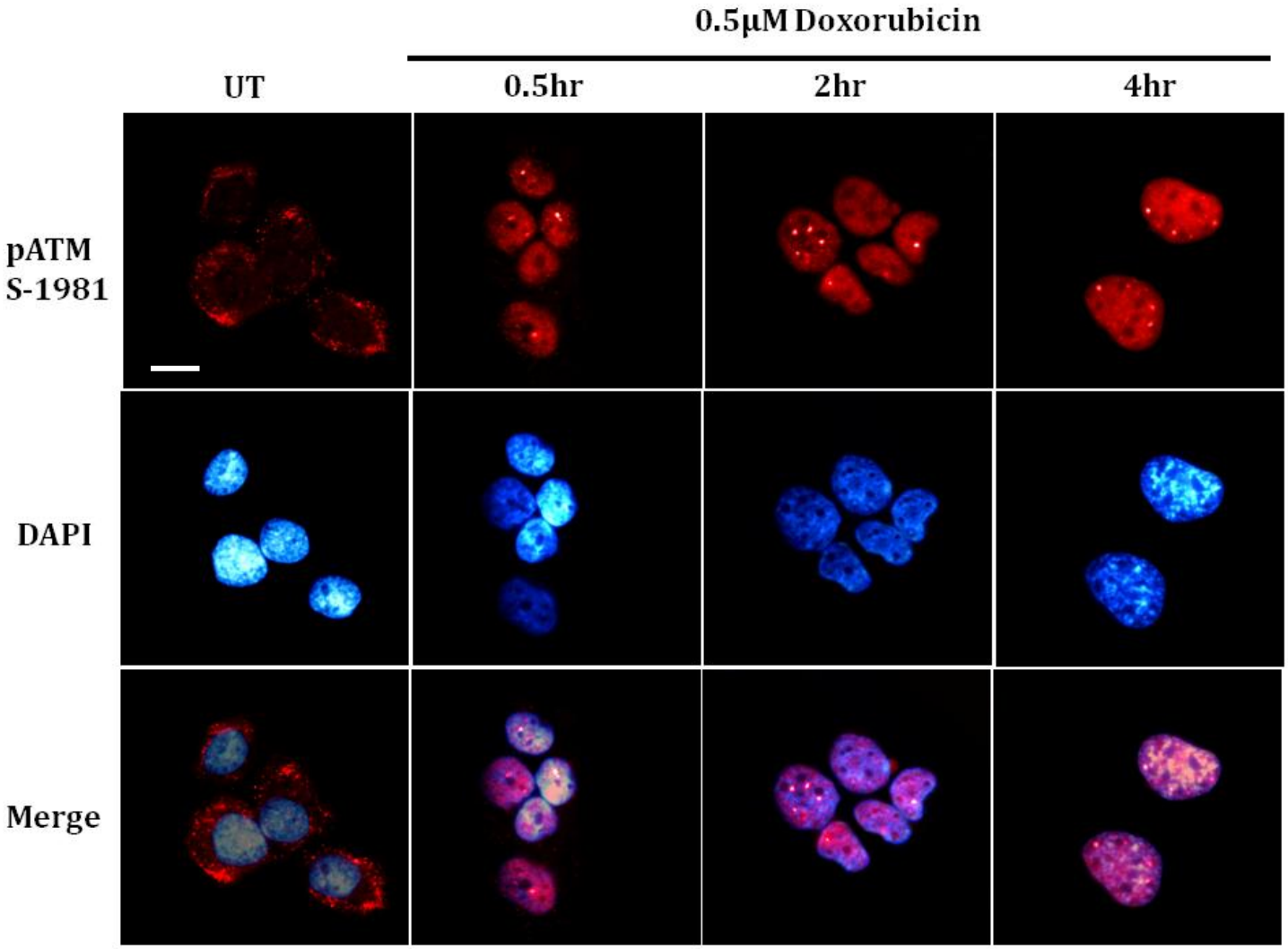
0.5µM Doxorubicin
UT
0.5hr
2hr
4hr
pATM S-1981
DAPI
Merge

**Figure 5.2: Double stranded DNA damage causes rapid disappearance of pATM from perinuclear region with a time dependent increase in its nuclear accumulation.** HaCat cells were seeded on Poly L lysine coated coverslips and grown until 70% confluent and treated as indicated. Immunostaining was performed with pATM S 1981 antibody using Alexa fluor® 568 conjugated secondary antibody. Nuclear reference is provided by merging of the DAPI stained nuclei of same cells. White arrows point towards pATM localisation at the perinuclear region. In the untreated state in HaCat cells, pATM was mostly localised at the perinuclear region with some residing in the nucleus. 0.5μM Dox treatment for 0.5, 2 or 4hr caused disappearance of the perinuclear pATM with an accompanying time dependent nuclear accumulation. These are representative images taken in different fields of views under 100x objective. Scale bar represents 10μm.

### *5.3.3. Extra nuclear pATM is mostly localised in the Golgi apparatus in HaCat cells.*

Next, in order to find the identity of this perinuclear region where pATM is localised in the untreated state, HaCat cells seeded on poly-L lysine coated cover slips were first transfected with constructs carrying different organelle specific genes tagged with fluorescence markers as described in materials and methods and then subjected to fluorescent immunolocalisation studies of pATM in the same cells. This allowed me to examine immunolabelled pATM and at the same time visualize individual organelles within the cell in different channels in order to identify the organelle where the immunostained cytoplasmic pATM was localised. Table 11 shows the genes tagged with fluorophores that were used as fluorescent organelle markers along with the type of secondary antibodies used for the subsequent immunostaining and localisational studies of pATM.

Table 11**:** Fluorescent gene constructs employed as organelle markers along with the type of fluorophore conjugated secondary antibodies used for immunostaining of pATM S-1981.

| **Gene** | **Organelle marker** | **Fluorophore** | **Secondary IgG** |
|---|---|---|---|
| RIC-3 | Endoplasmic reticulum (ER) | Red fluorescent protein | Alexa fluor 568 |
| Cyclooxygenase-II | Mitochondria | Red fluorescent protein | Alexa fluor 488 |
| Mannosidase II | Golgi apparatus | Green fluorescent protein | Alexa fluor 568 |
| DAPI | Nucleus | – | – |

After performing individual transfections with fluorescently tagged organelle specific gene constructs, the pATM localisation was carefully examined. Figure 5.3 shows RIC-RFP expression labelling Endoplasmic reticulum (Red) in HaCat cells and pATM immunostaining (green) in the same cell in the untreated HaCat cells. After merging of the two images captured in relevant channels to examine co-localisation, it was confirmed that pATM and ER were localised in different sub-cellular regions as no overlapping was observed between the fluorescent signals in the images (Fig 5.3).

Next, examination of the co-localisation of extra nuclear pATM with Cyclooxygenase II-RFP, a mitochondrial marker (red) was performed. After merging of the two images captured in relevant channels, it was confirmed that similar to what was observed for ER, mitochondria and pATM were also localised in different sub-cellular regions as there was no overlapping of the fluorescent signals in superimposed images (Fig. 5.4).

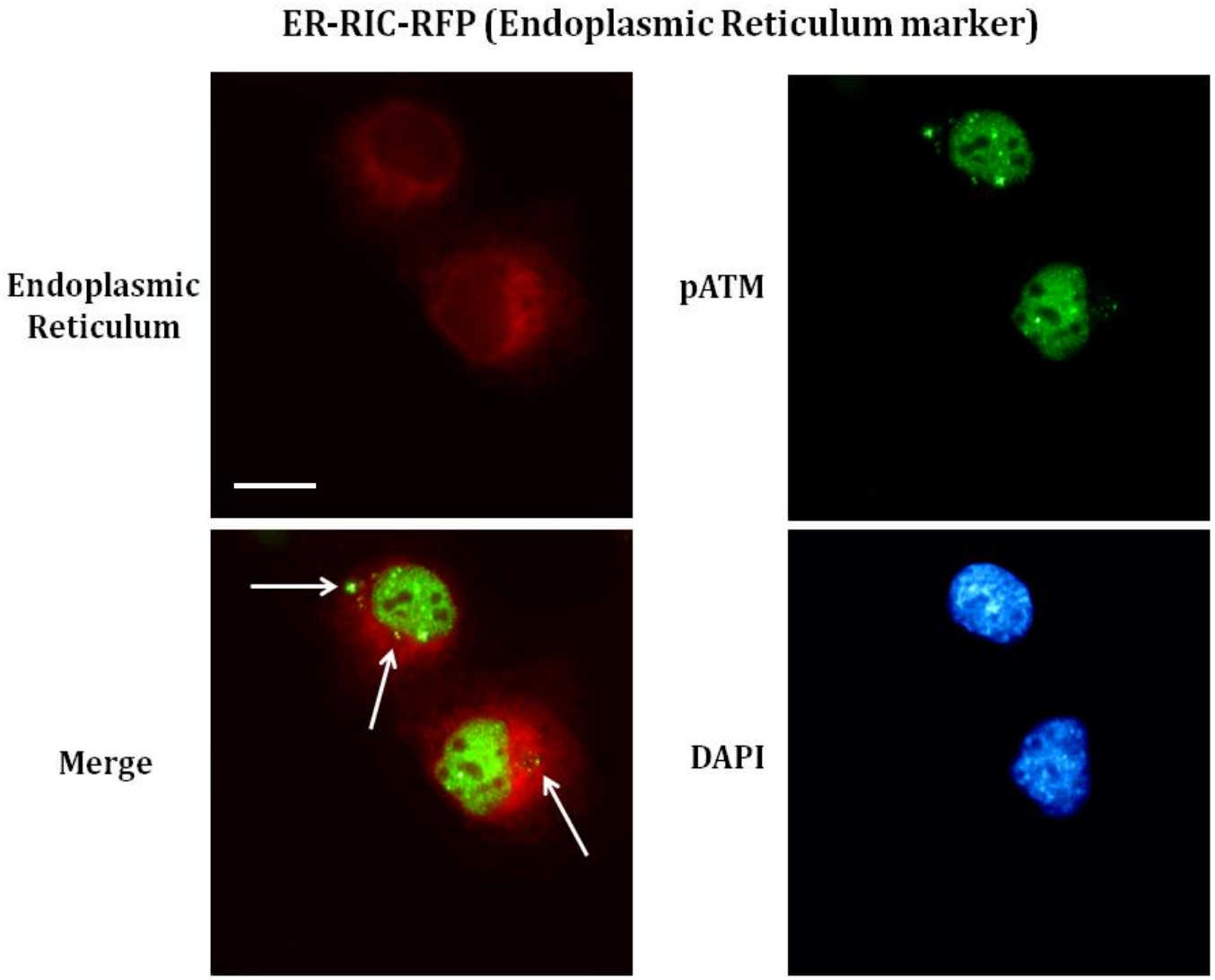


**Figure 5.3: Extra nuclear pATM does not localise in Endoplasmic reticulum in untreated HaCat cells.** HaCat cells were seeded on Poly L lysine coated coverslips and grown until 70% confluent. Cells were transfected with Endoplasmic reticulum marker gene, RIC3-RFP as described in materials and methods. After 16 hr of transfection, immunostaining was performed with pATM 1981 antibody using Alexa fluor 488 conjugated secondary antibody. Images were captured in relevant channels and co-localisation studies were performed by superimposition of the captured images. Nuclear reference is provided by staining the nuclei with DAPI. The extra nuclear pATM in the untreated HaCat cells did not co-localise with the ER marker, RIC3-RFP. White arrows indicate localisation of the extra nuclear pATM failing to overlap with ER. These are representative images taken in different fields of views under 100x objective. Scale bar represents 10μm.

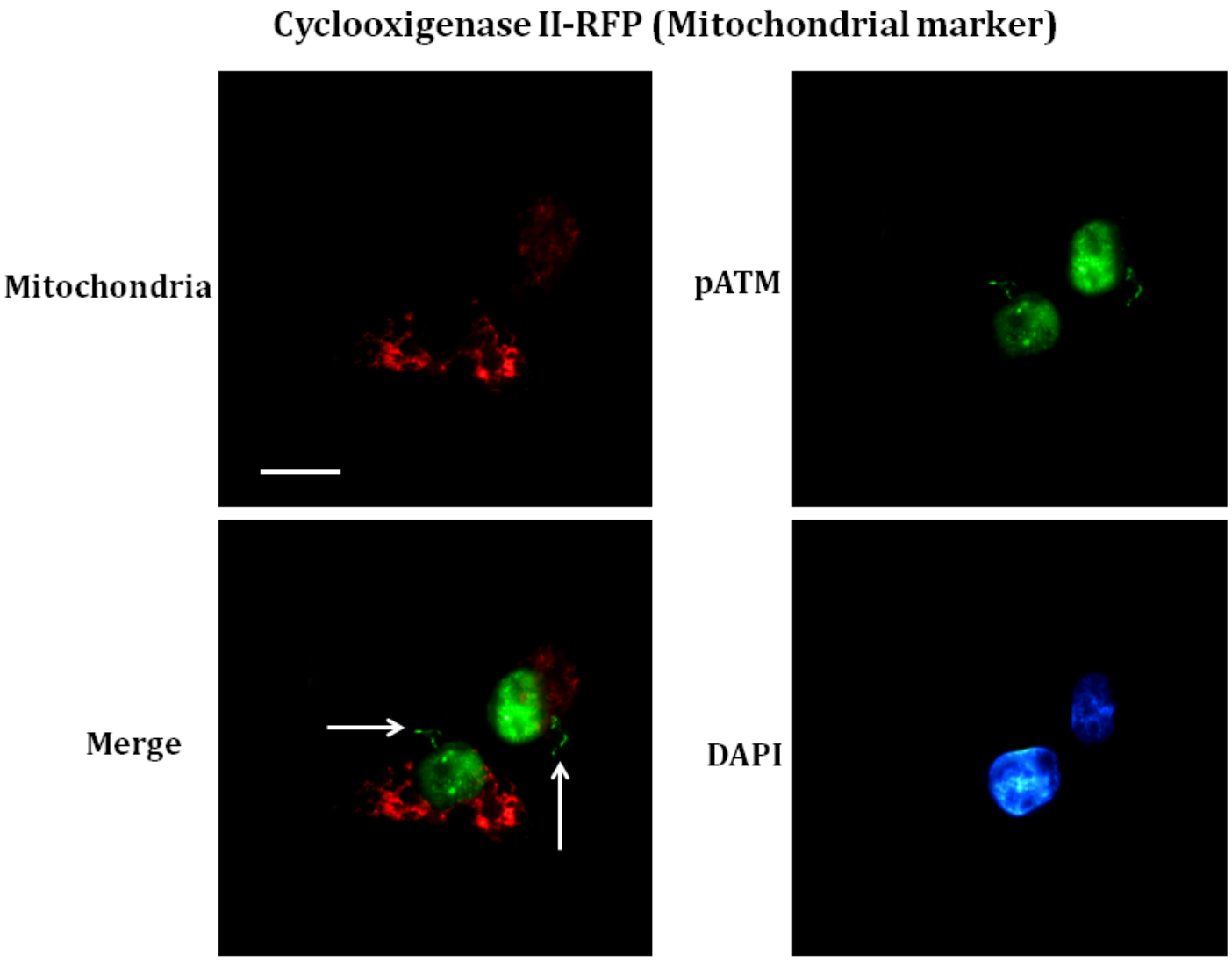


**Figure 5.4: Extra nuclear pATM does not localise in Mitochondria in untreated HaCat cells.** HaCat cells were seeded on Poly L lysine coated coverslips and grown until 70% confluent. Cells were transfected with Mitochondria marker gene, Cyclooxygenase II-RFP as described in materials and methods. After 16 hr of transfection, immunostaining was performed with pATM 1981 antibody using Alexa fluor 488 conjugated secondary antibody. Images were captured in relevant channels and co-localisation studies were performed by superimposition of the captured images. Nuclear reference is provided by staining the nuclei with DAPI. The extra nuclear pATM in the untreated HaCat cells did not co-localise with the Mitochondrial marker, RIC3-RFP. White arrows indicate localisation of the extra nuclear pATM failing to overlap with Mitochondria. These are representative images taken in different fields of views under 100x objective. Scale bar represents 10μm.

Interestingly, when the Golgi marker, Mannosidase-II-GFP was transfected into cells, allowed to express and analysed for its co-localisation with cytoplasmic pATM following its immunostaining, it was revealed that the two co-localised, indicating cytoplasmic pATM localisation in the Golgi apparatus. Hence, the merging of the two images via superimposition resulted in the appearance of yellow fluorescence, indicative of co-localisation between Alexa fluor 568 pATM signal and GFP of the Golgi marker in the untreated HaCat cells (Fig. 5.5). This result led me to confirm that in Fig. 5.2, the perinuclear region where pATM localized in HaCat cell is Golgi apparatus.

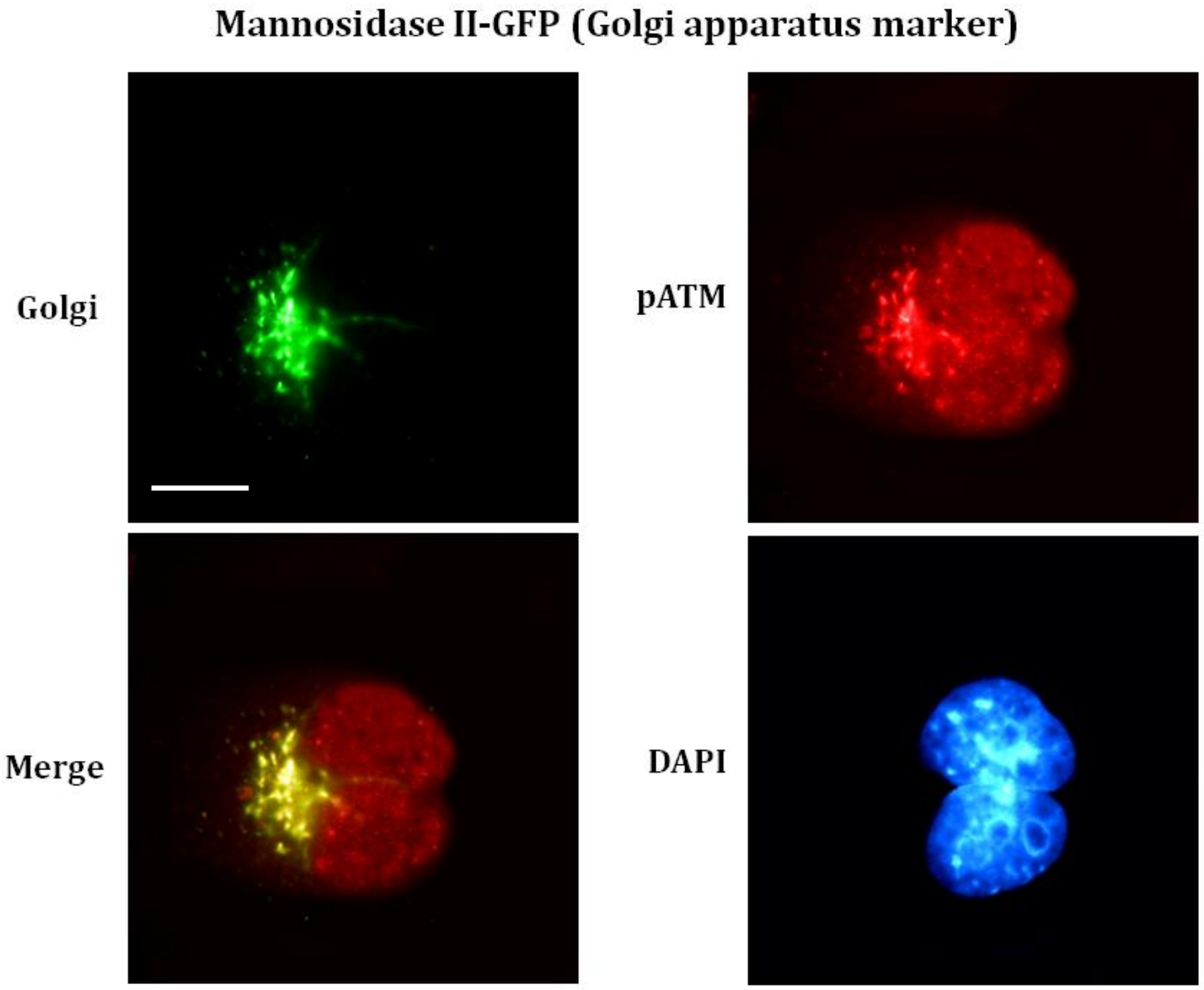


**Figure 5.5: Extra nuclear pATM localises in Golgi apparatus in untreated HaCat cells.** HaCat cells were seeded on Poly L lysine coated coverslips and grown until 70% confluent. Cells were transfected with Golgi marker gene, Mannosidase II-GFP as described in materials and methods. After 16 hr of transfection, immunostaining was performed with pATM 1981 antibody using Alexa fluor 568 conjugated secondary antibody. Images were captured in relevant channels and co-localisation studies were performed by superimposition of the captured images. Nuclear reference is provided by staining the nuclei with DAPI. The extra nuclear pATM in the untreated HaCat cells co-localised with the Golgi apparatus marker, Mannosidase II-GFP. The appearance of yellow fluorescence in the merged images of pATM and Golgi-GFP confirmed this co-localisation. These are representative images taken in different fields of views under 100x objective. Scale bar represents 10μm.

### 5.3.4. *Double stranded DNA damage causes rapid exit of Golgi resident pATM from Golgi apparatus with a concomitant increase in its nuclear accumulation and no localisation in endoplasmic reticulum or mitochondria.*

To determine pATM trafficking at the Golgi apparatus upon DNA damage, cells were next transfected with mannosidase II-GFP construct, exposed to 0.5μM of Dox and treated for 0.5, 2 and 4 hours. After Dox treatment, pATM S-1981 immunostaining was performed using Alexa fluor 568 conjugated secondary antibody. It was found that as soon as after 0.5 hr of Dox treatment, there was an exit of pATM from the Golgi apparatus with a corresponding and expected increase in its nuclear accumulation (Compare Fig. 5.5 and Fig. 5.6). At 2 and 4 hr time points of Dox, pATM continued to show nuclear induction without any transport to Golgi apparatus as determined by the merged images of mannosidase-II-GFP and pATM (Fig. 5.6).

To determine whether Dox induced DNA damage, in addition to causing the expected nuclear increase of pATM, also caused its transport to, and hence localisation in either endoplasmic reticulum or mitochondria, HaCat cells were next transfected with Ric-3-RFP and cyclooxygenase-II-RFP respectively. This was followed by exposing the cells to 0.5μM Dox for 0.5, 2 and 4 hr time points. Immunolabelling of pATM was performed using pATM primary and Alexa fluor 488 conjugated secondary antibody. Figure 5.7 and Figure 5.8 confirmed that DNA damage did not cause pATM transport to either mitochondria or endoplasmic reticulum respectively at all the time points tested. In each case, pATM showed nuclear increases with Dox treatment without any localisation in these organelles as evident by their merged images (Fig. 5.6, Fig 7. and Fig. 8).

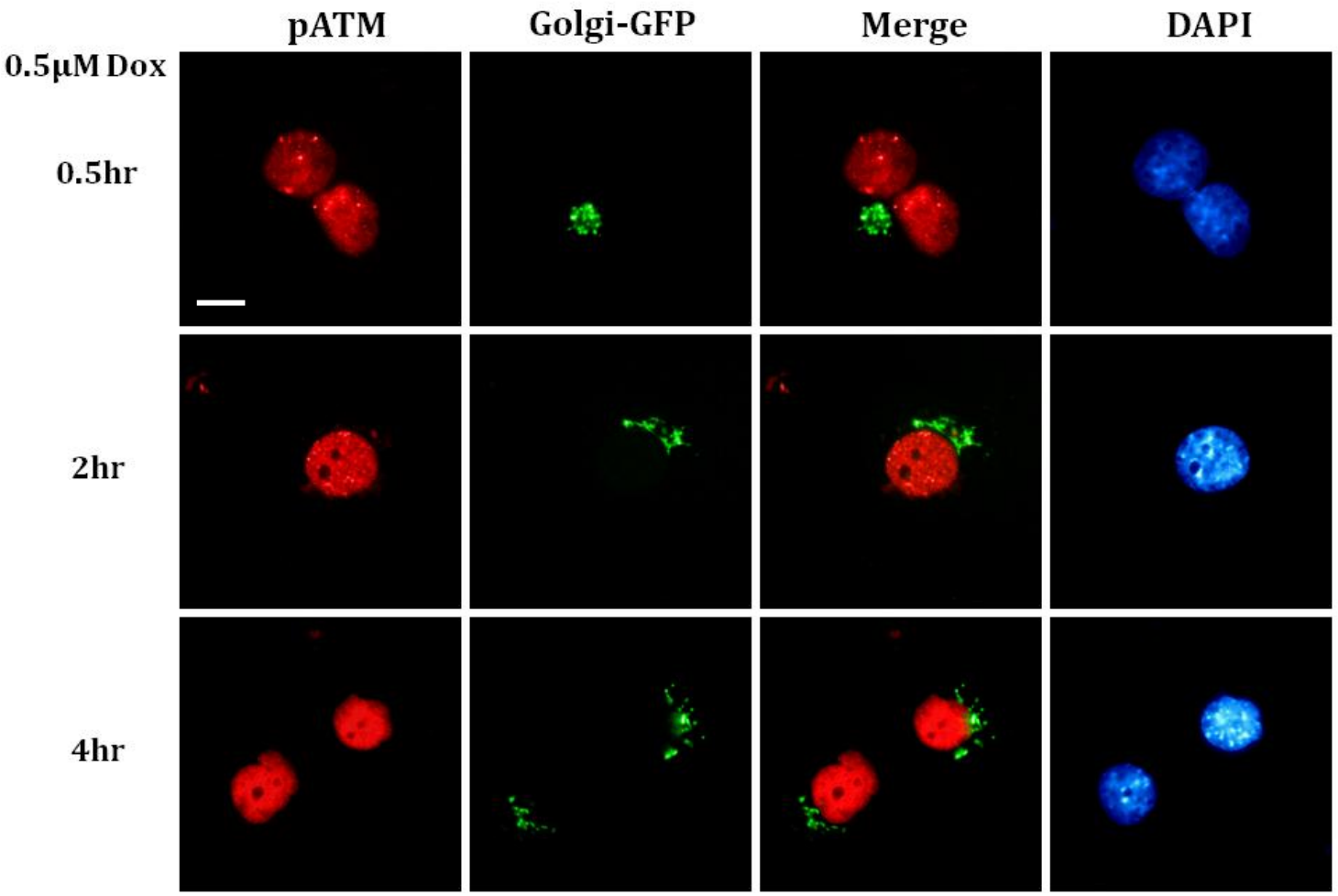
pATM
Golgi-GFP
Merge
DAPI
0.5µM Dox
0.5hr
2hr
4hr

**Figure 5.6: Double stranded DNA damage causes rapid exit of pATM from Golgi apparatus with an accompanying time dependent increase in the nucleus.** HaCat cells were seeded on Poly L lysine coated coverslips and grown until 70% confluent. Cells were transfected with Golgi marker gene, Mannosidase II-GFP as described in materials and methods. After 16hr of transfection, cells were exposed to 0.5μM Dox for 0.5, 2 and 4hr. This was followed by immunostaining with pATM 1981 antibody using Alexa fluor 568 conjugated secondary antibody. Images were captured in relevant channels and co-localisation studies were performed by superimposition of the captured images. Nuclear reference is provided by staining the nuclei with DAPI. The extra nuclear pATM in the HaCat cells that co-localised in the Golgi apparatus marker, MannosidaseII-GFP in untreated cells exhibited rapid exit from Golgi apparatus following DNA damage up to 4hr. Hence, co-localisation studies of the merged images of pATM and Golgi-GFP did not show any yellow fluorescent staining. These are representative images taken in different fields of views under 100x objective. Scale bar represents 10μm.

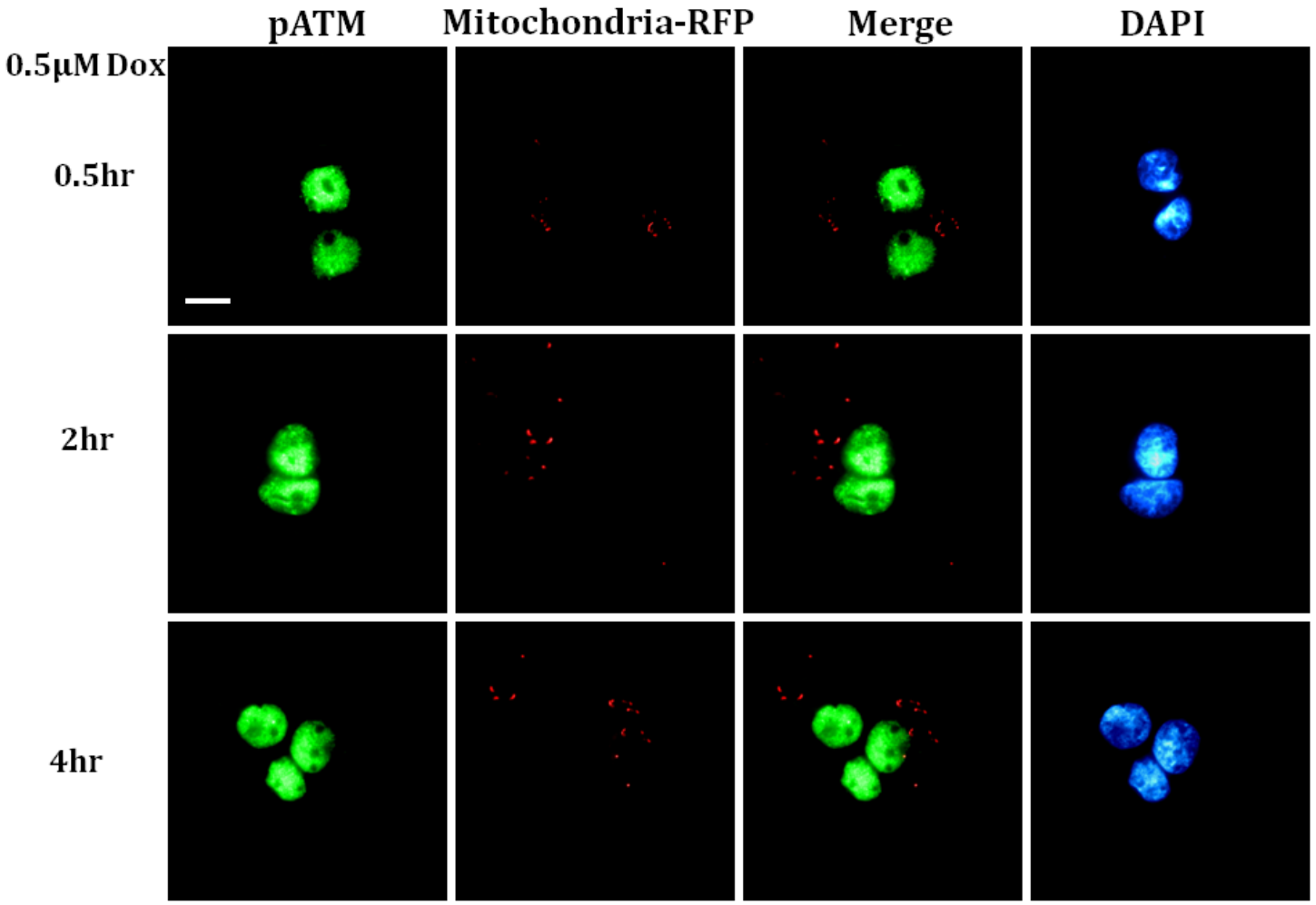
pATM
Mitochondria-RFP
Merge
DAPI
0.5µM Dox
0.5hr
2hr
4hr

**Figure 5.7: Double stranded DNA damage does not cause localisation of pATM in mitochondria but undergoes time dependent increase in the nucleus.** HaCat cells were seeded on Poly L lysine coated coverslips and grown until 70% confluent. Cells were transfected with Mitochondrial marker gene, Cyclooxygenase II-RFP as described in materials and methods. After 16hr of transfection, cells were exposed to 0.5μM Dox for 0.5, 2 and 4hr. This was followed by immunostaining with pATM 1981 antibody using Alexa fluor 488® conjugated secondary antibody. Images were captured in relevant channels and co-localisation studies were performed by superimposition of the captured images. Nuclear reference is provided by staining the nuclei with DAPI. Dox treatment did not cause pATM translocation to mitochondria at any of the time point tested. Hence, co-localisation studies of the merged images of pATM and Cyclooxygenase II-RFP did not show any yellow fluorescent staining. These are representative images taken in different fields of views under 100x objective. Scale bar represents 10μm.

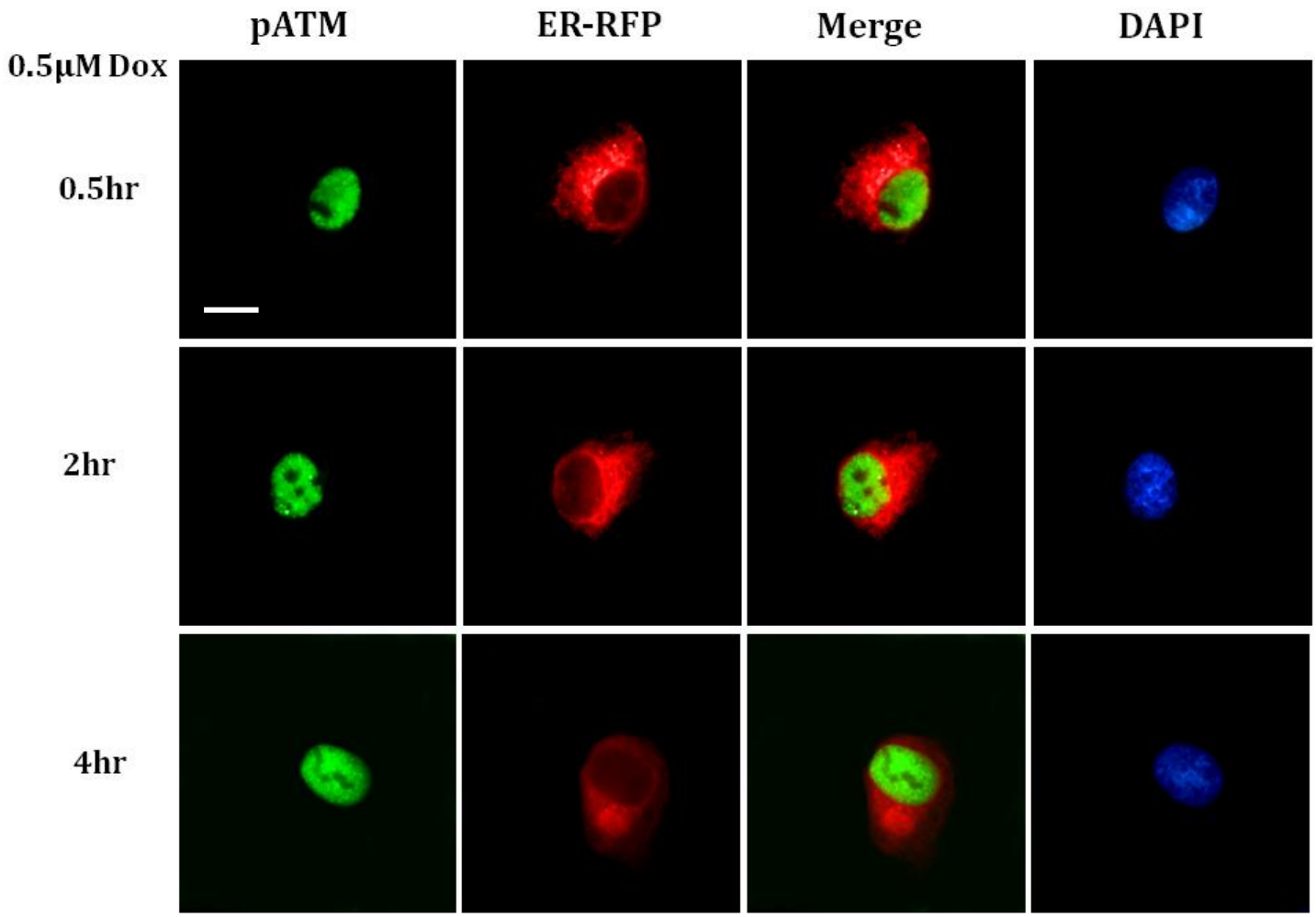
pATM
ER-RFP
Merge
DAPI
0.5μM Dox
0.5hr
2hr
4hr

**Figure 5.8: Double stranded DNA damage does not cause localisation of pATM in Endoplasmic Reticulum but undergoes time dependent increase in the nucleus.** HaCat cells were seeded on Poly L lysine coated coverslips and grown until 70% confluent. Cells were transfected with Endoplasmic reticulum marker gene, RIC3-RFP as described in materials and methods. After 16hr of transfection, cells were exposed to 0.5μM Dox for 0.5, 2 and 4hr. This was followed by immunostaining with pATM 1981 antibody using Alexa fluor 488® conjugated secondary antibody. Images were captured in relevant channels and co-localisation studies were performed by superimposition of the captured images. Nuclear reference is provided by staining the nuclei with DAPI. Dox treatment did not cause pATM translocation to Endoplasmic reticulum at any of the time point tested. Hence, co-localisation studies of the merged images of pATM and RIC3-RFP did not show any yellow fluorescent staining. These are representative images taken in different fields of views under 100x objective. Scale bar represents 10μm.

### *5.3.5 pATR, pChk2 and pChk1 are localised in Golgi apparatus in addition to nucleus in untreated HaCat cells and rapidly undergo DNA damage induced Golgi exit and nuclear accumulation.*

Previous reports have shown a functional link between ATM and ATR (Stiff T et al., 2006, Jazayeri A et al., 2006) while P53, checkpoint kinases Chk1 and Chk2 are known to be the substrates of ATM (Canman CE et al., 1998, Gatei M et al., 2003, Matsuoka S et al., 2000). Owing to this functional link between ATM activity and these substrates, I next set out to determine their localisation in HaCat cells in untreated condition as well as after genotoxic insults. This was done to examine whether the trafficking event identified for ATM during initiation of DDR is conserved for other DDR kinases as well. Cells were grown on coverslips and transfected with Golgi marker mannosidase-II-GFP followed by either leaving them untreated or exposing them to 0.5μM Dox for 0.5 and 4 hours. Next, immunostaining was performed for pATR S-428, pChk2 T-68, pChk1 S-296 and pP53 S-15 using Alexa fluor 568 conjugated secondary antibody as described in materials and methods section.

It was established that in untreated cells, in addition to pATM, interestingly other DDR kinases, pATR, pChk1 and pChk2 were also localised in Golgi apparatus (Fig.5.9 for pATR, Fig. 5.11 for pChk1 & Fig. 5.13 for pChk2). In contrast, pP53 was only found in the nucleus (5.15). However, after Dox induced DNA damage, these DDR kinases underwent rapid Golgi exit as soon as after 0.5 hr of treatment (Fig. 5.10 for pATR, Fig. 5.12 for pChk1 & Fig. 5.14 for pChk2) reminiscent of what was observed for pATM in previous figures. pP53 showed time dependent nuclear induction at 0.5 and 4 hr of Dox treatment (Fig. 16) with no localisation in any state in the Golgi.

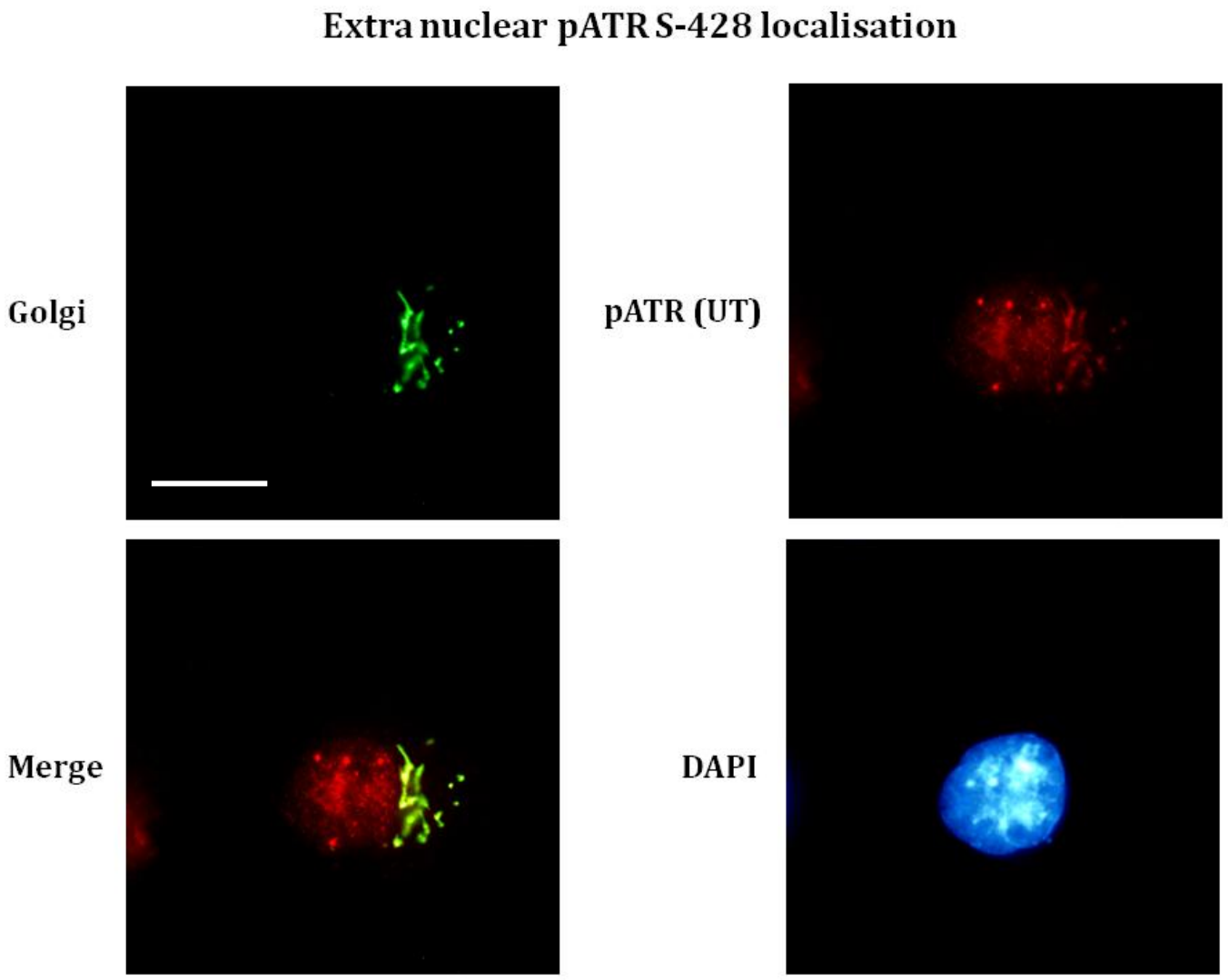


**Figure 5.9: Extra nuclear pATR localises in Golgi apparatus in untreated HaCat cells.** HaCat cells were seeded on Poly L lysine coated coverslips and grown until 70% confluent. Cells were transfected with Golgi marker gene, Mannosidase II-GFP as described in materials and methods. After 16 hr of transfection, immunostaining was performed with pATR S 428 antibody using Alexa fluor 568 conjugated secondary antibody. Images were captured in relevant channels and co-localisation studies were performed by superimposition of the captured images. Nuclear reference is provided by staining the nuclei with DAPI. The extra nuclear pATR in the untreated HaCat cells co-localised with the Golgi apparatus marker, Mannosidase II-GFP. The appearance of yellow fluorescence in the merged images of pATR and Golgi-GFP confirmed this co-localisation. These are representative images taken in different fields of views under 100x objective. Scale bar represents 10µm.

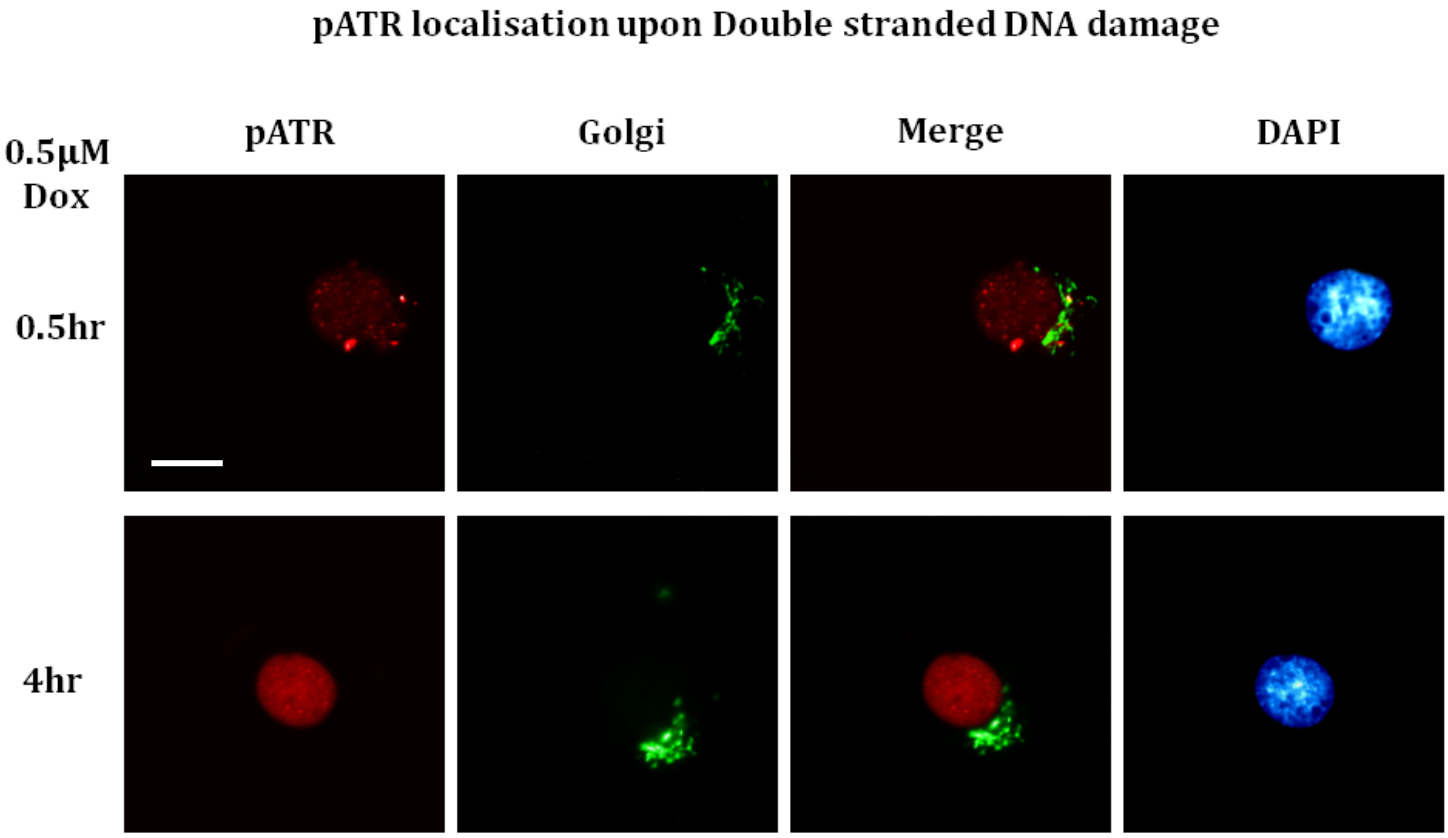
pATR localisation upon Double stranded DNA damage
pATR
Golgi
Merge
DAPI
0.5µM Dox
0.5hr
4hr

**Figure 5.10: Double stranded DNA damage causes rapid exit of pATR from Golgi apparatus with an accompanying increase in its nuclear accumulation.** HaCat cells were seeded on Poly L lysine coated coverslips and grown until 70% confluent. Cells were transfected with Golgi marker gene, Mannosidase II-GFP as described in materials and methods. After 16hr of transfection, cells were exposed to 0.5μM Dox for 0.5, and 4hr. This was followed by immunostaining with pATR S-428 antibody using Alexa fluor 568® conjugated secondary antibody. Images were captured in relevant channels and co-localisation studies were performed by superimposition of the captured images. Nuclear reference is provided by staining the nuclei with DAPI. The extra nuclear pATR in the HaCat cells that co-localised in the Golgi apparatus marker, MannosidaseII-GFP in untreated cells exhibited rapid exit from Golgi apparatus following DNA damage up to 4hr. Hence, co-localisation studies of the merged images of pATR and Golgi-GFP did not show any yellow fluorescent staining. These are representative images taken in different fields of views under 100x objective. Scale bar represents 10μm.

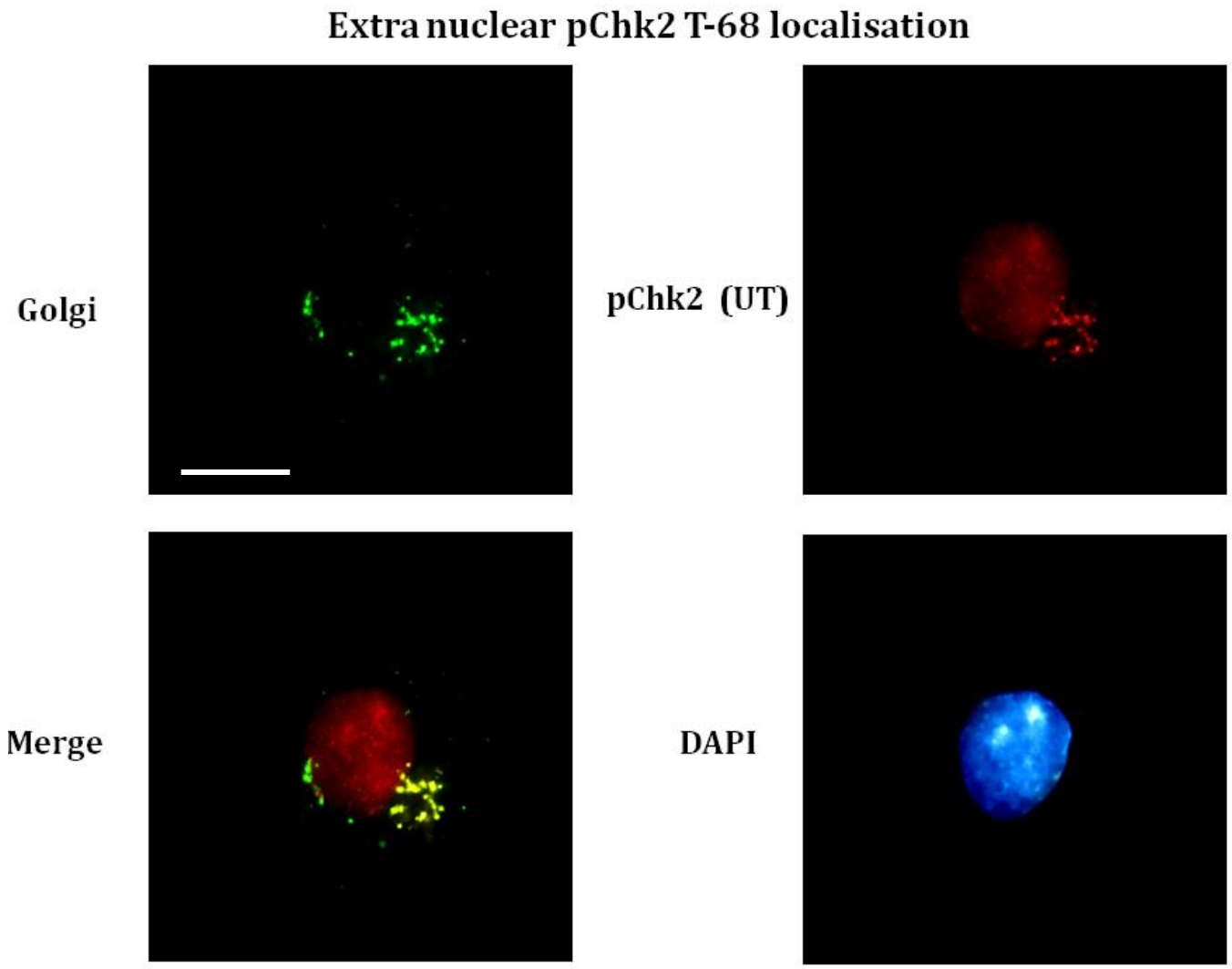


**Figure 5.11: Extra nuclear pChk2 localises in Golgi apparatus in untreated HaCat cells.** HaCat cells were seeded on Poly L lysine coated coverslips and grown until 70% confluent. Cells were transfected with Golgi marker gene, Mannosidase II-GFP as described in materials and methods. After 16 hr of transfection, immunostaining was performed with pChk2 T-68 antibody using Alexa fluor 568 conjugated secondary antibody. Images were captured in relevant channels and co-localisation studies were performed by superimposition of the captured images. Nuclear reference is provided by staining the nuclei with DAPI. The extra nuclear pChk2 in the untreated HaCat cells co-localised with the Golgi apparatus marker, Mannosidase II-GFP. The appearance of yellow fluorescence in the merged images of pChk2 and Golgi-GFP confirmed this co-localisation. These are representative images taken in different fields of views under 100x objective. Scale bar represents 10μm.

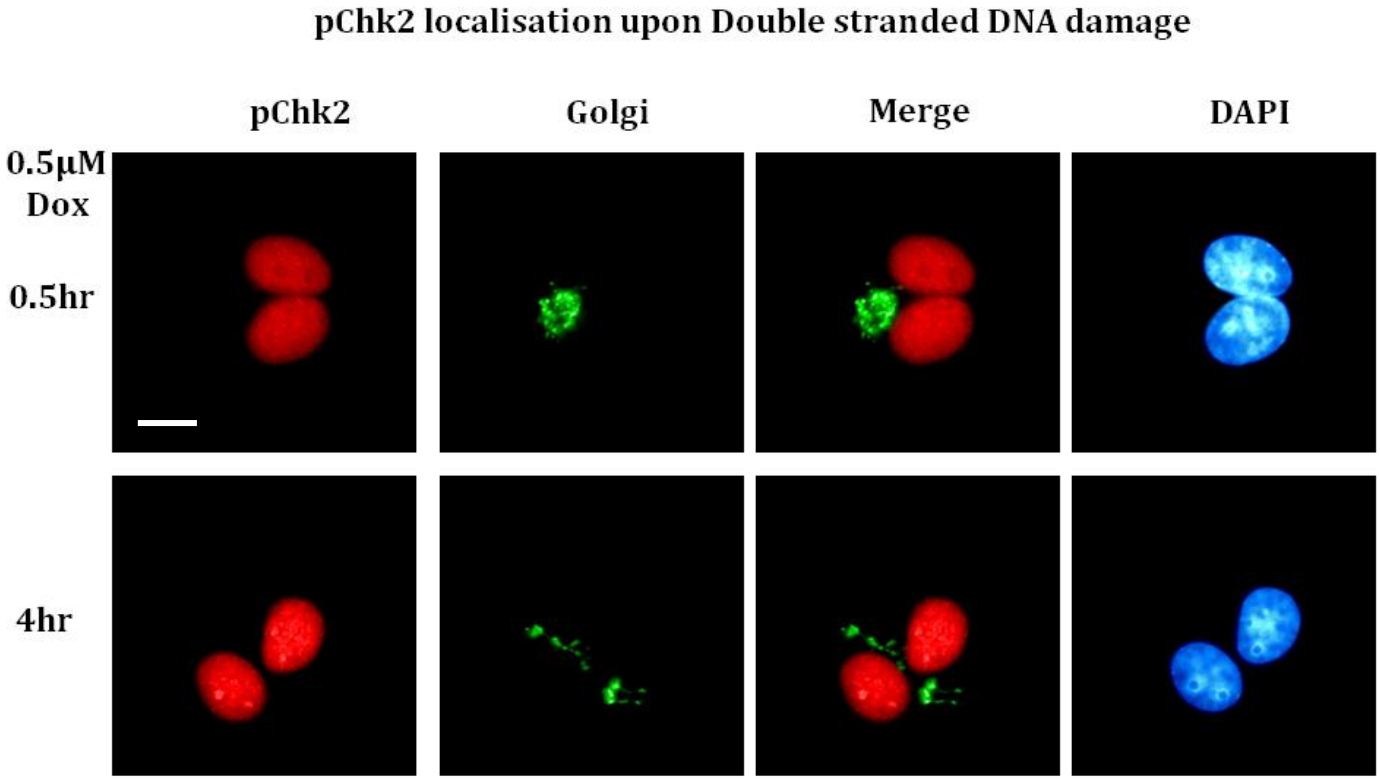
pChk2 localisation upon Double stranded DNA damage
pChk2
Golgi
Merge
DAPI
0.5µM Dox
0.5hr
4hr

**Figure 5.12: Double stranded DNA damage causes rapid exit of pChk2 from Golgi apparatus with an accompanying increase in its nuclear accumulation.** HaCat cells were seeded on Poly L lysine coated coverslips and grown until 70% confluent. Cells were transfected with Golgi marker gene, Mannosidase II-GFP as described in materials and methods. After 16hr of transfection, cells were exposed to 0.5μM Dox for 0.5, and 4hr. This was followed by immunostaining with pChk2 T-68 antibody using Alexa fluor 568® conjugated secondary antibody. Images were captured in relevant channels and co-localisation studies were performed by superimposition of the captured images. Nuclear reference is provided by staining the nuclei with DAPI. The extra nuclear pChk2 in the HaCat cells that co-localised in the Golgi apparatus marker, MannosidaseII-GFP in untreated cells exhibited rapid exit from Golgi apparatus following DNA damage up to 4hr. Hence, co-localisation studies of the merged images of pChk2 and Golgi-GFP did not show any yellow fluorescent staining. These are representative images taken in different fields of views under 100x objective. Scale bar represents 10μm.

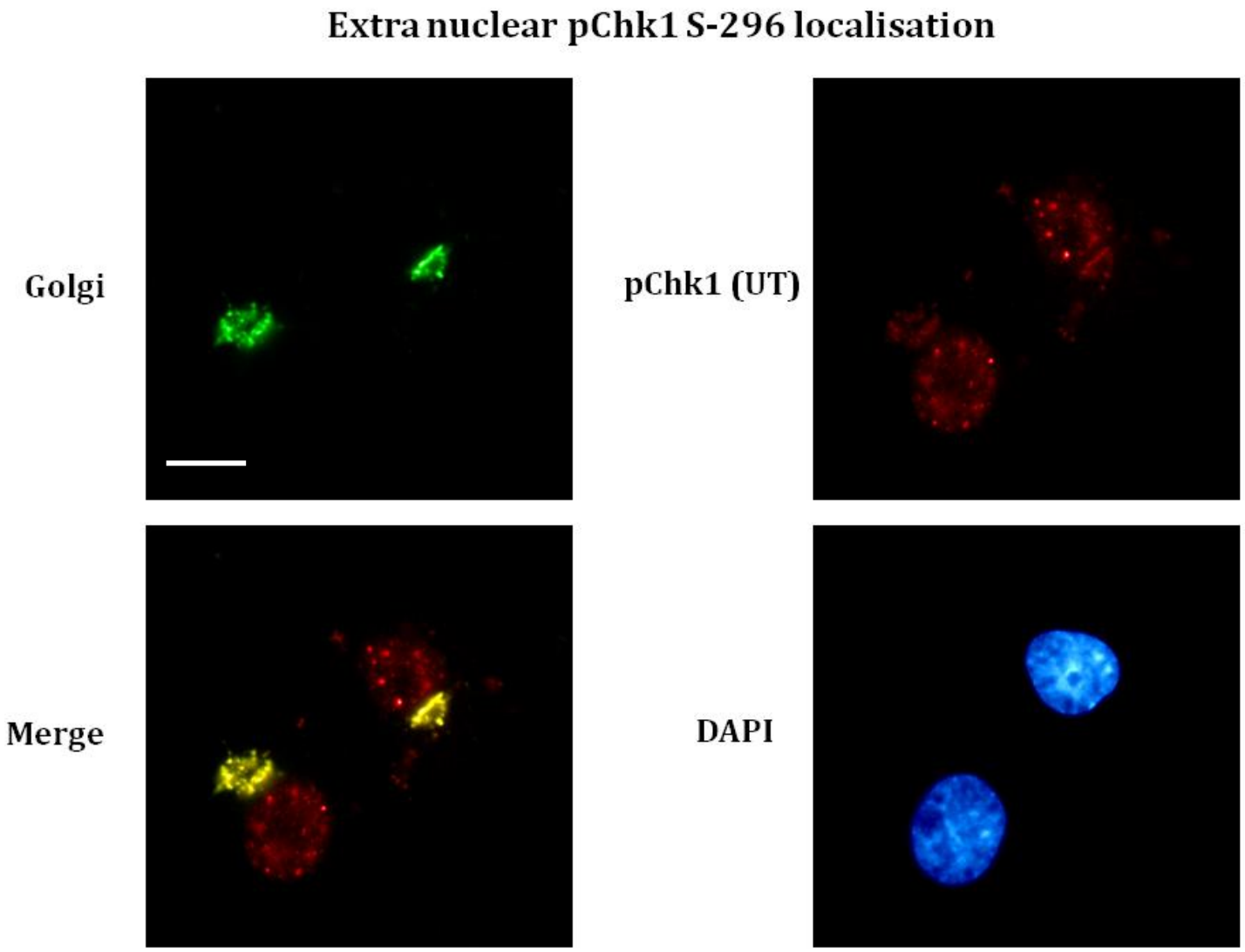


**Figure 5.13: Extra nuclear pChk1 localises in Golgi apparatus in untreated HaCat cells.** HaCat cells were seeded on Poly L lysine coated coverslips and grown until 70% confluent. Cells were transfected with Golgi marker gene, Mannosidase II-GFP as described in materials and methods. After 16 hr of transfection, immunostaining was performed with pChk1S-296 antibody using Alexa fluor 568 conjugated secondary antibody. Images were captured in relevant channels and co-localisation studies were performed by superimposition of the captured images. Nuclear reference is provided by staining the nuclei with DAPI. The extra nuclear pChk1 in the untreated HaCat cells co-localised with the Golgi apparatus marker, Mannosidase II-GFP. The appearance of yellow fluorescence in the merged images of pChk1 and Golgi-GFP confirmed this co-localisation. These are representative images taken in different fields of views under 100x objective. Scale bar represents 10μm.

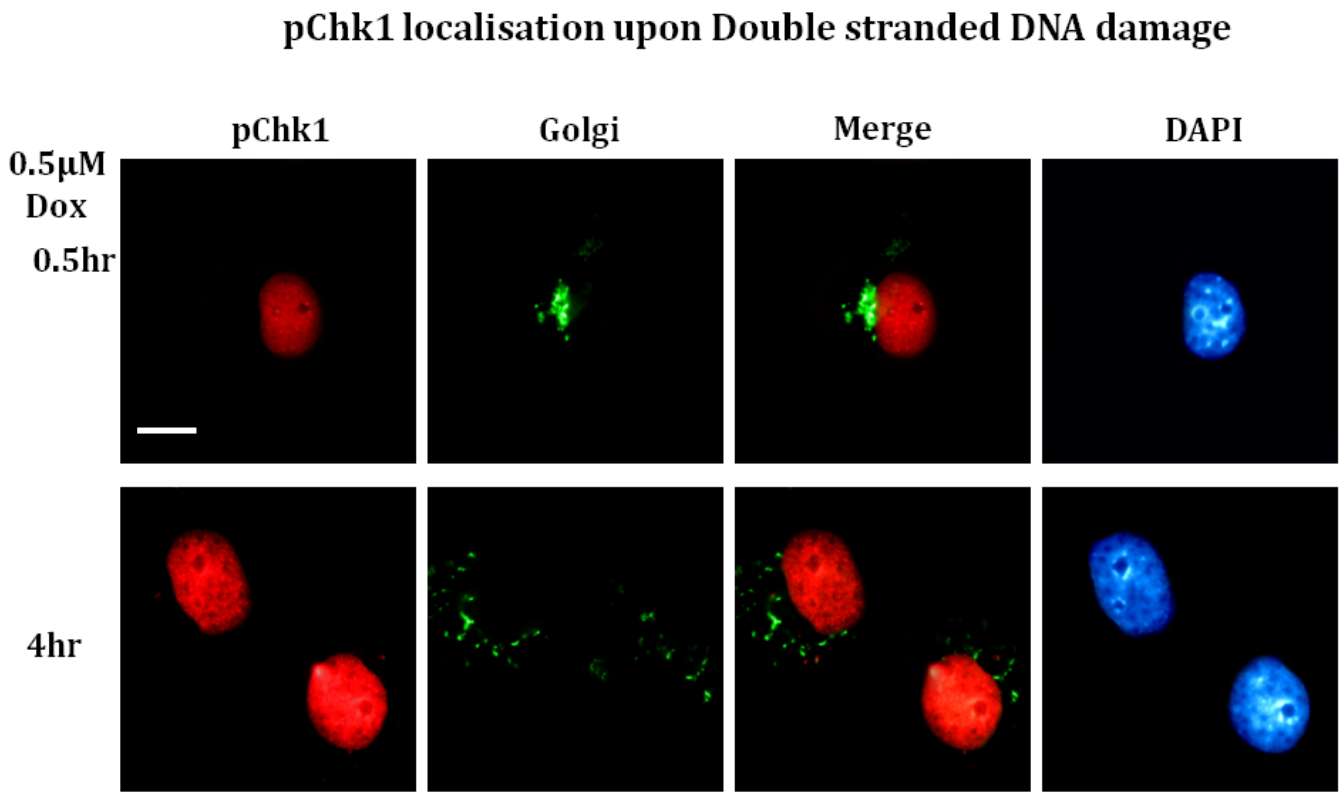
pChk1 localisation upon Double stranded DNA damage
pChk1
Golgi
Merge
DAPI
0.5µM Dox
0.5hr
4hr

**Figure 5.14: Double stranded DNA damage causes rapid exit of pChk1 from Golgi apparatus with an accompanying increase in its nuclear accumulation.** HaCat cells were seeded on Poly L lysine coated coverslips and grown until 70% confluent. Cells were transfected with Golgi marker gene, Mannosidase II-GFP as described in materials and methods. After 16hr of transfection, cells were exposed to 0.5μM Dox for 0.5, and 4hr. This was followed by immunostaining with pChk2 T-68 antibody using Alexa fluor 568® conjugated secondary antibody. Images were captured in relevant channels and co-localisation studies were performed by superimposition of the captured images. Nuclear reference is provided by staining the nuclei with DAPI. The extra nuclear pChk2 in the HaCat cells that co-localised in the Golgi apparatus marker, MannosidaseII-GFP in untreated cells exhibited rapid exit from Golgi apparatus following DNA damage up to 4hr. Hence, co-localisation studies of the merged images of pChk2 and Golgi-GFP did not show any yellow fluorescent staining. These are representative images taken in different fields of views under 100x objective. Scale bar represents 10μm.

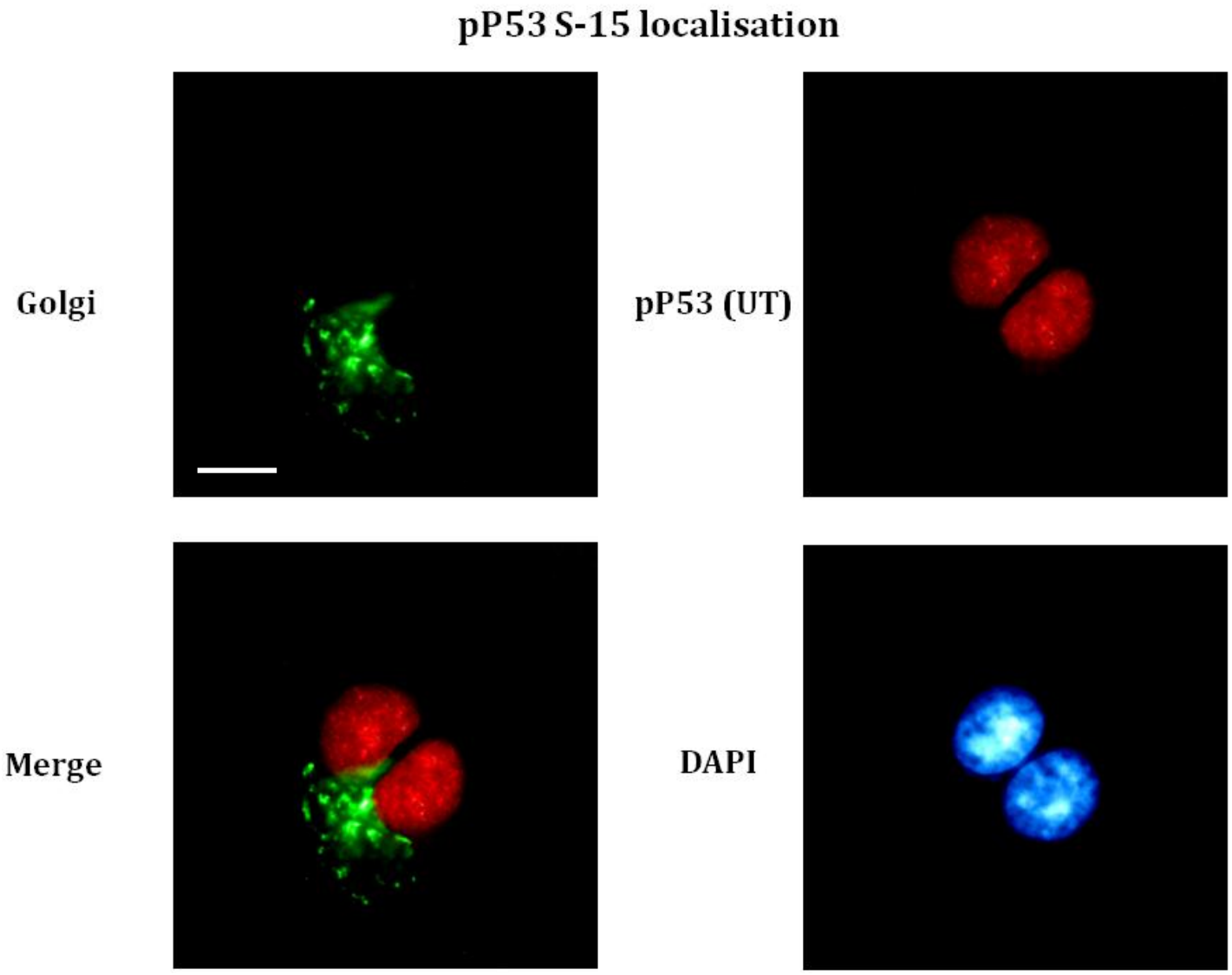


**Figure 5.15: pP53 does not localise in Golgi apparatus in untreated HaCat cells.** HaCat cells were seeded on Poly L lysine coated coverslips and grown until 70% confluent. Cells were transfected with Golgi marker gene, Mannosidase II-GFP as described in materials and methods. After 16 hr of transfection, immunostaining was performed with pP53 S-15 antibody using Alexa fluor 568 conjugated secondary antibody. Images were captured in relevant channels and co-localisation studies were performed by superimposition of the captured images. Nuclear reference is provided by staining the nuclei with DAPI. The pP53 in the untreated HaCat cells did not co-localise with the Golgi apparatus marker, Mannosidase II-GFP. Hence, co-localisation studies of the merged images of pP53 and Golgi-GFP did not show any yellow fluorescent staining. These are representative images taken in different fields of views under 100x objective. Scale bar represents 10μm.

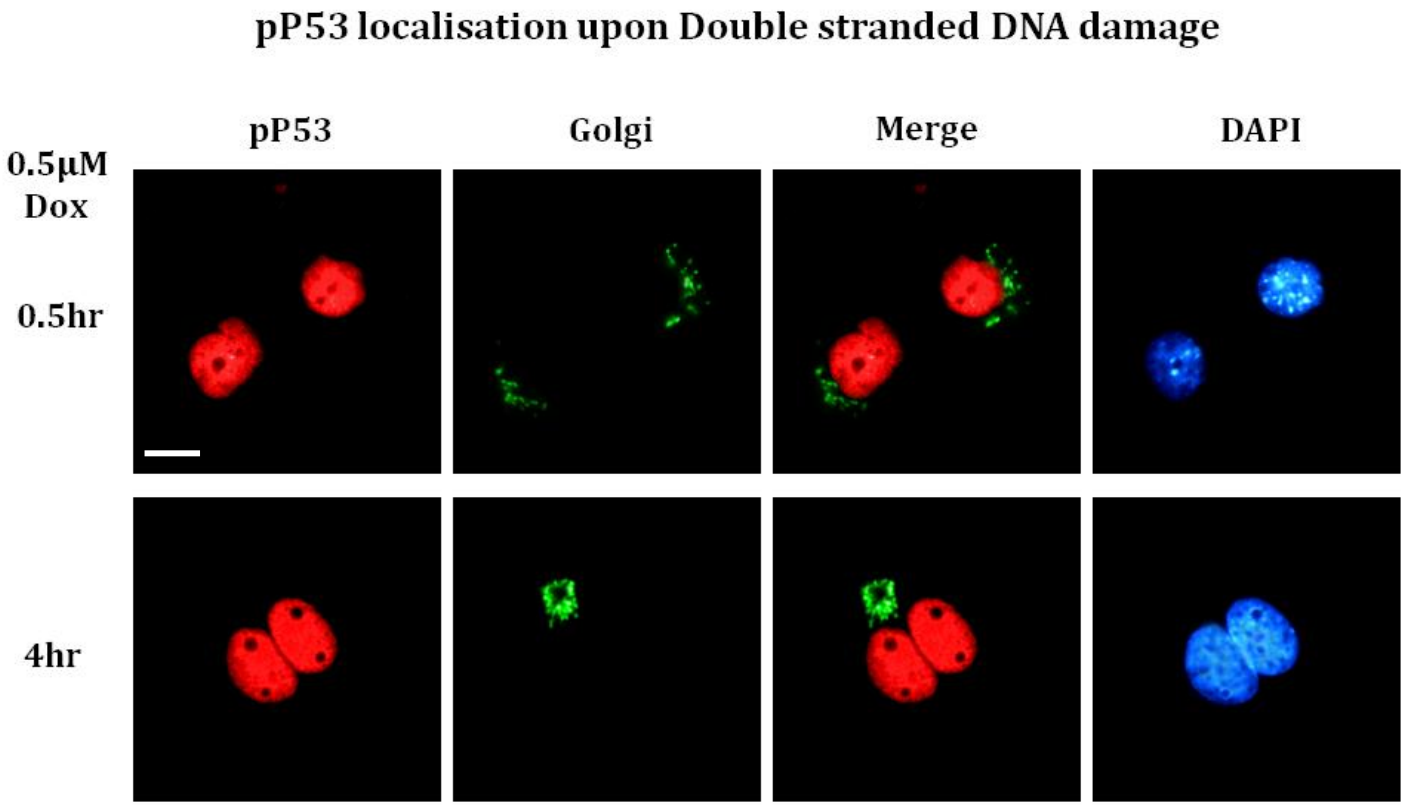
pP53 localisation upon Double stranded DNA damage
pP53
Golgi
Merge
DAPI
0.5µM Dox
0.5hr
4hr

**Figure 5.16: Double stranded DNA damage does not cause localisation of pP53 in Golgi apparatus but induces time dependent increase in its nuclear accumulation.** HaCat cells were seeded on Poly L lysine coated coverslips and grown until 70% confluent. Cells were transfected with Golgi marker gene, Mannosidase II-GFP as described in materials and methods. After 16hr of transfection, cells were exposed to 0.5μM Dox for 0.5, and 4hr. This was followed by immunostaining with pP53 S-15 antibody using Alexa fluor 568® conjugated secondary antibody. Images were captured in relevant channels and co-localisation studies were performed by superimposition of the captured images. Nuclear reference is provided by staining the nuclei with DAPI. pP53 did not co-localise with Golgi apparatus marker, MannosidaseII-GFP following DNA damage up to 4hr. Hence, co-localisation studies of the merged images of pP53 and Golgi-GFP did not show any yellow fluorescent staining. These are representative images taken in different fields of views under 100x objective. Scale bar represents 10μm.

These experiments confirmed that in addition to nuclearly localized pATM as well as pATR, pChk2 and pChk1, these DDR kinases also show localisation in Golgi apparatus in the untreated states and that DNA damage caused a rapid exit of these DDR proteins from Golgi apparatus while an accompanying induction in the nuclear fraction of these proteins. pP53 on the other hand, was not found to localise in Golgi and was predominantly nuclear where it showed induction following DNA damage.

### *5.3.6 Golgi export of pATM upon DNA damage is abrogated after inhibition of ATM kinase demonstrating an autoregulatory trafficking mechanism of ATM with no effect on pATR translocation.*

In order to determine if the kinase activity of ATM has any regulatory role in these early protein trafficking events, and hence in its autoregulation involving trafficking mechanism after DNA damage, I used the ATM kinase inhibitor KU in addition to DNA damage and examined its effects on the observed trafficking of pATM and its functional partner, pATR before and after the activation of DDR. Cells were transfected with the Golgi marker, mannosidase-II as before, and either left untreated, or treated with 0.5μM Dox plus 10μM KU for different time periods as indicated. Immunostaining was then performed for pATM and pATR and their localisation patterns were examined. It was found that addition of KU with Dox caused a reduction in the nuclear pATM as compared to untreated samples or only Dox treated samples (Compare Fig. 5.17 with Fig. 5.6). Surprisingly, I discovered that after the inhibition of ATM kinase, Golgi resident pATM failed to undergo Golgi export following DNA damage at 0.5 hr, 2 or an extended time period of 4 hr of Dox treatment. This was evident at the cellular level by the reappearance of yellow fluorescence in merged images between red fluorescence of pATM and green of Golgi apparatus (Fig. 5.18). This result demonstrated a novel autoregulatory trafficking mechanism of ATM where an active ATM kinase was required to induce pATM export from Golgi and subsequent nuclear accumulation following DNA damage.

On the other hand, the otherwise Golgi resident pATR showed normal Golgi exit and nuclear accumulation even in the presence of ATM kinase inhibitor, demonstrating an ATM independent trafficking mechanism after DNA damage (Fig. 5.16).

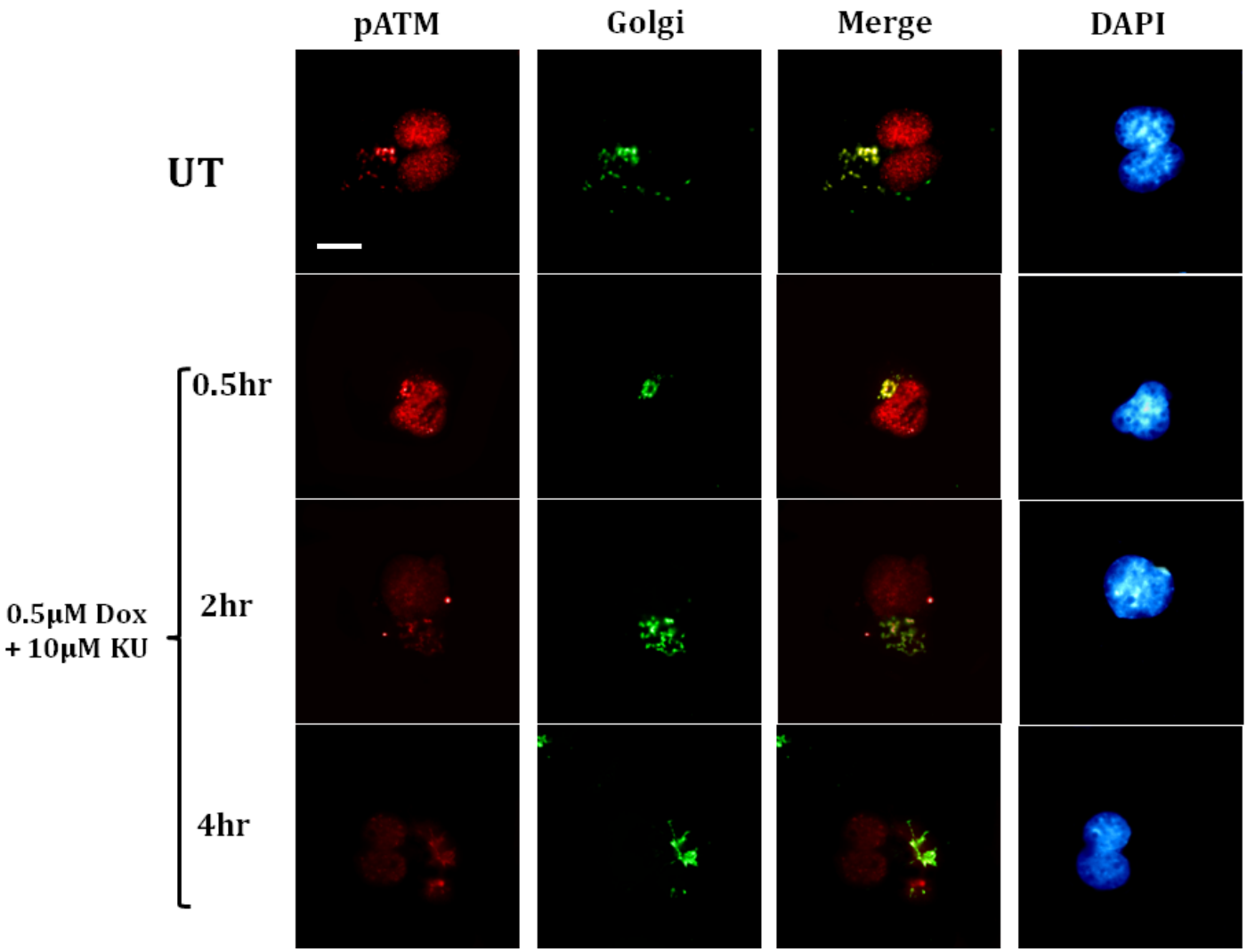
pATM
Golgi
Merge
DAPI
UT
0.5hr
2hr
4hr
0.5μM Dox
+ 10μM KU

**Figure 5.17: DNA damage induced Golgi exit of Golgi resident pATM requires ATM kinase activity in HaCat cells.** HaCat cells were seeded on Poly L lysine coated coverslips and grown until 70% confluent. Cells were transfected with Golgi marker gene, Mannosidase II-GFP as described in materials and methods. After 16hr of transfection, cells were either left untreated, or treated with 0.5μM Dox and 10μM KU for 0.5, 2 and 4hr. Immunostaining was performed with pATM S-1981 antibody using Alexa fluor 568® conjugated secondary antibody. Images were captured in relevant channels and co-localisation studies were performed by superimposition of the captured images. Nuclear reference is provided by staining the nuclei with DAPI. Inhibition of ATM kinase caused failure of pATM to undergo double stranded DNA damage induced Golgi exit at all the time points tested. The appearance of yellow fluorescence in the merged images of pATM and Golgi-GFP confirmed persistent co-localisation even after DNA damage. These are representative images taken in different fields of views under 100x objective. Scale bar represents 10μm.

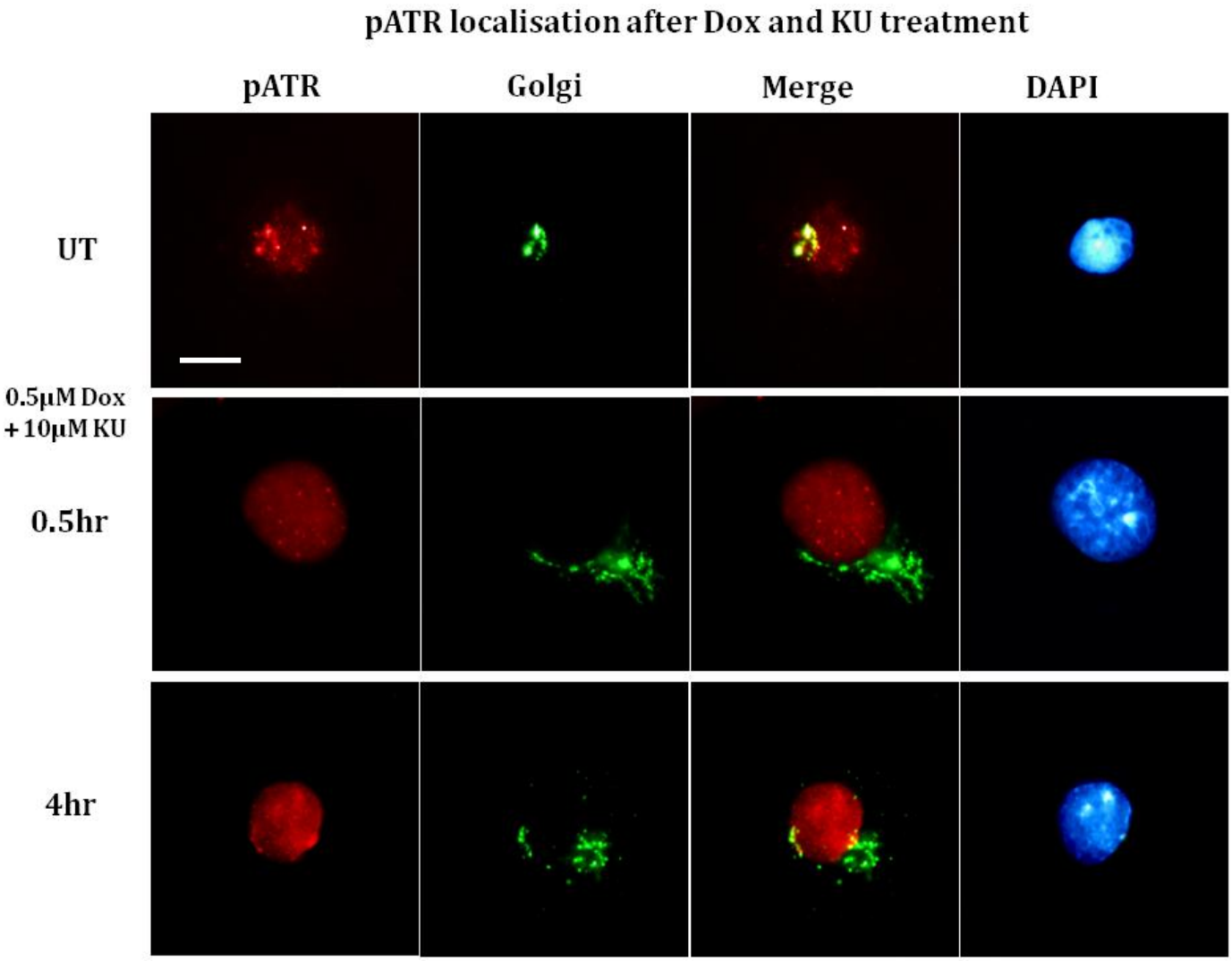
pATR localisation after Dox and KU treatment
pATR
Golgi
Merge
DAPI
UT
0.5μM Dox
+10μM KU
0.5hr
4hr

**Figure 5.18: DNA damage induced Golgi exit of Golgi resident pATR is independent of ATM function in HaCat cells.** HaCat cells were seeded on Poly L lysine coated coverslips and grown until 70% confluent. Cells were transfected with Golgi marker gene, Mannosidase II-GFP as described in materials and methods. After 16hr of transfection, cells were either left untreated, or treated with 0.5μM Dox and 10μM KU for 0.5, and 4hr. Immunostaining was performed with pATR S-428 antibody using Alexa fluor 568® conjugated secondary antibody. Images were captured in relevant channels and co-localisation studies were performed by superimposition of the captured images. Nuclear reference is provided by staining the nuclei with DAPI. Inhibition of ATM kinase did not prevent pATR exit from Golgi apparatus following double stranded DNA damage at the tested time points. Hence, co-localisation studies of the merged images of pATR and Golgi-GFP did not show any yellow fluorescent staining other than in untreated states. These are representative images taken in different fields of views under 100x objective. Scale bar represents 10μm.

These findings were significant as they demonstrated for the first time that the mechanism of sub-cellular ATM trafficking may be under the autoregulation of its kinase function. Furthermore, this mechanism was not found to be regulating pATR trafficking as it was insensitive to ATM inhibition.

### *5.3.7. Cancer cell lines show similar pATM localisation and transport upon double stranded DNA damage and ATM inhibition.*

Key findings of the differential localisation of DDR kinases upon DNA damage and after inhibition of ATM (sections 5.3.1-5.3.6) led me to determine if these early trafficking events are cell type specific or a conserved functional requirement. To determine this, same experiments were performed in other cell lines. Furthermore, another reason for including cancer cells was to identify any differences within ATM trafficking mechanism in normal and cancer cell lines. While conservation of this transport mechanism of ATM across difference cell lines would indicate its functional requirement and hence significance, any differences on the other hand, could be utilised to base therapeutic selectivity against cancer cells.

To this end, breast cancer cell lines MCF7 and MDB-MBA 231 were included in the current aspect of study. MCF7 cell line has a wild type P53 while MDA-MB 231 has a mutated P53. While experiments with such cell lines would fulfil the above mentioned objectives, these would also demonstrate if a functional P53 is required for this transport mechanism of ATM.

MCF 7 and MDA-MB 231 cells were transfected with Golgi marker, mannosidase-II-GFP and either left untreated, or treated with either 0.5μM Dox for 0.5, 2 and 4 hours or 0.5μM Dox plus 10μM KU for 0.5 and 4 hr. Following this, immunostaining was performed for pATM S-1981 using Alexa fluor 568 conjugated secondary antibody.

It was found that in both cancer cell lines, pATM was localized in the Golgi apparatus in the untreated states (Fig. 5.19 & 5.22). However, Dox treatment for all the time points tested resulted in Golgi exit of pATM in both MCF7 (Fig. 5.20) and MDA-MB 231 (Fig. 5.23) cell lines with an accompanying nuclear accumulation. Importantly, consistent with the findings for HaCat cell line, inhibition of ATM resulted in both failure of pATM to exit Golgi and nuclear accumulation after DNA damage in MCF7 (Fig. 5.21) as well as in MDA MB 231 (Fig. 5.24) cancer cell lines.

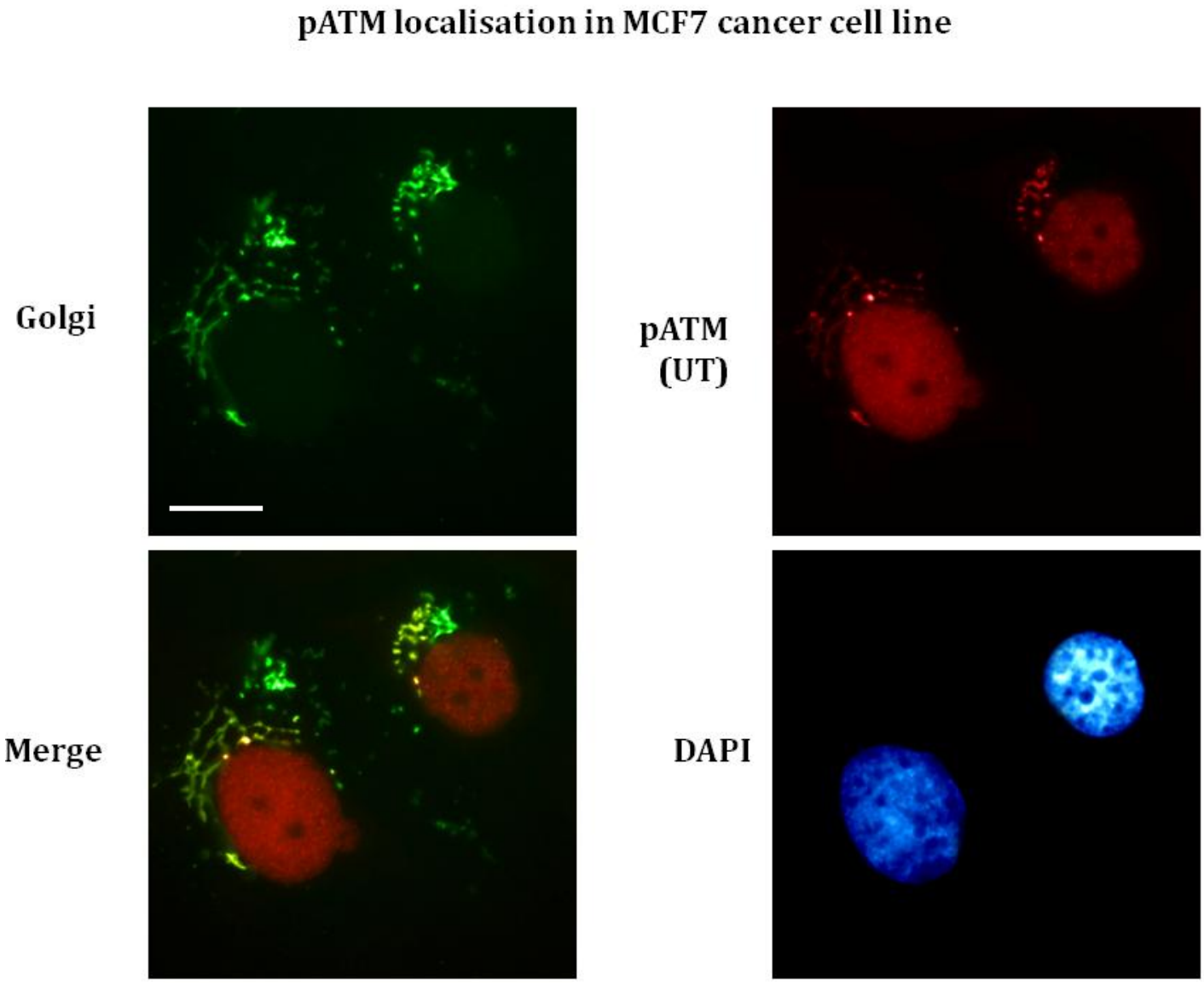


**Figure 5.19: In MCF7 breast cancer cell line, extra nuclear pATM localises in Golgi apparatus in untreated states.** Breast cancer cell line, MCF7 were seeded on Poly L lysine coated coverslips and grown until 70% confluent. Cells were transfected with Golgi marker gene, Mannosidase II-GFP as described in materials and methods. After 16 hr of transfection, immunostaining was performed with pATM 1981 antibody using Alexa fluor 568 conjugated secondary antibody. Images were captured in relevant channels and co-localisation studies were performed by superimposition of the captured images. Nuclear reference is provided by staining the nuclei with DAPI. The Extra nuclear pATM in the untreated MCF7 cells co-localised with Golgi apparatus marker, Mannosidase II-GFP. The appearance of yellow fluorescence in the merged images of pATM and Golgi-GFP confirmed this co-localisation. These are representative images taken in different fields of views under 100x objective. Scale bar represents 10µm.

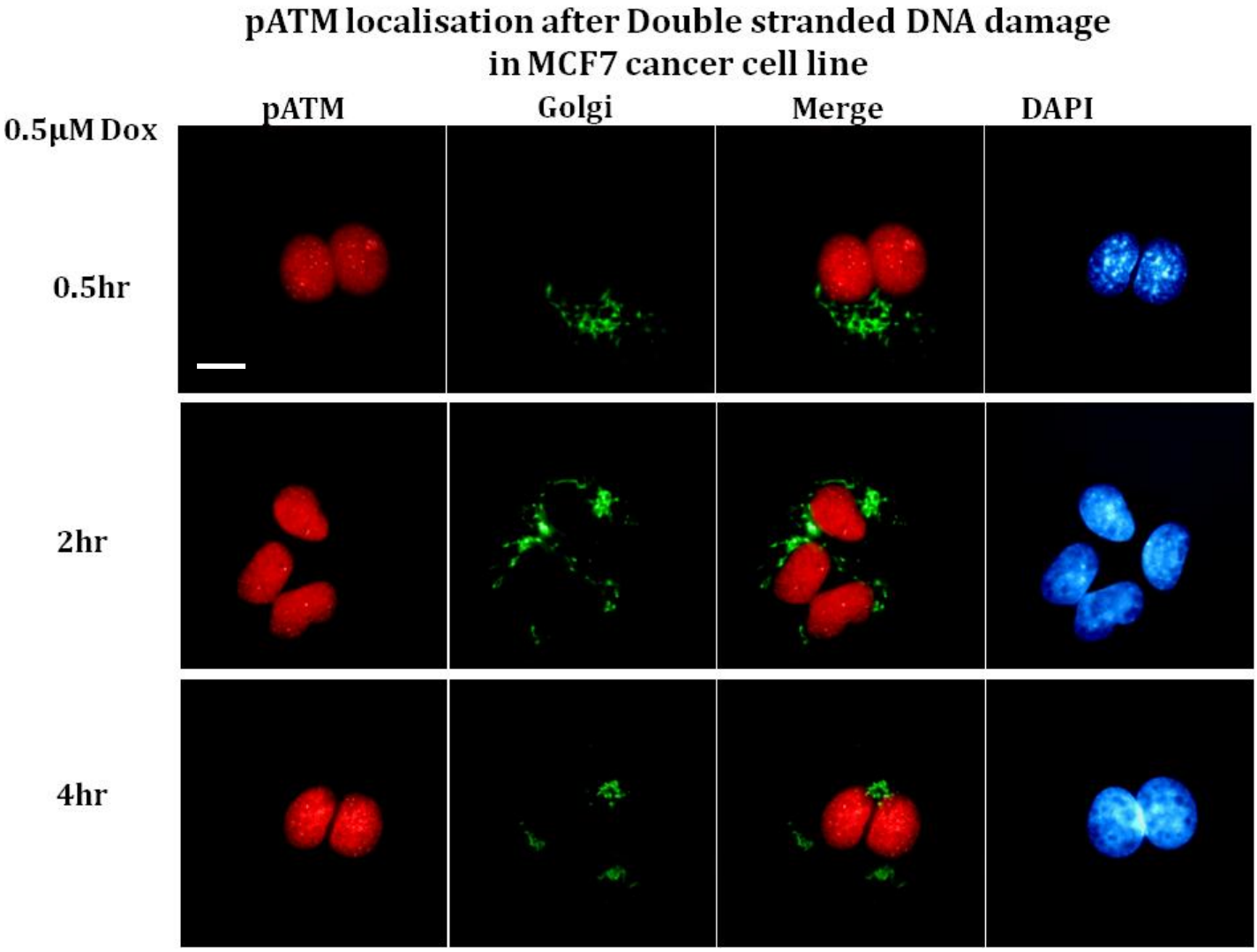
pATM localisation after Double stranded DNA damage
in MCF7 cancer cell line
pATM
Golgi
Merge
DAPI
0.5µM Dox
0.5hr
2hr
4hr

**Figure 5.20: In MCF7 breast cancer cell line, double stranded DNA damage causes rapid exit of pATM from Golgi apparatus with an accompanying time dependent increase in its nuclear accumulation.** Breast cancer cell line, MCF7 were seeded on Poly L lysine coated coverslips and grown until 70% confluent. Cells were transfected with Golgi marker gene, Mannosidase II-GFP as described in materials and methods. After 16hr of transfection, cells were exposed to 0.5μM Dox for 0.5, 2 and 4hr. This was followed by immunostaining with pATM 1981 antibody using Alexa fluor 568® conjugated secondary antibody. Images were captured in relevant channels and co-localisation studies were performed by superimposition of the captured images. Nuclear reference is provided by staining the nuclei with DAPI. The extra nuclear pATM in the MCF7 cells that co-localised in the Golgi apparatus marker, MannosidaseII-GFP in untreated state exhibited rapid exit from Golgi apparatus following DNA damage up to 4hr. Hence, co-localisation studies of the merged images of pATM and Golgi-GFP did not show any yellow fluorescent staining. These are representative images taken in different fields of views under 100x objective. Scale bar represents 10μm.

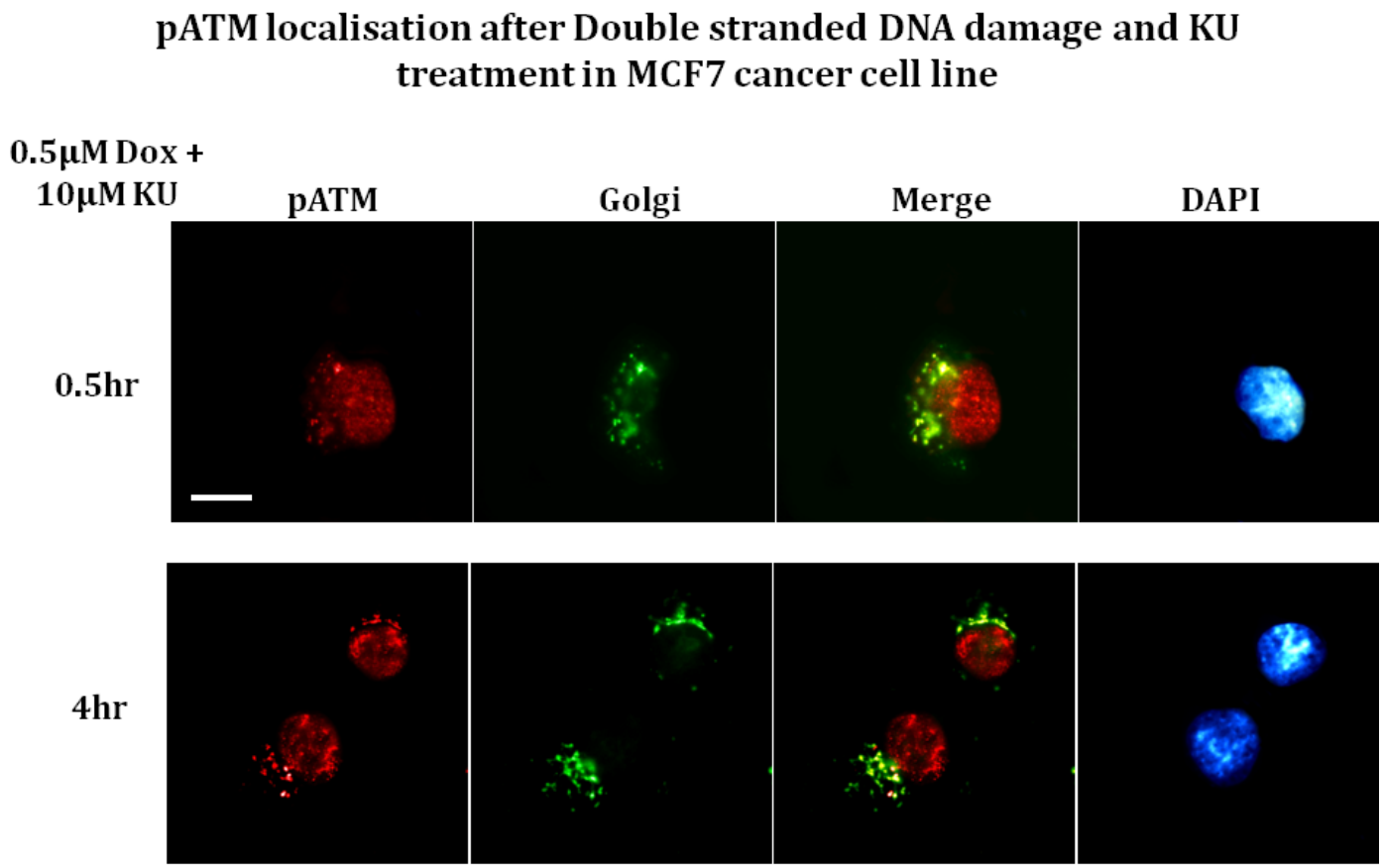


**Figure 5.21: In MCF7 breast cancer cell line, DNA damage induced Golgi exit of Golgi resident pATM and its subsequent nuclear accumulation requires ATM kinase activity.** Breast cancer cell lines, MCF7, were seeded on Poly L lysine coated coverslips and grown until 70% confluent. Cells were transfected with Golgi marker gene, Mannosidase II-GFP as described in materials and methods. After 16 hr of transfection, cells were either left untreated, or treated with 0.5µM Dox and 10µM KU for 0.5 and 4 hr. Immunostaining was performed with pATM S-1981 antibody using Alexa fluor 568 conjugated secondary antibody. Images were captured in relevant channels and co-localisation studies were performed by superimposition of the captured images. Nuclear reference is provided by staining the nuclei with DAPI. Inhibition of ATM kinase caused failure of pATM to undergo double stranded DNA damage induced Golgi exit at all the time points tested. The appearance of yellow fluorescence in the merged images of pATM and Golgi-GFP confirmed persistent co-localisation even after DNA damage. These are representative images taken in different fields of views under 100x objective. Scale bar represents 10µm.

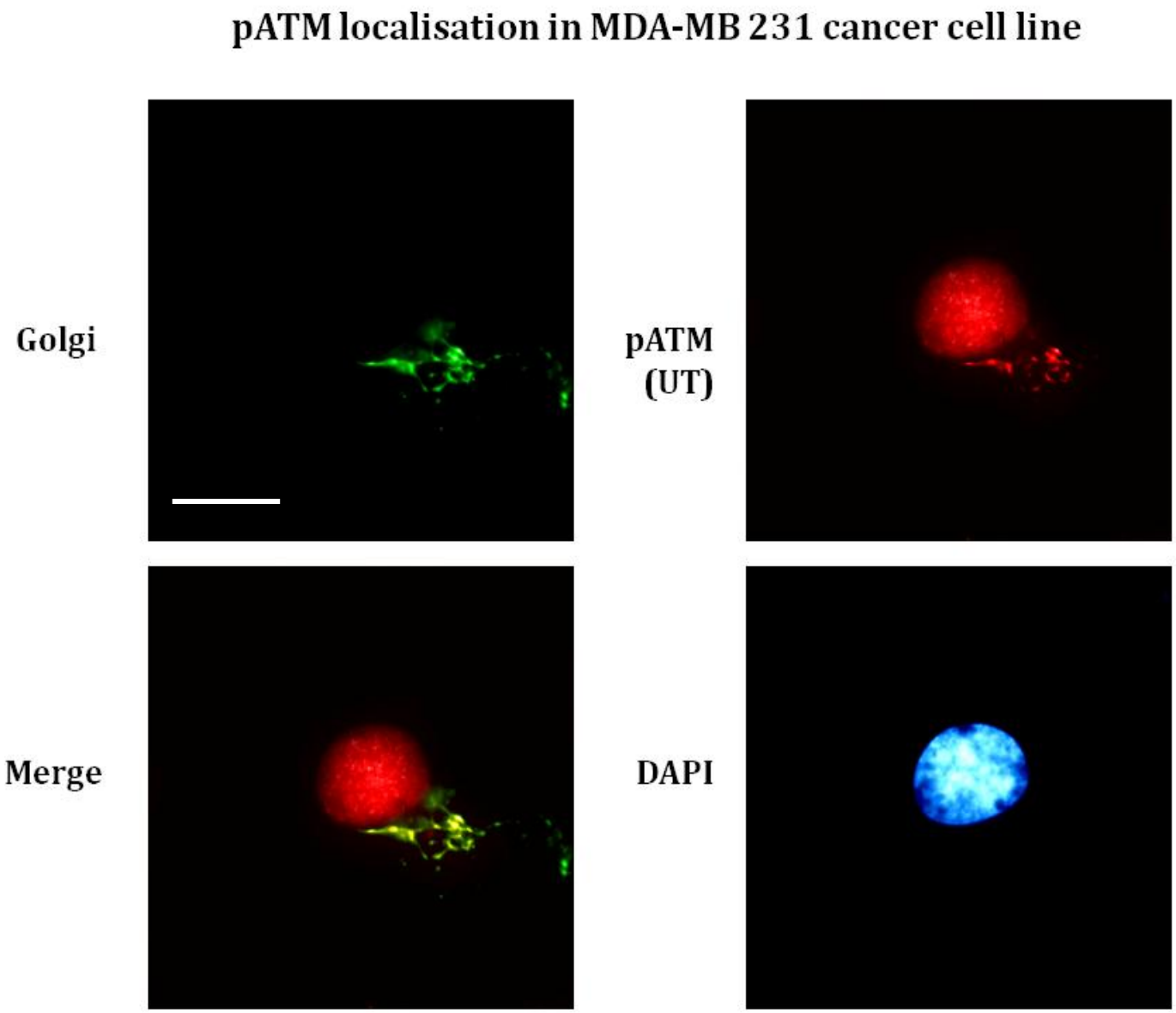


**Figure 5.22: In MDA-MB 231 breast cancer cell line, extra nuclear pATM co-localises in Golgi apparatus in untreated states.** Breast cancer cell line, MDA-MB 231 were seeded on Poly L lysine coated coverslips and grown until 70% confluent. Cells were transfected with Golgi marker gene, Mannosidase II-GFP as described in materials and methods. After 16 hr of transfection, immunostaining was performed with pATM 1981 antibody using Alexa fluor 568 conjugated secondary antibody. Images were captured in relevant channels and co-localisation studies were performed by superimposition of the captured images. Nuclear reference is provided by staining the nuclei with DAPI. The Extra nuclear pATM in the untreated MDA MB-231 cells co-localised with Golgi apparatus marker, Mannosidase II-GFP. The appearance of yellow fluorescence in the merged images of pATM and Golgi-GFP confirmed this co-localisation. These are representative images taken in different fields of views under 100x objective. Scale bar represents 10μm.

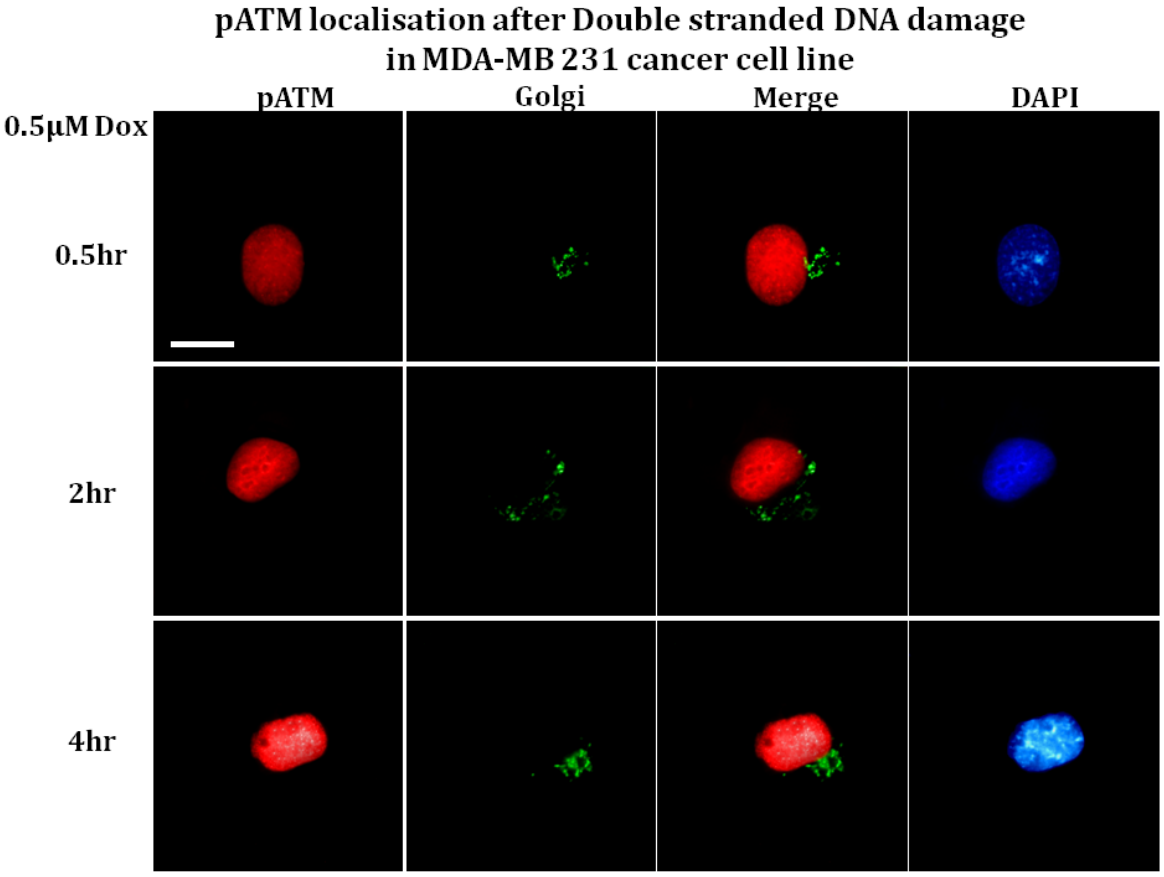
pATM localisation after Double stranded DNA damage
in MDA-MB 231 cancer cell line
pATM
Golgi
Merge
DAPI
0.5μM Dox
0.5hr
2hr
4hr

**Figure 5.23: In MDA-MB 231 breast cancer cell line, double stranded DNA damage causes rapid exit of pATM from Golgi apparatus with an accompanying time dependent increase in its nuclear accumulation.** Breast cancer cell line, MDA-MB 231 were seeded on Poly L lysine coated coverslips and grown until 70% confluent. Cells were transfected with Golgi marker gene, Mannosidase II-GFP as described in materials and methods. After 16 hr of transfection, cells were exposed to 0.5μM Dox for 0.5, 2 and 4 hr. This was followed by immunostaining with pATM 1981 antibody using Alexa fluor 568 conjugated secondary antibody. Images were captured in relevant channels and co-localisation studies were performed by superimposition of the captured images. Nuclear reference is provided by staining the nuclei with DAPI. The extra nuclear pATM in the MDA-MB 231 cells that co-localised in the Golgi apparatus marker, Mannosidase II-GFP in untreated state exhibited rapid exit from Golgi apparatus following DNA damage up to 4 hr. Hence, co-localisation studies of the merged images of pATM and Golgi-GFP did not show any yellow fluorescent staining. These are representative images taken in different fields of views under 100x objective. Scale bar represents 10μm.

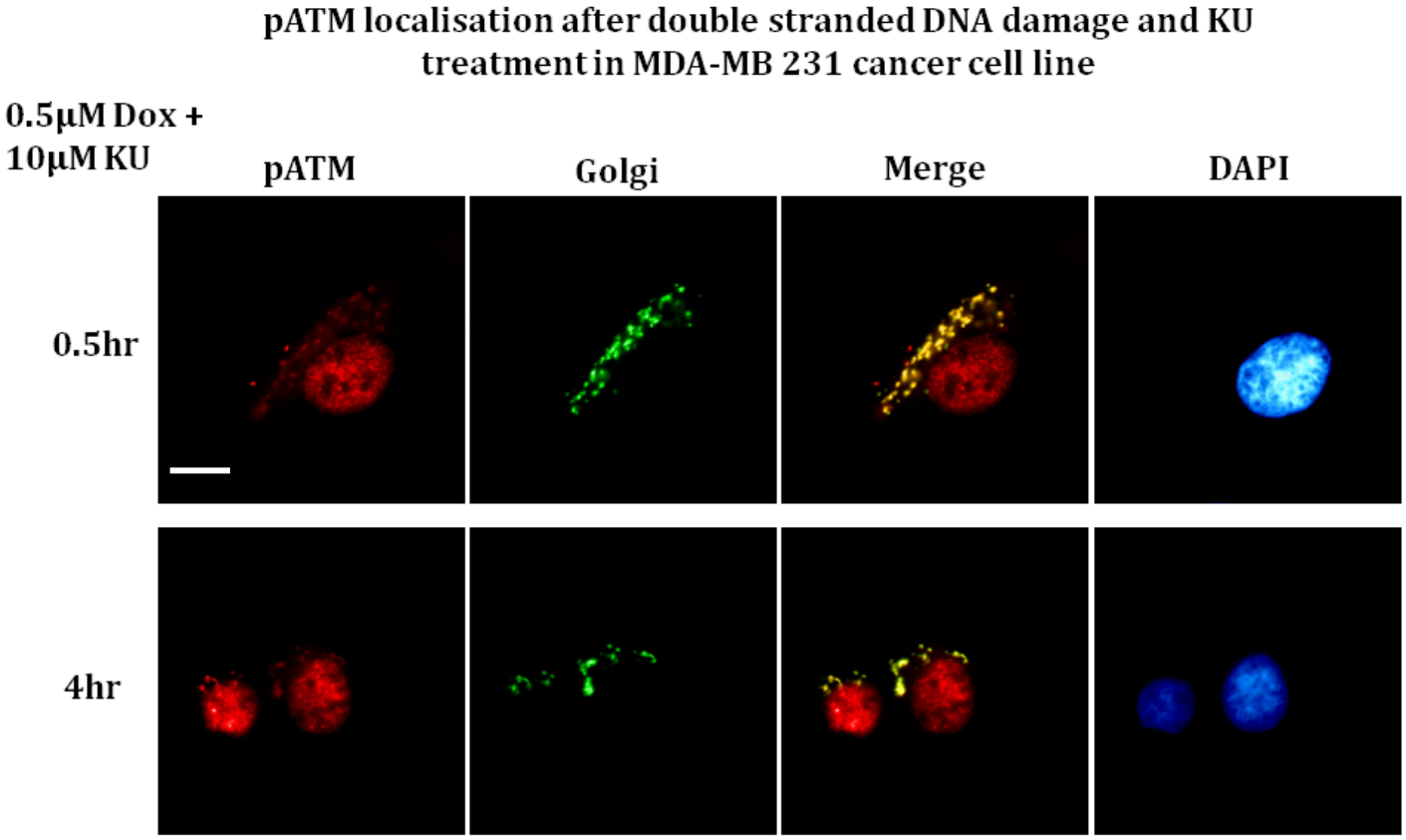
pATM localisation after double stranded DNA damage and KU treatment in MDA-MB 231 cancer cell line
0.5µM Dox + 10µM KU
pATM
Golgi
Merge
DAPI
0.5hr
4hr

**Figure 5.24: In MDA-MB 231 breast cancer cell line, DNA damage induced Golgi exit of Golgi resident pATM and its subsequent nuclear accumulation requires ATM kinase activity.** Breast cancer cell lines, MDA-MB 231, were seeded on Poly L lysine coated coverslips and grown until 70% confluent. Cells were transfected with Golgi marker gene, Mannosidase II-GFP as described in materials and methods. After 16hr of transfection, cells were either left untreated, or treated with 0.5μM Dox and 10μM KU for 0.5 and 4hr. Immunostaining was performed with pATM S-1981 antibody using Alexa fluor 568® conjugated secondary antibody. Images were captured in relevant channels and co-localisation studies were performed by superimposition of the captured images. Nuclear reference is provided by staining the nuclei with DAPI. Inhibition of ATM kinase caused failure of pATM to undergo double stranded DNA damage induced Golgi exit at all the time points tested. The appearance of yellow fluorescence in the merged images of pATM and Golgi-GFP confirmed persistent co-localisation even after DNA damage. These are representative images taken in different fields of views under 100x objective. Scale bar represents 10μm.

These experiments confirmed that pATM trafficking events determined in HaCat cell lines are not only ATM kinase dependent, indicating another autoregulatory aspect of ATM function, but they are also reproducible in cancer cell lines demonstrating cell type independence as well as indicating that this autoregulatory trafficking mechanism may be a conserved functional requirement for ATM. Furthermore, in MDA-MB231 cell line, which has a mutated P53, the conservation of ATM transport from Golgi to nucleus upon DNA damage illustrated that this traffic mechanism did not require normal function of P53.

### *5.3.8 Cytoplasmic pATM co-localises with coatomer protein subunit, β-COP-I in untreated HaCat cells while DNA damage causes discontinuation of this co-localisation.*

Localisation of pATM in the Golgi apparatus and its rapid exit following DNA damage with a subsequent nuclear accumulation points towards a trafficking event which may involve transport vesicles formed by coatomer proteins. If indeed coatomer proteins were involved in the previously demonstrated Golgi export of pATM, it should form complexes with one of the coatomer proteins within the Golgi apparatus. One candidate coatomer protein was COPI which reversibly associates with Golgi resident proteins within Golgi apparatus and is essential for retrograde transport away from Golgi membrane. COPI is also known to be a cytosolic protein that binds to di-lysine motifs (Beck R et al., 2009). The choice of COPI for pATM traffic was based on the biological insights, observations and previous reports listed in section 5.4. In order to determine ATM co-localisation and cross talk with COPI, and examine its sub-cellular changes during stress responses, the gene for the β-COP subunit of COPI, known to be an integral subunit of the hetero-heptamer complex of COPI and essential for its function (Eugster A et al., 2000), was first tagged with GFP at the N-terminal.

This construct was then cloned in PCDNA 3.1 vector (Full details of β-COPI cloning procedure are given in Appendix-I, section A1.3).

The β-COPI-GFP was transfected into HaCat cells, allowed to express for 24 hr, and then subjected to fluorescent immunolocalisation studies with immunolabelled pATM. This was the first ever study looking at pATM localisation with respect to COPI. Figure 5.25 shows N-terminally tagged β-COPI with GFP expression in HaCat cells under normal conditions. The β-COPI-GFP appeared to express in cytoplasm, Golgi apparatus and plasma membrane. While expression was concentrated more in the nuclear and Golgi sub-cellular compartments, it also diffused to other parts of the cell (Fig. 5.25).

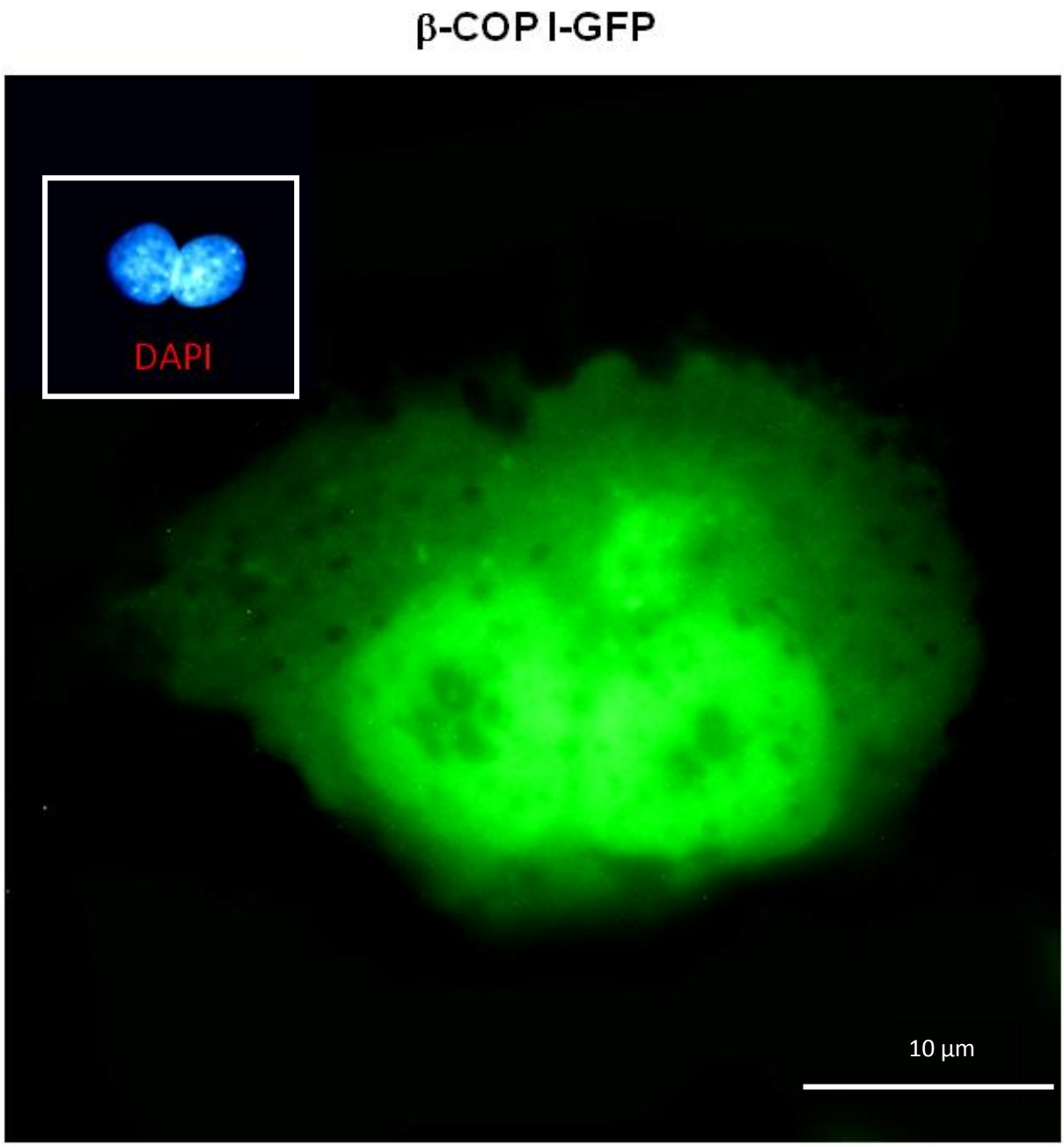


**Figure 5.25: N-terminal GFP tagged β-COPI expression in HaCat cells**. HaCat cells were seeded on Poly L lysine coated coverslips placed in 60mm tissue culture plates at a density of 8 x $10^5$ cells and allowed to grow until 70-90% confluent. 5µG of GFP-β-COPI DNA was transfected by Lipofection as described in materials and methods and cells allowed to grow for 16-24 hrs. For nuclear reference, DAPI staining was used. β-COPI was shown to express in the peripheral membranes, cytoplasm and Golgi apparatus. This is a representative image taken with 100x objective.

Strikingly, immunostained pATM with Alexa fluor 568 as secondary antibody (red fluorescence) revealed that the extra nuclear, Golgi resident pATM co-localised with β-COPI in the untreated cells, evident from the appearance of yellow fluorescence in the merged images of β-COPI expressing cell and extra nuclear pATM (Fig. 5.26). This was a novel finding, which for the first time demonstrated that extra nuclear pATM co-localised with β-COPI coatomer protein subunit.

When β-COPI transfected cells were exposed to 0.5μM Dox for 0.5, 2 and 4 hours, it was found that β-COPI showed some localisational rearrangement and seemed to restrict more to the nucleus (Fig. 5.27). Additionally, when β-COPI expressing cells were subjected to immunostaining for pATM, it was further revealed that β-COPI ceased to show the previously observed co-localisation with pATM at all the three time points with an accompanying induction of nuclear pATM (Fig. 5.27). The co-localisation detected between β-COPI and pATM in the untreated cells (Fig. 5.26) imply that COPI coatomer proteins may be involved in pATM transport and that upon DNA damage, it may mediate its rapid Golgi export and nuclear accumulation (Fig. 5.27).

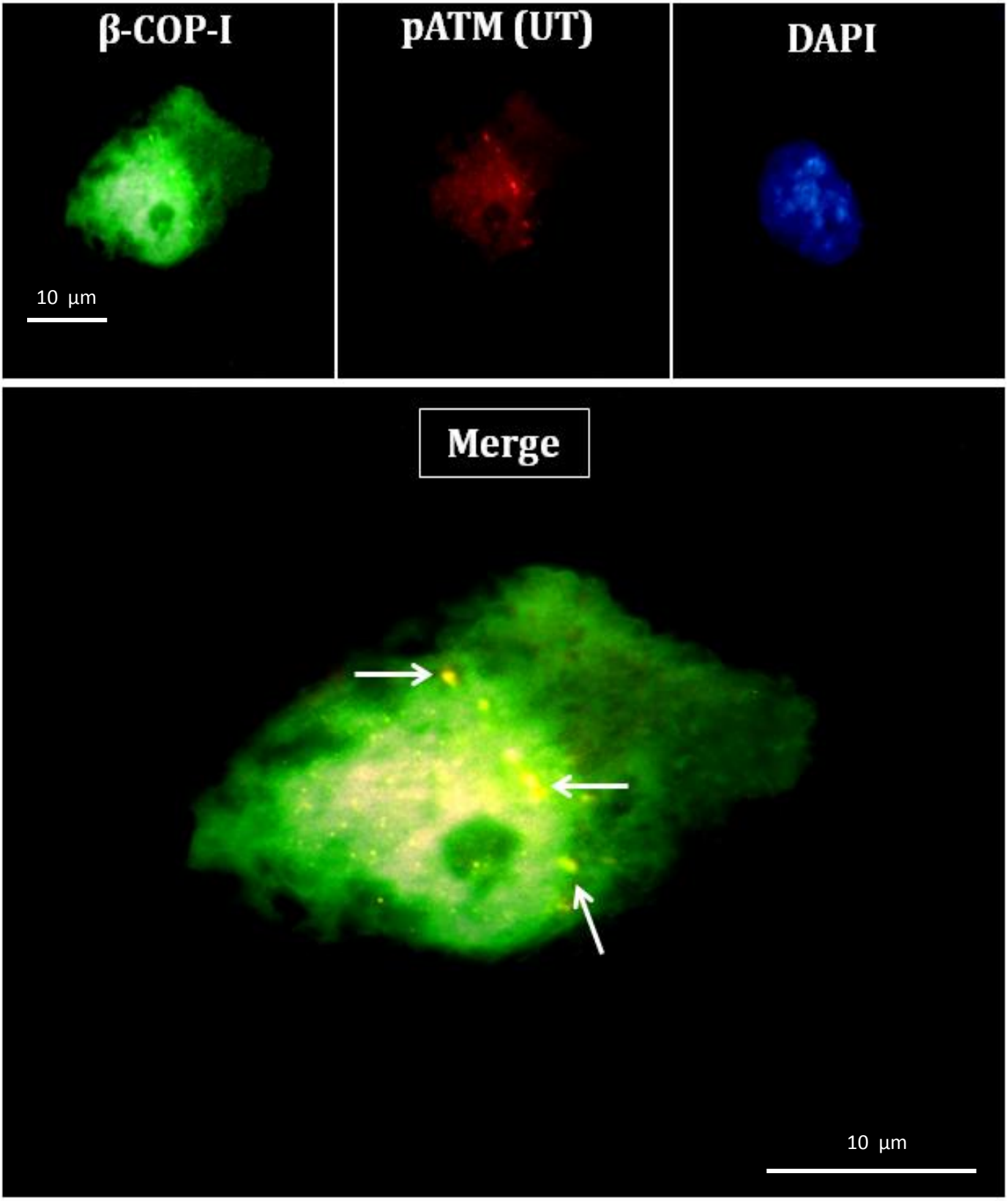
β-COP-I
pATM (UT)
DAPI
10 µm
Merge
10 µm

**Figure 5.26: β-COPI co-localises with Golgi resident pATM in untreated HaCat cells.** HaCat cells were seeded on Poly L lysine coated coverslips and grown until 70% confluent. Cells were transfected with N-terminal GFP tagged β-COPI as described in materials and methods. After 16 hr of transfection, immunostaining was performed with pATM 1981 antibody using Alexa fluor 568 conjugated secondary antibody. Images were captured in relevant channels and co-localisation studies were performed by superimposition of the captured images. Nuclear reference is provided by staining the nuclei with DAPI. β-COPI in the untreated HaCat cells co-localised with Golgi resident pATM. The appearance of yellow fluorescence in the merged images of β-COPI and pATM, indicated by white arrows, confirmed this co-localisation. These are representative images taken in different fields of views under 100x objective.

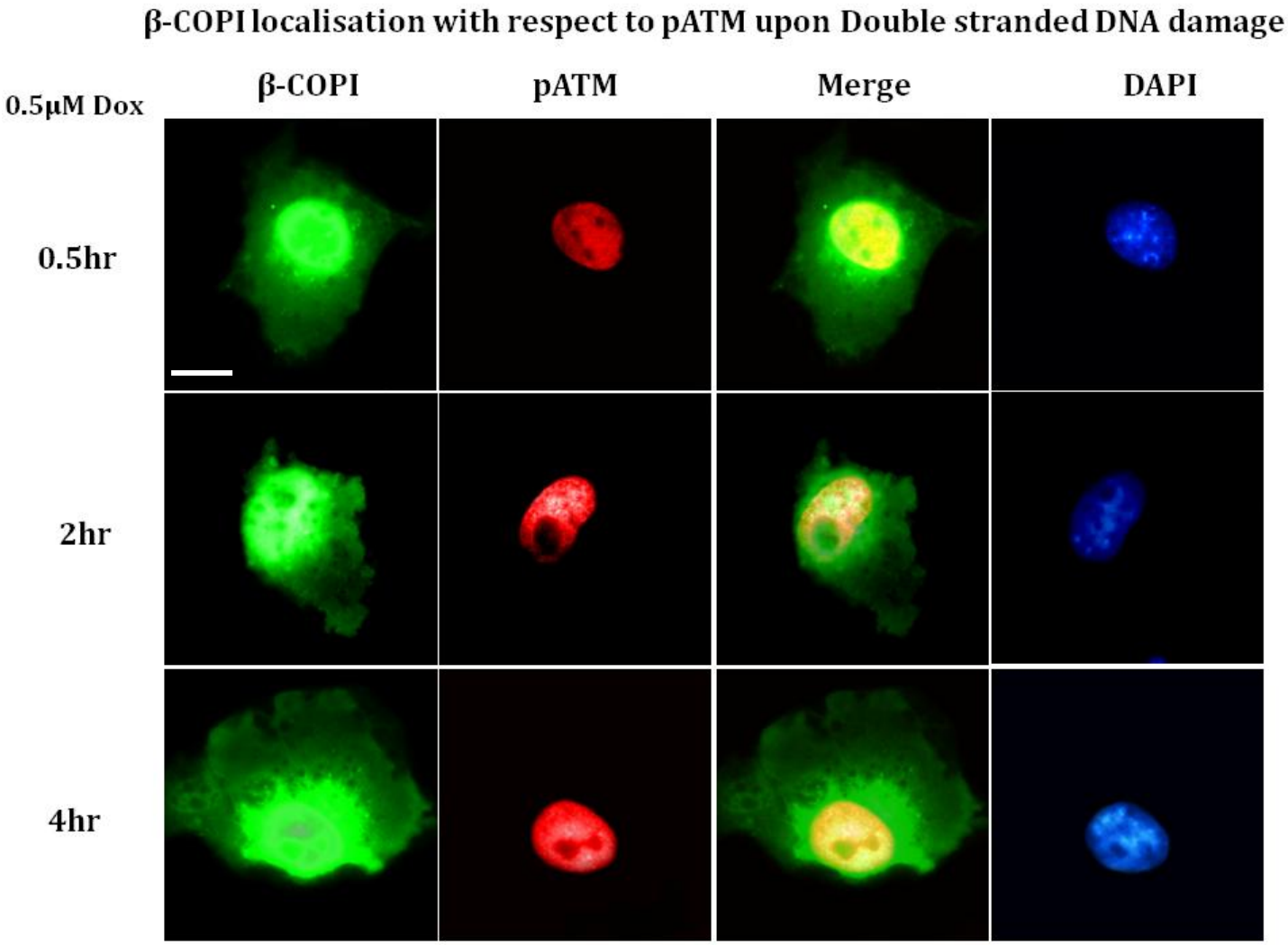


**Figure 5.27: β-COPI ceases to colocalise with pATM following double stranded DNA damage.** HaCat cells were seeded on Poly L lysine coated coverslips and grown until 70% confluent. Cells were transfected with N-terminal GFP tagged β-COPI as described in materials and methods. After 16 hr of transfection, cells were exposed to 0.5μM Dox for 0.5, 2 and 4 hr. This was followed by immunostaining with pATM 1981 antibody using Alexa fluor 568 conjugated secondary antibody. Images were captured in relevant channels and co-localisation studies were performed by superimposition of the captured images. Nuclear reference is provided by staining the nuclei with DAPI. Following Dox treatment, pATM discontinued to co-localise with β-COPI immediately after 0.5 hr of treatment and up to 4 hrs and showed nuclear induction. Hence, co-localisation studies of the merged images of pATM and Golgi-GFP did not show any yellow fluorescent staining. These are representative images taken in different fields of views under 100x objective. Scale bar represents 10μm.

### *5.3.9. Inhibition of ATM kinase disrupts the Golgi retained, cytoplasmic pATM co-localisation with β-COPI following double stranded DNA damage.*

I next argued that if Golgi resident pATM failed to exit from Golgi apparatus after its kinase inhibition (Fig. 5.17), and that if pATM export from Golgi was mediated by COPI coatomer protein, then inhibition of ATM should also result in disruption of its co-localisation with β-COPI. To answer this, HaCat cells were transfected with β-COPI and treated with 10μM KU in addition to Dox for 0.5, 2 and 4 hour time points followed by immunostaining such cells for pATM. This experiment helped to determine whether failure of pATM to exit Golgi apparatus upon its kinase inhibition also resulted in or was caused by disruption of its co-localisation with β-COPI.

A striking finding was that inhibition of ATM kinase, in addition to its expected retention in the Golgi apparatus, also resulted in disruption of co-localisation between β-COPI and Golgi resident pATM (Fig. 5.28). Furthermore, while the earliest time point of 0.5 hr treatment resulted in loss of co-localisation of pATM with β-COPI, these two molecules were still in closer proximity as evident in the corresponding merged image. However at further time points of 2 and 4 hour, they had completely dissociated. This result confirmed the above hypothesis and further supported the fact that ATM may undergo COPI mediated transport from Golgi apparatus upon DNA damage.

An additional observation was that the localisational changes of β-COPI seen in Fig. 5.27 after DNA damage, which caused a more restricted accumulation around nucleus, were still retained after KU treatment. Hence, while active ATM kinase was required for its own trafficking, its inhibition did not prevent distinct localisational changes in β-COPI itself in Fig. 5.28, which clearly demonstrated a time dependent restrictive accumulation of β-COPI in the nucleus.

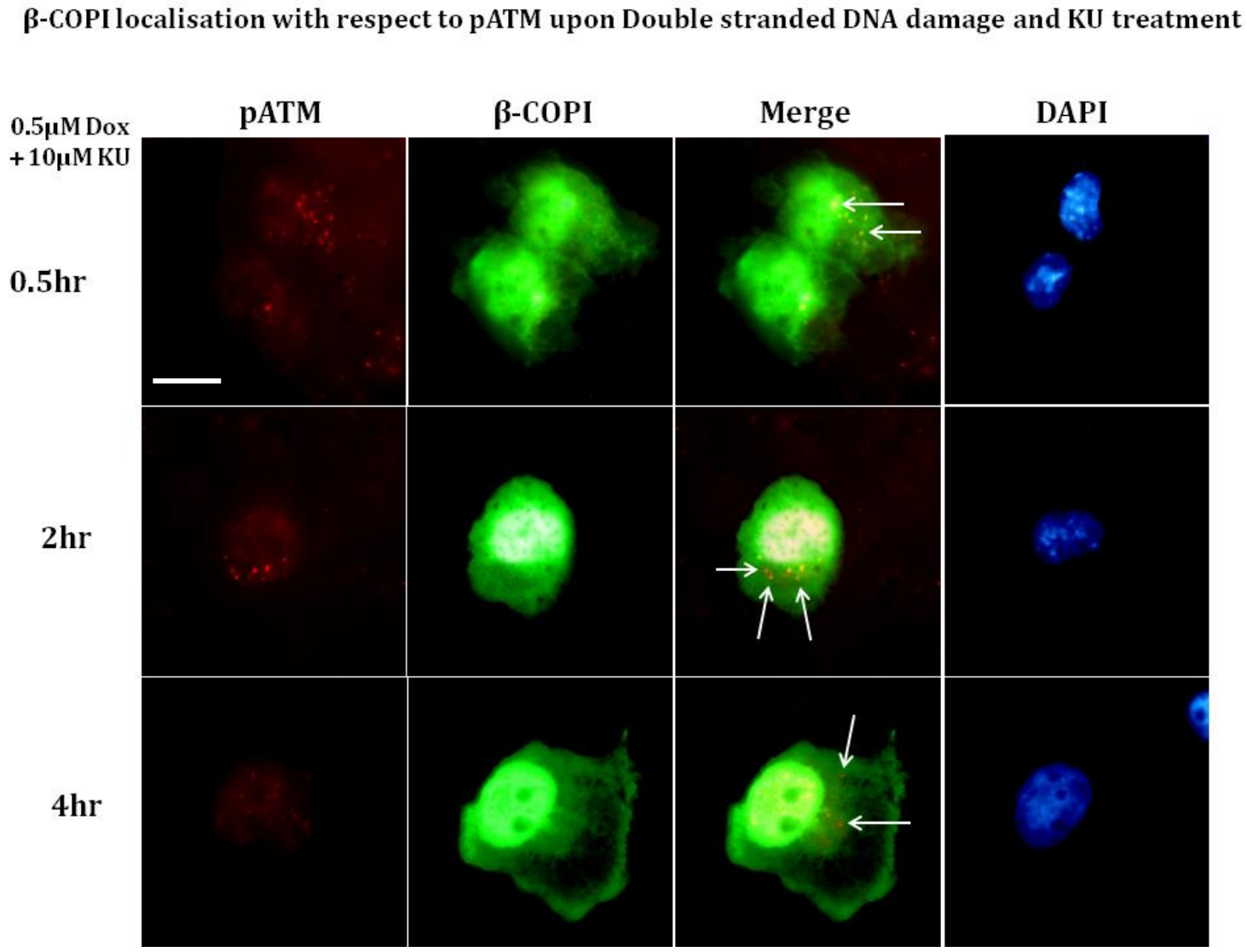


**Figure 5.28: ATM kinase inhibition causes disruption of co-localisation between β-COPI and Golgi retained pATM following DNA damage.** HaCat cells were seeded on Poly L lysine coated coverslips and grown until 70% confluent. Cells were transfected with N-terminal GFP tagged β-COPI as described in materials and methods. After 16 hr of transfection, cells were either left untreated, or treated with 0.5μM Dox and 10μM KU for 0.5, 2 and 4 hr. Immunostaining was performed with pATM S-1981 antibody using Alexa fluor 568 conjugated secondary antibody. Images were captured in relevant channels and co-localisation studies were performed by superimposition of the captured images. Nuclear reference is provided by staining the nuclei with DAPI. Inhibition of ATM kinase, in addition to causing its Golgi retention following DNA damage, also caused disruption of its co-localisation with β-COPI in the cytoplasm, as indicated by white arrows, at all the time points tested. Hence, co-localisation studies of the merged images of pATM and β-COPI-GFP did not show any yellow fluorescent staining. These are representative images taken in different fields of views under 100x objective. Scale bar represents 10μm.

### *5.3.10. N-terminal YFP tagged ATM is expressed similar to endogenous ATM and is kinase active.*

In order to get deeper insights of ATM transport and to be able to dissect its COPI mediated trafficking mechanism, the whole length, 9 kb ATM gene was tagged with yellow fluorescent protein (YFP) gene at its N-terminal and cloned into PCDNA3.1(+) vector (Invitrogen) as described in materials and methods section (Also see Appendix-I section A1.2.6 for cloning data). This construct was transfected into HaCat cells. After 48 hours of transfection, YFP-tagged ATM (YFP-ATM) expression was seen. Protein lysates of cells expressing YFP-ATM were also prepared and immunoblotted with GFP antibody (which detects YFP) to confirm over-expression of YFP-ATM in HaCat cells (Appendix-I, section A1.5) in addition to monitoring the fluorescence expression of YFP-ATM through fluorescence microscopy. The expression pattern of YFP-ATM was similar to the endogenous ATM with mostly nuclear and some extra nuclear expression (compare Fig. 5.1 with Fig. 5.29). Cells expressing YFP-ATM were next exposed to 0.5μM Dox for 0.5 and 4 hours to examine if cloned ATM gene product is kinase active. At 4 hr of Dox treatment, distinct ATM foci could be seen in the nucleus indicative of its kinase active status (Fig. 5.30).

An important feature of the expressed YFP-ATM was its localisation at the perinuclear region that appeared to be Golgi apparatus, in addition to its predominantly nuclear expression. In addition, exposure of cells to Dox resulted in the disappearance of this perinuclear distribution (compare Fig. 5.29 & 5.30). Thus the localisation pattern of YFP-ATM was recapitulative of the behaviour of endogenous ATM. This allowed me to continue further experiments on the tagged ATM construct to study ATM traffic and its mechanism of interaction with β-COPI.

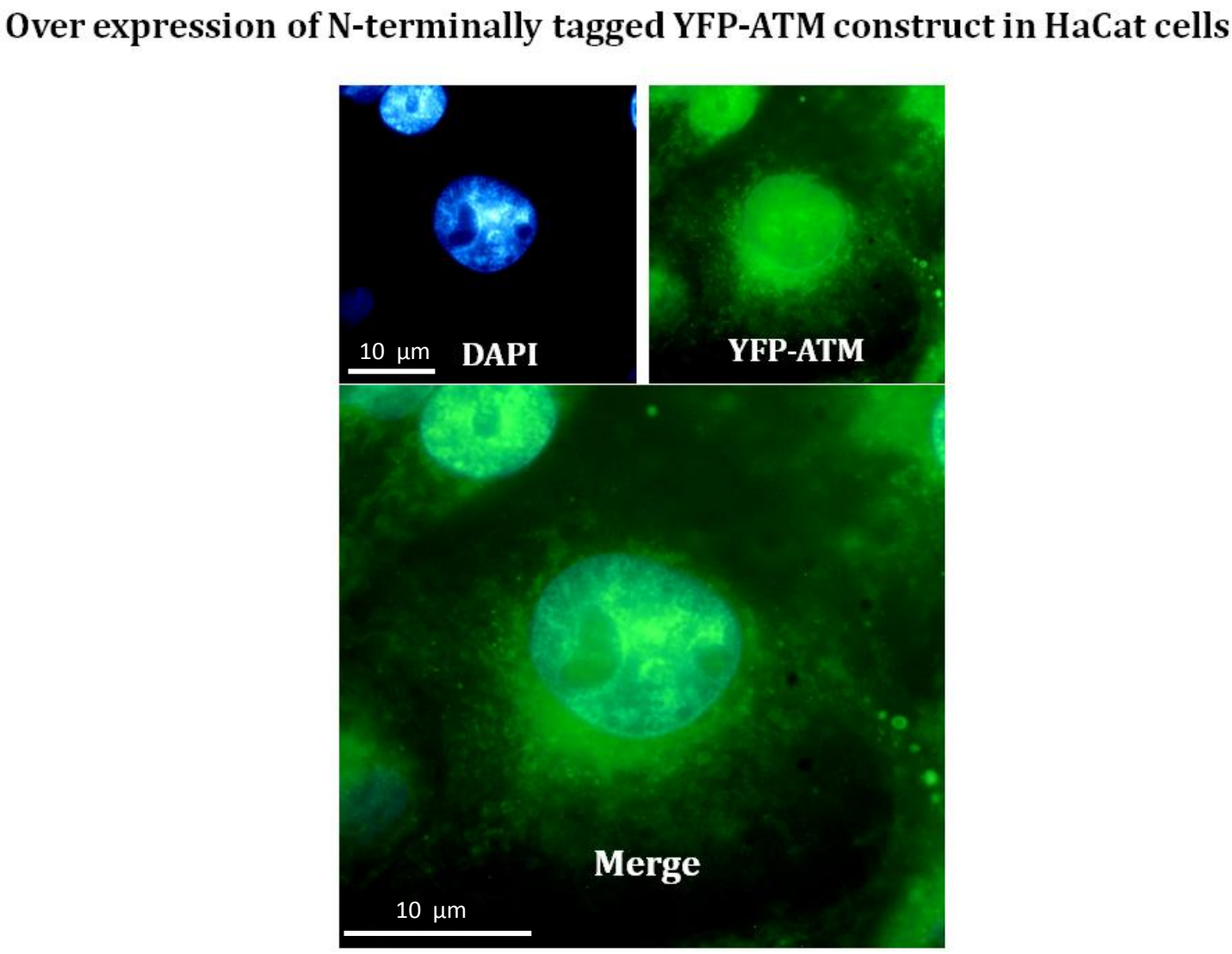


**Figure 5.29: N-terminal YFP tagged ATM expression in HaCat cells**. HaCat cells were seeded on Poly L lysine coated coverslips placed in 60mm tissue culture plates at a density of 8 x $10^5$ cells and allowed to grow until 70-90% confluent. 5µG of YFP-ATM DNA was transfected into cells as described in materials and methods and cells allowed to grow for 48 hrs. For nuclear reference, DAPI staining was used. YFP-ATM construct was expressed in a similar manner as endogenous ATM with mostly nuclear expression, and some perinuclear and cytoplasmic expression in untreated HaCat cell line. This is a representative image taken with 100x objective.

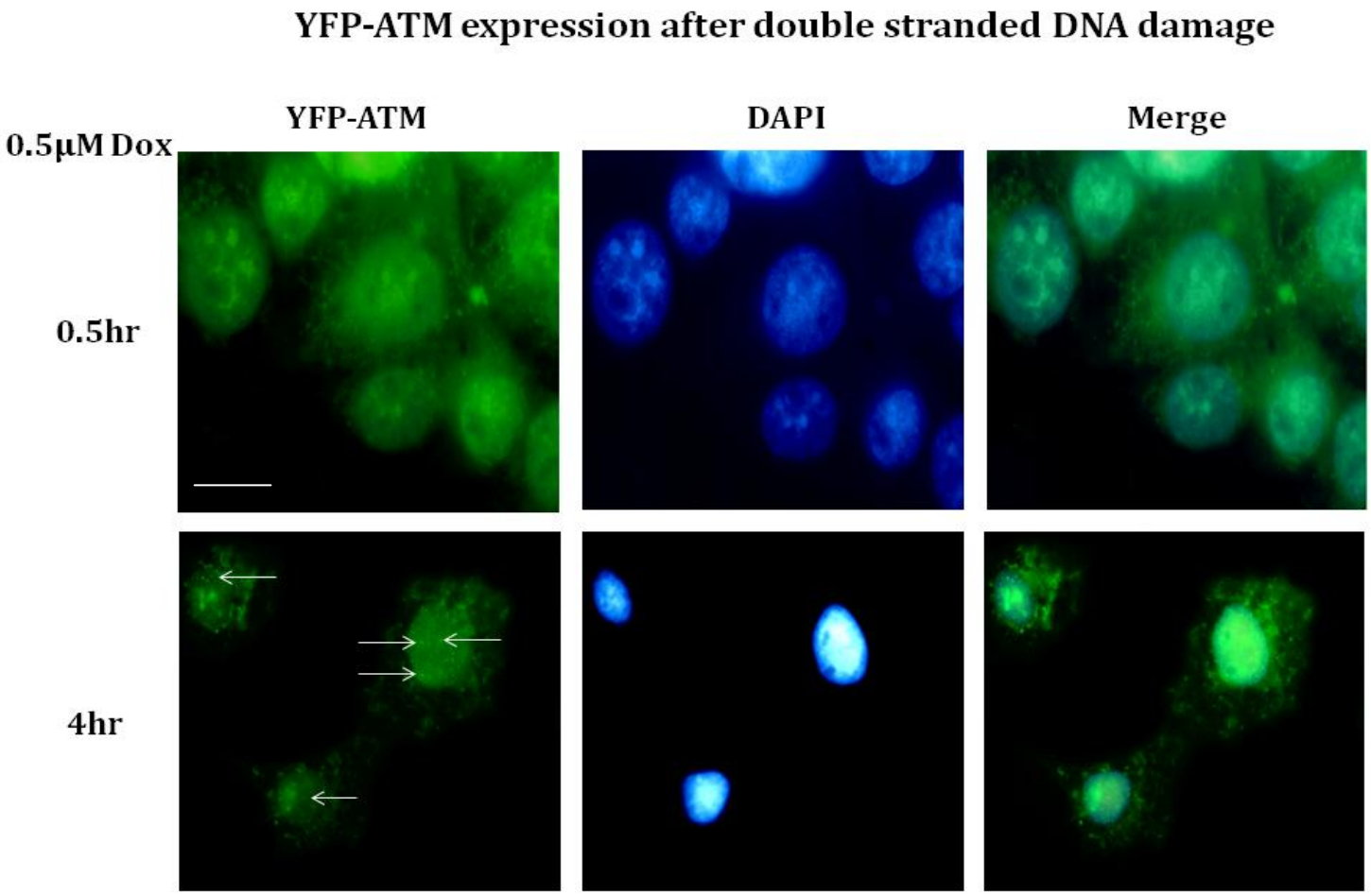
YFP-ATM expression after double stranded DNA damage
YFP-ATM
DAPI
Merge
0.5µM Dox
0.5hr
4hr

**Figure 5.30: YFP-ATM gene product is kinase active.** HaCat cells were seeded on Poly L lysine coated coverslips and grown until 70% confluent. Cells were transfected with N-terminal YFP-ATM gene construct as described in materials and methods. After 48 hr of transfection, cells were treated with 0.5μM Dox for 0.5 and 4 hr. Images were captured in relevant channel and co-localisation studies were performed by superimposition of the captured images. White arrows point towards appearance of distinct nuclear foci. Nuclear reference is provided by staining the nuclei with DAPI. Following double stranded DNA damage, the YFP-ATM gene product formed nuclear DNA damage foci, indicated by white arrows, confirming that the over expressed YFP-ATM gene product is kinase active. These are representative images taken in different fields of views under 100x objective.

### *5.3.11. Site directed mutagenesis of di-lysine motif (387-KK-388) of YFP-ATM results in its permanent extra nuclear retention and greatly reduced nuclear localisation in untreated, DNA damage and ATM kinase inhibited states.*

In order to establish direct role of COPI mediated transport system for Golgi exit of the cytoplasmic pATM upon DNA damage and to support the co-localisation data in Fig. 5.26, Site Directed mutagenesis (SDM) was performed on the ATM gene coding for the motif that is normally recognized by COP-I coatomer proteins for their traffic. To this end, bioinformatic analysis of ATM sequence was first carried out to first identify potential COPI recognizable domains in ATM. A di-Lysine motif at amino acid positions 387 and 388 was considered a potential candidate owing to the fact that COPI recognizes di-lysine residues in its substrates for retrograde transport from the Golgi membrane (Béthune J et a., 2006). Primers specific to the region surrounding the DNA sequence coding for 387-388 di-lysine motifs were designed replacing the di-Lysine to di-Alanine to disrupt this motif and site directed mutagenesis was performed as described in materials and methods (For additional data on SDM, see Appendix-I, section A1.2). The resulting construct, YFP tagged ATM with the mutated sequence 385-KRAA-388 (YFP-$ATM_{mut}$), was transfected into HaCat cells. The entire scheme is represented in Fig. 5.31.

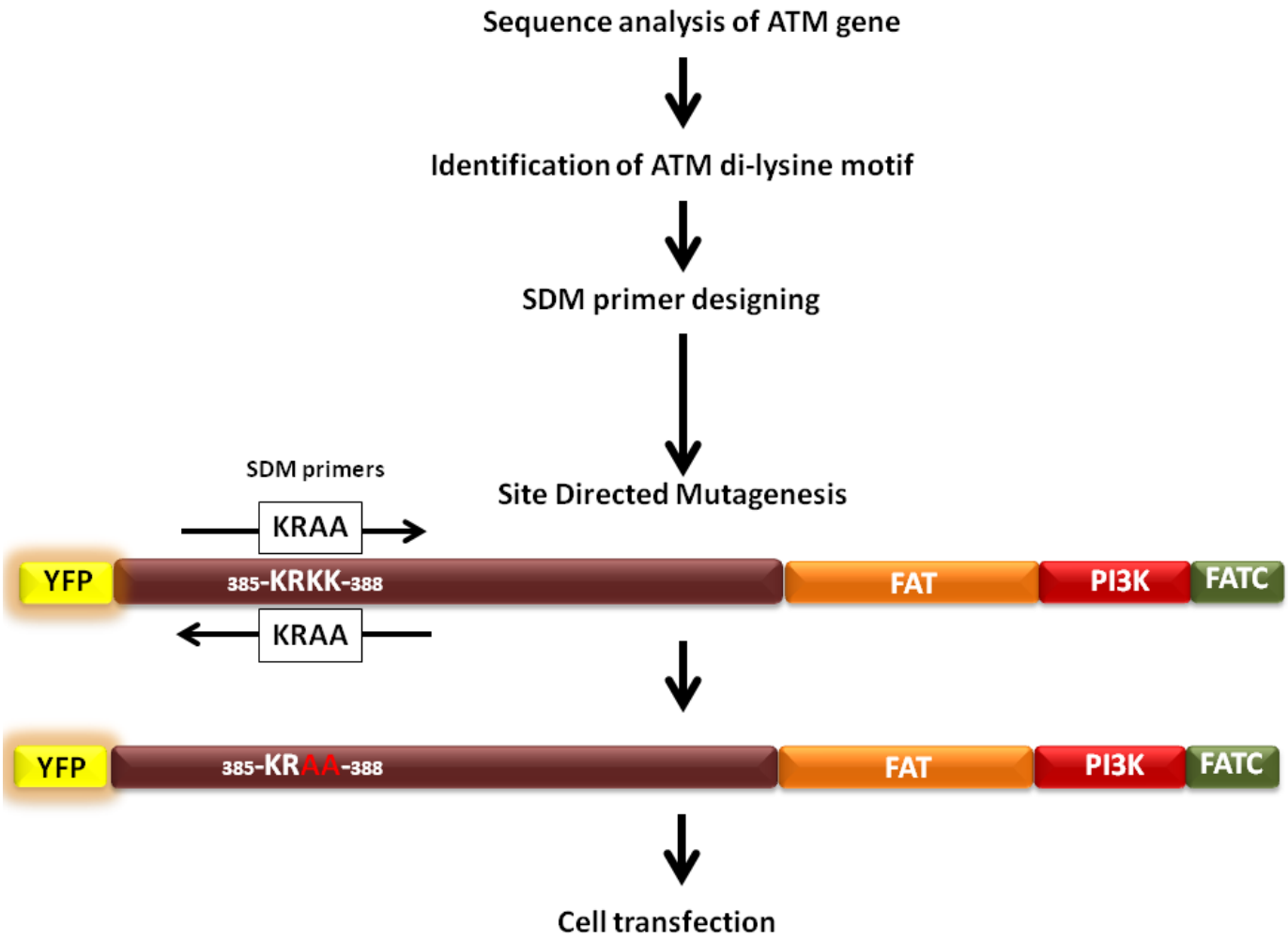


**Figure 5.31: The entire scheme of SDM mediated disruption of di-Lysine motif in YFP-ATM construct to produce YFP-ATM$_{mut}$.** The location of Di-lysine motif in ATM protein with respect to different ATM domains is shown. SDM was performed by using SDM primers targeting the region flanking the di-Lysine motif. The fidelity of the mutated ATM gene was confirmed by restriction digestion and sequencing.

After 48 hours of transfection, it was seen that YFP-$ATM_{mut}$ expression was mostly restricted to cytoplasm which appeared to be Golgi apparatus with a very minor localisation in the nucleus. This result suggested that even under undamaged conditions of DNA, ATM relies on 387-388 di-Lysine motif for its nuclear retention (Fig. 5.32).

Interestingly, YFP-$ATM_{mut}$ failed to undergo nuclear translocation upon DNA damage and showed persistent cytoplasmic retention when cells were exposed to either 0.5μM Dox alone or with the addition of 10μM KU, for 0.5, 2 and 4 hours (Fig. 5.33 & Fig. 5.34).

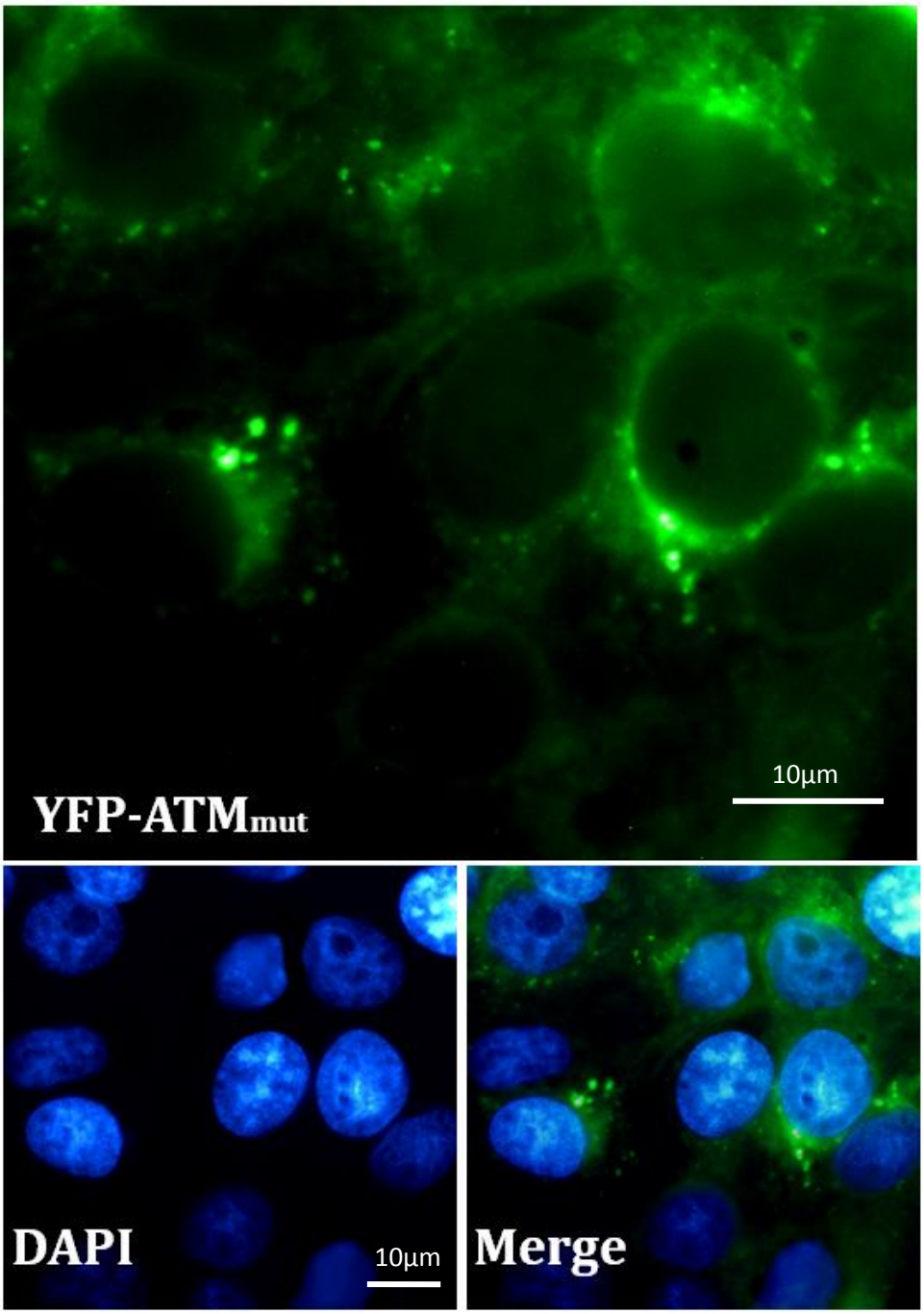


**Figure 5.32: Disruption of di-Lysine motif 387-KK-388 of ATM causes predominantly cytoplasmic and a minor nuclear expression of ATM.** HaCat cells were seeded on Poly L lysine coated coverslips and grown until 70% confluent. Cells were transfected with YFP-$ATM_{mut}$ gene construct as described in materials and methods. After 48 hr of transfection, YFP-$ATM_{mut}$ expression could be seen. Images were captured in relevant channel and co-localisation studies were performed by superimposition of the captured images. Nuclear reference is provided by staining the nuclei with DAPI. It was found that YFP-$ATM_{mut}$ expression was mostly restricted to the cytoplasm with almost no expression in the nucleus in the untreated HaCat cell line. This demonstrated requirement of the di-Lysine motif for nuclear retention of ATM. These are representative images taken in different fields of views under 100x objective.

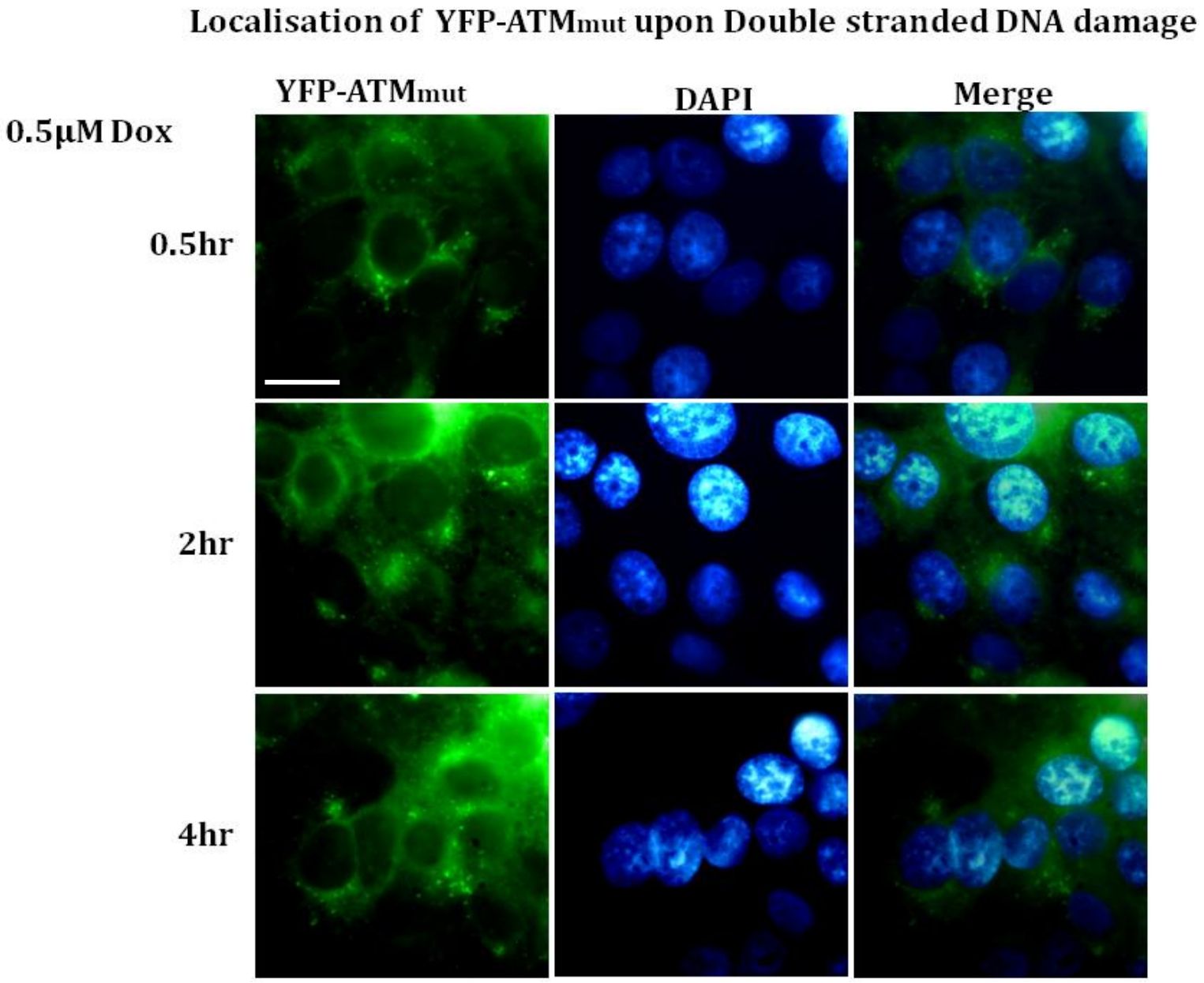


**Figure 5.33: YFP-ATM$_{mut}$ fails to undergo DNA damage induced Golgi exit and shows persistent retention in the cytoplasm.** HaCat cells were seeded on Poly L lysine coated coverslips and grown until 70% confluent. Cells were transfected with YFP-ATM$_{mut}$ gene construct as described in materials and methods. After 48 hr of transfection, cells were exposed to 0.5µM Dox for 0.5, 2 and 4 hr and YFP-ATM$_{mut}$ expression studied. Images were captured in relevant channel and co-localisation studies were performed by superimposition of the captured images. Nuclear reference is provided by staining the nuclei with DAPI. It was found that YFP-ATM$_{mut}$ showed permanent retention in the cytoplasm and failed to undergo DNA damage induced exit or localisation in the nucleus, demonstrating functional requirement of the di-Lysine motif. These are representative images taken in different fields of views under 100x objective. Scale bar represents 10µm.

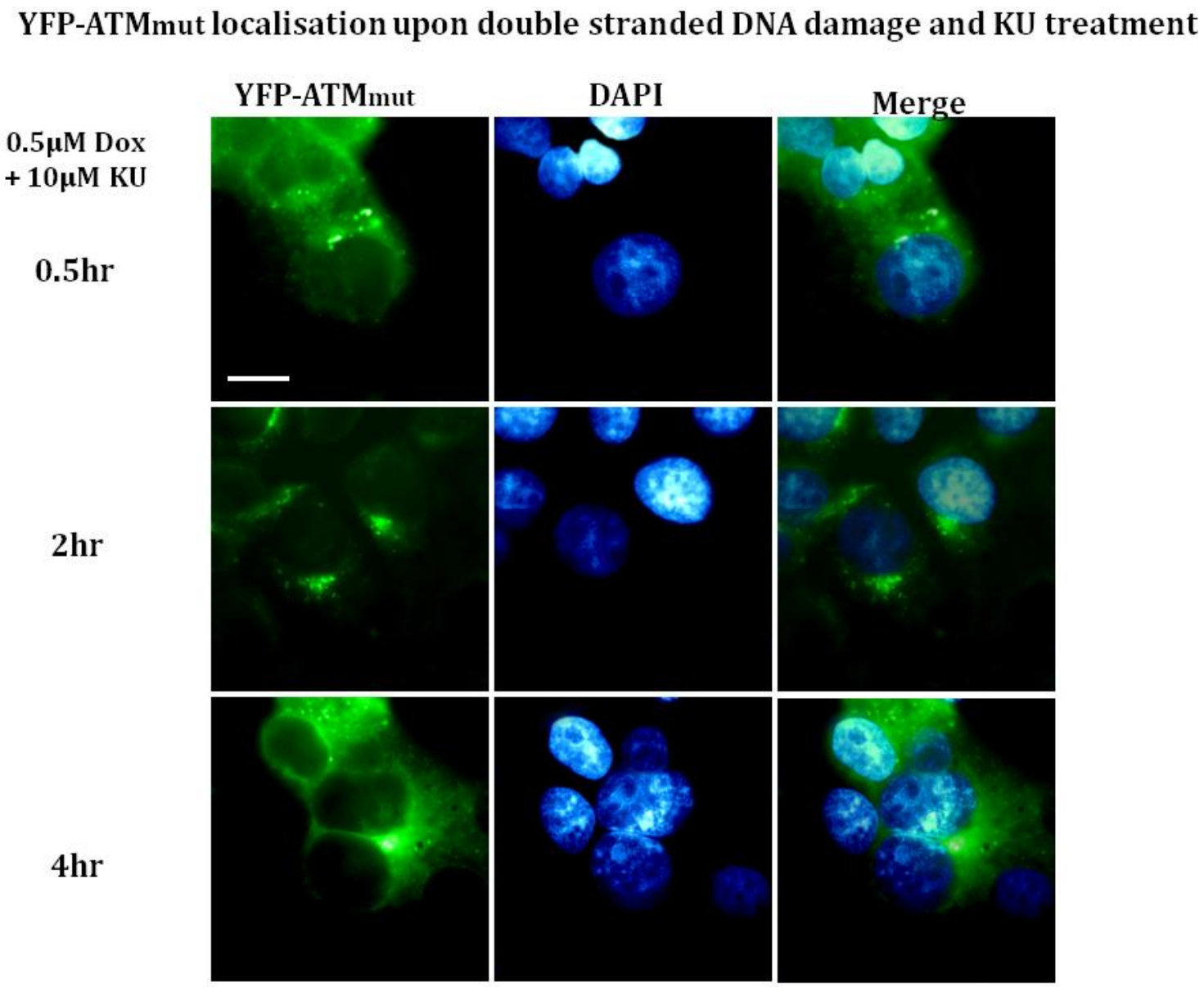


**Figure 5.34: YFP-ATM$_{mut}$ shows permanent cytoplasmic retention during ATM kinase inhibited states upon DNA damage in HaCat cells.** HaCat cells were seeded on Poly L lysine coated coverslips and grown until 70% confluent. Cells were transfected with YFP-ATM$_{mut}$ gene construct as described in materials and methods. After 48 hr of transfection, cells were exposed to 0.5µM Dox and 10µM KU for 0.5, 2 and 4 hr and YFP-ATM$_{mut}$ expression studied. Images were captured in relevant channel and co-localisation studies were performed by superimposition of the captured images. Nuclear reference is provided by staining the nuclei with DAPI. It was found that YFP-ATM$_{mut}$ showed permanent retention in the cytoplasm and failed to undergo DNA damage induced exit or localisation in the nucleus, demonstrating functional requirement of the di-Lysine motif. These are representative images taken in different fields of views under 100x objective. Scale bar represents 10µm.

Taken together, these novel findings illustrated that under non-damaging conditions of DNA, the Golgi resident pATM co-localized with β-COPI and underwent rapid Golgi export upon DNA damage. Inhibition of the kinase activity of ATM disrupted its co-localisation with β-COPI and resulted in failure of pATM to undergo Golgi export upon damage. Moreover, mutation of the potential COPI recognizable di-Lysine motif in the ATM sequence also caused a permanent cytoplasmic retention of YFP-$ATM_{mut.}$ These findings led to the conclusion that the di-Lysine 377-388 motif is essential for the nuclear translocation of ATM under normal and in DNA damaging conditions and further supported the involvement of COPI mediated transport system, which uses the di-Lysine motifs for substrate recognition and subsequent Golgi exit.

## 5.4 Key findings and their significance

In this section of the research, the following new findings were made:

i) In addition to its predominantly nuclear localisation, pATM also resides in Golgi apparatus in multiple cell lines in untreated states.

ii) Golgi localised pATM undergoes rapid Golgi exit following DNA damage with a concomitant nuclear accumulation as soon as after 30 min of genotoxic insult. This trafficking mechanism is conserved in cancer cell lines both with and without wild type P53.

iii) The above were also found to occur for ATM substrates pChk1 and pChk2 and its functional partner, pATR.

iv) The trafficking events for pATM were autoregulatory in nature, as they were sensitive to and hence abrogated upon ATM kinase inhibition, demonstrating a requirement of ATM kinase activity for its Golgi export and sub-cellular localisation in an autoregulatory manner.

v) Golgi resident cytoplasmic pATM was found to co-localise with a retrograde transport coat protein, β-COPI. This co-localisation was disrupted after inhibition of ATM kinase accompanied by its persistent cytoplasmic retention after DNA damage and failure to undergo nuclear accumulation.

vi) Mutagenesis of a di-Lysine 387-388 motif caused permanent cytoplasmic retention of ATM with almost no nuclear expression in the untreated, DNA damage or ATM kinase inhibited states.

Golgi apparatus to nuclear transport of pATM upon DNA damage could be vital step in the initiation of DDR signalling cascade following double stranded DNA damage. Disruption of DDR signalling following ATM inhibition as demonstrated in earlier chapters could not only result from block of ATM signalling, but may well be as a result of contribution from failure of pATM to undergo Golgi export into nucleus and substrate interaction.

These new findings were importantly found conserved in cancer cell lines and this could thus lead to revision or improvement of current strategies that modulate DDR signalling which, in addition to involving inhibition of DDR kinases for cancer therapeutics, could also be aided by inhibiting key intra-cellular trafficking events that contribute in the initiation of specific DDR signalling cascades. Hence, different peptide inhibitors that block the di-Lysine motif, or general Golgi to nuclear transport inhibitors could be employed that would decrease the overall load on small molecular inhibitors of different kinases to achieve therapeutic DDR intervention for sensitization of cancer cells.

# Chapter Six

# Elucidation of the role of ATM signalling pathway in cytoprotection and apoptosis and generation of time series data for parameterization of mathematical model for *in silico* prediction of ATM signalling

From time immemorial, man has desired to comprehend the complexity of nature in terms of as few elementary concepts as possible.

Abdus Salam, Theoretical physicist (1926–1996).

## 6.1 Abstract

*Over the past decade, tremendous progress has been made in our qualitative understanding of the signal transduction pathways, their molecular mechanisms, activity, regulation and the associated outcome on cell-fate. While this has helped us immensely in conceptualising intervention strategies in diseased states, the mere descriptive nature of the information regarding key cellular pathways has prevented their use in mathematical and computational modelling application which could potentially identify new therapeutic targets and help us devise treatment regimens. In an attempt to provide semi quantitative data of the proteins involved in the ATM signalling pathway, drug treatments were performed with high temporal resolution and the resulting quantitative estimations of induction of eight different proteins of DDR, based on high throughput ELISA technique were carried out. Furthermore, the precise role of ATM in such temporal induction of DDR proteins was elucidated at a lower and higher scale of DNA damage. It was found that both in dose dependent and time dependent treatments of Dox, there was higher cell death when ATM was inhibited than without inhibition but only at lower dosage or at early time points of genotoxic treatment. This indicated a cytoprotective role of ATM, functioning mainly in damage repair and survival at lower scale of DNA damage. However, at a higher dose of DNA damaging agent or during longer course of treatments, ATM inhibition on the contrary, resulted in lower cell death as compared to ATM active state, indicating a switch in its function from its cytoprotective role to a role in inducing cell death or apoptosis at more extensive DNA damage. Moreover, the difference in sensitivities of normal and cancer cells towards genotoxic agents were found to correlate well with the differences in kinetics of activation of ATM following genotoxic treatments in these cell lines, which was suggestive of the role of ATM in determining overall sensitivity. These results not only unveiled the underlying ATM dependent DDR signalling pathway and provided semi quantitative protein induction data, but also demonstrated the importance of first determining the appropriate scale of DNA damage while employing ATM inhibition strategies to achieve cellular sensitisation.*

## 6.2 Introduction

A prerequisite of a molecularly targeted anticancer approach is a detailed understanding of the underlying mechanisms contributing in tumour development. This involves changes in both the types and extents of molecular interactions governing key process in a cell that may predispose it to cancer. Additionally, a thorough understanding of the cell microenvironment, proliferation, growth and stress signals are vital before a successful anticancer approach could be devised. Failure to do so is one reason why theoretically, very effective anticancer strategies could be conceptualised, while they still fail to actualise. Until recently, strategies for therapeutic intervention via the modulation of key molecular pathways targeted individual components of the global regulatory network. This was based on the assumption that different pathways transmit signals through independent mechanisms. However, with the advent of new molecular techniques and bioinformatic tools, remarkable progress has been made and new insights have been gained into the nature of the intracellular signalling networks. It is now known that numerous key proteins have multiple functions in different pathways and that the downstream signalling choice of a particular protein depends on a number of variables. ATM is central to a number of key pathways as mentioned before. These pathways act in concert in order to phosphorylate P53 at a number of sites, some having overlapping functions and others being specific for a particular response. In this micro-environment, the effect of inhibiting ATM protein is not fully predictable especially owing to the fact that ATM function can contribute both in cell cycle arrest to allow time for DNA repair, as well as in apoptotic induction. Prediction is further complicated by the finding that ATM may self-regulate its own protein levels (Chapter Four and Khalil HS et al., 2011 & 2012).

In this complex and unpredictable situation, the efficacy of potential ATM inhibitors would have to be assessed in terms of the effects it exerts, not only on ATM activity and its immediate substrates e.g. ATM→pATM→pP53→DNA repair, but on a number of connected key proteins in the DNA repair, cell cycle and apoptotic pathways and the overall impact of such pathways on cell-fate.

It is increasingly becoming obvious that complexity in determining the absolute effects of kinase inhibition necessitates parallel theoretical and experimental considerations. This could be best addressed by employing a systems biology approach to the problem, involving mathematical modelling of biological processes (Clyde RG et al., 2006). Such a model could be capable of predicting the global phosphorylation status of important proteins e.g. ATM, ATR, P53, E2F1 and BRCA, the activity levels of checkpoint kinases e.g. Chk1 and Chk2 and pro and anti-apoptotic proteins, and their outcome on cellular fate. Also, such a model could be able to provide for varying levels of drug input over variable time courses as well as being capable of incorporating combinations of intervention strategies e.g. involving both ionizing radiation and chemical carcinogens in conjunction with ATM or other DDR protein inhibitors.

Successful computational modelling of molecular pathways triggered by multifunctional proteins like ATM can not only provide predictive behaviour of this kinase in a specific treatment regimen in terms of either DNA repair or apoptotic function, but also highlight key differences in pathway choices between normal and cancer cells within a single treatment regime. These predictions could then be tested at experimental level to examine the degree of accuracy of these models.

As a first step towards providing quantitative time series data of the DDR pathway proteins after drug intervention for the development of experiment based deterministic model, I performed time series experiments under different conditions targeting all major proteins that respond to DNA damage and carried out their semi quantitative analysis. Relative quantifications of each protein were performed by high throughput HRP based ELISA. Readings for each treatment were based on means from quadruplets treatments with each experiment performed on three independent occasions. Hence, a data consistent profiling of the dynamic processes within biological system was performed by measuring quantitative changes in these important proteins for up to 24 hrs to provide kinetic parameters for a systems biology application.

To determine the consequences of these phosphorylational events and relative quantitative changes of DDR proteins for cell survival and health, NR-uptake based cell cytotoxicity assays were also performed after treatments. This allowed parallel study of the degree of the activation of these proteins and the effect that such temporal induction exerted on cell survival along these treatments. Since ATM inhibition was also used along with the drug treatments, the precise role of ATM in either cell cycle arrest or cell death (as determined by comparative analysis between degrees of cell death with and without ATM inhibition during DNA damage) could also be inferred. This enabled the interpretation of pathway activation on overall cell-fate.

Finally, the next aim was to determine key treatment regimes based on ATM activity that allowed targeted cellular sensitivity. To achieve this, a normal epithelial cell line, MCF10A and cancer epithelial cell line MCF7A were exposed to dose dependent treatments of doxorubicin with and without ATM inhibition.

This not only elucidated ATM role in apoptotic induction based on dose dependent treatments (as opposed to time courses), but also identified differences in its relative activation between normal and cancer cell lines following genotoxic treatments.

Extensive biological analyses were then carried out on the generated data on the basis of existing literature and biological insight for validation and the data were then passed on to mathematical modellers (Michael Idowu, Prof James Bown, University of Abertay Dundee) for the prospective development of experiment based mathematical model. The development of a successful model of biological system was expected to further our insights and provide clues for successful therapeutic intervention by isolating and targeting key protein interactions within a broader signalling network, by which, cell-fate is greatly influenced. Full list of objectives that I set out and formulated based on the prospective successful model are listed in section 6.4. Table 12 lists the different conditions at which cytotoxicity assays were performed while table 13 and 14 list the important DDR proteins for which relative measurements were carried out.

Table 12: Different conditions at which Cell cytotoxicity assay were performed.

| | **Cell cytotoxicity assay (NR-uptake) conditions** | | | |
|---|---|---|---|---|
| | **100nM Dox** | **100nM Dox + 10µM KU** | **400nM Dox** | **400nM Dox + 10µM KU** |
| **Time Points** | UT | UT | UT | UT |
| | 2 hr | 2 hr | 2 hr | 2 hr |
| | 4 hr | 4 hr | 4 hr | 4 hr |
| | 8 hr | 8 hr | 8 hr | 8 hr |
| | 12 hr | 12 hr | 12 hr | 12 hr |
| | 16 hr | 16 hr | 16 hr | 16 hr |
| | 20 hr | 20 hr | 20 hr | 20 hr |
| | 24 hr | 24 hr | 24 hr | 24 hr |

Table 13**:** Time series treatments at lower concentration (1x) and higher concentration (4x) DNA damage with and without ATM inhibition performed for the activity analysis of key DDR protein kinases.

| **DDR Kinases** | **100nM Dox** | **100nM Dox + 10µM KU** | **400nM Dox** | **400nM Dox + 10µM KU** |
|---|---|---|---|---|
| **pATM S 1981** | UT | UT | UT | **UT** |
| | 2 hr | 2 hr | 2 hr | 2 hr |
| | 4 hr | 4 hr | 4 hr | 4 hr |
| | 8 hr | 8 hr | 8 hr | 8 hr |
| | 12 hr | 12 hr | 12 hr | 12 hr |
| | 16 hr | 16 hr | 16 hr | 16 hr |
| | 20 hr | 20 hr | 20 hr | 20 hr |
| | 24 hr | 24 hr | 24 hr | 24 hr |
| **pATR S 428** | UT | UT | UT | UT |
| | 2 hr | 2 hr | 2 hr | 2 hr |
| | 4 hr | 4 hr | 4 hr | 4 hr |
| | 8 hr | 8 hr | 8 hr | 8 hr |
| | 12 hr | 12 hr | 12 hr | 12 hr |
| | 16 hr | 16 hr | 16 hr | 16 hr |
| | 20 hr | 20 hr | 20 hr | 20 hr |
| | 24 hr | 24 hr | 24 hr | 24 hr |
| **pChk 2 T 68** | UT | UT | UT | UT |
| | 2 hr | 2 hr | 2 hr | 2 hr |
| | 4 hr | 4 hr | 4 hr | 4 hr |
| | 8 hr | 8 hr | 8 hr | 8 hr |
| | 12 hr | 12 hr | 12 hr | 12 hr |
| | 16 hr | 16 hr | 16 hr | 16 hr |
| | 20 hr | 20 hr | 20 hr | 20 hr |
| | 24 hr | 24 hr | 24 hr | 24 hr |
| **pChk1 S 296** | UT | UT | UT | UT |
| | 2 hr | 2 hr | 2 hr | 2 hr |
| | 4 hr | 4 hr | 4 hr | 4 hr |
| | 8 hr | 8 hr | 8 hr | 8 hr |
| | 12 hr | 12 hr | 12 hr | 12 hr |
| | 16 hr | 16 hr | 16 hr | 16 hr |
| | 20 hr | 20 hr | 20 hr | 20 hr |
| | 24 hr | 24 hr | 24 hr | 24 hr |

Table 14: Time series treatments at lower concentration (1x) and higher concentration (4x) DNA damage with and without ATM inhibition performed for the activity analysis of key DDR protein substrates implicated in DNA repair, cell cycle arrest and apoptosis.

| DDR substrates | 100nM Dox | 100nM Dox + 10µM KU | 400nM Dox | 400nM Dox + 10µM KU |
|---|---|---|---|---|
| pP53 S 15 | UT | UT | UT | UT |
| | 2 hr | 2 hr | 2 hr | 2 hr |
| | 4 hr | 4 hr | 4 hr | 4 hr |
| | 8 hr | 8 hr | 8 hr | 8 hr |
| | 12 hr | 12 hr | 12 hr | 12 hr |
| | 16 hr | 16 hr | 16 hr | 16 hr |
| | 20 hr | 20 hr | 20 hr | 20 hr |
| | 24 hr | 24 hr | 24 hr | 24 hr |
| pBRCA1 S 1524 | UT | UT | UT | UT |
| | 2 hr | 2 hr | 2 hr | 2 hr |
| | 4 hr | 4 hr | 4 hr | 4 hr |
| | 8 hr | 8 hr | 8 hr | 8 hr |
| | 12 hr | 12 hr | 12 hr | 12 hr |
| | 16 hr | 16 hr | 16 hr | 16 hr |
| | 20 hr | 20 hr | 20 hr | 20 hr |
| | 24 hr | 24 hr | 24 hr | 24 hr |
| E2F1 | UT | UT | UT | UT |
| | 2 hr | 2 hr | 2 hr | 2 hr |
| | 4 hr | 4 hr | 4 hr | 4 hr |
| | 8 hr | 8 hr | 8 hr | 8 hr |
| | 12 hr | 12 hr | 12 hr | 12 hr |
| | 16 hr | 16 hr | 16 hr | 16 hr |
| | 20 hr | 20 hr | 20 hr | 20 hr |
| | 24 hr | 24 hr | 24 hr | 24 hr |
| γ–H2AX | UT | UT | UT | UT |
| | 2 hr | 2 hr | 2 hr | 2 hr |
| | 4 hr | 4 hr | 4 hr | 4 hr |
| | 8 hr | 8 hr | 8 hr | 8 hr |
| | 12 hr | 12 hr | 12 hr | 12 hr |
| | 16 hr | 16 hr | 16 hr | 16 hr |
| | 20 hr | 20 hr | 20 hr | 20 hr |
| | 24 hr | 24 hr | 24 hr | 24 hr |

## 6.3 Results

### *6.3.1 Time series treatment of 100nM Doxorubicin with and without ATM inhibition revealed cytoprotective role of ATM signalling pathway with extensive effects on DDR protein induction in HaCat cells.*

HaCat cells were seeded in 96 well plates as described in materials and methods. After 24 hr of incubation, cells were washed once with warm PBS and were either left untreated, or treated with 100nM Dox with and without 10μM KU. Four replicates of each treatment were carried out as listed in table 6.1 and 6.2 followed by performing ELISA. In addition, cells grown in other 96 well plates were treated in the same manner and subjected to NR-uptake assay to determine cell viability after treatments.

Doxorubicin treatment in this section of experiments was set to 100nM because this is a physiologically relevant concentration currently being employed in chemotherapy (Gajewski E et al., 2007). This allowed me to not only look at the underlying mechanism and kinetics of DDR at each time point with overall high temporal resolution, but also to correlate these kinetics with rates of cell death in ATM dependent and independent manner at exactly the same time points. Figure 6.1 illustrates these for pATM S 1981. The % cell death, as compared to 0% cell death in the untreated state after treatment with 100nM Dox or 100nM Dox plus 10μM KU is shown in figure 6.9.

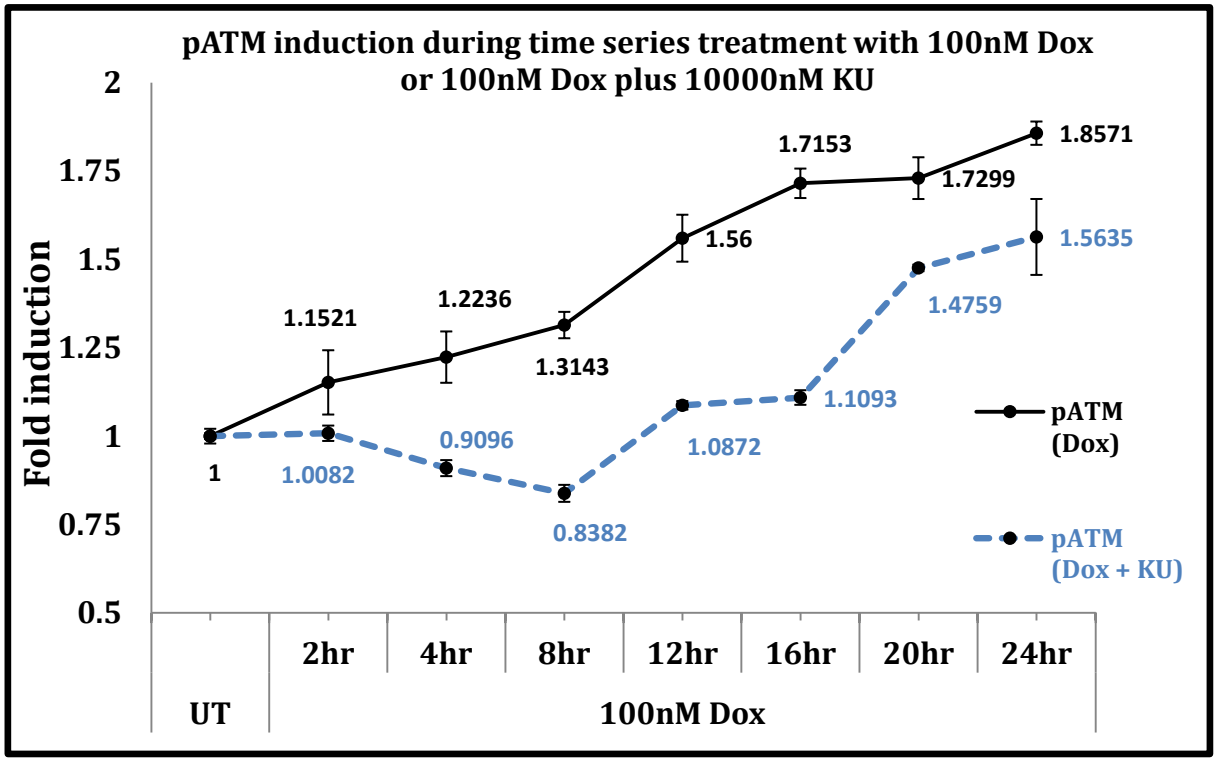


**Figure 6.1: pATM induction during time series treatment of 100nM Dox with and without 10µM ATM kinase inhibitor (KU).** HaCat cells were seeded in 96-well plates at a density of 2.5 x $10^3$ cells per well. After 24 hr of incubation, cells were either left untreated or treated with 100nM Dox or 100nM Dox plus 10µM KU for the indicated time points. After treatments, cells were subjected to ELISA as described in materials and methods for the determination of pATM S-1981 induction using HRP conjugated secondary antibody and Amplex Red® detection system. Readings were taken in Modulus template® 96-well plate reader using excitation emission maxima of 570/585 nm. Each value is based on means of the fluorescence values acquired from quadruplet of treatments and normalized to the mean value of untreated control (UT) expressed as 1. The data is based on three independent experiments.

Treatment with 100nM Dox resulted in pATM induction starting with the first time point at 2 hr, up to the 24 hr of treatment. Hence, a lower scale damage of 100nM Dox was still enough to induce pATM induction. However, the kinetics of induction were slow with < two fold maximum induction at 24 hr time point (Fig. 6.1). Addition of ATM inhibitor, KU, to the Dox treatment resulted in disruption of pATM induction up until the 12 hr time point. Interestingly however, furthering the treatment with Dox plus KU resumed pATM induction slightly at 16 hr onwards to around 1.5 fold at 24 hr time point.

Hence, it appeared that while ATM inhibition caused earlier disruption of pATM induction, at later time points, the induction slightly resumed resulting in overall delayed kinetics of pATM activation (Fig. 6.1).

A possible explanation of the resumption of pATM induction post 12 hr treatment with 100nM Dox could be the fact that KU is a reversible inhibitor of ATM and may only form a transient effective inhibitory complex and lose its affinity during long term treatments in the presence of DNA damage. Furthermore, while KU was previously shown to upregulate total ATM levels resulting in a transient induction of pATM at 0.5 hr of treatment (chapter 4), this cellular mechanism of combating ATM inhibition might have taken place at other further time points. Finally, another possible reason of pATM induction at later time points is to do with KU stability. HPLC stability graph of KU showed good overall stability for up to 30 hr. However, there was a slight reduction in stability at and after 16 hr in the media (Appendix I, A1.6). Analysis of cell death of cells treated in the same manner revealed that while cells underwent cell death with both functional and inhibited states of ATM during 100nM of Dox treatment, ATM inhibition resulted in overall greater cell death (45% cell death at 24 hr time point with the addition of KU, as compared to 35% without KU) (Fig. 6.9). This confirmed ATM signalling role in cytoprotection and survival at this particular extent of DNA damage. This fitted well with the function of ATM whereby it promotes DNA repair and ensures cell survival at a repairable scale of DNA damage. This is brought about both by its DNA damage induced phosphorylation of P53 which exerts CIP/KIP mediated cell cycle arrest by sequestering E2F1 activities (Banin S et al., 1998, Chehab NH et al., 2000, Maya R et al., 2001), as well as its phosphorylational activation of checkpoint kinases which further phosphorylate and inhibit phosphatase activities of Cdc25 (Falk J et al., 2001, Kramer A et al., 2004).

This study used HaCat cell line, which contains two point mutations in P53. While these mutations cause disruption of p53 mediated upregulation of p21 (role in cell cycle arrest and repair), these cells still undergo P53 upregulation and P53 dependent apoptosis following genotoxic insults (Henseleit U et al., 1997). Hence, in terms of cell cycle arrest and repair, ATM may signal via ATM→ Chk1/2→x Cdc25 →CELL CYCLE ARREST pathway or in a P63 and P73 dependent manner in HaCat cells. Inhibition of this link via KU treatment would allow Cdc25 activities unchecked resulting in cell cycle progression and failure to cause checkpoint arrested and provide adequate time for DNA repair.

While ATM is also implicated in apoptosis induction (Xu Y et al., 1996), from the cytotoxicity assay, it could be inferred that at 100nM Dox, its major function was to arrest the cells and ensure cellular survival rather than apoptosis. Therefore, its inhibition would induce greater cell death as illustrated in figure 6.9. This hypothesis was further supported in subsequent figures below.

Analysis of pATR S-428 induction at 100nM of Dox treatment revealed no major change through all the time points tested (Fig. 6.2). This can be explained by the fact that ATR activity is mostly implicated in DNA damage following UV exposure or replication folk stalling (Guo Z et al., 2000) and that a lower double stranded DNA damage alone is not enough to induce pATR up to 24 hr of treatment. Interestingly, however, with the addition of ATM inhibitor, pATR levels dropped below those in untreated cells at 2, 4 and 8 hr time points while showed an induction starting at 12 hr of treatment and continuing further till 24 hr time point (Fig. 6.2). It is already known that double stranded DNA damage may still activate ATR but at later time points as compared to ATM activation (Adams KE et al., 2006).

In the text, the sign → indicates activation, →x indicates inhibition or disruption of that signal, = indicates an outcome

The observation that pATR levels dropped below those in the untreated cells at earlier time points could be explained by the fact that ATR function upon double stranded DNA damage requires functional ATM (Adams KE et al., 2006) at least earlier in the damage. On the other hand, the fact that absence of ATM activity caused pATR activation at later time points of 100nM Dox treatment may be as a result of emergency response of cell where ATR may perform overlapping function of ATM (Fig. 6.2). Secondly, in chapter 4, KU induced pATR upregulation was reported at 0.5 hr post treatment (Fig. 4.3a & b). Here, KU induced upregulation of pATR at 12 hr post treatment may possibly have taken place because of the same mechanism.

Finally, it is likely that the up regulated fraction of pATR post 12 hr in ATM inhibited state induced apoptosis, since this induction correlated with increased cell death that was observed during KU + Dox treatments in cytotoxicity assay after 12 hr of treatment (Compare Fig. 6.2 with Fig. 6.9 Dox + KU treatments). Additionally, the role of ATR in apoptosis induction has already been reported at least in cases of cisplatin (Pabla N et al., 2008) and hydroxyurea (Kuman S et al., 2005) treatments.

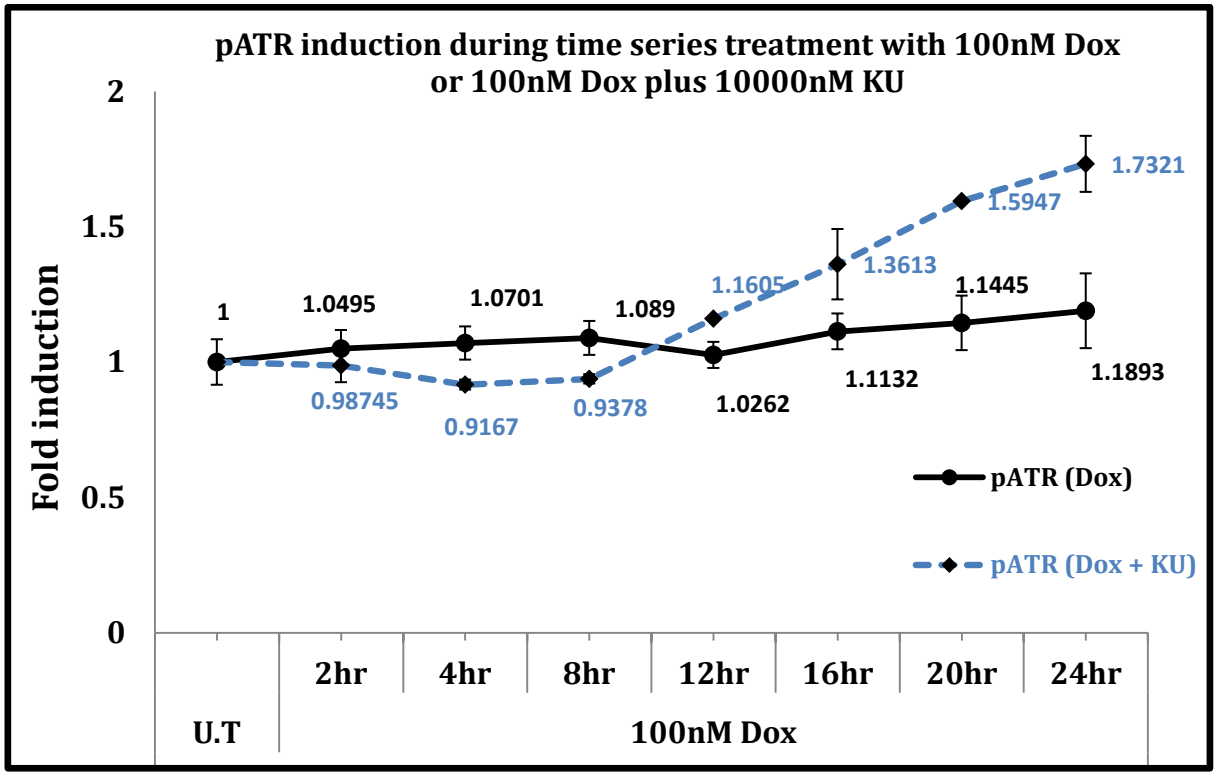


**Figure 6.2: pATR induction during time series treatment of 100nM Dox with and without 10µM ATM kinase inhibitor (KU).** HaCat cells were seeded in 96-well plates at a density of 2.5 x $10^3$ cells per well. After 24 hr of incubation, cells were either left untreated or treated with 100nM Dox or 100nM Dox plus 10µM KU for the indicated time points. After treatments, cells were subjected to ELISA as described in materials and methods for the determination of pATR S-428 induction using HRP conjugated secondary antibody and Amplex Red® detection system. Readings were taken in Modulus template® 96-well plate reader using excitation emission maxima of 570/585 nm. Each value is based on means of the fluorescence values acquired from quadruplet of treatments and normalized to the mean value of untreated control (UT) expressed as 1. The data is based on three independent experiments.

Analysis of the checkpoint kinases pChk1 S-296 and pChk2 T-68 at 100nM of Dox treatment revealed minimal induction until 8 hr of treatment. However, at further time points, both of these kinases showed an induction but at different kinetics (Fig. 6.3 & 6.4).

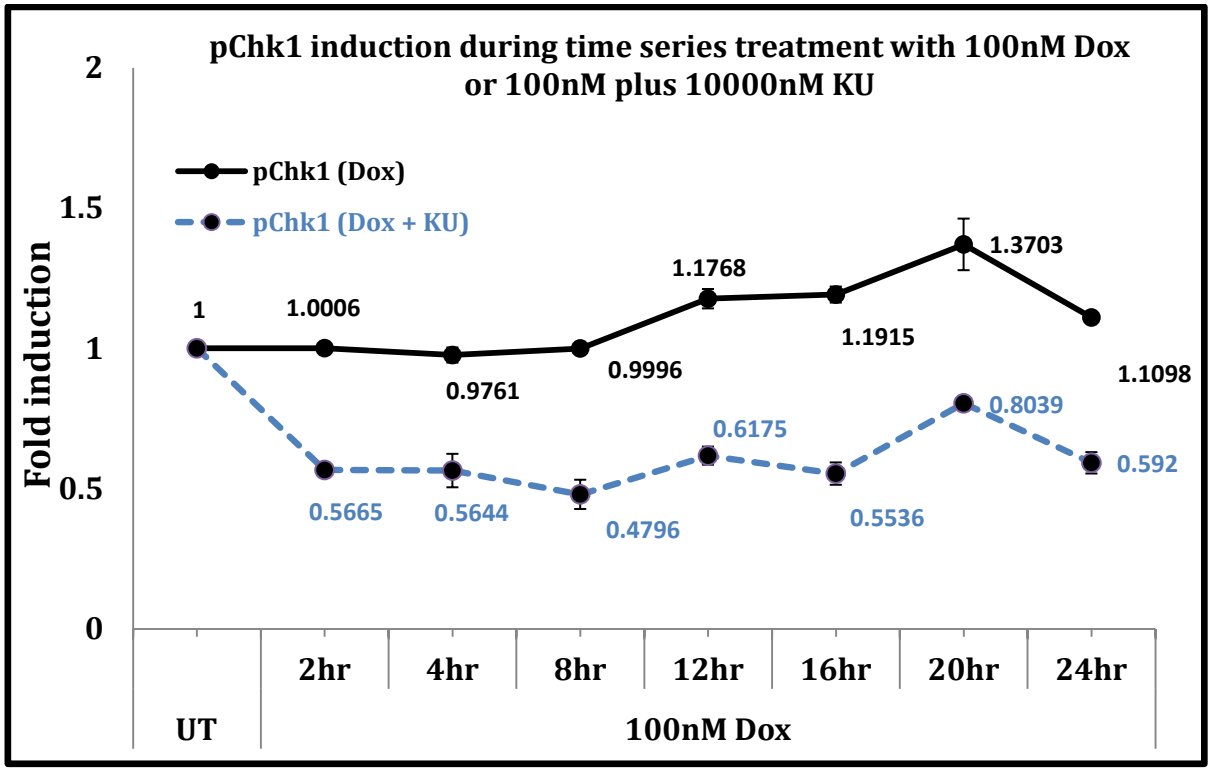


**Figure 6.3: pChk1 induction during time series treatment of 100nM Dox with and without 10µM ATM kinase inhibitor (KU).** HaCat cells were seeded in 96-well plates at a density of 2.5 x $10^3$ cells per well. After 24 hr of incubation, cells were either left untreated or treated with 100nM Dox or 100nM Dox plus 10µM KU for the indicated time points. After treatments, cells were subjected to ELISA as described in materials and methods for the determination of pChk1 S-296 induction using HRP conjugated secondary antibody and Amplex Red® detection system. Readings were taken in Modulus template® 96-well plate reader using excitation emission maxima of 570/585 nm. Each value is based on means of the fluorescence values acquired from quadruplet of treatments and normalized to the mean value of untreated control (UT) expressed as 1. The data is based on three independent experiments.

pChk2 showed an overall greater induction than pChk1, fitting well with pChk2 being the primary effector molecule downstream of pATM following double stranded DNA damage (Matsuoka S et al., 2000). The fact that both pChk1 and pChk2 showed induction following Dox treatment supported the earlier hypothesis of ATM mediating checkpoint kinase dependent cell cycle arrest.

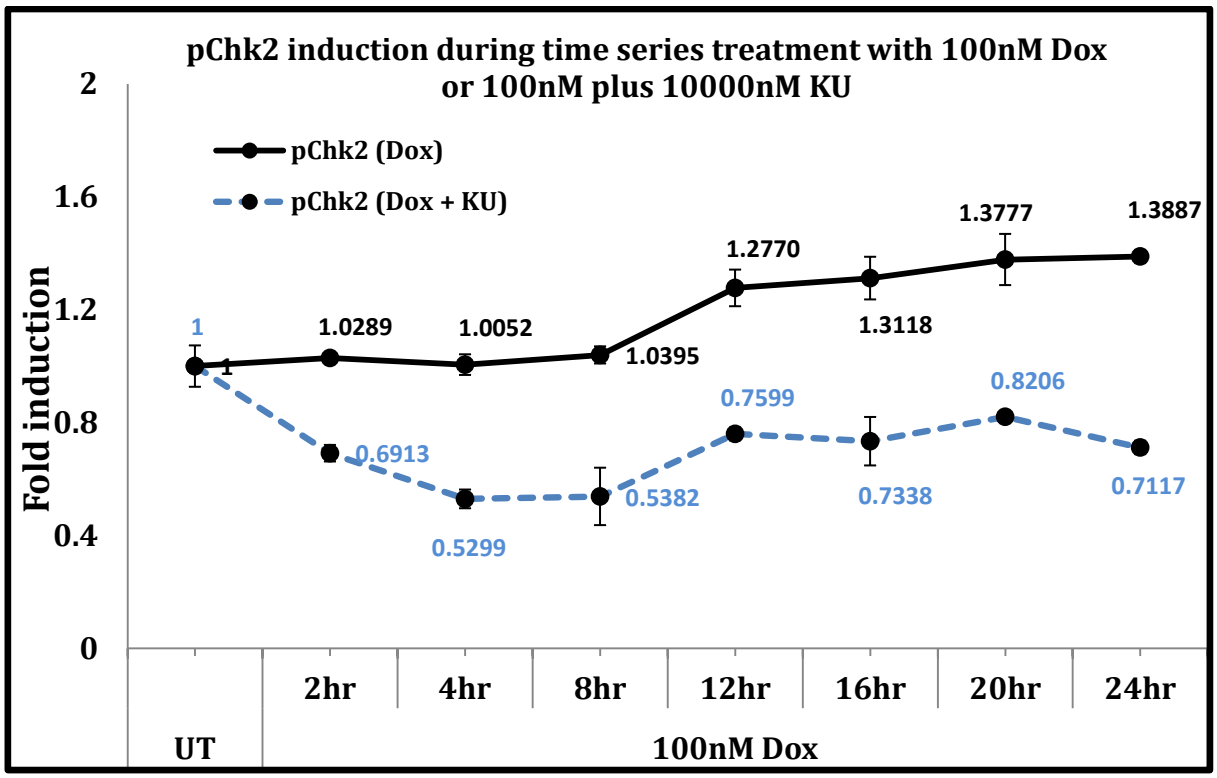


**Figure 6.4: pChk2 induction during time series treatment of 100nM Dox with and without 10µM ATM kinase inhibitor (KU).** HaCat cells were seeded in 96-well plates at a density of 2.5 x $10^3$ cells per well. After 24 hr of incubation, cells were either left untreated or treated with 100nM Dox or 100nM Dox plus 10µM KU for the indicated time points. After treatments, cells were subjected to ELISA as described in materials and methods for the determination of pChk2 T-68 induction using HRP conjugated secondary antibody and Amplex Red® detection system. Readings were taken in Modulus template® 96-well plate reader using excitation emission maxima of 570/585 nm. Each value is based on means of the fluorescence values acquired from quadruplet of treatments and normalized to the mean value of untreated control (UT) expressed as 1. The data is based on three independent experiments.

The late kinetics of activation of checkpoint kinases possibly pointed towards G2/M arrest of the cell cycle rather than inducing apoptosis through ATM→pATM→pChk1/pChk2→X Cdc25 = G2/M CELL CYCLE ARREST pathway. The reason could be that ATM inhibition in KU treated states totally disrupted this later induction of the checkpoint kinases which was accompanied by greater degree of cell death while the activation of these checkpoints in ATM functional state correlated with reduced cell death (Fig. 6.9).

Contrastingly, examination of pP53, another substrate of ATM, at the same time points revealed an earlier time dependent induction that continued steadily up until the 20 hr time point (Fig. 6.5). ATM mediated pP53 induction following mild DNA damage has been reported to result in G1/S cell cycle arrest (Prokopkova J et al., 2006). Hence, it indicated that at earlier time points of lower scale of DNA damage, pATM may signal via the induction of pP53 which can contribute in causing arrest and induce DNA repair signalling, in addition to ATM→Chk1/2→xCdc25 pathway.

Interestingly, pP53 induction was totally disrupted after ATM inhibition up until 16 hr of treatment, a time point where the degree of cell death between ATM inhibited and ATM active states were similar (Compare Fig. 6.5 & 6.9). However, at 20 and 24 hr time point of 100nM Dox treatment in ATM inhibited state, pP53 levels were rapidly induced which tightly correlated with a surge in cell death in the cytotoxicity assay at these time points (Fig. 6.9). This probably demonstrated P53 mediated ATM independent mode of apoptosis post 12 hr. The likely signalling pathway triggered by these treatments leading to apoptosis at later time points could be DNA DAMAGE→XATM = ATR→pP53→Apoptotic proteins →Cell death. Other likely kinases responsible for this P53 induction could be DNA-PK (Shiey SY et al., 1997).

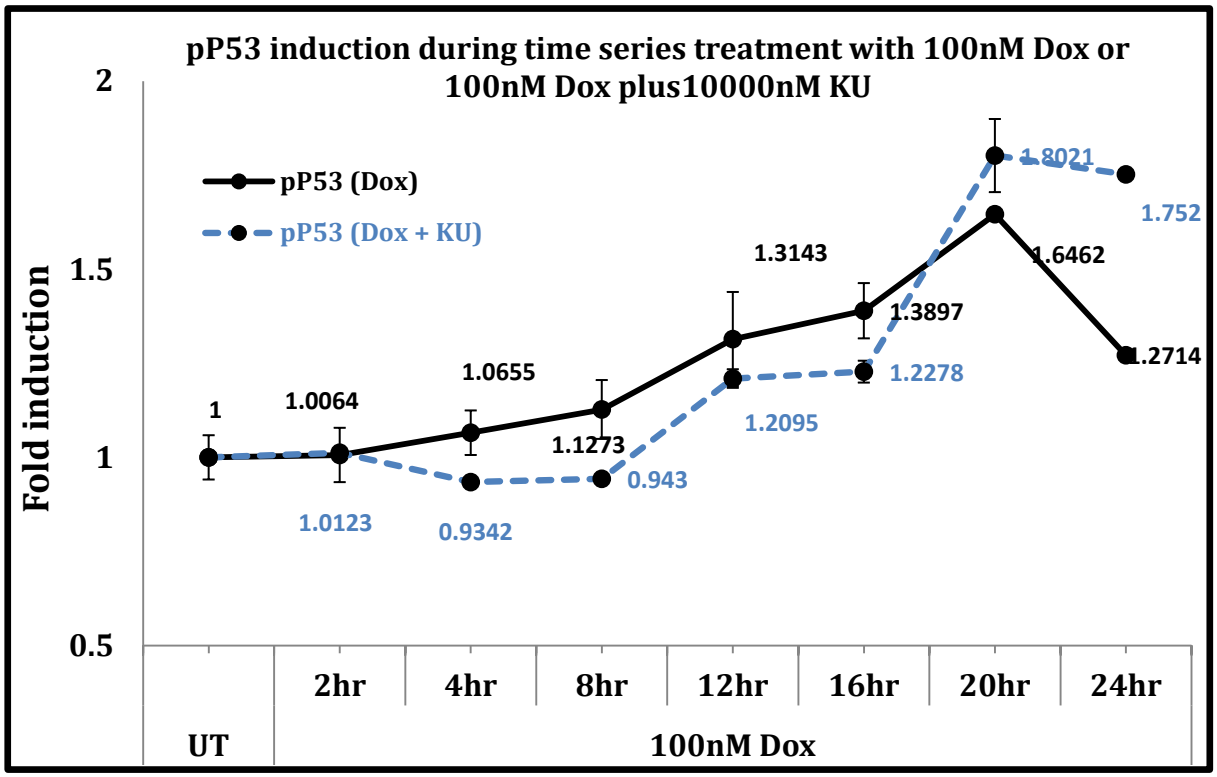


**Figure 6.5: pP53 S-15 induction during time series treatment of 100nM Dox with and without 10µM ATM kinase inhibitor (KU).** HaCat cells were seeded in 96-well plates at a density of 2.5 x $10^3$ cells per well. After 24 hr of incubation, cells were either left untreated or treated with 100nM Dox or 100nM Dox plus 10µM KU for the indicated time points. After treatments, cells were subjected to ELISA as described in materials and methods for the determination of pP53 S-15 induction using HRP conjugated secondary antibody and Amplex Red® detection system. Readings were taken in Modulus template® 96-well plate reader using excitation emission maxima of 570/585 nm. Each value is based on means of the fluorescence values acquired from quadruplet of treatments and normalized to the mean value of untreated control (UT) expressed as 1. The data is based on three independent experiments.

Next, levels of E2F1 transcription factor, implicated in both cell cycle progression (Ohtani K et al., 1995) as well as apoptosis (Wu X et al., 1994) were examined. It was found that as early as 2 hr post 100nM Dox treatment, there was a sharp reduction of E2F1 levels with lowest at 4 hr post treatment. Lower levels of E2F1 were maintained through the whole treatment regime of 2-24 hr but with a single peak at 12 hr time point (Fig. 6.6). Hence, at lower scale of damage, pATM activation (Fig. 6.1) resulting in an accompanying pP53 induction (Fig. 6.5) was also accompanied by reduction in E2F1 levels which fits well with the conventional pathway of ATM dependent, P53 mediated Rb induced block of E2F1 activity causing G1/S arrest (Helen K et al., 1993).

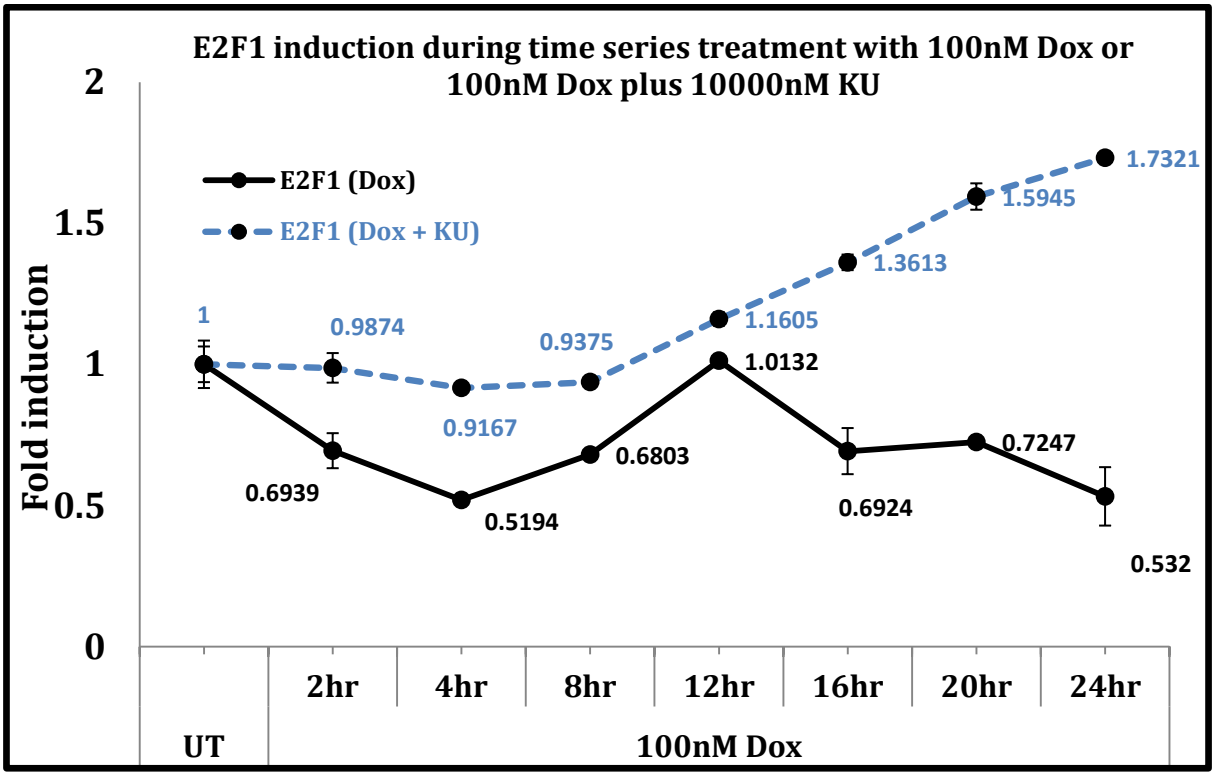


**Figure 6.6: E2F1 induction during time series treatment of 100nM Dox with and without 10µM ATM kinase inhibitor (KU).** HaCat cells were seeded in 96-well plates at a density of 2.5 x $10^3$ cells per well. After 24 hr of incubation, cells were either left untreated or treated with 100nM Dox or 100nM Dox plus 10µM KU for the indicated time points. After treatments, cells were subjected to ELISA as described in materials and methods for the determination of E2F1induction using HRP conjugated secondary antibody and Amplex Red® detection system. Readings were taken in Modulus template® 96-well plate reader using excitation emission maxima of 570/585 nm. Each value is based on means of the fluorescence values acquired from quadruplet of treatments and normalized to the mean value of untreated control (UT) expressed as 1. The data is based on three independent experiments.

Taken together, the earlier assumption of pATM induction at earlier time points of 100nM Dox causing a G1/S arrest is supported by Figure 6.6, while the involvement of checkpoint kinases also suggested G2/M checkpoint arrest. Further support of pATM induced G1/S arrest via ATM → P53 → Rb → x E2F1→CELL CYCLE ARREST pathway is also provided by the fact that, this reduction of E2F1 levels following 100nM Dox treatment was disrupted in ATM inhibited states (Fig. 6.6, Dox + KU panel) whereby E2F1 levels show a time dependent induction which also corresponded with increased cell death observed in cytotoxicity assays (Fig. 6.9). Since E2F1 levels were induced in KU treated states, it pointed towards an ATM independent mechanism of E2F1 activation and apoptosis. Chk2, also known to activate E2F1 following double stranded DNA damage (Steven C et al., 2003) does not seem to be the prime candidate as pChk2 T-68 levels were also disrupted after ATM inhibition. ATR, which showed some induction post 12 hr of treatment, could be a possible candidate causing E2F1 mediated apoptosis. Indeed E2F1 activation has also been reported in pATM and pChk2 independent mechanisms after doxorubicin treatments involving histone acetyl transferase activities (Martínez-Balbás MA et al., 2000, Ianari A et al., 2004).

The γ-H2AX levels, as expected were induced starting at first time point examined and showed time dependent increase until the 24 hr time point of 100nM Dox treatment. Treatment with ATM inhibitor resulted in total disruption of this induction at all the time points tested (Fig. 6.7). This indicated total ATM dependence for γ-H2AX formation after doxorubicin treatment.

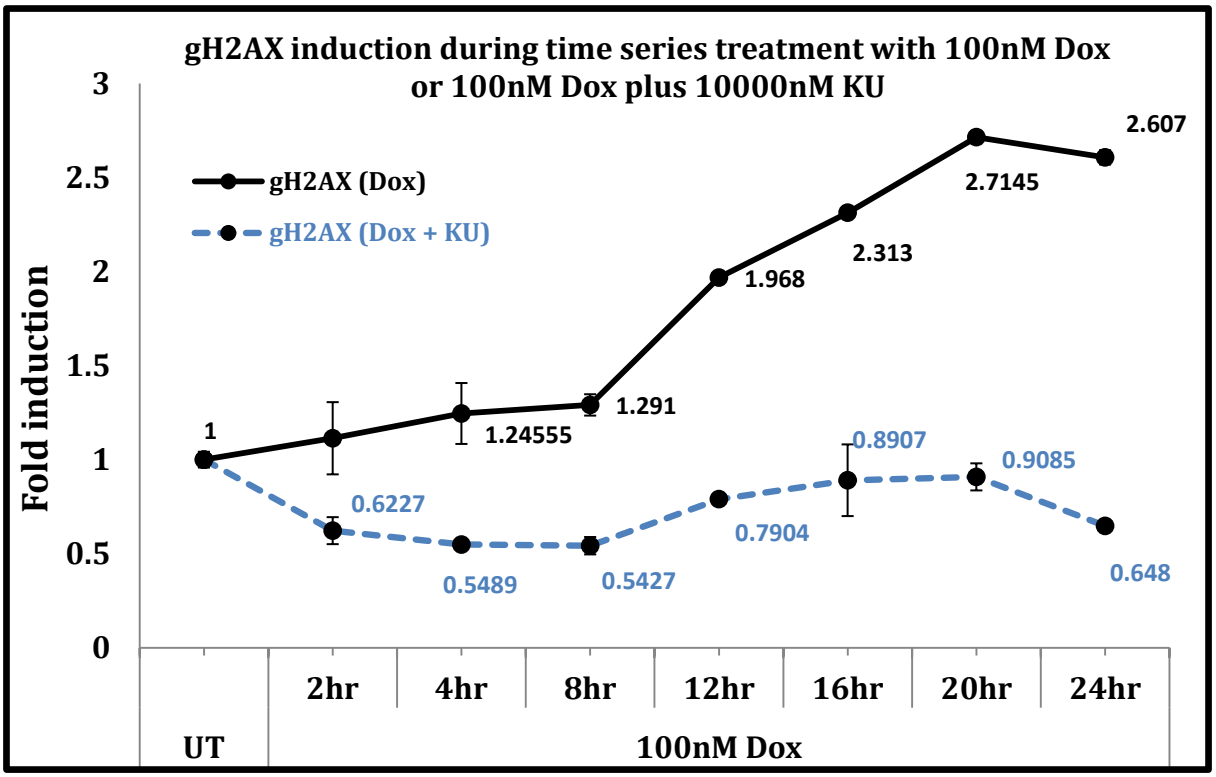


**Figure 6.7: γH2AX induction during time series treatment of 100nM Dox with and without 10μM ATM kinase inhibitor (KU).** HaCat cells were seeded in 96-well plates at a density of 2.5 x $10^3$ cells per well. After 24 hr of incubation, cells were either left untreated or treated with 100nM Dox or 100nM Dox plus 10μM KU for the indicated time points. After treatments, cells were subjected to ELISA as described in materials and methods for the determination of γH2AX induction using HRP conjugated secondary antibody and Amplex Red® detection system. Readings were taken in Modulus template® 96-well plate reader using excitation emission maxima of 570/585 nm. Each value is based on means of the fluorescence values acquired from quadruplet of treatments and normalized to the mean value of untreated control (UT) expressed as 1. The data is based on three independent experiments.

Similarly, BRCA1, an important downstream substrate of ATM also showed ATM dependence for its induction (Fig. 6.8). While BRCA1was reported to induce apoptosis in both P53 dependent (Zhang H et al., 1998) and independent mechanisms (Harkin DP et al., 1999), under the conditions tested, and it terms of ATM signalling, BRCA1 exhibited a complete dependence on ATM for its induction (Fig. 6.8).

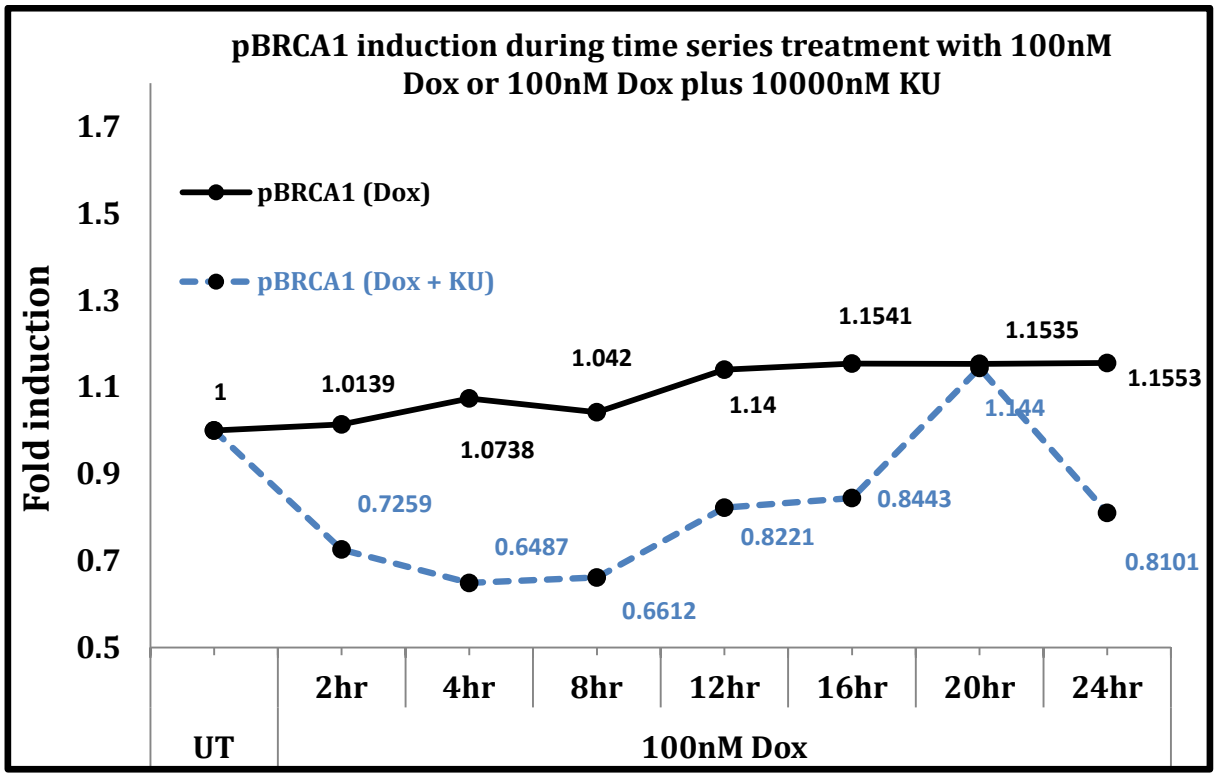


**Figure 6.8: pBRCA1 induction during time series treatment of 100nM Dox with and without 10µM ATM kinase inhibitor (KU).** HaCat cells were seeded in 96-well plates at a density of 2.5 x $10^3$ cells per well. After 24 hr of incubation, cells were either left untreated or treated with 100nM Dox or 100nM Dox plus 10µM KU for the indicated time points. After treatments, cells were subjected to ELISA as described in materials and methods for the determination of pBRCA1 S-1524 induction using HRP conjugated secondary antibody and Amplex Red® detection system. Readings were taken in Modulus template® 96-well plate reader using excitation emission maxima of 570/585 nm. Each value is based on means of the fluorescence values acquired from quadruplet of treatments and normalized to the mean value of untreated control (UT) expressed as 1. The data is based on three independent experiments.

Taken together, the data generated with a lower DNA damage of 100nM Doxorubicin demonstrated that ATM kinase functioned as a DNA damage sensor causing G1/S arrest or G2/M arrest rather than apoptosis indicating its role in cytoprotection and DNA repair. Furthermore, the treatment resulted in DDR activation in a characteristic way whereby different ATM substrates showed different kinetics of activation as well as dissimilar sensitivity towards ATM inhibition. The numerical data generated with eight different proteins tested at two different conditions and data collected over eight different time points was passed on to mathematical modellers (Michael Idowu and Prof James Bown, University of Abertay Dundee) to compute a data driven deterministic model of the biological pathway (See section 6.4).

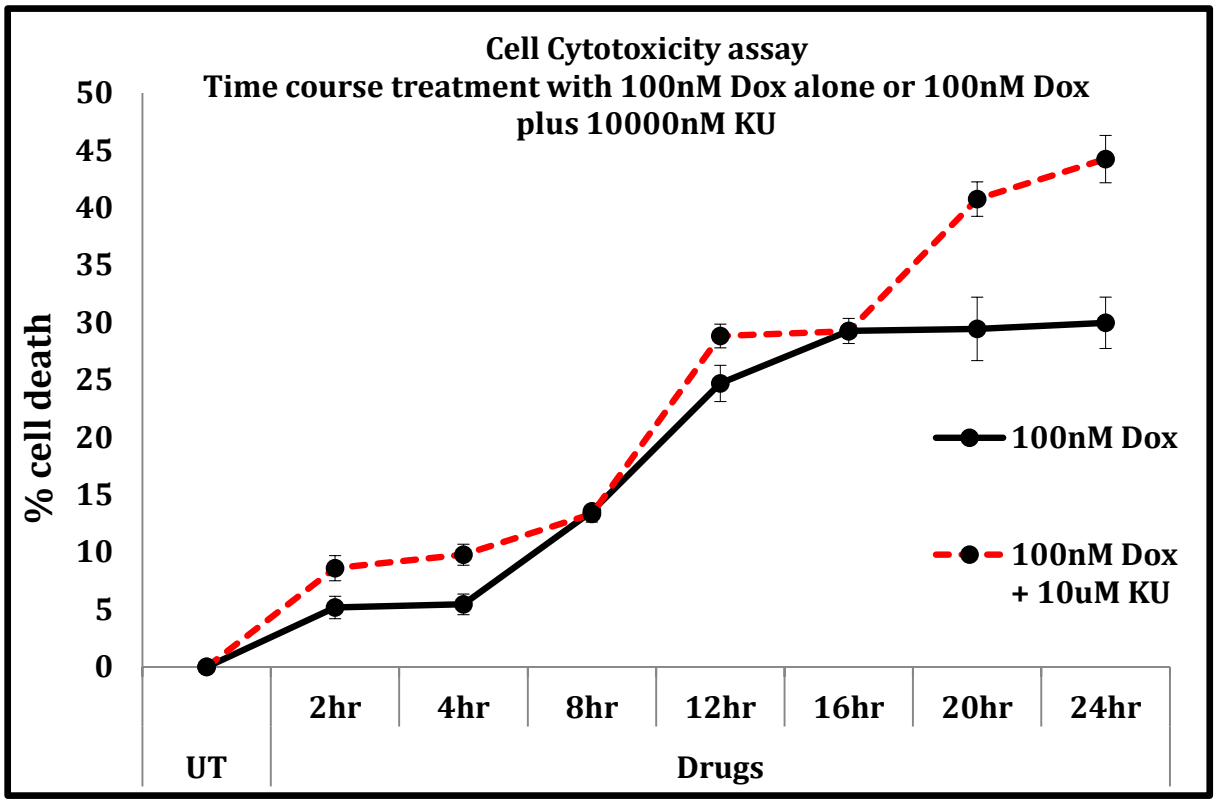


**Figure 6.9: NR-uptake based cell cytotoxicity assay during time course treatment with 100nM Dox alone, or with the addition of 10µM ATM kinase inhibitor (KU).** HaCat cells were seeded in 96-well plates at a density of 2.3 x $10^3$ cells per well. After 24 hr of incubation, cells were either left untreated or treated with 100nM Dox or 100nM Dox plus 10µM KU for the indicated time points. After treatments, cells were subjected to NR-uptake cell cytotoxicity assay as described in materials and methods for the determination of cell viability. Readings were taken in Modulus template® 96-well plate reader by measuring the absorbance at 540nm. Each value is based on means of the absorbance values acquired from quadruplet of treatments and normalized to the mean value of untreated control (UT) and expressed as % cell death with the formula 100 – [($Abs_{540}$ treated sample/$Abs_{540}$ untreated sample) × 100]. The data is based on three independent experiments.

### *6.3.2 Time series treatment of 400nM Doxorubicin with and without ATM inhibition revealed time dependent dual roles of ATM in determining cellular sensitivity towards genotoxicity in HaCat cells.*

Once the kinetic parameters of DDR activation at relatively low level of DNA damage was determined, I next set out to perform the same experiment at higher degree of DNA damage by increasing Doxorubicin concentration four times (400nM Dox). The logic behind performing experiment at higher degree of DNA damage was based on the following:

i) To determine whether increasing DNA damage has any affect on relative contribution of ATM in apoptotic induction as compared to what was observed at lower scale of DNA damage.

ii) To determine whether increasing DNA damage causes the resulting DDR activation more ATM independent (by examining substrate induction in KU treated states).

iii) To determine if there is a linear relationship between the independent variable i.e. drug treatment and a dependent variable i.e. DDR activation. This would be determined by computational modelling experiments using data generated in these experiments.

iv) To test the potential of computational modelling in predicting DDR kinetics at higher damage, based on data acquired at lower damage.

Cytotoxicity assay of cells treated with either 400nM Dox alone or with the addition of 10μM KU revealed striking results and quite different from those observed in section 6.3.1.

Firstly, greater apoptosis was seen both with and without addition of ATM inhibitor at 400nM of Dox treatment as compared to lower DNA damage incurred at 100nM of Dox. Interestingly, addition of ATM inhibitor along with 400nM Dox resulted in higher apoptosis only at earlier time points of 2, 4 and 8 hr of treatments as compared to 400nM Dox alone. Furthering the treatment regime contrastingly resulted in a lower cell death with the addition of ATM inhibitor then without, at 12, 16, 20 and 24 hr time points. Furthermore, this difference in relative percentages of cell death between Dox only and Dox plus KU treatments post 8 hr kept increasing until the final time point (Fig. 6.10).

Hence, it was inferred that at earlier time points, ATM kinase mainly performed a cytoprotective function by signalling in cell cycle arrest and DNA repair pathways as it ensured greater cell survival until 8 hr time point, as compared to that in ATM inhibition state. On the other hand, at a greater extent of DNA damage beyond 8 hr of treatment, its function switched towards apoptosis, as there was higher cell death in functional ATM state than in inhibited state (Fig. 6.10).

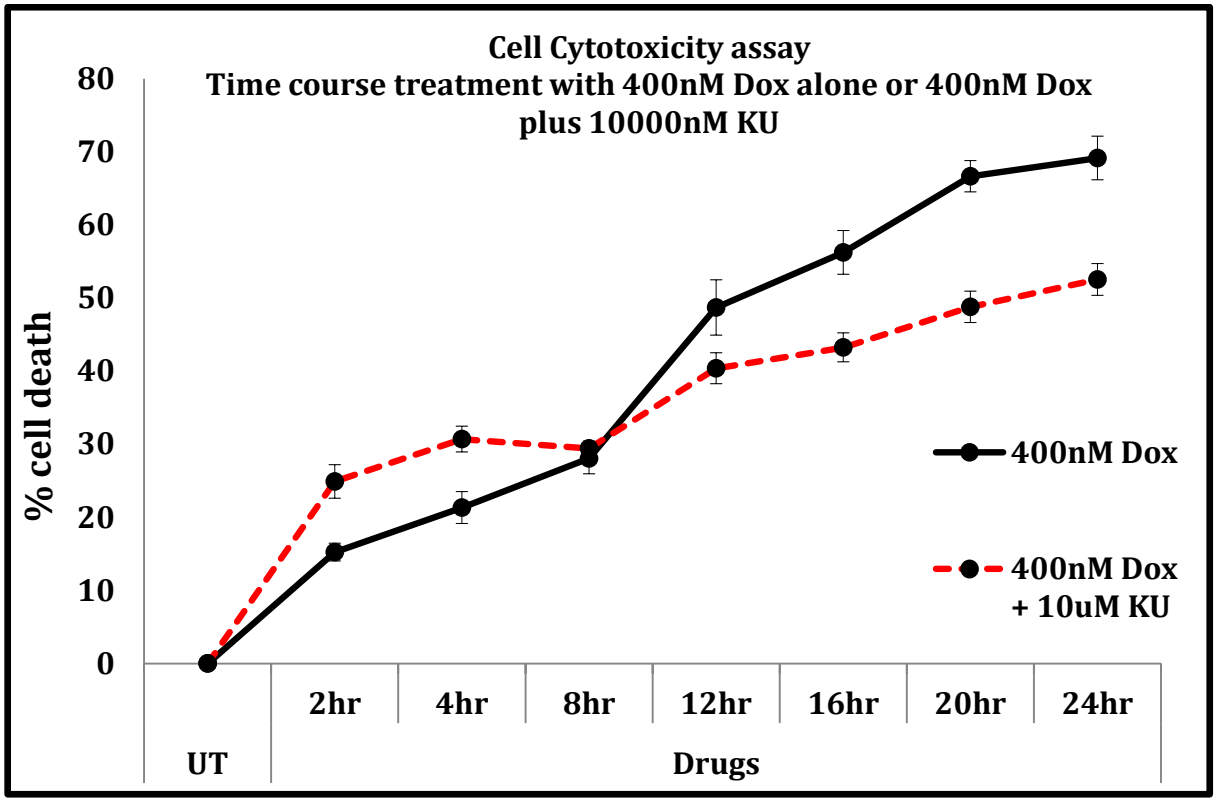


**Figure 6.10: NR-uptake based cell cytotoxicity assay during time course treatment with 400nM Dox alone, or with the addition of 10µM ATM kinase inhibitor (KU).** HaCat cells were seeded in 96-well plates at a density of 2.3 x $10^3$ cells per well. After 24 hr of incubation, cells were either left untreated or treated with 400nM Dox or 400nM Dox plus 10µM KU for the indicated time points. After treatments, cells were subjected to NR-uptake cell cytotoxicity assay as described in materials and methods for the determination of cell viability. Readings were taken in Modulus template® 96-well plate reader by measuring the absorbance at 540nm. Each value is based on means of the absorbance values acquired from quadruplet of treatments and normalized to the mean value of untreated control (UT) and expressed as % cell death with the formula 100 – [($Abs_{540}$ treated sample/$Abs_{540}$ untreated sample) × 100]. The data is based on three independent experiments.

This was an important observation that clearly demonstrated time dependent switch of ATM kinase function between having a cytoprotective role to having a role in apoptotic pathway. This result also demonstrated the importance of timing ATM kinase inhibition during a genotoxic treatment regime, whereby, if the objective is to achieve higher cellular sensitivity, it is best to inhibit ATM during time points where it is functioning as a DNA repair kinase as opposed to apoptosis inducer.

Next, the underlying DDR mechanism under these conditions was studied. Treatment of HaCat cells with 400nM Dox resulted in a rapid pATM induction reaching >3 fold at the first time point of 2 hr, where only 15% cell death was seen as opposed to 25% during its inhibition, and maintaining time dependent induction up until 16 hr of treatment (>5 fold increase). At 20 and 24 hr time points, there was a reduction in pATM levels with the lowest at 24 hr time point but still 2 fold higher than at untreated state (Fig. 6.11). One reason of this reduction, where a higher cell death was observed could be a previously reported caspase dependent ATM cleavage (Smith GC et al., 1999). Addition of ATM inhibitor, as expected, resulted in disruption of Dox mediated pATM induction (Fig. 6.11).

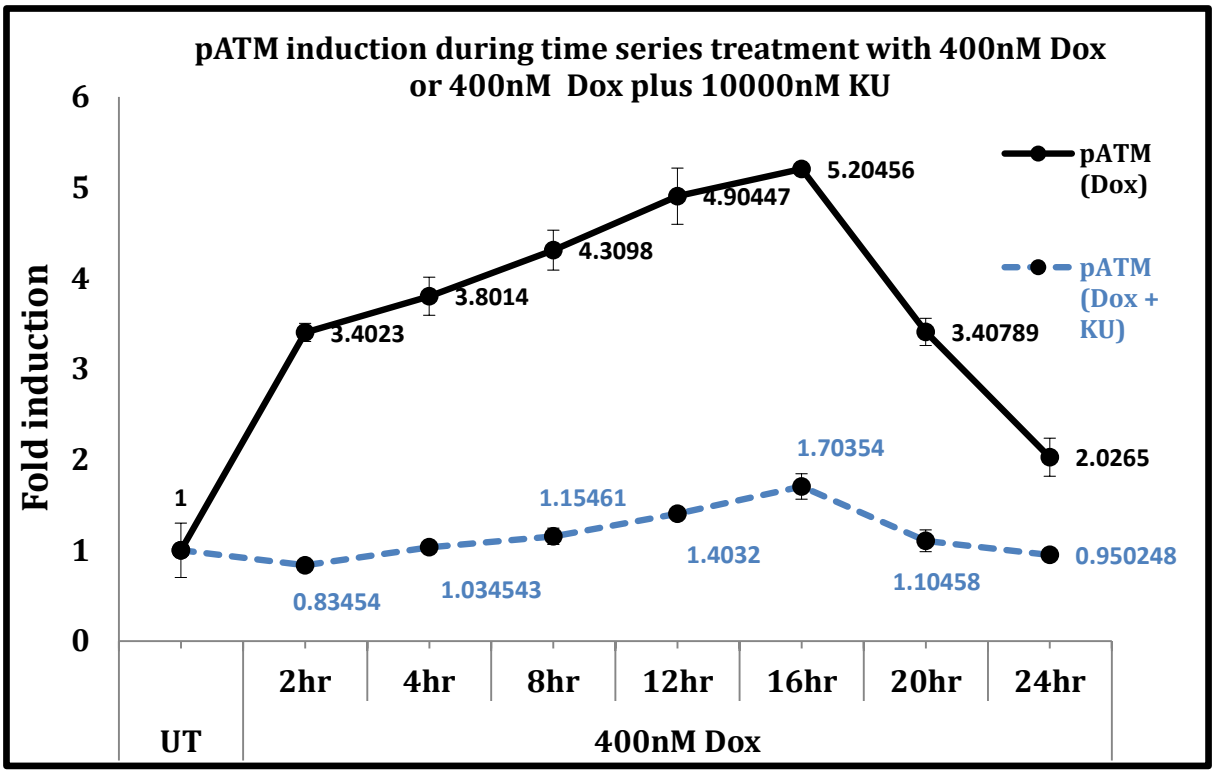


**Figure 6.11: pATM induction during time series treatment of 400nM Dox with and without 10µM ATM kinase inhibitor (KU).** HaCat cells were seeded in 96-well plates at a density of 2.5 x $10^3$ cells per well. After 24 hr of incubation, cells were either left untreated or treated with 400nM Dox or 400nM Dox plus 10µM KU for the indicated time points. After treatments, cells were subjected to ELISA as described in materials and methods for the determination of pATM S-1981 induction using HRP conjugated secondary antibody and Amplex Red® detection system. Readings were taken in Modulus template® 96-well plate reader using excitation emission maxima of 570/585 nm. Each value is based on means of the fluorescence values acquired from quadruplet of treatments and normalized to the mean value of untreated control (UT) expressed as 1. The data is based on three independent experiments.

Interestingly, at a higher damage of 400nM Dox, pATR also showed induction, starting at 8 hr and maximum at 16 hr time points (6.12). The kinetics of this induction, however, were slower than those of pATM. It is not surprising as in a previous study, pATR was found to be recruited to DSBs at later time points than pATM (Adams KE et al., 2006). Furthermore, while addition of ATM inhibitor at a lower damage of 100nM Dox resulted in a minor induction of pATR post 12 hr treatment as compared to Dox only treatment (Fig. 6.2), addition of it with 400nM Dox surprisingly resulted in higher induction starting at 2 hr post treatment and maximum at 12 hr time point (6.12). While Jazayeri A et al., 2006 reported a functional requirement of ATM for ATR function in double stranded DNA damage, this result suggests KU dependent induction of pATR. Analysis of this induction with the results obtained from cytotoxicity assay (Fig. 6.10) suggested the role of this transient pATR induction in apoptosis during ATM inhibited states where cells fail to arrest in G1/S state. For example, with the addition of ATM inhibitor, pATR was up-regulated at 2, 4 and 8 hours, time points where cells showed higher cell death, whereas, it was rapidly down regulated at 12, 16 and 20 hours, time points where cells showed an overall lower cell death (Compare Fig. 6.10 and 6.12). Hence one candidate for inducing higher apoptosis in ATM inhibited states till 8 hr time point seemed to be ATR activity.

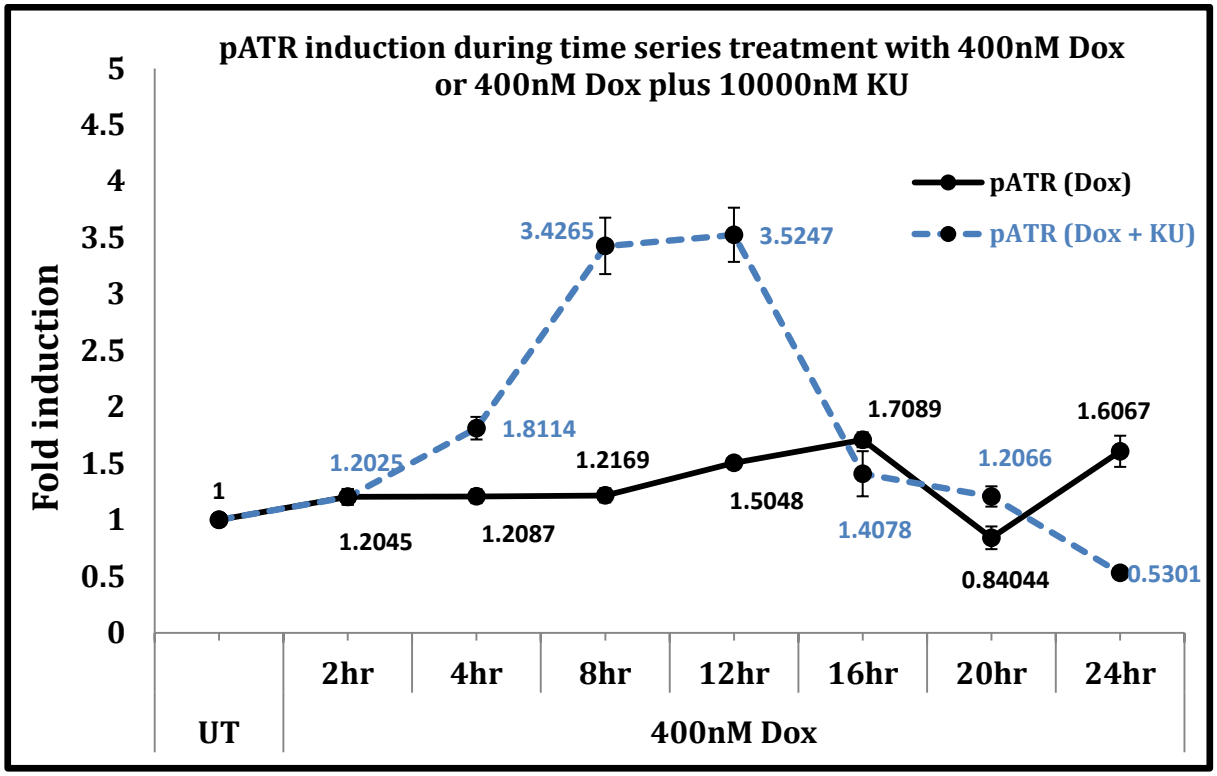


**Figure 6.12: pATR induction during time series treatment of 400nM Dox with and without 10µM ATM kinase inhibitor (KU).** HaCat cells were seeded in 96-well plates at a density of 2.5 x $10^3$ cells per well. After 24 hr of incubation, cells were either left untreated or treated with 400nM Dox or 400nM Dox plus 10µM KU for the indicated time points. After treatments, cells were subjected to ELISA as described in materials and methods for the determination of pATR S-428 induction using HRP conjugated secondary antibody and Amplex Red® detection system. Readings were taken in Modulus template® 96-well plate reader using excitation emission maxima of 570/585 nm. Each value is based on means of the fluorescence values acquired from quadruplet of treatments and normalized to the mean value of untreated control (UT) expressed as 1. The data is based on three independent experiments.

In terms of checkpoint kinase activities of Chk1 and Chk2, while Fig. 6.3 and 6.4 revealed comparable Dox induced activation and KU induced disruption of induction between these kinases, at a higher scale of damage of 400nM Dox, these kinases showed significantly different sensitivities toward ATM inhibition. Overall, pChk2 showed earlier induction following Dox treatment as compared to pChk1, starting at 2 hr time point and continuing until 16 hr of treatment, and staying constant henceforth (Fig. 6.14). pChk1, on the other hand, showed a delayed induction but a very high single spike at 16 hr of treatment and reducing at further time points of 20 and 24 hr (Fig. 6. 13).

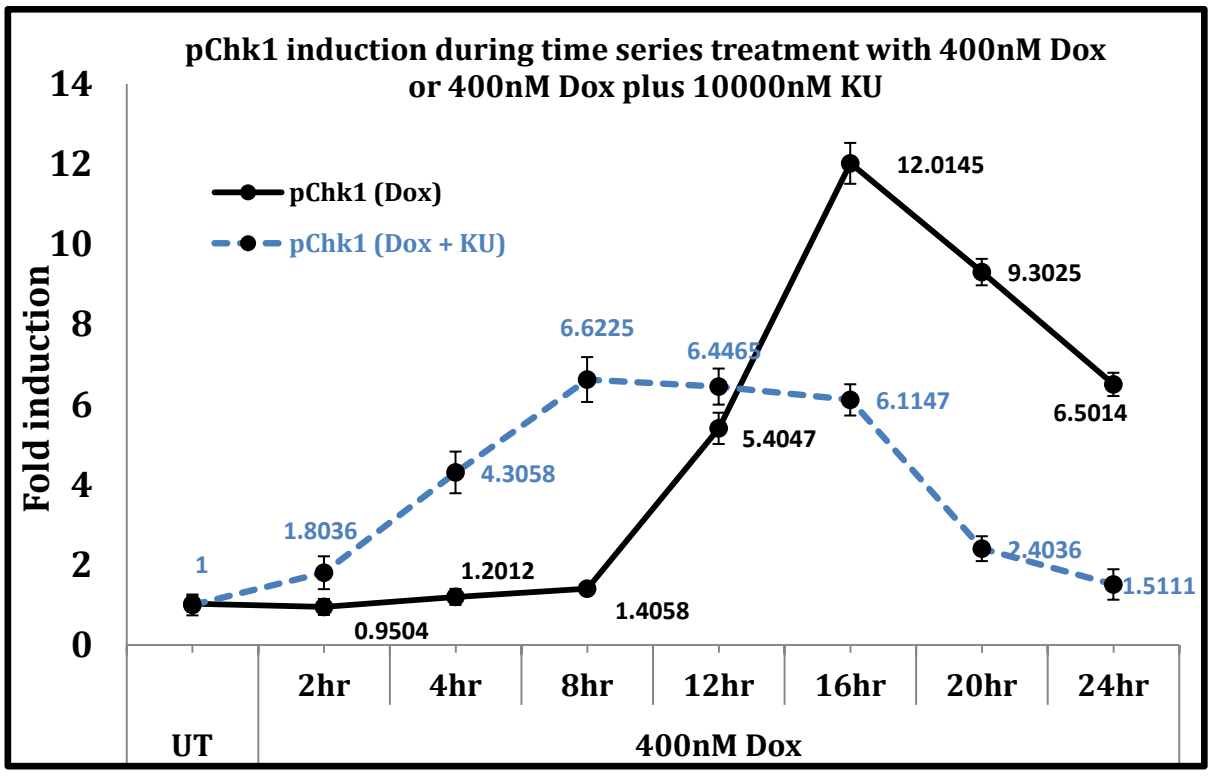


**Figure 6.13: pChk1 induction during time series treatment of 400nM Dox with and without 10µM ATM kinase inhibitor (KU).** HaCat cells were seeded in 96-well plates at a density of 2.5 x $10^3$ cells per well. After 24 hr of incubation, cells were either left untreated or treated with 400nM Dox or 400nM Dox plus 10µM KU for the indicated time points. After treatments, cells were subjected to ELISA as described in materials and methods for the determination of pChk1 S-296 induction using HRP conjugated secondary antibody and Amplex Red® detection system. Readings were taken in Modulus template® 96-well plate reader using excitation emission maxima of 570/585 nm. Each value is based on means of the fluorescence values acquired from quadruplet of treatments and normalized to the mean value of untreated control (UT) expressed as 1. The data is based on three independent experiments.

Addition of ATM inhibitor along with 400nM Dox resulted in total disruption of pChk2 levels at all the time points, confirming that the dependency of Chk2 on ATM for its Threonine 68 phosphorylation is unaltered even at higher scale of DNA damage (Fig. 6.14). These results further demonstrate that pChk2 induction, which was totally dependent on ATM activity, was implicated in effecting the cytoprotective function of ATM at relatively lower scale of DNA damage, whereas promoted apoptotic signalling at a higher scale of DNA damage. This result is also supported by previously well explained ATM dependent role of Chk2 in apoptotic induction (Steven C et al., 2003, Rogoff HA et al., 2004).

pChk1, on the other hand, while being sensitive to ATM inhibition at lower Dox concentration of 100nM, showed ATM independent induction at a higher Dox concentration of 400nM, starting at 2 hr time point, and remaining > 6 fold high until 16 hr of treatment, after which, showing reduction (Fig. 6.13). Interestingly, the kinetics of pATR and pChk1 induction during ATM inhibited state at 400nM Dox were very similar (Compare Fig. 6.12 and 6.13). Furthermore, this activation in ATM inhibited state was tightly correlated with cell death. For example, at 2, 4 and 8 hr of 400nM Dox plus KU, there was induction of pATR and pChk1 accompanied by higher cell death. By 16, 20 and 24 hr of such treatment, both pATR and pChk1 levels reduced whereby, there was also reduction in comparative cell death. Since pChk1 is a direct substrate of pATR, these results point towards an ATM independent and ATR dependent apoptotic induction via KU→xATM = ATR→pChk1→APOPTOSIS pathway.

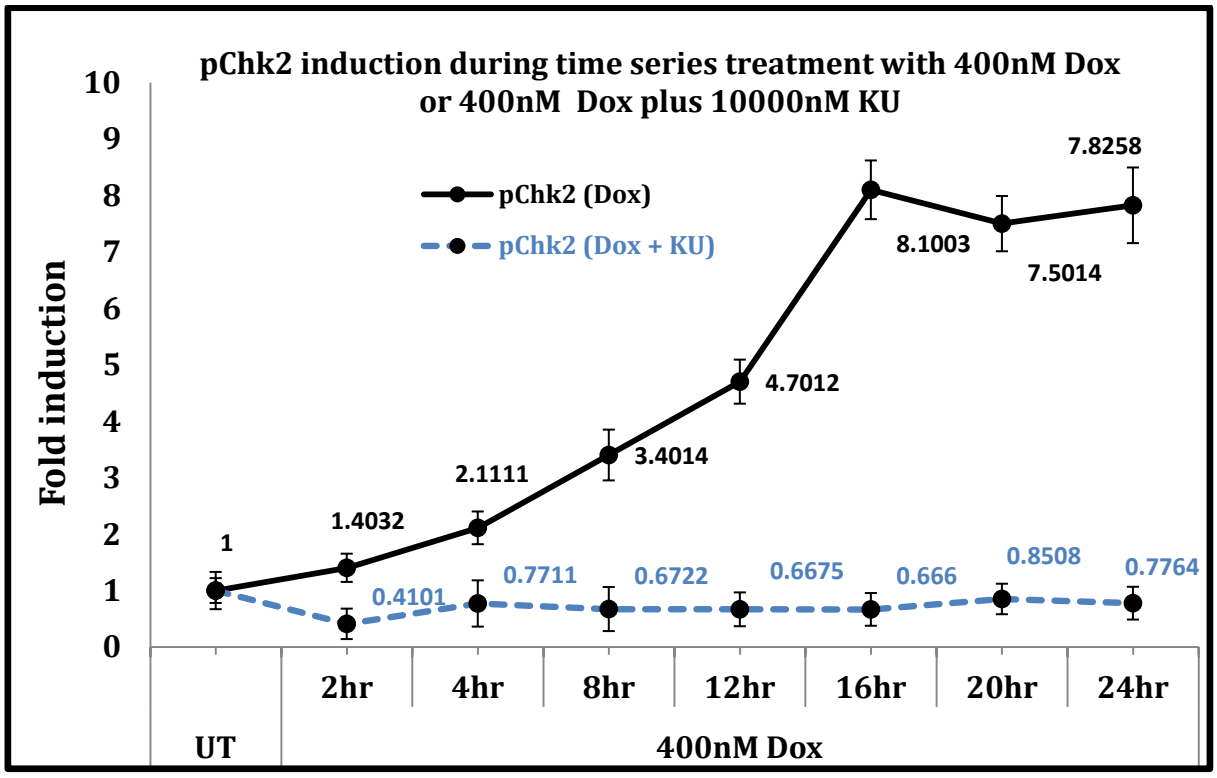


**Figure 6.14: pChk2 induction during time series treatment of 400nM Dox with and without 10µM ATM kinase inhibitor (KU).** HaCat cells were seeded in 96-well plates at a density of 2.5 x $10^3$ cells per well. After 24 hr of incubation, cells were either left untreated or treated with 400nM Dox or 400nM Dox plus 10µM KU for the indicated time points. After treatments, cells were subjected to ELISA as described in materials and methods for the determination of pChk2 T-68 induction using HRP conjugated secondary antibody and Amplex Red® detection system. Readings were taken in Modulus template® 96-well plate reader using excitation emission maxima of 570/585 nm. Each value is based on means of the fluorescence values acquired from quadruplet of treatments and normalized to the mean value of untreated control (UT) expressed as 1. The data is based on three independent experiments.

Another candidate for pChk1 activation could be DNA-PK, which has been shown to have a functional interaction with it (Goudelock DM et al., 2003) and thus pChk1 induction at higher scale of damage in ATM inhibited state may demonstrate an overlapping function of DNA-PK with ATM which may still ensure DDR activation (Stiff T et al., 2004). Overall, both in ATM active and inhibited states, pChk1 induction fitted well with the degree of cell death in such treatments. Hence, while lower scale of DNA damage, pChk1 was classified as effecting the cytoprotective function of ATM, at higher scale of DNA damage, it promoted cytotoxicity both in ATM dependent and independent manner.

Owing to a rapid induction of pATM and pChk2 after 400nM Dox treatment, it was expected to induce pP53 S-15 levels. Figure 6.15 shows rapid and very high pP53 induction >9 fold at the first time point of 2 hr treatment and maximum at 24 hr time point (> 20 fold induction). Hence, so far, the higher degree of cell death with Dox only treatment is proposed to have an underlying DDR pathway involving ATM→Chk2/Chk1→P53→Bad/Bax/Caspase cleavage → Apoptosis. Addition of ATM inhibitor with 400nM Dox disrupted pP53 induction only showing a slight transient rise at 12 hr time point (Fig. 6.15). Nevertheless, pP53 levels in Dox + KU treated cells always remained below those in Dox treated cells, unlike what was observed in figure 6.5, where at 24 hr time point, KU addition to 100nM Dox resulted in higher levels of pP53. This result also suggested the involvement of P53 in ATM mediated cell death after 400nM of Dox treatment.

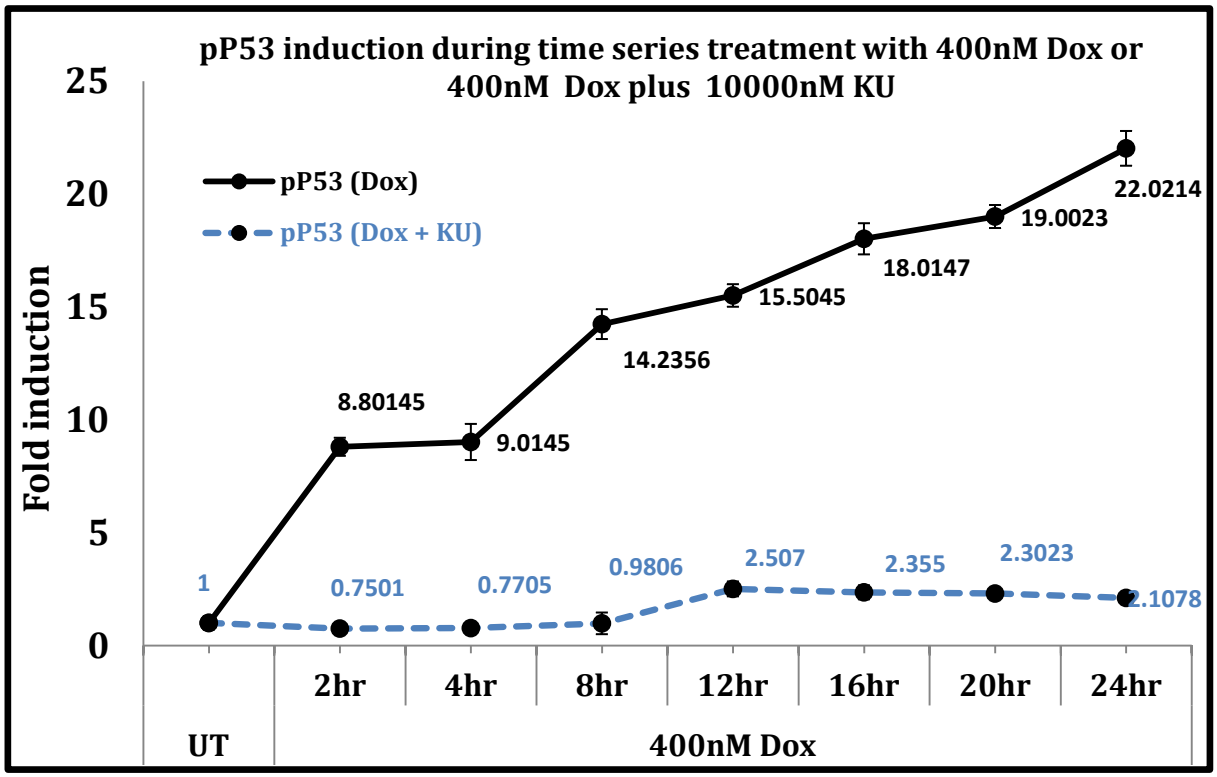


**Figure 6.15: pP53 induction during time series treatment of 400nM Dox with and without 10µM ATM kinase inhibitor (KU).** HaCat cells were seeded in 96-well plates at a density of 2.5 x $10^3$ cells per well. After 24 hr of incubation, cells were either left untreated or treated with 400nM Dox or 400nM Dox plus 10µM KU for the indicated time points. After treatments, cells were subjected to ELISA as described in materials and methods for the determination of pP53 S-15 induction using HRP conjugated secondary antibody and Amplex Red® detection system. Readings were taken in Modulus template® 96-well plate reader using excitation emission maxima of 570/585 nm. Each value is based on means of the fluorescence values acquired from quadruplet of treatments and normalized to the mean value of untreated control (UT) expressed as 1. The data is based on three independent experiments.

As E2F1 is already mentioned earlier to have a prominent role in ATM mediated apoptosis (Lin WC et al., 2001, Rogoff HA et al., 2004), the greater cell death seen in 400nM Dox treatments was expected to be accompanied by E2F1 induction. Indeed, E2F1 was found to be induced in a time dependent manner and showed greater than 12 fold induction at 20 hr post Dox treatment (Fig. 6.16).

Interestingly, while a lower scale damage of 100nM Dox resulted in ATM dependent reduction in E2F1 levels (proposed earlier via the pathway ATM → P53 → Rb → x E2F1→CELL CYCLE ARREST), which were abrogated after ATM inhibition (Fig. 6.6), at a higher scale damage of 400nM Dox, E2F1 contrastingly showed ATM dependent induction, which was abrogated during ATM inhibition (Fig. 6.16). This clearly demonstrated dual roles of E2F1 during lower and higher scale damage, being inhibited at lower scale damage to prevent cell cycle progression in order to arrest and repair cells, hence ensuring cell survival, while activated at higher scale damage, to promote ATM dependent apoptosis. The proposed pathway for this apoptotic mechanism could be ATM → (directly or via pChk2)→ E2F1 → p300/ARF→ P53 or P73 → Apoptosis. These results reemphasized the importance of ATM function in performing multiple cellular roles, dependent upon state of cellular DNA, which in this instance was via differential regulation of E2F1.

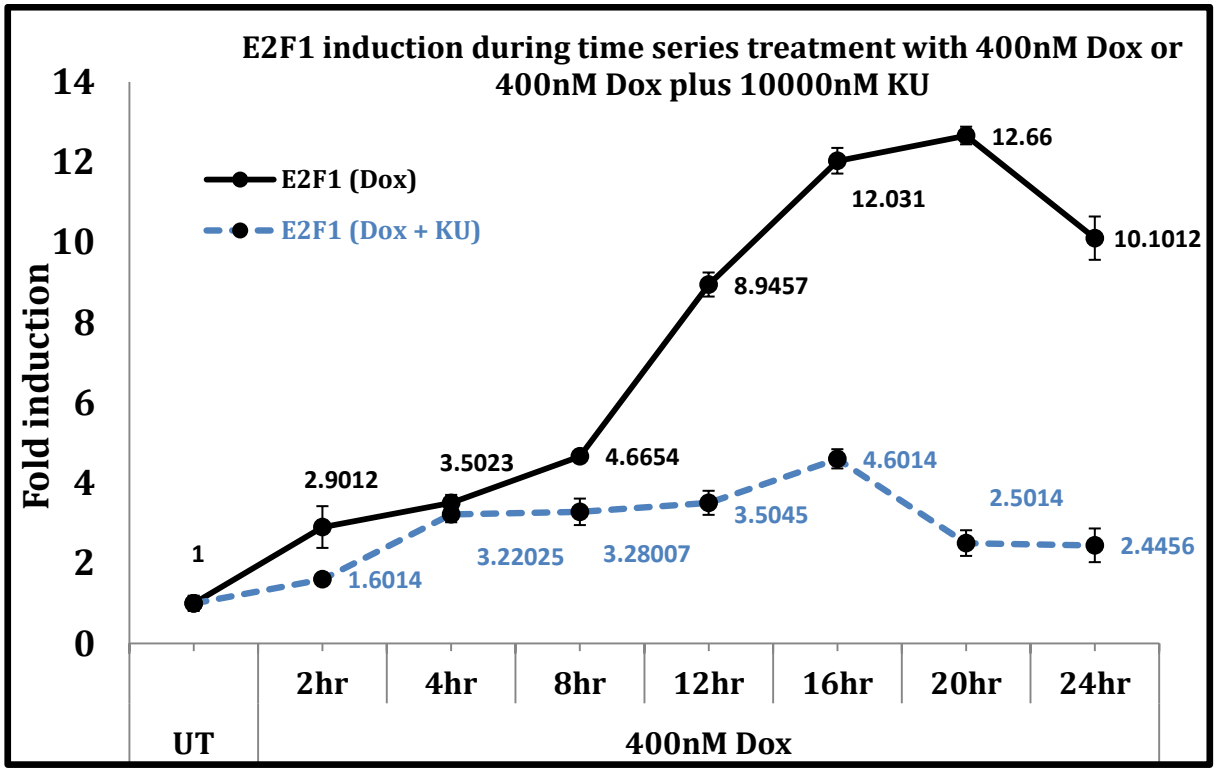


**Figure 6.16: E2F1 induction during time series treatment of 400nM Dox with and without 10µM ATM kinase inhibitor (KU).** HaCat cells were seeded in 96-well plates at a density of 2.5 x $10^3$ cells per well. After 24 hr of incubation, cells were either left untreated or treated with 400nM Dox or 400nM Dox plus 10µM KU for the indicated time points. After treatments, cells were subjected to ELISA as described in materials and methods for the determination of E2F1 induction using HRP conjugated secondary antibody and Amplex Red® detection system. Readings were taken in Modulus template® 96-well plate reader using excitation emission maxima of 570/585 nm. Each value is based on means of the fluorescence values acquired from quadruplet of treatments and normalized to the mean value of untreated control (UT) expressed as 1. The data is based on three independent experiments.

γ–H2AX S-139 (Fig. 6.17) and pBRCA1 S-1524 (Fig. 6.18) both showed a time dependent induction in their levels following treatment with 400nM Dox while disruption of this induction during ATM inhibition. This again demonstrated a sole requirement of ATM function during these DNA damage dependent inductions.

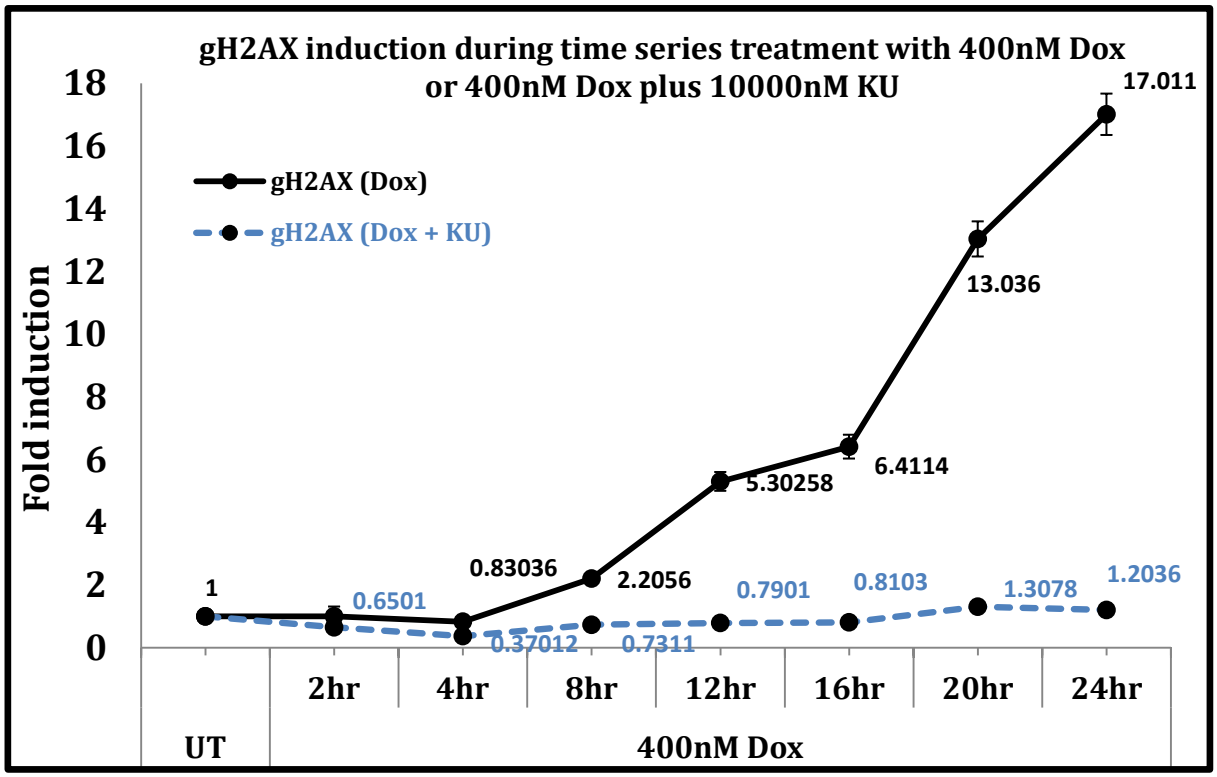


**Figure 6.17: γH2AX induction during time series treatment of 400nM Dox with and without 10μM ATM kinase inhibitor (KU).** HaCat cells were seeded in 96-well plates at a density of 2.5 x $10^3$ cells per well. After 24 hr of incubation, cells were either left untreated or treated with 400nM Dox or 400nM Dox plus 10μM KU for the indicated time points. After treatments, cells were subjected to ELISA as described in materials and methods for the determination of γH2AX induction using HRP conjugated secondary antibody and Amplex Red® detection system. Readings were taken in Modulus template® 96-well plate reader using excitation emission maxima of 570/585 nm. Each value is based on means of the fluorescence values acquired from quadruplet of treatments and normalized to the mean value of untreated control (UT) expressed as 1. The data is based on three independent experiments.

While BRCA1 phosphorylation has been reported to occur in an overlapping manner by other DDR kinases (Gatei M et al., 2001), the antibody used in the current research detects S-1524 which is demonstrated to get completely disrupted after ATM inhibition (Fig. 6.18).

γ–H2AX showed the highest levels at 24 hr time point during Dox treatments. pBRCA1 induction, as mentioned earlier, could be associated with the increased cell death seen in figure 6.10 at 12, 16, 20 and 24 hr time points during Dox treated states.

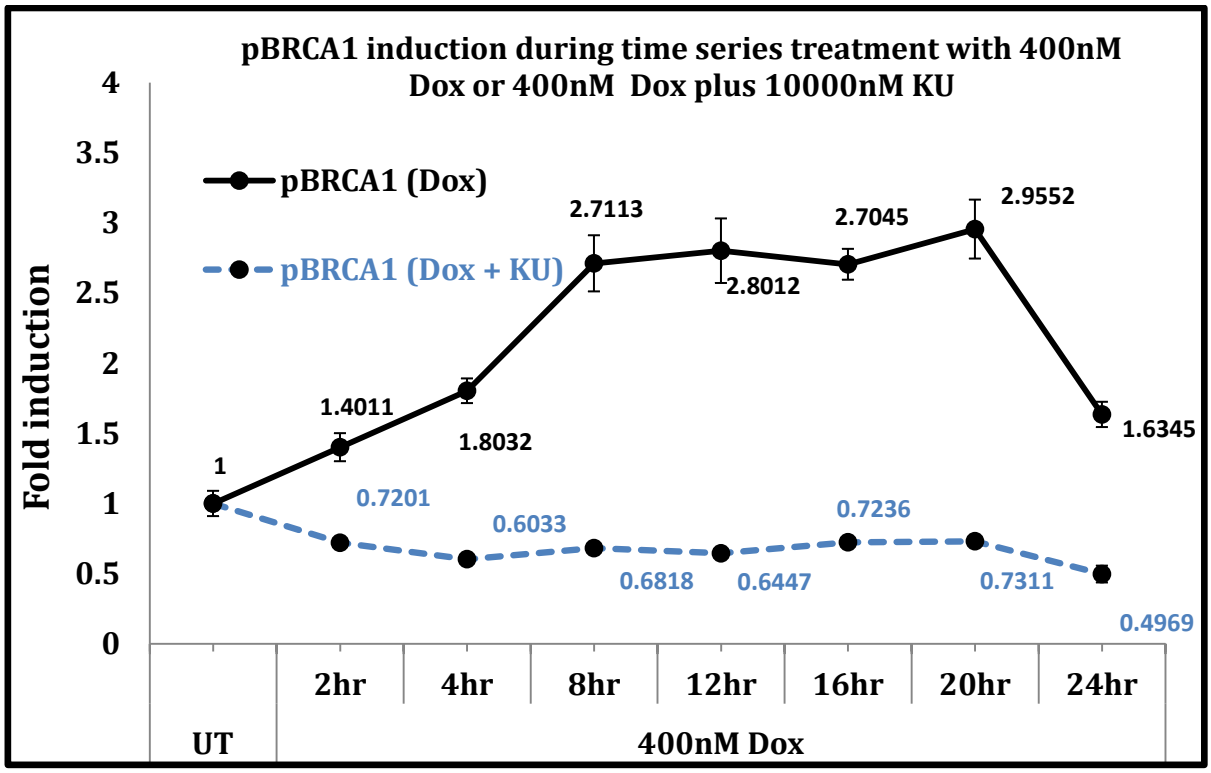


**Fig. 6.18: pBRCA1 induction during time series treatment of 400nM Dox with and without 10μM ATM kinase inhibitor (KU).** HaCat cells were seeded in 96-well plates at a density of 2.5 x $10^3$ cells per well. After 24 hr of incubation, cells were either left untreated or treated with 400nM Dox or 400nM Dox plus 10μM KU for the indicated time points. After treatments, cells were subjected to ELISA as described in materials and methods for the determination of pBRCA1 S-1524 induction using HRP conjugated secondary antibody and Amplex Red® detection system. Readings were taken in Modulus template® 96-well plate reader using excitation emission maxima of 570/585 nm. Each value is based on means of the fluorescence values acquired from quadruplet of treatments and normalized to the mean value of untreated control (UT) expressed as 1. The data is based on three independent experiments.

These experiments not only provided time series quantitative data of the differential kinetics of DDR induction in different conditions, but also elucidated its impact on overall cellular survival and health. These experiments allowed the quantitative data generated to be employed for the development of dynamic mathematical modelling and visualization networks. Furthermore, the cytotoxicity assays revealed multiple roles that ATM might play by the modulation in its substrate preferences in a time dependent manner. These results reemphasised on the importance of timing the DDR inhibition regimes during genotoxic treatments to achieve greater cytotoxic sensitivity as the ATM kinase can function both in survival as well as apoptotic pathways.

### *6.3.3 Dose dependent treatment of Doxorubicin with and without ATM inhibition revealed cytoprotective function of ATM at lower (100-250nM), while a role in apoptosis at higher (≥500nM) dose in HaCat cells.*

After the initial experiments discovered dual outcomes of ATM inhibition on cell survival during a time course genotoxic treatment regime, I next set out dose dependent experiments to manipulate ATM activity in order to establish treatment regimes that could enable targeted cellular sensitivity towards cancer cells, as opposed to their normal counter parts.

Since it was already established in sections 6.3.2 and 6.3.3 that ATM function caused cell survival during lower extent of DNA damage (at 100nM Dox and only at earlier time points at 400nM Dox), dose dependent Dox treatments ranging from a lower scale of 100nM Dox to 7000nM Dox were next performed for 12 hr of treatment to identify the point where ATM function switches to apoptotic mode in normal epithelial cell line (MCF10A).

Once this was established, same experiments were performed on MCF7 (cancer) cell line, data collected and then compared in order to determine differences in dose responses and cell survival.

Figure 6.19 demonstrated that MCF10 cells showed a dose dependent cell death after treatments with the indicated doses of Dox starting at the lowest dose of 100nM Dox (6.12% cell death). 50% cell death was achieved at 1000nM of Dox treatment. 74% of cells death was seen at the highest concentration of 7000nM after 12 hr of treatment. Interestingly, in the same figure, ATM inhibition was shown to result in opposing effects on cell survival in a dose dependent manner. While the addition of ATM inhibitor at 100 and 250 nM Dox resulted in greater sensitivity towards the genotoxic agent, and hence greater cell death, increasing the dosage to and above 500nM Dox strikingly resulted in reduced cell death in ATM inhibited state than ATM active state. This again demonstrated the switch in ATM signalling from cytoprotection to cytotoxicity between 250nM-500nM of Dox treatment for 12 hr in HaCat cells. For example, when ATM was inhibited, 50% cell death occurred at a relatively higher concentration of 5000nM Dox, as compared to 1000nM in ATM active state. These results recapitulated the effects of time series treatment of Dox (Fig. 6.10) whereby a lower damage supported ATM role in DNA repair and cell survival, while higher damage suggested its role in apoptotic induction where its inhibition caused a higher survival.

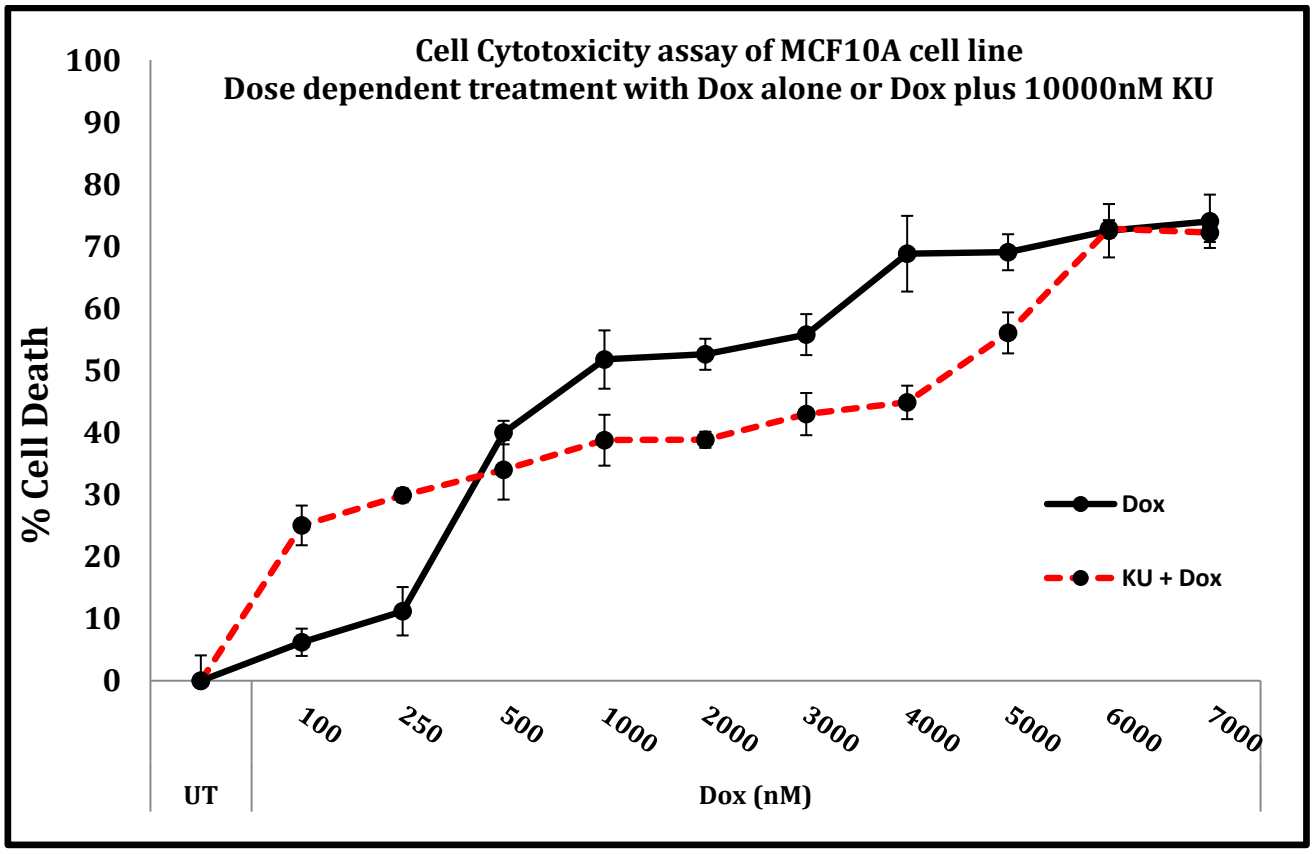


**Figure 6.19: NR-uptake based cell cytotoxicity assay during dose dependent treatment of 100nM-7000nM of Dox alone, or with the addition of 10µM ATM kinase inhibitor KU in MCF10 cell line.** MCF10 cells were seeded in 96-well plates at a density of 2.3 x $10^3$ cells per well. After 24 hr of incubation, cells were either left untreated or treated with 100nM-7000nM dose range of Dox alone or with the addition of 10µM KU for 12 hours. After treatments, cells were subjected to NR-uptake cell cytotoxicity assay as described in materials and methods for the determination of cell viability. Readings were taken in Modulus template® 96-well plate reader by measuring the absorbance at 540nm. Each value is based on means of the absorbance values acquired from quadruplet of treatments and normalized to the mean value of untreated control (UT) and expressed as % cell death with the formula 100 – [($Abs_{540}$ treated sample/$Abs_{540}$ untreated sample) × 100]. The data is based on three independent experiments.

To elucidate this dual ATM functionality in cancer cell line, MCF7 cells were subjected to dose treatment of Dox in the same manner as above. It was observed that MCF7 cell line was more sensitive to the genotoxic agent than MCF10A cell line at lower dosage of DNA damage, with 50% cell death occurring at 500nM Dox as opposed to 1000nM in MCF10A cell line (Fig. 6.20). Furthermore, at 1000nM Dox, MCF7 cell line showed almost 70% cell death. However, increasing the Dox dosage beyond 1000nM did not substantially cause further cell death as there was only an increase of around 7% cell death between 2000-7000nM Dox range. Interestingly, as was observed for MCF10A cell line, inhibition of ATM caused higher cell death only at lower doses of Dox treatment The increased sensitivity to Dox after ATM inhibition was only in the dosage range of 100-250nM, same as for MCF10A (Fig. 6.20). Increasing the dosage to and beyond 500nM resulted in ATM function to switch to apoptosis as KU addition during higher dose range reduced cell death as compared to Dox only treatment.

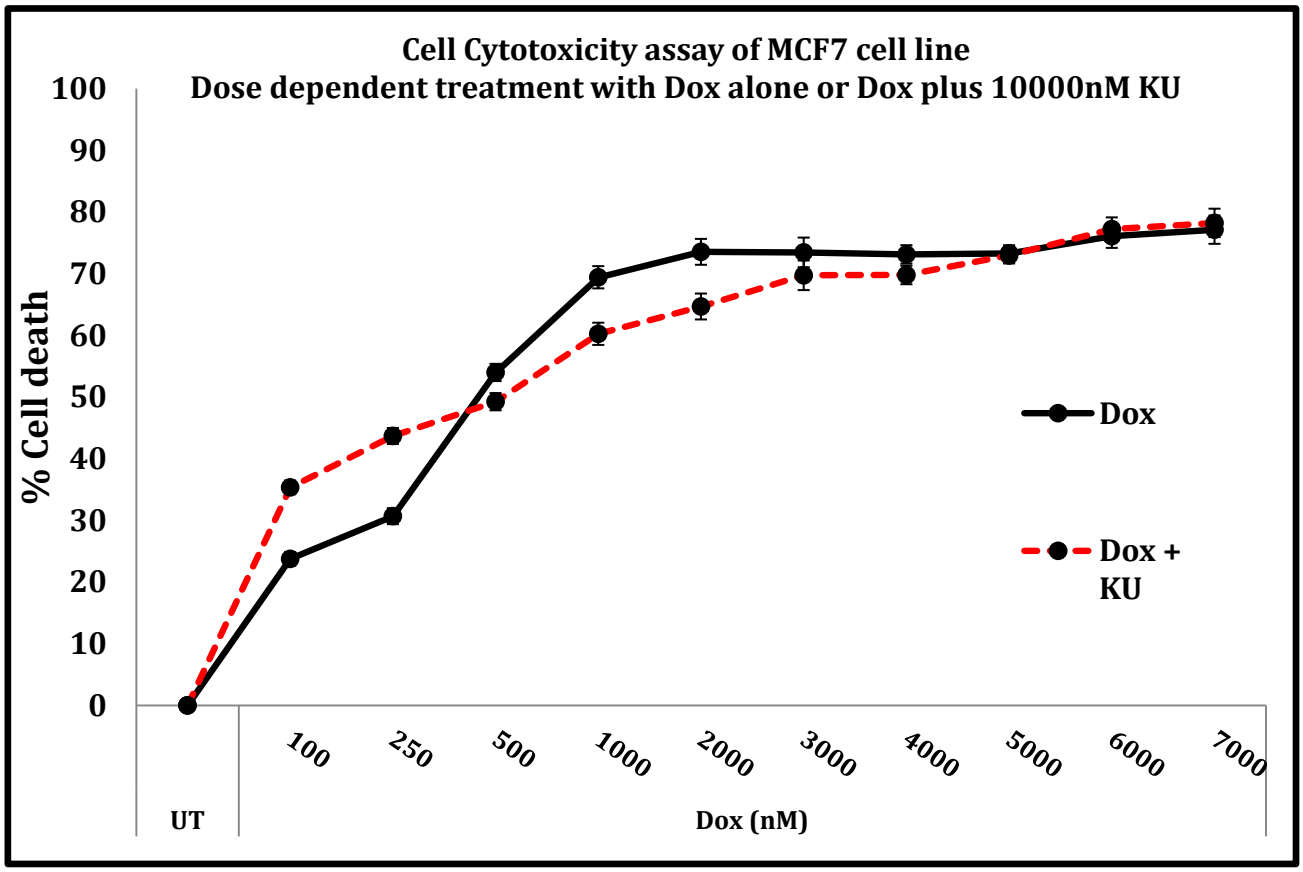


**Figure 6.20: NR-uptake based cell cytotoxicity assay during dose dependent treatment with Dox alone, or with the addition of 10µM ATM kinase inhibitor KU in MCF7 breast cancer cell line.** MCF7 cells were seeded in 96-well plates at a density of 2.3 x $10^3$ cells per well. After 24 hr of incubation, cells were either left untreated or treated with 100nM-7000nM dose range of Dox alone or with the addition of 10µM KU for 12 hours. After treatments, cells were subjected to NR-uptake cell cytotoxicity assay as described in materials and methods for the determination of cell viability. Readings were taken in Modulus template® 96-well plate reader by measuring the absorbance at 540nm. Each value is based on means of the absorbance values acquired from quadruplet of treatments and normalized to the mean value of untreated control (UT) and expressed as % cell death with the formula 100 – [($Abs_{540}$ treated sample/$Abs_{540}$ untreated sample) × 100]. The data is based on three independent experiments.

Figures 6.19 and 6.20 clearly demonstrated the different outcomes of combinatorial drug treatments on cell survival based on ATM activity. Taken together, these results in normal and cancer epithelial cell lines demonstrated an important observation that inhibition of DDR activity, via modulation of ATM activity during DNA damage could result in higher sensitivity only in a specific range of genotoxic treatment. Additionally, comparison of percent cell death between the normal and cancer cell lines tested showed differences in sensitivities towards Dox only at a lower dosage range where the cancer cell line was more sensitive (Fig. 6.19 & 6.20). Application of such treatment regimens to which cancer cells are more susceptible, as demonstrated, could help achieve targeted cellular sensitivity.

### *6.3.4. Differences in cell survival between normal and cancer cells during dose dependent genotoxic treatments were also accompanied by differences in kinetics of pATM induction.*

After demonstrating that the normal, MCF10 and cancer, MCF7 cell lines exhibited differences in cellular sensitivity towards Dox during dose dependent treatments, and that in both cases, status of ATM greatly influenced the survival outcome of cells, I next set up experiments to determine if these differences are also accompanied by underlying differences in the kinetics of activation of pATM. The cell lines were treated in the same manner as above and the relative induction of pATM, and hence of the DDR pathway during the treatment regimes especially where these cell lines exhibited greatest differences in survival (lower doses of Dox), was determined.

It was revealed that following treatments with similar doses of Dox, there were differences in the degree of pATM induction, and hence in the kinetics of activation of DDR, in MCF10 and MCF7 cell lines (Fig. 21).

Importantly, analysis of the % cell death and its correlation with the degree of pATM induction revealed that Dox dose range where MCF7 cells exhibited higher sensitivity showed lower induction of pATM than MCF10A, while dose range that induced similar cell death also showed similar pATM induction between the cell lines.

This was an important observation pointing towards the already attributed role of ATM induction in cell cycle arrest and hence survival at lower DNA damage. This would mean that failure of MCF7 cells to induce pATM activation to certain threshold at low dosages may have rendered it more sensitive to the genotoxic agent.

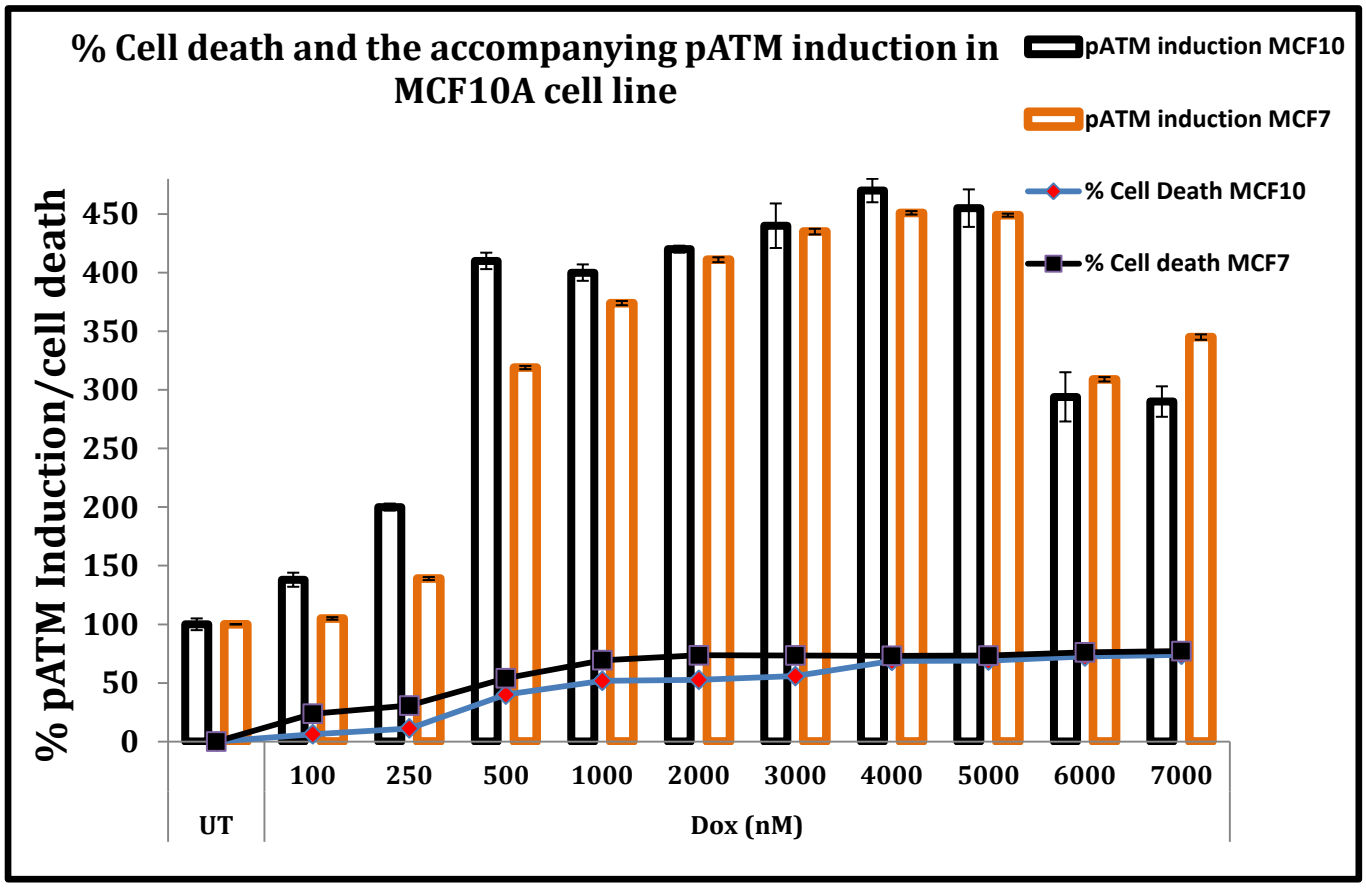
% Cell death and the accompanying pATM induction in MCF10A cell line
pATM induction MCF10
pATM induction MCF7
% Cell Death MCF10
% Cell death MCF7
% pATM Induction/cell death
450
400
350
300
250
200
150
100
50
0
UT
100
250
500
1000
2000
3000
4000
5000
6000
7000
Dox (nM)

**Figure 6.21: Comparative analysis of kinetics of pATM induction between normal and cancer cell line and its correlation with degree of cell death during dose dependent Dox treatment.** MCF10 or MCF7 cells were seeded in 96-well plates at a density of 2.5 x $10^3$ cells per well. After 24 hr of incubation, cells were either left untreated or treated with 100nM-7000nM dose range of Dox alone or with addition of 10μM KU for 12 hours. After treatments, cells were subjected to ELISA as described in materials and methods for the determination of pATM S-1981 induction using HRP conjugated secondary antibody and Amplex Red® detection system. Readings were taken in Modulus template® 96-well plate reader using excitation emission maxima of 570/585 nm. Each value is based on means of the fluorescence values acquired from quadruplet of treatments and normalized to the mean value of untreated control (UT) expressed as 100%. The data is based on three independent experiments. For comparative analysis, % cell death data from Fig. 6.19 and 6.20 Dox only treatments have been included.

Figure 6.21 suggested that intrinsic cellular differences in kinetics of activation of ATM after genotoxic agents could not only have an impact on cell survival and hence be a key determinant in cellular sensitivity towards genotoxic agents, but this difference could also be utilised to devise cancer cell specific treatment regimes. For example, a dosage range of 100-1000nM Dox for 12 hr evokes a higher pATM induction in normal cells making them more resistant to genotoxicity as compared to their cancerous counterparts and hence this dosage allows for cancer cell selectivity as opposed to dosage of ≥1000nM Dox.

## 6.4 Key findings and their significance

In this section of the current research work, the consequences of ATM inhibition on cell survival after different degrees of double stranded DNA damage in a normal cell lines (HaCat and MCF10A) and breast cancer cell line (MCF7) were evaluated. This was done to clearly illustrate its dual roles in cytoprotection and cytotoxicity. Further to this, cellular differences in sensitivities towards genotoxic treatments were determined and evaluated for their therapeutic potential. Outcomes of the of drug dose treatments with and without ATM function were first evaluated in terms responses generated in downstream signalling proteins involved in DNA repair signalling (BRCA1, γ-H2AX), cell cycle checkpoint kinases (Chk1, Chk2 and ATR), cell cycle regulatory protein (E2F1), and apoptosis signalling (P53). Next, the consequences of the generated responses on overall cell survival were examined in normal and cancer cell lines.

Figures 6.9, 6.10, 6.19 and 6.20 clearly reported the effects of combinatorial drug treatments on the survival of cells based on status of ATM activity, time of treatment and dose range. The variation in degrees of cell survival provided with different options of treatment regimens to achieve a desired degree of cell death as well as selectivity.

It was found that inhibition of ATM during 400nM Dox treatment resulted in greater cell death only at earlier time points of 2, 4 and 8 hr of treatment and lower cell death at further time points of 12, 16, 20 and 24 hr of treatment (as compared to Dox only treated cells) in HaCat cells. Similarly, both in normal and cancer epithelial cell lines, dose dependent treatment of Dox, ranging from 100nM-7μM for 12 hr, revealed that ATM inhibition resulted in greater cell death only at lower concentration range of 100-250nM Dox, as determined by cytotoxicity assays. At a higher concentration of ≥500nM Dox, ATM inhibition on the contrary, enhanced the survival rate as compared to only Dox treated cells.

Taken together, these data indicated a role of ATM in modulating both cell survival and apoptosis and that this decision was based on the scale of DNA damage. From these results, it could be concluded that at earlier time points or at lower scale of DNA damage, ATM function ensured cell survival by causing cell cycle arrest and DNA repair, while at later time points or higher scale of DNA damage, ATM mediated cell death as inhibition of its function caused higher survival, hence making it ineffective strategy to sensitise cells at this particular state of DNA damage in these cell lines.

These experiments not only established significant features of ATM functioning in time as well as dosage dependent genotoxic treatments but also uncovered the underlying DDR pathway, brought about my other kinases and DDR substrates in the signalling network. Furthermore, these experiments generated valuable quantitative estimations of protein activities implicated in DDR pathway under different conditions. The changes in the relative abundance of different proteins, expressed as semi quantitative numerals, provided valuable data for the design, calibration and parameterization of deterministic mathematical model for DDR pathway. The kinetic parameters established were also correlated with the degree of cell survival after treatments in order to ascertain the functional consequences of the induced pathways.

These data sets were then passed on to the mathematical modellers along with a thorough explanation of the underlying biology and signalling networks to develop a dynamic and visualization based network model.

I set out the following objectives for successful development of non-linear half-system based *in-silico* mathematical model of the DDR signalling network:

i) To predict or project activation kinetics of ATM and its substrates at later time points based on the initial activation kinetics of first four data points at a given scale of DNA damage.

ii) To predict activation kinetics of ATM at a higher scale of damage, based on the predictions made with (i).

iii) To develop a dynamic network topology with ATM at the nodal point at each of the data point with signalling links to all the other proteins in a given scale of DNA damage.

iv) To carryout *in silico* prediction of effects of ATM inhibition on the network topology model created in (iii).

v) To form a correlation between a given state of network kinetics of all the proteins analysed at a particular data point of a given treatment, with the degree of survival or cell death.

vi) Based on the correlation obtained from (v), to predict time of treatment required, or dose of treatment required to achieve a desired state of network kinetics which would in turn determine the degree of cell death at that state.

vii) Based on (vi), to determine differences in state of network kinetics, and hence of degree of cell death, between different cell lines (cancer and normal) at particular treatment regimes which would finally enable researchers to achieve targeted cellular sensitivity.

# Chapter Seven

# Discussion and Conclusion

Today we have discovered the secret of life!

Francis Crick, Molecular biologist (1916 – 2004)

## 7.1 Discussion

The current research work was carried out to further our knowledge of functional regulation, mechanism of activation and trafficking of ATM kinase in different conditions and cell lines specifically, and gaining an overall understanding of how activated ATM initiates DDR pathway in general. The latter was done by examining the phospho-induction, stabilisation, co-localisation and trafficking of functional partners and substrates of ATM during ATM signalling. Subsequently, key discoveries made in these domains were further elaborated and transformed into the generation of valuable biotechnological tools for application in cell based kinase assays and data generation for a prospective predictive mathematical modelling of complex signalling network with ATM at its nodal point. This research work not only unveiled novel spatio-temporal autoregulatory mechanisms of ATM functioning but also aided tremendously in our general understanding of the complex signalling network that comprises DDR signalling pathway surrounding the ATM. This research also highlighted the intricate nature of these responses and the need to acquire full elucidation of pathways surrounding and emerging from ATM before a successful intervention could be conceptualized and then actualized to achieve therapeutic goals in cancer biology.

### 7.1.2 Cell cycle dependent ATM expression, activity and localisation: Responses generated by DSB inducing agents and ATM kinase inhibition and its impact on DDR signalling pathway in normal Human epithelial cell line.

This section of study reported on ATM regulation and its sub cellular localisation upon serum stimulation and in early phases of cell cycle, and the effects of this regulation on its immediate substrates during cell cycle.

Furthermore, the kinase activation of ATM upon different extents of DNA damage through radiomimetic drugs, and its effects on phospho-induction and consequences for subsequent localisation of downstream signalling molecules in a time dependant manner were also examined. These experiments were performed in human epithelial cell line, MCF10A that helped elucidate how ATM orchestrates signalling cascades that first elicit DDR pathway and then modulate it.

There are mixed reports of the effects of different growth hormones on the expression and activity levels of ATM. While Gueven N et al., in 2001 demonstrated that epidermal growth factor downregulated ATM expression at the transcriptional level, Fukao T et al., (1999) had earlier shown that ATM is up regulated during mitogenic response in peripheral blood mononuclear cells. On the other hand, treatment with Insulin was reported to upregulate ATM kinase activity that stimulated cell cycle progression and proliferation via PKB signalling pathway (Halaby MJ et al., 2008, Yang DQ et al., 2000). I found out that addition of foetal bovine serum not only stimulated ATM protein levels by 3 fold, but the activity of ATM (as determined by pATM levels, which is its own substrate) was also enhanced by >2 fold. The consequences of this enhanced expression and activity levels after serum stimulation may reach its downstream substrates as, at the same time point, upregulation of E2F1 and pChk2 levels were also seen (Fig. 3.2).

Previous reports have also shown that the activity of ATM is regulated both in cell cycle dependent (Jazayeri A et al., 2006) as well as independent manner (Golding SE et al., 2004). These reports demonstrated that ATM showed a variable dependence on cell cycle in terms of signalling to its downstream substrates.

Experiments performed on $G_1$ synchronized MCF10A epithelial cell line showed that release of these cells into cell cycle after serum stimulation cause total ATM levels to undergo slight changes during cell cycle progression at particular time points, but mostly remained constant. It could be argued that these slight changes in total ATM have an impact on constitutively active DNA repair pathway as these changes were accompanied by alteration in ATM activity as well. Most notably, cell cycle progression after serum stimulation in MCF10A cells resulted in upregulation of both ATM and pATM post 2 hr, apart from the initial induction and incurred a decrease at 8 hr time point post serum addition. This induction at specific time points, which interestingly also coincided with induction of E2F1 and pChk2 indicated cell cycle progression, where an upregulation of E2F1 (~4 hrs after serum addition) was previously reported to be associated with reduction in cyclin D levels through G1/S transition (Watanabe G et al., 1998).

pP53 levels in undamaged cells exhibited same pattern of induction. However, an exception was that serum stimulation of G1 quiescent cells resulted in downregulation of both total P53 and its phosphorylated form at 0.5 hr post treatment. This was consistent with previous studies reporting P53 function during cellular quiescence and temporary arrest (Itahana K et al., 2002).

Under DNA damaging conditions of 0.5μM Dox, while levels of total ATM were almost unaltered, upregulation of the phospho forms of ATM, P53, E2F1 and Chk2 was seen, demonstrating a functional DDR pathway in this cell line.

While initial induction as soon as 30 minutes after damage was observed for pATM and all its substrates, maximum induction, comparing with the previous time point, was observed at 2 hr after which, a continued upregulation was seen up until 8 hr of drug treatment.

Previous reports have demonstrated both doxorubicin induced cell cycle arrest as well as apoptosis (Gajewski E et al., 2007). The time dependent pATM induction seen in Fig. 3.3a & b may indicate that the earlier lower induction (prior to 2 hr time point) may result in an initial cell cycle arrest after Dox treatment while the later higher induction (2 hr and post 2 hr induction) may be as a result of switch to apoptosis. The fact that E2F1, which in lower and repairable states of DNA damage undergoes Rb induced block (Helen K et al., 1993) while at unrepairable state is up regulated and promotes apoptosis (Lin WC et al., 2001, Rogoff HA et al., 2004), is also up regulated post 2 hr of 0.5μM Dox treatment also supports the switch to apoptosis in these cells.

In terms of localisation, very distinct peri nuclear ATM was detected in serum starved cells and in the early time points post serum stimulation. The same was observed for pATM as well. However, DNA damage caused disappearance of these from the extra nuclear region. While this section of ATM research was more focussed on regulation of ATM protein and ATM dependent sub cellular induction of DDR substrates in cell cycle and DNA damage settings, in terms of its localisation and trafficking, a more in-depth study was undertaken in chapter Six that not only revealed the identity of this distinct perinuclear localisation but also proposed its function (Section 7.3).

ATM inhibition via the use of specific small molecular inhibitor of ATM, not only totally disrupted induction of pATM after 0.5μM Dox treatment, but also of ATM substrates pP53 and pChk2, most notably at and post 2hr of treatment. These results demonstrated the prime requirement of ATM signalling in DDR induction following double stranded DNA damage at least after Dox treatment for up to 8 hr in MCF10A cell line.

It was demonstrated that the DDR mechanism for DNA damaging agents other than doxorubicin was not completely dependent on ATM signalling. For these experiments, induction of phosphorylated P53 at serine 15 was used as a measure of DDR activation. First of all, the kinetics of pP53 induction were determined after treatments with Bleomycin, Hydroxyurea and Cisplatin in a time dependent manner. Second, the effects of ATM inhibition were examined on the above kinetics (Fig. 9). These experiments established that while addition of ATM inhibitor along with these drugs altered the kinetics of pP53 induction, it did not fully disrupt this induction. Furthermore, while sensitivity of pP53 induction to ATM inhibition was to different extents for each of these drugs, the most affected time points were 1 and 1.5 hr of treatment. However, in each case, the pP53 levels at 2 hr of treatment with the genotoxic drugs in the ATM inhibited state were almost comparable to those in the drugs without ATM inhibitor treatment. One explanation for this earlier sensitivity of pP53 induction to ATM inhibition could be greater dependence on ATM signalling early in the damage followed by the activation of other DDR kinases with overlapping function with ATM for phosphorylation of pP53 at higher scale damage. Another possibility could be that the activation of other DDR kinases was an emergency response as a result of ATM inhibition. The fact that pP53 levels following Bleomycin treatment were higher when ATM was inhibited than without inhibition supports the second possibility (Fig. 3.9b).

Hydroxyurea induced pP53 activation seemed to be the least affected with KU inhibition consistent with previous reports stating ATR dependence for DDR after Hydroxyurea or UV treatments (Turchi JJ et al., 1996). In case of Cisplatin treatment, while DNA-PK activity might not be required, ATR is reported to be activated (Nakayama Y et al., 2009). Bleomycin induced pP53 may be as a result of either ATR and/or DNA-PK activity (Chen BP et al., 2005).

### 7.1.2 Inhibition of ATM kinase causes transient induction of its transcription and increase in its activity via a novel autoregulatory mechanism.

In this section of research work, I discovered a novel mode of ATM regulation, which involved an autoregulatory mechanism governed at the transcriptional level that also influenced the phosphorylated levels of ATM protein with the effects reaching up to other ATM substrates in the DDR signalling pathway. There had been a number of previous speculations about regulation of ATM. It was originally described as a constitutively expressed gene, regulated only post translationally via autophosphorylation and dimer to monomer transition with no appreciable change in the actual levels of the protein (Bakkenist MB et al., 2003, Kobayashi J et al., 2009). Previous reports have also described the expression levels and sub cellular distribution of total ATM before and after damage to be almost unaffected (Gately DP et al., 1998, Brown KD et al., 1997). However, there are contrary reports demonstrating ATM induction after damage or during mitogenic response (Fukao T et al., 1999, Hirai Y et al., 2001), reduction after treatments with growth hormones (Gueven N et al., 2001) while some studies also reported the possibility of ATM to be regulated at the transcriptional level (Clyde RG et al., 2009, Gueven N et al., 2003, & 2006, Khalil HS et al., 2011 & 2012).

In this section of my research, I found out that inhibition of ATM kinase activity by small molecular inhibitor, KU resulted in an induction followed by oscillation of total ATM protein levels. Furthermore, through protein stability experiments and promoter characterisation, it was confirmed that this regulation was governed at the transcriptional level. The initial induction was indicative of an autoregulatory mode of ATM regulation providing a negative feed-back loop independent of cell cycle.

A possibility exists that the observed upregulation of luciferase activity in Fig. 4.11 may have resulted from increased stabilisation of luciferase protein caused by KU treatment. While this could be determined by employing a different constitutively active promoter for luciferase assay, the increased induction of ATM at protein level as well (Fig. 4.1) supports that this upregulation of Luc signal is not caused by Luciferase protein stabilisation and takes place via promoter regulation.

From these results, it could be hypothesised that equilibrium may exist between ATM activity and amount of ATM expressed and that ATM enzymatic activity may monitor its own expression levels under normal conditions. With the addition of KU, this equilibrium would be disturbed, resulting in oscillation, as observed in this study.

Interestingly, the rise in ATM levels at 0.5 hr post KU treatment also resulted in a rise in pATM levels which may suggest that the up regulated fraction of ATM is kinase active. This result is explained by the fact that the kinase inhibitor, KU used in this study is a reversible small molecular inhibitor which binds to the ATP binding pocket of ATM, blocking its kinase function. At 10μM KU concentration, most of the pre-existing ATM molecules are blocked and stop signalling. However, any *de novo* synthesis of ATM protein e.g. at 0.5 hr KU induction, would be in a free state and may exceed the number of KU molecules in the cell, and restore its role in DDR signalling.

Therefore, the kinase inhibition-induced up regulated fraction of ATM may be free from KU, and therefore functional, and be able to induce a temporary DDR by activating its substrates. This hypothesis was tested by looking at the levels of pATM and other ATM substrates.

E2F1 and P53, which are known to regulate ATM transcription by directly binding to its promoter (Craig AI et al., 2010, Berkovich E et al., 2003) and ATR, that was previously demonstrated to have a functional link with ATM (Stiff T et al., 2006, Jazayeri A et al., 2006) showed transient induction after treatment with KU in a cell cycle independent manner.

In terms of ATR activity, a previous study has shown its dependence on ATM in a cell cycle dependent manner (Jazayeri A et al., 2006). However, here we show a cell cycle independent upregulation upon ATM kinase inhibition, which may be a different mechanism of dependence on ATM. This may imply an important scenario where any higher concentration of KU, sufficient to inhibit all the transiently up regulated molecules of ATM kinase may still not completely prevent a downstream DDR signal because of pATR induction. The fact that this novel ATM auto regulation points towards a negative feedback loop between its activity and expression is also supported by the observation that the activation of ATM kinase after DNA damage caused a reduction in the total ATM levels at 0.5 hr post treatment (Fig. 3.3a & b).

E2F1, which can directly bind the ATM promoter and up-regulate it (Berkovich E et al., 2003) and P53, known to be a negative regulator of ATM (Craig AL et al., 2010), may participate in this ATM autoregulation in the following manner:

Firstly, KU-induced ATM inhibition will cause deactivation of P53's transcriptional ability (Turenne GA et al., 2007) and decreased constitutive P53 activity. This will be followed by a reduction in the CIP/KIP family P21 and P27, which otherwise mediate the RB induced check

on E2F1 transcriptional activities (el-Deiry WS et al., 1993). As a result, ATM induction following inhibition of its kinase activity will occur via two mechanisms.

One is the deactivation of P53, which is otherwise a negative regulator of ATM and the second is the release of E2F1, which is known to up regulate ATM.

On the other hand, increased E2F1 accumulation above a certain level itself can cause P53 activation at the protein level (Zhu JW et al., 1999) or transcriptionally by binding to the P53 promoter (Choi M et al., 2002). The upregulation of P53, a transcriptional repressor of ATM may explain the reason for the reduction in initial ATM induction post 0.5 hr. Hence, ATM may maintain a balance between its expression and activity by modulating E2F1 and P53 function under normal conditions, which might be disturbed by inhibiting its kinase activity. This proposed mechanism is illustrated in Figure 7.1. While this could be a possible explanation, further insights into this mechanism could be provided by studying this phenomenon in P53 or E2F1 null cell lines.

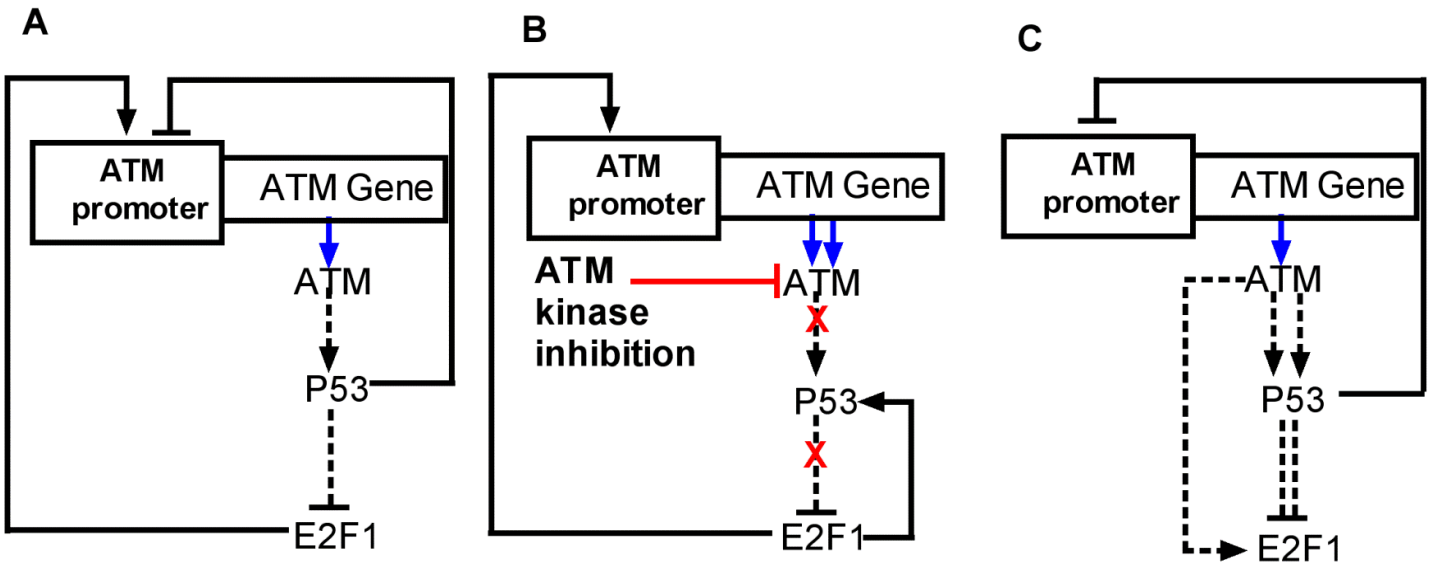
A
ATM promoter
ATM Gene
ATM
P53
E2F1
B
ATM promoter
ATM Gene
ATM kinase inhibition
ATM
P53
E2F1
C
ATM promoter
ATM Gene
ATM
P53
E2F1

**Figure 7.1: Proposed scheme of ATM regulation under normal, DNA damage or Kinase inhibited states.** Lines with arrow heads indicate transcriptional up regulation while lines with bars indicate transcriptional repression. Red line with bar head indicates Kinase inhibition via KU. Blue lines with arrowhead indicate translation. Dotted lines with arrowheads indicate phosphorylational activation while dotted lines with bar heads indicate inactivation. Dotted lines with arrows or bar heads with "X" denote disruption of that signal while two arrows or two bar headed lines indicate enhancement of that signal **(A)** Under normal (undamaged) state, stable constitutive ATM expression is maintained by the activities of P53 and E2F1 transcription factors, which repress or induce ATM expression respectively. **(B)** Under ATM kinase inhibition, the ATM stops signalling to P53, which loses its transcriptional potential and thus ATM is released from the transcriptional repression of P53. Also, decreased P53 stability no longer keeps the ATM transcription activator, E2F1 in the RB-check, which will bind to ATM promoter and induce ATM expression, evident after KU mediated ATM kinase inhibition. **(C)** Under DNA damage condition, ATM kinase is activated, which rapidly stabilizes P53 which in turn will not only cause E2F1 block via the Rb pathway, thus preventing E2F1 binding to ATM promoter, but also bind directly to ATM promoter and repress it, as evident in the Dox mediated down regulation of ATM. State B and C are both temporary and will ultimately restore to normal state A, as excess E2F1 as in state B, itself is a positive regulator of P53 which will balance the system back to state A, while excess damage in state C can cause ATM to phosphorylate and stabilize E2F1, which will abrogate the ATM repression by P53 and hence bring the pathway back to state A.

Involvement of DDR kinase in its negative autoregulation via P53 has also been described earlier for Chk1 (Gottifredi V et al., 2001). It would be interesting to see if Chk1 levels upon its kinase inhibition are similarly up regulated and if this causes a change in activities of its interacting proteins.

To find the origin of this autoregulation, I blocked protein synthesis with cycloheximide (CHX) treatment and left cells untreated or exposed to KU or Dox. This abrogated the KU induced oscillation, suggesting a regulation at transcriptional machinery.

The ATMpr/PGL3 and ATMpr/Ptimer-1 confirmed KU induced upregulation of the promoter activity and this upregulation likewise was followed by oscillatory signals.

The discovery of this novel autoregulation of ATM was employed to generate novel reporter assays for screening ATM kinase inhibitors as well as detecting ATM kinase activation. The induction of ATM promoter signal, which occurs at a precise time point, could be used to report ATM kinase inhibition. On the other hand, the slight down regulation of ATM following its activation can be reported through these reporters and hence be employed as detectors of DNA damage within the cells, as early as after 15 min of genotoxic insult (Fig. 4.11). The Response of ATMpr constructs to KU treatment in various transfected cell lines (data not shown) has shown a similar induction of the promoter signal upon ATM kinase inhibition. These results implicate the use of ATMpr as a valuable reporter tool.

### 7.1.3 A novel autoregulatory trafficking mechanism of ATM involves β-COPI mediated Golgi to nuclear transport of pATM S-1981 during initiation of DDR signalling.

In this part of the current research, novel and important findings of ATM translocation and localisation were determined which add to the complexity and give another dimension to the mechanisms via which regulation of ATM activity is brought about.

It was found that ATM and pATM are localized at a perinuclear region in untreated immortalized human keratinocytes in addition to their nuclear localisation. While ATM was found to be more spread out in the cytoplasm, pATM was restricted to the perinuclear region, which was later identified as Golgi apparatus. The cytoplasmic ATM appeared to form distinct puncta. The appearance of cytoplasmic puncta may denote ATM localisation in vesicular structures. Indeed, ATM has previously been found to exist in cytoplasmic vesicles (Watters D et al., 1997, Lim DS et al., 1998, Kuljis RO et al., 1999, Watters D et al., 1999).

While the perinuclear pATM was found to be localized in Golgi apparatus, double stranded DNA damage caused a rapid pATM export from Golgi, evident at 0.5 hr of 0.5μM Dox treatment with an accompanying increase in the nuclear pATM. It was also established that DNA damage induced Golgi exit of pATM required active ATM kinase as exposure to specific inhibitor of ATM kinase, 10μM KU, resulted in persistent Golgi retention of pATM even after DNA damage for up to 4 hr. This new insight of ATM trafficking mechanism established novel role of ATM in its autoregulation via the modulation of its trafficking mechanism. This yet another autoregulatory mechanism of ATM regulation can provide for additional means by which ATM activity could be controlled.

This study used HaCat cell line, an immortalized human skin cell line. The choice of this cell line was based on the fact that the DDR pathway in skin cell line may behave slightly different owing to its constant exposure to genotoxic agents.

Therefore, this increased environmental susceptibility was expected to result in distinct localisation or trafficking behaviour of ATM, identification of which was the aim of the current study.

Interestingly, these new findings of pATM localisation were not restricted to HaCat cell line and were demonstrated in breast cancer cell lines as well. While pATM did not show co-localisation with mitochondria in any of the conditions tested, (Fig. 4, Fig. 8), mitochondria did show DNA damage induced structural changes both in the presence and absence of KU. These discrete structural changes in mitochondria could be as a result of stress response. While exact mechanisms of DNA damage induced protein trafficking at the mitochondrial membrane are largely unknown, a number of proteins are known to traffic to mitochondria upon DNA damage induced by both IR and genotoxic chemicals (Marchenko ND et al., 2000, Essmann F et al., 2005, Kharbanda S et al., 2000, Tong T et al., 2005).

The finding of pATM localisation in Golgi apparatus could be explained in the following way. The Golgi resident pATM may provide for storage of already monomerized and thus activated ATM molecules. Upon DNA damage, these already constitutively active molecules may rapidly undergo nuclear translocation and induce DDR pathway. This would avoid the delay of dimer to monomer transition during emergency situation of DNA damage. Secondly, extra nuclear storage of pATM may also be explained by the fact that such sequestration of activated ATM from the nucleus would prevent its interaction with DDR substrates and thus unnecessary induction of DDR.

Another interesting and important hypothesis for the function of Golgi resident pATM and checkpoint kinases is that of apoptosis regulation. Caspases (Cysteine dependent Aspartate specific proteases) are important cellular proteases that carryout proteolytic cleavage of cellular substrates, a hallmark of apoptotic cell death (Krumschnabel G et al., 2008). Caspase 2 is the only protease in the caspase family that is known to co-localize in the Golgi apparatus (Mancini M et al., 2000). Interestingly, it has been reported that Chk1 protein inhibits caspase 2 apoptotic function in ATM/ATR dependent manner (Sidi S et al., 2008). Hence, under undamaged conditions of DNA, the Golgi resident pATM, pChk1 and pATR may keep Golgi localized caspase 2 function in check to prevent unwanted apoptotic induction, while Golgi exit of these kinases following DNA damage may partly activate apoptotic pathway via loss of caspase 2 inhibition at Golgi apparatus.

Alternatively, the disappearance of pATM from Golgi apparatus after damage may just be because of dephosphorylation of pATM without actual translocation to the nucleus. However, this is unlikely for two reasons:

Firstly, DNA damage also caused redistribution of total ATM from the perinuclear region, in addition to pATM (Fig. 5.1), hence it is not a merely a dephosphorylation event. Secondly, dephosphorylation of pATM upon DNA damage is altogether highly unlikely, especially earlier after DNA damage (0.5 hr post damage).

Another novel finding in the current part of research was that Golgi resident pATM also co-localized with β-COPI and that inhibition of ATM kinase disrupted this co-localisation. The likely hood of involvement of β-COPI coatomer protein in ATM trafficking events was based on the following observations:

1. Firstly, COPI is the major coatomer protein responsible for retrograde transport of proteins from Golgi membrane to other parts of cell, an event observed for pATM.

2. Secondly, the presence of a di-Lysine motif in ATM, which is recognition sequence for all COPI mediated transport from Golgi, and which was previously reported to be important for nuclear retention of ATM (Young DB et al., 2005).

3. β-COPI protein has significant sequence homology with β-Adaptin (Pairwise alignment shown in Fig. 7.2), which is a component of the AP-2 adaptor complex, and was previously reported to be recognized by, and bind to ATM in cytoplasmic vesicles (Lim DS et al., 1998).

4. and finally analysis of β-COPI amino acid sequence revealed three distinct ATM recognizable SQ and three TQ phosphorylational motifs (Fig. 7.3) further suggesting strongly its interaction with ATM.

The presence of multiple SQ motifs in β-COPI, the di-Lysine motif in ATM and the fact that ATM kinase inhibition disrupts its co-localisation with β-COPI, all support the likelihood of a functional link between the two. Based on the experimentation and observation in Figures 5.26-5.28, and 5.32, it could be hypothesised that in untreated state, both the constitutively phosphorylated ATM and β-COPI are present in the Golgi. Upon DNA damage, full activation of ATM kinase caused by dimer to monomer transition occurs. This results in two events. First is the full exposure of the 387-388 di-Lysine recognition motif of ATM and second is the enhanced ATM kinase activity towards β-COPI via the recognition of SQ motifs in β-COPI sequence.

The latter event may increase the functional interaction between the two leading β-COPI to recognize and bind the di-Lysine motif of ATM and trigger its transport away from Golgi into the nucleus upon DNA damage, where a subsequent rise in pATM accumulation was seen.

Since phospho specific β-COPI antibodies at these SQ motifs are not commercially available, the phosphorylation event could not be determined. However, both the inhibition of ATM kinase and the disruption of the di-Lysine motif within ATM were shown to cause retention of pATM in Golgi apparatus.

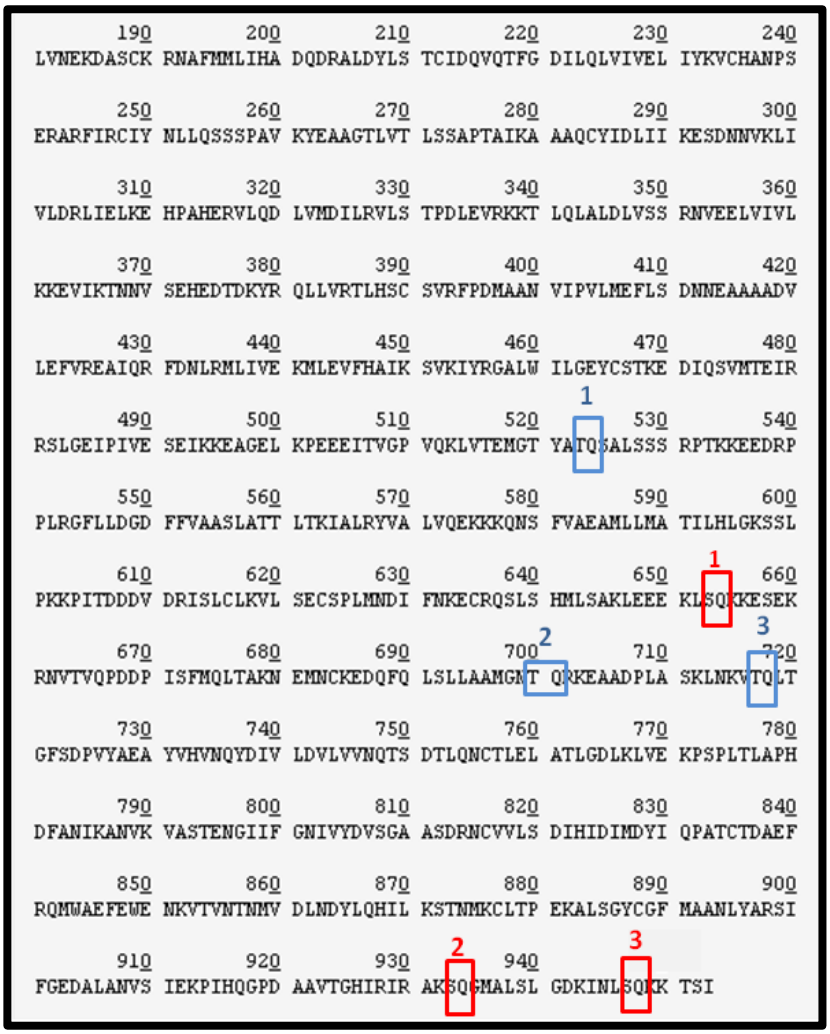


**Figure 7.2: ATM recognizable SQ and TQ motifs in β-COPI protein sequence.** Protein sequence of human β-COPI was retrieved from Uniprot protein information resource (http://www.uniprot.org/) and analysed for the presence of SQ motifs as indicated by red squares and TQ motifs indicated in blue squares.

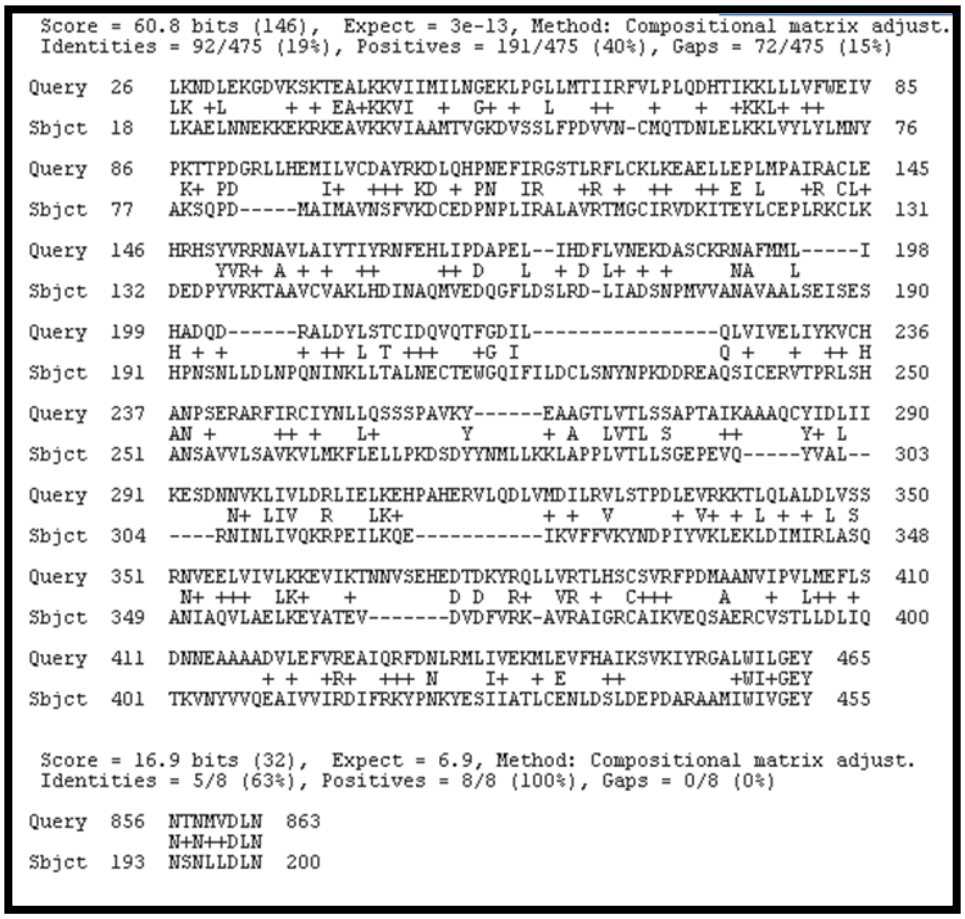

```
 Score = 60.8 bits (146),  Expect = 3e-13, Method: Compositional matrix adjust.
 Identities = 92/475 (19%), Positives = 191/475 (40%), Gaps = 72/475 (15%)

Query  26   LKNDLEKGDVKSKTEALKKVIIMILNGEKLPGLLMTIIRFVLPLQDHTIKKLLLVFWEIV  85
            LK +L     + + EA+KKVI  +  G+ +  L   ++   +   +  +KKL+ ++
Sbjct  18   LKAELNNEKKEKRKEAVKKVIAAMTVGKDVSSLFPDVVN-CMQTDNLELKKLVYLYLMNY  76

Query  86   PKTTPDGRLLHEMILVCDAYRKDLQHPNEFIRGSTLRFLCKLKEAELLEPLMPAIRACLE  145
             K+ PD       I+  +++ KD + PN  IR   +R +  ++  ++ E L   +R CL+
Sbjct  77   AKSQPD-----MAIMAVNSFVKDCEDPNPLIRALAVRTMGCIRVDKITEYLCEPLRKCLK  131

Query  146  HRHSYVRRNAVLAIYTIYRNFEHLIPDAPEL--IHDFLVNEKDASCKRNAFMML-----I  198
                YVR+ A + +  ++     ++ D   L  + D L+ + +     NA   L
Sbjct  132  DEDPYVRKTAAVCVAKLHDINAQMVEDQGFLDSLRD-LIADSNPMVVANAVAALSEISES  190

Query  199  HADQD------RALDYLSTCIDQVQTFGDIL----------------QLVIVELIYKVCH  236
            H + +      + ++ L T +++   +G I                  Q +   +  ++ H
Sbjct  191  HPNSNLLDLNPQNINKLLTALNECTEWGQIFILDCLSNYNPKDDREAQSICERVTPRLSH  250

Query  237  ANPSERARFIRCIYNLLQSSSPAVKY------EAAGTLVTLSSAPTAIKAAAQCYIDLII  290
            AN +     ++ +   L+       Y      + A  LVTL S    ++     Y+ L
Sbjct  251  ANSAVVLSAVKVLMKFLELLPKDSDYYNMLLKKLAPPLVTLLSGEPEVQ-----YVAL--  303

Query  291  KESDNNVKLIVLDRLIELKEHPAHERVLQDLVMDILRVLSTPDLEVRKKTLQLALDLVSS  350
                 N+ LIV  R   LK+            + +  V     + V+ + L + + L S
Sbjct  304  ----RNINLIVQKRPEILKQE-----------IKVFFVKYNDPIYVKLEKLDIMIRLASQ  348

Query  351  RNVEELVIVLKKEVIKTNNVSEHEDTDKYRQLLVRTLHSCSVRFPDMAANVIPVLMEFLS  410
             N+ +++  LK+   +        D D  R+  VR +  C+++    A   +  L++ +
Sbjct  349  ANIAQVLAELKEYATEV-------DVDFVRK-AVRAIGRCAIKVEQSAERCVSTLLDLIQ  400

Query  411  DNNEAAAADVLEFVREAIQRFDNLRMLIVEKMLEVFHAIKSVKIYRGALWILGEY  465
                + +  +R+  +++ N    I+  + E   ++          +WI+GEY
Sbjct  401  TKVNYVVQEAIVVIRDIFRKYPNKYESIIATLCENLDSLDEPDARAAMIWIVGEY  455


 Score = 16.9 bits (32),  Expect = 6.9, Method: Compositional matrix adjust.
 Identities = 5/8 (63%), Positives = 8/8 (100%), Gaps = 0/8 (0%)

Query  856  NTNMVDLN  863
            N+N++DLN
Sbjct  193  NSNLLDLN  200
```

**Figure 7.3: Demonstration of sequence homology between β-COPI and β-Adaptin through pair-wise sequence alignment.** Protein sequences for β-COPI and β-Adaptin were retrieved from Uniprot protein data resource (http://www.uniprot.org/) and their FASTA formats were subjected to EMBL-EBI pair-wise protein sequence alignment (http://www.ebi.ac.uk/Tools/psa/).

The novel insights of ATM trafficking gained from this part of research opens up the possibility of devising therapeutic strategies that modulate ATM activity via the interference in its transport machinery to gain cellular sensitivity to genotoxic agents. Since in addition to pATM, other DDR kinases pATR, pChk1 and pChk2 were also shown to undergo DNA damage dependent Golgi export, such inhibition of transport machinery could prove to be an effective strategy.

### 7.1.4 Elucidation of the role of ATM signalling pathway in cytotoxicity and apoptosis and generation of time series data for parameterization of mathematical model for *in silico* prediction of ATM signalling.

Research in this part of the thesis was conducted to meet two main objectives. One was to characterise and clearly demonstrate and distinguish the role of ATM in either cytoprotection via DNA repair and cell cycle arrest or in the induction of cytotoxicity via cell death and apoptosis through time courses and dose dependent treatments of genotoxic agent. The second and more general objective was to elucidate the underlying DDR signalling pathway leading to the observed cellular fates (comparisons of degree of survival) and generate highly consistent semi quantitative data of DDR signal transduction pathway with high degree of temporal resolution. These kinetic determinations were aimed to be utilised in a systems biology approach for parameterization of prospective mathematical modelling of ATM signalling pathway both while playing a cytoprotective role and in triggering apoptosis. This could help the biologist in predicting the role of ATM in a given treatment regimen for a specific cell line.

Previous mathematical modelling attempts have shown that the design and construction of a deterministic mathematical model of the molecular interactions that underpin the DDR require new kind of time series quantitative data (Prof. Jim Bown UAD, personal communication). This data must be consistent, have high temporal resolution and spatial consideration and provide the kinetic parameters of larger number of different proteins involved in a single pathway. While qualitative data are easily available, quantitative data pertaining to key signalling molecules that would allow speedy calibrations and provide kinetic parameters for the construction of mathematical model is scarce.

Over the years, a tremendous progress has been in producing qualitative signalling data that provide for the explanation for different cellular events. In terms of therapeutic intervention of such pathways, a mere descriptive knowledge is not enough. The decision making property of these pathways may involve oscillations and concentration thresholds that require a quantitative approach, calculations and numeral analysis for data collection and interpretation. Once such time series data is available for use in mathematical logic, they can not only shed light on the mechanism of functioning of these vital cellular pathways but could also be predictive in nature in terms of outcomes of interventions.

In an attempt to better understand the complex signalling network surrounding ATM, to find correlations between substrate preference of ATM and its impact on cell survival following drug interventions, and to interpret these signalling networks in the form of concentration thresholds and numerals, relative quantitative estimations were carried out of ATM and its substrates, and NR-uptake based cell cytotoxicity assays were performed following different treatments to evaluate relative cell death. Substrates analysed were those involved in DNA repair signalling (BRCA1, γ-H2AX), cell cycle checkpoint kinases (Chk1, Chk2 and ATR), cell cycle regulatory protein (E2F1), and apoptosis signalling (P53).

Doxorubicin treatments were performed in time courses as well as in a dose dependent manner. As a starting point, the concentration dose of 100nM Dox for time course was based on the fact that this is a clinically achievable concentration which is currently employed in chemotherapy for cancer patients. Since some of these cancer patients develop secondary malignancies in otherwise normal tissues after Dox treatments owing to extensive DNA damage (Gajewski E et al., 2007), I was interested to perform DDR profiling in normal cells exposed to 100nM Dox, to elucidate the underlying signalling responses generated in such cells and also assay for cell death.

Important discoveries in chapter six and those in previous chapters provided information about oscillation, spatial patterning, sequential interactions and concentration thresholds of ATM and other important DDR proteins. While ATM is thought to exist in the form of bi-stable switch, it appeared that ATM provided a graded input. However, elucidation of role of ATM through time courses and dose dependent drug intervention in cytotoxicity assays revealed that the mechanism of shift between arrest and apoptosis may follow a switch like output. Figures 6.19 and 6.20 showed that this switch of function between cytoprotection and cytotoxicity of ATM signalling took place between DNA damage of 250nM-500nM of Dox concentration. The prediction of this switch like ATM function during different combinatorial drug treatment regimens in other cell lines is vital in determining the final outcome of therapeutic intervention involving genotoxicity. This prediction in particular settings could be provided by network simulations and quantitative data driven mathematical models. These models, at the outset, could assist in furthering our understanding of protein-protein spatio-temporal interaction and dynamics in complex signalling networks and could be calibrated initially at the stage of the experimental assay. This would involve the quantitative measurement at the molecular level of a large number of inputs in terms of drug concentration, radiation dose, culture media, as well as measurement of the corresponding outputs in terms of a range of key molecules on the relevant pathways.

The new insights obtained from the initial model could also possibly not only predict treatment regimens involving time dependent administration of DNA damaging agents and DDR inhibitors to get a desired outcome in a cell line, but also pin point key differences in cancer and normal cell lines. These dissimilarities between normal and cancer cell lines, owing to their differences in protein repertoire and genetic backgrounds, can hence determine and revise treatment regimens to allow for achieving targeted cellular sensitivity.

Thus, tremendous assistance could be provided in researching potential drug treatment options for certain types of cancers based on *in silico* predictions. Following this, and if other potential ways are found for inhibition of the DDR pathway, a secondary calibration stage could be carried out along with the initial clinical trials. This would permit the model to be developed as a clinical application to be used in conjunction with the drug treatment regimes.

Such an application would enable clinicians to determine the optimum timing and level of drug dose and radiation for use in the individual patient where the DDR pathway status has already been established by the measurement of key protein levels in that patient. In the terms of this approach the optimal outcome is taken to be the highest number of cancer cells damaged by the drug and/or radiation which are directed toward apoptosis.

## 7.2 Conclusion

The current PhD. study of ATM signalling pathway and its substrates covered aspects ranging from their regulation, activation, localisation and trafficking associated with the progression of cell cycle, in the DNA damaged states, during DDR manipulation and up to the final outcome on cell-fate. In the course of such functional and regulatory elucidation of ATM, its DDR substrates and its functional partners in both normal and cancer cell lines, I discovered two autoregulatory mechanisms of ATM function; First mechanism involved its kinase dependent transcriptional modulation via its promoter activity. The second means of autoregulation comprised of its kinase dependent trafficking mechanism via β-COPI mediated Golgi to nuclear transport.

One of the major challenges for cancer biologists is to identify and target key survival pathways in cancerous cells that could provide selectivity against them. While this is a challenging task owing to the complexity in responses generated by different types of cancers, age and in different settings (Hong MY et al., 2005, Tummala H et al., 2011), taking a systems biology approach to study these complex molecular networks and key differences between normal and cancer cells has helped researchers to identify pathways and novel drug targets (Faratian D et al., 2009, Clyde RG et al., 2006 & 2011). It is now known that an increased sensitivity of cancer cells towards genotoxic agents could be achieved by inhibiting the DDR proteins implicated in G2/M checkpoint e.g. via inhibition of ATM kinase (Bolderson E et al., 2009). This forms the rationale of targeting DNA damage response proteins for therapeutic intervention in cancer. This study clearly indicated that inhibition of the ATM kinase activity leads to upregulation of the ATM protein, giving rise to a temporary peak in its activity accompanied by induction in P53, pATR and E2F1. This temporary increase in DDR activity may hinder the therapeutic effect of G2/M checkpoint abrogation, providing an opportunity to repair the DNA in cancer cells.

A luciferase reporter assay of ATM promoter not only established a transcriptional basis for this change but also demonstrated the precise timing of this upregulation in the ATM levels after its inhibition. This particular oscillation pattern might differ in its timing and regulation in different types of cancers. However, the novel information in this study could be used to time the chemotherapy or radiotherapy treatments to precise time points after ATM inhibition, when the ATM levels are at their lowest hence allowing a better therapeutic intervention. The reporter assay designed whose conceptual framework is based on the novel finding can help in screening new inhibitors or for the detection of DNA damage. Furthermore, novel autoregulatory trafficking mechanism of ATM following DNA damage has revealed the involvement of β-COPI mediated transport for activated ATM, and possibly ATR and checkpoint kinases. This provides another means by which the kinase activity of ATM could autoregulate its function by triggering its DNA damage induced sub-cellular compartmentalisation. As such this finding provides another dimension through which the DDR responses in general, or those of ATM kinase specifically could be manipulated i.e. via intervention within the DNA damage induced trafficking events. While inhibition of Golgi to nuclear protein trafficking will have far reaching effects, specificity could be achieved via the manipulation of the identified di-Lysine motif in the current research.

The novel findings in the current research work have not only extended our current state of knowledge regarding the mechanism of ATM expression, activation, trafficking, differential functioning in cytoprotection and cytotoxicity specifically and working machinery of DDR in general, they also highlight the intricate nature of the signalling pathways and the complexity involved in these cellular systems. Before the most successful therapeutic intervention in cancer could be achieved, a thorough understanding of cellular systems that govern cell cycle, DNA repair and apoptosis is necessary. This research is a step towards achieving that.

# Chapter Eight

# References

Every scientific truth goes through three states: first, people say it conflicts with the Bible; next, they say it has been discovered before; lastly, they say they always believed it.

Louis Agassiz, Palaeontologist (1807-1873)

Adair GM, Rolig RL, Moore-Faver D, Zabelshansky M, Wilson JH, Nairn RS. Role of ERCC1 in removal of long non-homologous tails during targeted homologous recombination. EMBO J. 2000 Oct 16;19(20):5552-1.

Adams KE, Medhurst AL, Dart DA, Lakin ND. Recruitment of ATR to sites of ionising radiation-induced DNA damage requires ATM and components of the MRN protein complex. Oncogene. 2006 Jun 29;25(28):3894-904. Epub 2006 Feb 13.

Ahmed KM, Li JJ. ATM-NF-kappaB connection as a target for tumor radiosensitization. Curr Cancer Drug Targets. 2007 Jun;7(4):335-42.

Alao JP, Sunnerhagen P.. The ATM and ATR inhibitors CGK733 and caffeine suppress cyclin D1 levels and inhibit cell proliferation. Radiat Oncol. 2009 Nov 10;4:51.

Arienti KL, Brunmark A, Axe FU, McClure K, Lee A, Blevitt J, Neff DK, Huang L, Crawford S, Pandit CR, Karlsson L, Breitenbucher JG. Checkpoint kinase inhibitors: SAR and radioprotective properties of a series of 2-arylbenzimidazoles. J Med Chem. 2005 Mar 24;48(6):1873-85.

Bakkenist CJ, Kastan MB. DNA damage activates ATM through intermolecular autophosphorylation and dimer dissociation. Nature. 2003 Jan 30;421(6922):499-506.

Banin S, Moyal L, Shieh S, Taya Y, Anderson CW, Chessa L, Smorodinsky NI, Prives C, Reiss Y, Shiloh Y, Ziv Y. Enhanced phosphorylation of P53 by ATM in response to DNA damage. Science. 1998 Sep 11;281(5383):1674-7.

Bao S, Tibbetts RS, Brumbaugh KM, Fang Y, Richardson DA, Ali A, Chen SM, Abraham RT, Wang XF. ATR/ATM-mediated phosphorylation of human Rad17 is required for genotoxic stress responses. Nature. 2001 Jun 21;411(6840):969-74.

Barlow C, Liyanage M, Moens PB, Tarsounas M, Nagashima K, Brown K, Rottinghaus S, Jackson SP, Tagle D, Ried T, Wynshaw-Boris A. Atm deficiency results in severe meiotic disruption as early as leptonema of prophase I. Development. 1998 Oct;125(20):4007-17.

Barlow C, Ribaut-Barassin C, Zwingman TA, Pope AJ, Brown KD, Owens JW, Larson D, Harrington EA, Haeberle AM, Mariani J, Eckhaus M, Herrup K, Bailly Y, Wynshaw-Boris A. ATM is a cytoplasmic protein in mouse brain required to prevent lysosomal accumulation. Proc Natl Acad Sci U S A. 2000 Jan 18;97(2):871-6.

Beck R, Rawet M, Wieland FT, Cassel D. The COPI system: molecular mechanisms and function. FEBS Lett. 2009 Sep 3;583(17):2701-9.

Berkovich E, Ginsberg D. ATM is a target for positive regulation by E2F-1. Oncogene. 2003 Jan 16;22(2):161-7.

Bernardi R, Scaglioni PP, Bergmann S, Horn HF, Vousden KH, Pandolfi PP. PML regulates P53 stability by sequestering Mdm2 to the nucleolus. Nat Cell Biol. 2004 Jul;6(7):665-72.

Béthune J, Wieland F, Moelleken J. COPI-mediated transport. J Membr Biol. 2006; 211(2):65-79. Epub 2006 Oct 14.

Blasina A, Hallin J, Chen E, Arango ME, Kraynov E, Register J, Grant S, Ninkovic S, Chen P, Nichols T, O'Connor P, Anderes K. Breaching the DNA damage checkpoint via PF-00477736, a novel small-molecule inhibitor of checkpoint kinase 1. Mol Cancer Ther. 2008 Aug;7(8):2394-404.

Bolderson E, Richard DJ, Zhou BB, Khanna KK. Recent advances in cancer therapy targeting proteins involved in DNA double-strand break repair. Clin Cancer Res. 2009 Oct 15;15(20):6314-20. Epub 2009 Oct 6.

Broderick S, Rehmet K, Concannon C, Nasheuer HP. Eukaryotic single- stranded DNA binding proteins: central factors in genome stability. Subcell Biochem. 2010;50:143-63.

Brown KD, Ziv Y, Sadanandan SN, Chessa L, Collins FS, Shiloh Y, Tagle DA. The ataxia-telangiectasia gene product, a constitutively expressed nuclear protein that is not up-regulated following genome damage. Proc Natl Acad Sci U S A. 1997 Mar 4;94(5):1840-5.

Byrd PJ, Cooper PR, Stankovic T, Kullar HS, Watts GD, Robinson PJ, Taylor MR. A gene transcribed from the bidirectional ATM promoter coding for a serine rich protein: amino acid sequence, structure and expression studies. Hum Mol Genet. 1996 Nov;5(11):1785-91.

Canman CE, Lim DS, Cimprich KA, Taya Y, Tamai K, Sakaguchi K, Appella E, Kastan MB, Siliciano JD. Activation of the ATM kinase by ionizing radiation and phosphorylation of P53. Science. 1998 Sep 11;281(5383):1677-9.

Carcagno AL, Ogara MF, Sonzogni SV, Marazita MC, Sirkin PF, Ceruti JM, Cánepa ET. E2F1 transcription is induced by genotoxic stress through ATM/ATR activation.IUBMB Life. 2009 May;61(5):537-43.

Carney JP, Maser RS, Olivares H, Davis EM, Le Beau M, Yates JR 3rd, Hays L, Morgan WF, Petrini JH. The hMre11/hRad50 protein complex and Nijmegen breakage syndrome: linkage of double-strand break repair to the cellular DNA damage response. Cell. 1998 May 1;93(3):477-86.

Carter T, Vancurová I, Sun I, Lou W, DeLeon S. A DNA-activated protein kinase from HeLa cell nuclei. Mol Cell Biol. 1990 Dec;10(12):6460-71.

Chan DW, Lees-Miller SP. The DNA-dependent protein kinase is inactivated by autophosphorylation of the catalytic subunit. J Biol Chem. 1996 Apr 12;271(15):8936-41.

Chehab NH, Malikzay A, Appel M, Halazonetis TD. Chk2/hCds1 functions as a DNA damage checkpoint in G(1) by stabilizing P53. Genes Dev. 2000 Feb 1;14(3):278-88.
Chen G, Lee EYHP. The product of the ATM gene is a 370-kDa nuclear phosphoprotein. J Biol Chem. 1996 Dec 27;271(52):33693-7.

Chen L, Trujillo K, Sung P, Tomkinson AE. Interactions of the DNA ligase IV-XRCC4 complex with DNA ends and the DNA-dependent protein kinase. J Biol Chem. 2000 Aug 25;275(34):26196-205.

Chen X, Yang L, Udar N, Liang T, Uhrhammer N, Xu S, Bay JO, Wang Z, Dandakar S, Chiplunkar S, Klisak I, Telatar M, Yang H, Concannon P, Gatti RA. CAND3: a ubiquitously expressed gene immediately adjacent and in opposite transcriptional orientation to the ATM gene at 11q23.1. Mamm Genome. 1997 Feb;8(2):129-33.

Chen BP, Chan DW, Kobayashi J, Burma S, Asaithamby A, Morotomi-Yano K, Botvinick E, Qin J, Chen DJ. Cell cycle dependence of DNA-dependent protein kinase phosphorylation in response to DNA double strand breaks. J Biol Chem. 2005 Apr 15;280(15):14709-15. Epub 2005 Jan 26.

Choi M, Lee H, Rho HM. E2F1 activates the human P53 promoter and overcomes the repressive effect of hepatitis B viral X protein (Hbx) on the P53 promoter. IUBMB Life. 2002 Jun;53(6):309-17.

Chipuk JE, Bouchier-Hayes L, Kuwana T, Newmeyer DD, Green DR. PUMA couples the nuclear and cytoplasmic proapoptotic function of p53. Science. 2005 Sep 9;309(5741):1732-5.

Chong MJ, Murray MR, Gosink EC, Russell HR, Srinivasan A, Kapsetaki M, Korsmeyer SJ, McKinnon PJ. Atm and Bax cooperate in ionizing radiation-induced apoptosis in the central nervous system. Proc Natl Acad Sci U S A. 2000 Jan 18;97(2):889-94.

Clyde RG, Bown JL, Hupp TR, Zhelev N, Crawford JW. The role of modelling in identifying drug targets for diseases of the cell cycle. J R Soc Interface. 2006 Oct 22;3(10):617-27.

Clyde RG, Craig AL, de Breed L, Bown JL, Forrester L, Vojtesek B, Smith G, Hupp T, Crawford J. A novel ataxia-telangiectasia mutated autoregulatory feedback mechanism in murine embryonic stem cells. J R Soc Interface. 2009 Dec 6;6(41):1167-77. Epub 2009 Mar 4.

Clyde R, Tummala H, Khalil HS, Goszcz K, Lucka I, Tupone MG, Zwirek M, Cavicchi L, Vallatur J, Stoyanova V, Mitev V, Zhelev N. A novel quantitative systems biology approach to cancer research and treatment. Curr Opin Biotechnol 2011; 22(S): S58.

Collis SJ, Swartz MJ, Nelson WG, DeWeese TL. Enhanced radiation and chemotherapy-mediated cell killing of human cancer cells by small inhibitory RNA silencing of DNA repair factors. Cancer Res. 2003 Apr 1;63(7):1550-4.

Cortez D. Caffeine inhibits checkpoint responses without inhibiting the ataxia-t elangiectasia-mutated (ATM) and ATM- and Rad3-related (ATR) protein kinases. J Biol Chem. 2003 Sep 26;278(39):37139-45.

Craig AL, Holcakova J, Finlan LE, Nekulova M, Hrstka R, Gueven N, DiRenzo J, Smith G, Hupp TR, Vojtesek B. DeltaNp63 transcriptionally regulates ATM to control P53 Serine-15 phosphorylation. Mol Cancer. 2010 Jul 21;9:195.

Crescenzi E, Palumbo G, de Boer J, Brady HJ. Ataxia telangiectasia mutated and P21CIP1 modulate cell survival of drug-induced senescent tumor cells: implications for chemotherapy. Clin Cancer Res. 2008 Mar 15;14(6):1877-87.

Daub H, Olsen JV, Bairlein M, Gnad F, Oppermann FS, Körner R, Greff Z, Kéri G, Stemmann O, Mann M. Kinase-selective enrichment enables quantitative phosphoproteomics of the kinome across the cell cycle. Mol Cell. 2008 Aug 8;31(3):438-48.

De Marco N, Buono M, Troise F, Diez-Roux G. Optineurin increases cell survival and translocates to the nucleus in a Rab8-dependent manner upon an apoptotic stimulus. J Biol Chem. 2006 Jun 9;281(23):16147-56.

Duckett DR, Murchie AI, Diekmann S, von Kitzing E, Kemper B, Lilley DM. The structure of the Holliday junction, and its resolution. Cell. 1988 Oct 7;55(1):79-89.

el-Deiry WS, Tokino T, Velculescu VE, Levy DB, Parsons R, Trent JM, Lin D, Mercer WE, Kinzler KW, Vogelstein B. WAF1, a potential mediator of P53 tumor suppression. Cell. 1993 Nov 19;75(4):817-25.

Elliott B, Jasin M. Double-strand breaks and translocations in cancer. Cell Mol Life Sci. 2002 Feb;59(2):373-85.

Elson A, Wang Y, Daugherty CJ, Morton CC, Zhou F, Campos-Torres J, Leder P. Pleiotropic defects in ataxia-telangiectasia protein-deficient mice. Proc Natl Acad Sci U S A. 1996 Nov 12;93(23):13084-9.

Enomoto M, Goto H, Tomono Y, Kasahara K, Tsujimura K, Kiyono T, Inagaki M. Novel positive feedback loop between Cdk1 and Chk1 in the nucleus during G2/M transition. J Biol Chem. 2009 Dec 4;284(49):34223-30.

Essmann F, Pohlmann S, Gillissen B, Daniel PT, Schulze-Osthoff K, Jänicke RU. Irradiation-induced translocation of P53 to mitochondria in the absence of apoptosis. J Biol Chem. 2005 Nov 4;280(44):37169-77.

Eugster A, Frigerio G, Dale M, Duden R. COP I domains required for coatomer integrity, and novel interactions with ARF and ARF-GAP. EMBO J. 2000 Aug 1;19(15):3905-17.

Falck J, Mailand N, Syljuåsen RG, Bartek J, Lukas J. The ATM-Chk2-Cdc25A checkpoint pathway guards against radioresistant DNA synthesis. Nature. 2001 Apr 12;410(6830):842-7.

Fang ZM, Lee CS, Sarris M, Kearsley JH, Murrell D, Lavin MF, Keating K, Clarke RA. Rapid radiation-induction of ATM protein levels in situ. Pathology. 2001 Feb;33(1):30-6.

Faratian D, Goltsov A, Lebedeva G, Sorokin A, Moodie S, Mullen P, Kay C, Um IH, Langdon S, Goryanin I, Harrison DJ. Systems biology reveals new strategies for personalizing cancer medicine and confirms the role of PTEN in resistance to trastuzumab. Cancer Res. 2009 Aug 15;69(16):6713-20. Epub 2009 Jul 28.

Fong PC, Boss DS, Yap TA, Tutt A, Wu P, Mergui-Roelvink M, Mortimer P, Swaisland H, Lau A, O'Connor MJ, Ashworth A, Carmichael J, Kaye SB, Schellens JH, de Bono JS. Inhibition of poly(ADP-ribose) polymerase in tumors from BRCA mutation carriers. N Engl J Med. 2009 Jul 9;361(2):123-34. Epub 2009 Jun 24.

Foray N, Marot D, Gabriel A, Randrianarison V, Carr AM, Perricaudet M, Ashworth A, Jeggo P. A subset of ATM- and ATR-dependent phosphorylation events requires the BRCA1 protein. EMBO J. 2003 Jun 2;22(11):2860-71.

Foray N, Priestley A, Alsbeih G, Badie C, Capulas EP, Arlett CF, Malaise EP. Hypersensitivity of ataxia telangiectasia fibroblasts to ionizing radiation is associated with a repair deficiency of DNA double-strand breaks. Int J Radiat Biol. 1997 Sep;72(3):271-83.

Frederick H., Barbara K. H.. Cancer in Ataxia-telangiectasia patients. Cancer Genetics and Cytogenetics 1990; Volume 46, Issue 1, Pages 9-19.

Frossi B, Tell G, Spessotto P, Colombatti A, Vitale G, Pucillo C. H(2)O(2) induces translocation of APE/Ref-1 to mitochondria in the Raji B-cell line. J Cell Physiol. 2002 Nov;193(2):180-6.

Fukao T, Kaneko H, Birrell G, Gatei M, Tashita H, Yoshida T, Cross S, Kedar P, Watters D, Khana KK, Misko I, Kondo N, Lavin MF. ATM is upregulated during the mitogenic response in peripheral blood mononuclear cells. Blood. 1999 Sep 15;94(6):1998-2006.

Gao Y, Hayes RB, Huang WY, Caporaso NE, Burdette L, Yeager M, Chanock SJ, Berndt SI. DNA repair gene polymorphisms and tobacco smoking in the risk for colorectal adenomas. Carcinogenesis. 2011 Jun;32(6):882-7. Epub 2011 Apr 18.

Gajewski E, Gaur S, Akman SA, Matsumoto L, van Balgooy JN, Doroshow JH. Oxidative DNA base damage in MCF-10A breast epithelial cells at clinically achievable concentrations of doxorubicin. Biochem Pharmacol. 2007 Jun 15;73(12):1947-56. Epub 2007 Mar 24.

Gatei M, Sloper K, Sorensen C, Syljuäsen R, Falck J, Hobson K, Savage K, Lukas J, Zhou BB, Bartek J, Khanna KK. Ataxia-telangiectasia-mutated (ATM) and NBS1-dependent phosphorylation of Chk1 on Ser-317 in response to ionizing radiation. J Biol Chem. 2003 Apr 25;278(17):14806-11.

Gatei M, Sloper K, Sorensen C, Syljuäsen R, Falck J, Hobson K, Savage K, Lukas J, Zhou BB, Bartek J, Khanna KK. Ataxia-telangiectasia-mutated (ATM) and NBS1-dependent phosphorylation of Chk1 on Ser-317 in response to ionizing radiation. J Biol Chem. 2003 Apr 25;278(17):14806-11. Epub 2003 Feb 14.

Gatei M, Zhou BB, Hobson K, Scott S, Young D, Khanna KK. Ataxia telangiectasia mutated (ATM) kinase and ATM and Rad3 related kinase mediate phosphorylation of BRCA1 at distinct and overlapping sites. In vivo assessment using phospho-specific antibodies. J Biol Chem. 2001 May 18;276(20):17276-80. Epub 2001 Feb 13.

Gately DP, Hittle JC, Chan GK, Yen TJ. Characterization of ATM expression, localization, and associated DNA-dependent protein kinase activity. Mol Biol Cell. 1998 Sep;9(9):2361-74.

Gatti RA, Berkel I, Boder E, Braedt G, Charmley P, Concannon P, Ersoy F, Foroud T, Jaspers NG, Lange K, et al. Localization of an ataxia-telangiectasia gene to chromosome 11q22-23. Nature. 1988 Dec 8;336(6199):577-80.

Gatti RA, Swift M. Ataxia-telangiectasia: Genetics, Neuropathology, and Immunology of a Degenerative Disease of Childhood. New York: 1985; Alan R. Liss (pub).

Gentilini F, Turba ME, Forni M, Cinotti S. Complete sequencing of full-length canine ataxia telangiectasia mutated mRNA and characterization of its putative promoter. Vet Immunol Immunopathol. 2009 Apr 15;128(4):437-40. Epub 2008 Dec 6.

Gerson SL. MGMT: its role in cancer aetiology and cancer therapeutics. Nat Rev Cancer. 2004 Apr;4(4):296-307.

Gilad S, Bar-Shira A, Harnik R, Shkedy D, Ziv Y, Khosravi R, Brown K, Vanagaite L, Xu G, Frydman M, Lavin MF, Hill D, Tagle DA, Shiloh Y. Ataxia-telangiectasia: founder effect among north African Jews. Hum Mol Genet. 1996 Dec;5(12):2033-7.

Gjerset RA, Bandyopadhyay K. Regulation of p14ARF through subnuclear compartmentalization. Cell Cycle. 2006 Apr;5(7):686-90.

Golding SE, Rosenberg E, Valerie N, Hussaini I, Frigerio M, Cockcroft XF, Chong WY, Hummersone M, Rigoreau L, Menear KA, O'Connor MJ, Povirk LF, van Meter T, Valerie K. Improved ATM kinase inhibitor KU-60019 radiosensitizes glioma cells, compromises insulin, AKT and ERK prosurvival signaling, and inhibits migration and invasion. Mol Cancer Ther. 2009 Oct;8(10):2894-902. Epub 2009 Oct 6.

Golub EI, Gupta RC, Haaf T, Wold MS, Radding CM. Interaction of human rad51 recombination protein with single-stranded DNA binding protein, RPA. Nucleic Acids Res. 1998 Dec 1;26(23):5388-93.

Gottifredi V, Karni-Schmidt O, Shieh SS, Prives C. P53 down-regulates CHK1 through P21 and the retinoblastoma protein. Mol Cell Biol. 2001 Feb;21(4):1066-76.

Goudelock DM, Jiang K, Pereira E, Russell B, Sanchez Y. Regulatory interactions between the checkpoint kinase Chk1 and the proteins of the DNA-dependent protein kinase complex. J Biol Chem. 2003 Aug 8;278(32):29940-7. Epub 2003 May 19.

Gueven N, Fukao T, Luff J, Paterson C, Kay G, Kondo N, Lavin MF. Regulation of the Atm promoter in vivo. Genes Chromosomes Cancer. 2006 Jan;45(1):61-71.

Gueven N, Keating K, Fukao T, Loeffler H, Kondo N, Rodemann HP, Lavin MF. Site-directed mutagenesis of the ATM promoter: consequences for response to proliferation and ionizing radiation. Genes Chromosomes Cancer. 2003 Oct;38(2):157-67.

Gueven N, Keating KE, Chen P, Fukao T, Khanna KK, Watters D, Rodemann PH, Lavin MF. Epidermal growth factor sensitizes cells to ionizing radiation by down-regulating protein mutated in ataxia-telangiectasia. J Biol Chem. 2001 Mar 23;276(12):8884-91. Epub 2000 Nov 15.

Guha C, Guha U, Tribius S, Alfieri A, Casper D, Chakravarty P, Mellado W, Pandita TK, Vikram B. Antisense ATM gene therapy: a strategy to increase the radiosensitivity of human tumors. Gene Ther. 2000 May;7(10):852-8.

Guo Z, Kozlov S, Lavin MF, Person MD, Paull TT. ATM activation by oxidative stress. Science. 2010 Oct 22;330(6003):517-21.

Guo Z, Kumagai A, Wang SX, Dunphy WG. Requirement for ATR in phosphorylation of Chk1 and cell cycle regulation in response to DNA replication blocks and UV-damaged DNA in Xenopus egg extracts. Genes Dev. 2000 Nov 1;14(21):2745-56.

Halaby MJ, Hibma JC, He J, Yang DQ. ATM protein kinase mediates full activation of Akt and regulates glucose transporter 4 translocation by insulin in muscle cells. Cell Signal. 2008 Aug;20(8):1555-63. Epub 2008 Apr 26.

Hanahan D, Jessee J, Bloom FR. Plasmid transformation of Escherichia coli and other bacteria. Methods Enzymol. 1991;204:63-113.

Harkin DP, Bean JM, Miklos D, Song YH, Truong VB, Englert C, Christians FC, Ellisen LW, Maheswaran S, Oliner JD, Haber DA. Induction of GADD45 and JNK/SAPK-dependent apoptosis following inducible expression of BRCA1. Cell. 1999 May 28;97(5):575-86.

Hartwell LH, Weinert TA. Checkpoints: controls that ensure the order of cell cycle events. Science. 1989 Nov 3;246(4930):629-34.

Helin K, Harlow E, Fattaey A. Inhibition of E2F-1 transactivation by direct binding of the retinoblastoma protein. Mol Cell Biol. 1993 Oct;13(10):6501-8.

Henseleit U, Zhang J, Wanner R, Haase I, Kolde G, Rosenbach T. Role of p53 in UVB-induced apoptosis in human HaCaT keratinocytes. J Invest Dermatol. 1997 Dec;109(6):722-7.

Hickson I, Zhao Y, Richardson CJ, Green SJ, Martin NM, Orr AI, Reaper PM, Jackson SP, Curtin NJ, Smith GC. Identification and characterization of a novel and specific inhibitor of the ataxia-telangiectasia mutated kinase ATM. Cancer Res. 2004 Dec 15;64(24):9152-9.

Hirai Y, Hayashi T, Kubo Y, Hoki Y, Arita I, Tatsumi K, Seyama T. X-irradiation induces up-regulation of ATM gene expression in wild-type lymphoblastoid cell lines, but not in their heterozygous or homozygous ataxia-telangiectasia counterparts. Jpn J Cancer Res. 2001 Jun;92(6):710-7.

Hong MY, Turner ND, Carroll RJ, Chapkin RS, Lupton JR. Differential response to DNA damage may explain different cancer susceptibility between small and large intestine. Exp Biol Med (Maywood). 2005 Jul;230(7):464-71.

Ianari A, Gallo R, Palma M, Alesse E, Gulino A. Specific role for p300/CREB-binding protein-associated factor activity in E2F1 stabilization in response to DNA damage. J Biol Chem. 2004 Jul 16;279(29):30830-5.

Imai T, Sugawara T, Nishiyama A, Shimada R, Ohki R, Seki N, Sagara M, Ito H, Yamauchi M, Hori T. The structure and organization of the human NPAT gene. Genomics. 1997 Jun 15;42(3):388-92.

Imai T, Yamauchi M, Seki N, Sugawara T, Saito T, Matsuda Y, Ito H, Nagase T, Nomura N, Hori T. Identification and characterization of a new gene physically linked to the ATM gene. Genome Res. 1996 May;6(5):439-47.

Imamura S, Kishi S, Amatruda JF, Kanki JP, Green DR, D'Andrea AA, Look AT. Chk1 suppresses a caspase-2 apoptotic response to DNA damage that bypasses P53, Bcl-2, and caspase-3. Cell. 2008 May 30;133(5):864-77.

Ismail F, Ikram M, Purdie K, Harwood C, Leigh I, Storey A. Cutaneous squamous cell carcinoma (SCC) and the DNA damage response: pATM expression patterns in pre-malignant and malignant keratinocyte skin lesions. PLoS One. 2011;6(7):e21271. Epub 2011 Jul 1.

Itahana K, Dimri GP, Hara E, Itahana Y, Zou Y, Desprez PY, Campisi J. A role for P53 in maintaining and establishing the quiescence growth arrest in human cells. J Biol Chem. 2002 May 17;277(20):18206-14. Epub 2002 Mar 5.

Ivanova IA, Vespa A, Dagnino L. A novel mechanism of E2F1 regulation via nucleocytoplasmic shuttling: determinants of nuclear import and export. Cell Cycle. 2007 Sep 1;6(17):2186-95.

Powers JT, Hong S, Mayhew CN, Rogers PM, Knudsen ES, Johnson DG. E2F1 uses the ATM signaling pathway to induce P53 and Chk2 phosphorylation and apoptosis. Mol Cancer Res. 2004 Apr;2(4):203-14.

Jamieson ER, Lippard SJ. Structure, Recognition, and Processing of Cisplatin-DNA Adducts. Chem Rev. 1999 Sep 8;99(9):2467-98.

Jazayeri A, Falck J, Lukas C, Bartek J, Smith GC, Lukas J, Jackson SP. ATM-and cell cycle-dependent regulation of ATR in response to DNA double-strand breaks. Nat Cell Biol. 2006 Jan;8(1):37-45.

Jung M, Dritschilo A. 2001. NF-kappa B signalling pathway as a target for human tumor radiosensitization. Semin Radiat Oncol. ;11(4):346-51.

Karmakar P, Piotrowski J, Brosh RM Jr, Sommers JA, Miller SP, Cheng WH, Snowden CM, Ramsden DA, Bohr VA. Werner protein is a target of DNA-dependent protein kinase in vivo and in vitro, and its catalytic activities are regulated by phosphorylation. J Biol Chem. 2002 May 24;277(21):18291-302.

Kastan MB, Bartek, J.. Cell cycle checkpoints and cancer. Nature 2004; 432, 316-323.

Khalil HS, Tummala H, Oluwaseun OA, Zhelev N. Novel insights of Ataxia Telangiectasia Mutated (ATM) regulation and its potential as a target for therapeutic intervention in cancer. Curr. Opin. Biotechnol 2011; 22(S) :S115- 116.

Khanna KK, Jackson SP. DNA double-strand breaks: signaling, repair and the cancer connection. Nat Genet. 2001 Mar;27(3):247-54.

Kharbanda S, Saxena S, Yoshida K, Pandey P, Kaneki M, Wang Q, Cheng K, Chen YN, Campbell A, Sudha T, Yuan ZM, Narula J, Weichselbaum R, Nalin C, Kufe D. Translocation of SAPK/JNK to mitochondria and interaction with Bcl-x(L) in response to DNA damage. J Biol Chem. 2000 Jan 7;275(1):322-7. Erratum in: J Biol Chem 2000 Jun 23;275(25):19433.

Kim ST, Xu B, Kastan MB. Involvement of the cohesin protein, Smc1, in Atm-dependent and independent responses to DNA damage. Genes Dev. 2002 Mar 1;16(5):560-70.

Koniaras K, Cuddihy AR, Christopoulos H, Hogg A, O'Connell MJ. Inhibition of Chk1-dependent G2 DNA damage checkpoint radiosensitizes P53 mutant human cells. Oncogene. 2001 Nov 8;20(51):7453-63.

Kozlov SV, Graham ME, Peng C, Chen P, Robinson PJ, Lavin MF. Involvement of novel autophosphorylation sites in ATM activation. EMBO J. 2006 Aug 9;25(15):3504-14. Epub 2006 Jul 13.

Krämer A, Mailand N, Lukas C, Syljuåsen RG, Wilkinson CJ, Nigg EA, Bartek J, Lukas J. Centrosome-associated Chk1 prevents premature activation of cyclin-B-Cdk1 kinase. Nat Cell Biol. 2004 Sep;6(9):884-91.

Krumschnabel G, Sohm B, Bock F, Manzl C, Villunger A. The enigma of caspase-2: the laymen's view. Cell Death Differ. 2009 Feb;16(2):195-207. Epub 2008 Nov 21.

Kuge O, Hara-Kuge S, Orci L, Ravazzola M, Amherdt M, Tanigawa G, Wieland FT, Rothman JE. zeta-COP, a subunit of coatomer, is required for COP-coated vesicle assembly. J Cell Biol. 1993 Dec;123(6 Pt 2):1727-34.

Kuljis RO, Chen G, Lee EY, Aguila MC, Xu Y. ATM immunolocalisation in mouse neuronal endosomes: implications for ataxia-telangiectasia. Brain Res. 1999 Sep 25;842(2):351-8.

Kumar S, Dodson GE, Trinh A, Puchalski JR, Tibbetts RS. ATR activation necessary but not sufficient for P53 induction and apoptosis in hydroxyurea-hypersensitive myeloid leukemia cells. Cell Cycle. 2005 Nov;4(11):1667-74.

Lee Y, McKinnon PJ. ATM dependent apoptosis in the nervous system. Apoptosis. 2000 Dec;5(6):523-9.

Leemput J, Masson C, Bigot K, Errachid A, Dansault A, Provost A, Gadin S, Aoufouchi S, Menasche M, Abitbol M. ATM localization and gene expression in the adult mouse eye. Mol Vis. 2009;15:393-416. Epub 2009 Feb 20.

Levitt NC, Hickson ID. Caretaker tumour suppressor genes that defend genome integrity. Trends Mol Med. 2002 Apr;8(4):179-86.

Liang SH, Clarke MF. Regulation of P53 localization. Eur J Biochem. 2001 May;268(10):2779-83.

Li C, Chen L, Chen J. DNA damage induces MDMX nuclear translocation by P53-dependent and -independent mechanisms. Mol Cell Biol. 2002 Nov;22(21):7562-71.

Li J, Han YR, Plummer MR, Herrup K. Cytoplasmic ATM in neurons modulates synaptic function. Curr Biol. 2009 Dec 29;19(24):2091-6. Epub 2009 Dec 3.

Lim DS, Kim ST, Xu B, Maser RS, Lin J, Petrini JH, Kastan MB. ATM phosphorylates p95/nbs1 in an S-phase checkpoint pathway. Nature. 2000 Apr 6;404(6778):613-7.

Lim DS, Kirsch DG, Canman CE, Ahn JH, Ziv Y, Newman LS, Darnell RB, Shiloh Y, Kastan MB. ATM binds to beta-adaptin in cytoplasmic vesicles. Proc Natl Acad Sci U S A. 1998 Aug 18;95(17):10146-51.

Lin WC, Lin FT, Nevins JR. Selective induction of E2F1 in response to DNA damage, mediated by ATM-dependent phosphorylation. Genes Dev. 2001 Jul 15;15(14):1833-44.

Lopez-Girona A, Furnari B, Mondesert O, Russell P. Nuclear localisation of Cdc25 is regulated by DNA damage and a 14-3-3 protein. Nature. 1999 Jan 14;397(6715):172-5.

Ma Y, Pannicke U, Schwarz K, Lieber MR. Hairpin opening and overhang processing by an Artemis/DNA-dependent protein kinase complex in nonhomologous end joining and V(D)J recombination. Cell. 2002 Mar 22;108(6):781-94.

Madhusudan S, Smart F, Shrimpton P, Parsons JL, Gardiner L, Houlbrook S, Talbot DC, Hammonds T, Freemont PA, Sternberg MJ, Dianov GL, Hickson ID. Isolation of a small molecule inhibitor of DNA base excision repair. Nucleic Acids Res. 2005 Aug 19;33(15):4711-24. Print 2005.

Mahajan KN, Nick McElhinny SA, Mitchell BS, Ramsden DA. Association of DNA polymerase mu (pol mu) with Ku and ligase IV: role for pol mu in end-joining double-strand break repair. Mol Cell Biol. 2002 Jul;22(14):5194-202.

Mancini M, Machamer CE, Roy S, Nicholson DW, Thornberry NA, Casciola-Rosen LA, Rosen A. Caspase-2 is localized at the Golgi complex and cleaves golgin-160 during apoptosis. J Cell Biol. 2000 May 1;149(3):603-12.

Marchenko ND, Zaika A, Moll UM. Death signal-induced localisation of P53 protein to mitochondria. A potential role in apoptotic signaling. J Biol Chem. 2000 May 26;275(21):16202-12.

Martínez-Balbás MA, Bauer UM, Nielsen SJ, Brehm A, Kouzarides T. Regulation of E2F1 activity by acetylation. EMBO J. 2000 Feb 15;19(4):662-71.

Matsuoka S, Ballif BA, Smogorzewska A, McDonald ER 3rd, Hurov KE, Luo J, Bakalarski CE, Zhao Z, Solimini N, Lerenthal Y, Shiloh Y, Gygi SP, Elledge SJ. ATM and ATR substrate analysis reveals extensive protein networks responsive to DNA damage. Science. 2007 May 25;316(5828):1160-6.

Matsuoka S, Rotman G, Ogawa A, Shiloh Y, Tamai K, Elledge SJ. Ataxia telangiectasia-mutated phosphorylates Chk2 in vivo and in vitro. Proc Natl Acad Sci U S A. 2000 Sep 12;97(19):10389-94.

Maya R, Balass M, Kim ST, Shkedy D, Leal JF, Shifman O, Moas M, Buschmann T, Ronai Z, Shiloh Y, Kastan MB, Katzir E, Oren M. ATM-dependent phosphorylation of mdm2 on serine 395: role in P53 activation by DNA damage. Genes Dev. 2001 May 1;15(9):1067-77.

McMahon HT, Mills IG. COP and clathrin-coated vesicle budding: different pathways, common approaches. Curr Opin Cell Biol. 2004 Aug;16(4):379-91.

Meyn MS. Ataxia-telangiectasia, cancer and the pathobiology of the ATM gene. Clin Genet. 1999 May;55(5):289-304.

Mitui M, Nahas SA, Du LT, Yang Z, Lai CH, Nakamura K, Arroyo S, Scott S, Purayidom A, Concannon P, Lavin M, Gatti RA. Functional and computational assessment of missense variants in the ataxia-telangiectasia mutated (ATM) gene: mutations with increased cancer risk. Hum Mutat. 2009 Jan;30(1):12-21.

Morgan SE, Lovly C, Pandita TK, Shiloh Y, Kastan MB. Fragments of ATM which have dominant-negative or complementing activity. Mol Cell Biol. 1997 Apr;17(4):2020-9.

Nakayama Y, Igarashi A, Kikuchi I, Obata Y, Fukumoto Y, Yamaguchi N. Bleomycin-induced over-replication involves sustained inhibition of mitotic entry through the ATM/ATR pathway. Exp Cell Res. 2009 Sep 10;315(15):2515-28. Epub 2009 Jun 13.

Neijenhuis S, Verwijs-Janssen M, van den Broek LJ, Begg AC, Vens C. Targeted radiosensitization of cells expressing truncated DNA polymerase {beta}. CancerRes. 2010 Nov 1;70(21):8706-14. Epub 2010 Oct 26.

Oberkovitz G, Regev L, Gross A. Nucleocytoplasmic shuttling of BID is involved in regulating its activities in the DNA-damage response. Cell Death Differ. 2007 Sep;14(9):1628-34.

Ohtani K, DeGregori J, Nevins JR. Regulation of the cyclin E gene by transcription factor E2F1. Proc Natl Acad Sci U S A. 1995 Dec 19;92(26):12146-50.

Oka A, Takashima S. Expression of the ataxia-telangiectasia gene (ATM) product in human cerebellar neurons during development. Neurosci Lett. 1998 Aug 21;252(3):195-8.

Okada S, Ouchi T. Cell cycle differences in DNA damage-induced BRCA1 phosphorylation affect its subcellular localisation. J Biol Chem. 2003 Jan 17;278(3):2015-20.

Oppermann FS, Gnad F, Olsen JV, Hornberger R, Greff Z, Kéri G, Mann M, Daub H. Large-scale proteomics analysis of the human kinome. Mol Cell Proteomics. 2009 Jul;8(7):1751-64. Epub 2009 Apr 15.

Pabla N, Huang S, Mi QS, Daniel R, Dong Z. ATR-Chk2 signaling in P53 activation and DNA damage response during cisplatin-induced apoptosis. J Biol Chem. 2008 Mar 7;283(10):6572-83. Epub 2007 Dec 27. Erratum in: J Biol Chem. 2008 May 30;283(22):15512.

Palade G. Intracellular aspects of the process of protein synthesis. Science. 1975 Aug 1;189(4200):347-58.

Paull TT, Rogakou EP, Yamazaki V, Kirchgessner CU, Gellert M, Bonner WM. A critical role for histone H2AX in recruitment of repair factors to nuclear foci after DNA damage. Curr Biol. 2000 Jul 27-Aug 10;10(15):886-95.

Peasland A, Wang LZ, Rowling E, Kyle S, Chen T, Hopkins A, Cliby WA, Sarkaria J, Beale G, Edmondson RJ, Curtin NJ. Identification and evaluation of a potent novel ATR inhibitor, NU6027, in breast and ovarian cancer cell lines. Br J Cancer. 2011 Jul 26;105(3):372-81. Epub 2011 Jul 5.

Perlman S, Becker-Catania S, Gatti RA. Ataxia-telangiectasia: diagnosis and treatment. 2003; Volume 10, Issue 3, Pages 173-182.

Peterson RD, Funkhouser JD, Tuck-Muller CM, Gatti RA. Cancer susceptibility in ataxia-telangiectasia. Leukemia. 1992; 6 Suppl 1:8-13.

Platzer M, Rotman G, Bauer D, Uziel T, Savitsky K, Bar-Shira A, Gilad S, Shiloh Y, Rosenthal A. Ataxia-telangiectasia locus: sequence analysis of 184 kb of human genomic DNA containing the entire ATM gene. Genome Res. 1997 Jun;7(6):592-605.

Plummer R, Jones C, Middleton M, Wilson R, Evans J, Olsen A, Curtin N, Boddy A, McHugh P, Newell D, Harris A, Johnson P, Steinfeldt H, Dewji R, Wang D, Robson L, Calvert H. Phase I study of the poly(ADP-ribose) polymerase inhibitor, AG014699, in combination with temozolomide in patients with advanced solid tumors. Clin Cancer Res. 2008 Dec 1;14(23):7917-23.

Powers JT, Hong S, Mayhew CN, Rogers PM, Knudsen ES, Johnson DG. E2F1 uses the ATM signaling pathway to induce P53 and Chk2 phosphorylation and apoptosis. Mol Cancer Res. 2004 Apr;2(4):203-14.

Prokopcova J, Kleibl Z, Banwell CM, Pohlreich P. The role of ATM in breast cancer development. Breast Cancer Res Treat. 2007 Aug;104(2):121-8. Epub 2006 Oct 24.

Qi J, Shackelford R, Manuszak R, Cheng D, Smith M, Link CJ, Wang S. Functional expression of ATM gene carried by HSV amplicon vector in vitro and in vivo. Gene Ther. 2004 Jan;11(1):25-33.

Rainey MD, Charlton ME, Stanton RV, Kastan MB. Transient inhibition of ATM kinase is sufficient to enhance cellular sensitivity to ionizing radiation. Cancer Res. 2008 Sep 15;68(18):7466-74.

Reed WB, Epstein WL, Boder E, Sedgwick R. Cutaneous manifestations of ataxia-telangiectasia. JAMA. 1966; 28;195(9):746-53.

Repetto G, del Peso A, Zurita JL. Neutral red uptake assay for the estimation of cell viability/cytotoxicity. Nat Protoc. 2008;3(7):1125-31.

Riesterer O, Matsumoto F, Wang L, Pickett J, Molkentine D, Giri U, Milas L, Raju U. A novel Chk inhibitor, XL-844, increases human cancer cell radiosensitivity through promotion of mitotic catastrophe. Invest New Drugs. 2011 Jun;29(3):514-22. Epub 2009 Dec 22.

Rodriguez JA, Schüchner S, Au WW, Fabbro M, Henderson BR. Nuclear-Cytoplasmic shuttling of BARD1 contributes to its proapoptotic activity and is regulated by dimerization with BRCA1. Oncogene. 2004 Mar 11;23(10):1809-20.

Rodriguez R, Meuth M. Chk1 and P21 cooperate to prevent apoptosis during DNA replication fork stress. Mol Biol Cell. 2006 Jan;17(1):402-12.

Rogatcheva MB, Fritz KL, Rund LA, Pollock CB, Beever JE, Counter CM, Schook LB.. Characterization of the porcine ATM gene: towards the generation of a novel non-murine animal model for Ataxia-Telangiectasia. Gene. 2007; 15;405(1-2):27-35. Epub 2007 Aug 30.

Rogoff HA, Pickering MT, Frame FM, Debatis ME, Sanchez Y, Jones S, Kowalik TF. Apoptosis associated with deregulated E2F activity is dependent on E2F1 and Atm/Nbs1/Chk2. Mol Cell Biol. 2004 Apr;24(7):2968-77.

Ross JB., 2006. Dynamics of DNA damage recognition. In: Siede W., Kow YW., Doestsch PW, ed. 2006. DNA damage recognition. Taylor and Francis.

Sahu RP, Batra S, Srivastava SK. Activation of ATM/Chk1 by curcumin causes cell cycle arrest and apoptosis in human pancreatic cancer cells. Br J Cancer. 2009 May 5;100(9):1425-33.

Sanal O, Wei S, Foroud T, Malhotra U, Concannon P, Charmley P, Salser W, Lange K, Gatti RA. Further mapping of an ataxia-telangiectasia locus to the chromosome 11q23 region. Am J Hum Genet. 1990 Nov;47(5):860-6.

Sanchez Y, Wong C, Thoma RS, Richman R, Wu Z, Piwnica-Worms H, Elledge SJ. Conservation of the Chk1 checkpoint pathway in mammals: linkage of DNA damage to Cdk regulation through Cdc25. Science. 1997 Sep 5;277(5331):1497-501.

Sarkaria JN, Busby EC, Tibbetts RS, Roos P, Taya Y, Karnitz LM, Abraham RT. Inhibition of ATM and ATR kinase activities by the radiosensitizing agent, caffeine. Cancer Res. 1999 Sep 1;59(17):4375-82.

Sarkaria JN, Tibbetts RS, Busby EC, Kennedy AP, Hill DE, Abraham RT. Inhibition of phosphoinositide 3-kinase related kinases by the radiosensitizing agent wortmannin. Cancer Res. 1998 Oct 1;58(19):4375-82.

Savitsky K, Bar-Shira A, Gilad S, Rotman G, Ziv Y, Vanagaite L, Tagle DA, Smith S, Uziel T, Sfez S, Ashkenazi M, Pecker I, Frydman M, Harnik R, Patanjali SR, Simmons A, Clines GA, Sartiel A, Gatti RA, Chessa L, Sanal O, Lavin MF, Jaspers NG, Taylor AM, Arlett CF, Miki T, Weissman SM, Lovett M, Collins FS, Shiloh Y. A single ataxia telangiectasia gene with a product similar to PI-3 kinase. Science. 1995 Jun 23;268(5218):1749-53.

Savitsky K, Platzer M, Uziel T, Gilad S, Sartiel A, Rosenthal A, Elroy-Stein O, Shiloh Y, Rotman G. Ataxia-telangiectasia: structural diversity of untranslated sequences suggests complex post-transcriptional regulation of ATM gene expression. Nucleic Acids Res. 1997 May 1;25(9):1678-84.

Scott SP, Zhang N, Khanna KK, Khromykh A, Hobson K, Watters D, Lavin MF. 1998. Cloning and expression of the ataxia-telangiectasia gene in baculovirus. Biochem Biophys Res Commun. 1998 7;245(1):144-8.

Shafman T, Khanna KK, Kedar P, Spring K, Kozlov S, Yen T, Hobson K, Gatei M, Zhang N, Watters D, Egerton M, Shiloh Y, Kharbanda S, Kufe D, Lavin MF. Interaction between ATM protein and c-Abl in response to DNA damage. Nature. 1997 May 29;387(6632):520-3.

Shen Z., Nickoloff JA. Mammalian homologous recombination repair and cancer intervention. In: Wei Q, Li L, Chen DJ, EDS. DNA repair, genetic instability, and cancer. Singapore: World scientific publishing Co., 2007: 119-156.

Shieh SY, Ahn J, Tamai K, Taya Y, Prives C. The human homologs of checkpoint kinases Chk1 and Cds1 (Chk2) phosphorylate P53 at multiple DNA damage-inducible sites. Genes Dev. 2000 Feb 1;14(3):289-300. Erratum in: Genes Dev 2000 Mar 15;14(6):750.

Shieh SY, Ikeda M, Taya Y, Prives C. DNA damage-induced phosphorylation of P53 alleviates inhibition by MDM2. Cell. 1997 Oct 31;91(3):325-34.

Shrivastav M, De Haro LP, Nickoloff JA. Regulation of DNA double-strand break repair pathway choice. Cell Res. 2008 Jan;18(1):134-47.

Sidi S, Sanda T, Kennedy RD, Hagen AT, Jette CA, Hoffmans R, Pascual J, Imamura S, Kishi S, Amatruda JF, Kanki JP, Green DR, D'Andrea AA, Look AT. Chk1 suppresses a caspase-2 apoptotic response to DNA damage that bypasses P53, Bcl-2, and caspase-3. Cell. 2008 May 30;133(5):864-77.

Smith GC, d'Adda di Fagagna F, Lakin ND, Jackson SP. Cleavage and inactivation of ATM during apoptosis. Mol Cell Biol. 1999 Sep;19(9):6076-84.

Smith GC, Jackson SP. The DNA-dependent protein kinase. Genes Dev. 1999 Apr 15;13(8):916-34.

Smaili SS, Hsu YT, Sanders KM, Russell JT, Youle RJ. Bax translocation to mitochondria subsequent to a rapid loss of mitochondrial membrane potential. Cell Death Differ. 2001 Sep;8(9):909-20.

Smith J, Tho LM, Xu N, Gillespie DA. The ATM-Chk2 and ATR-Chk1 pathways in DNA damage signaling and cancer. Adv Cancer Res. 2010;108:73-112.

Soares HD, Morgan JI, McKinnon PJ. Atm expression patterns suggest a contribution from the peripheral nervous system to the phenotype of ataxia-telangiectasia. Neuroscience. 1998 Oct;86(4):1045-54.

Sørensen CS, Syljuåsen RG, Falck J, Schroeder T, Rönnstrand L, Khanna KK, Zhou BB, Bartek J, Lukas J. Chk1 regulates the S phase checkpoint by coupling the physiological turnover and ionizing radiation-induced accelerated proteolysis of Cdc25A. Cancer Cell. 2003 Mar;3(3):247-58.

Spector BD, AH Filipovich, GS Perry, JH Kersey. Epidemiology of cancer in ataxia-telangiectasia. Newyork: John wiley and sons Ltd, 1982; 103-138.

Stenzel D, Hobson K, Kozlov S, Zhang N, Farrell A, Ramsay J, Gatti R, Lavin M. Cellular localisation of the ataxia-telangiectasia (ATM) gene product and discrimination between mutated and normal forms. Oncogene. 1997 Apr 24;14(16):1911-21.

Stevens C, Smith L, La Thangue NB. Chk2 activates E2F-1 in response to DNA damage. Nat Cell Biol. 2003 May;5(5):401-9.

Stiewe T, Pützer BM. Role of the P53-homologue P73 in E2F1-induced apoptosis. Nat Genet. 2000 Dec;26(4):464-9.

Stiff T, O'Driscoll M, Rief N, Iwabuchi K, Löbrich M, Jeggo PA. ATM and DNA-PK function redundantly to phosphorylate H2AX after exposure to ionizing radiation. Cancer Res. 2004 Apr 1;64(7):2390-6.

Stiff T, Walker SA, Cerosaletti K, Goodarzi AA, Petermann E, Concannon P, O'Driscoll M, Jeggo PA. ATR-dependent phosphorylation and activation of ATM in response to UV treatment or replication fork stalling. EMBO J. 2006 Dec 13;25(24):5775-82. Epub 2006 Nov 23.

Su Y, Swift M. Mortality rates among carriers of ataxia-telangiectasia mutant alleles. Ann Intern Med. 2000 Nov 21;133(10):770-8.

Sun Y, Jiang X, Chen S, Fernandes N, Price BD. A role for the Tip60 histone acetyltransferase in the acetylation and activation of ATM. Proc Natl Acad Sci U S A. 2005 Sep 13;102(37):13182-7.

Sun Y, Xu Y, Roy K, Price BD. DNA damage-induced acetylation of lysine 3016 of ATM activates ATM kinase activity. Mol Cell Biol. 2007 Dec;27(24):8502-9. Epub 2007 Oct 8.

Swagemakers SM, Essers J, de Wit J, Hoeijmakers JH, Kanaar R. The human RAD54 recombinational DNA repair protein is a double-stranded DNA-dependent ATPase. J Biol Chem. 1998 Oct 23;273(43):28292-7.

Swift M. Genetic aspects of ataxia-telangiectasia. Immunodefic Rev; 1990; 2(1):67-81.

Swift M. Genetics and epidemiology of ataxia-telangiectasia. Kroc Found Ser. 1985;19:133-46.

Takata M, Sasaki MS, Sonoda E, Morrison C, Hashimoto M, Utsumi H, Yamaguchi-Iwai Y, Shinohara A, Takeda S. Homologous recombination and non-homologous end-joining pathways of DNA double-strand break repair have overlapping roles in the maintenance of chromosomal integrity in vertebrate cells. EMBO J. 1998 Sep 15;17(18):5497-508.

Taniguchi T, Garcia-Higuera I, Xu B, Andreassen PR, Gregory RC, Kim ST, Lane WS, Kastan MB, D'Andrea AD. Convergence of the fanconi anemia and ataxia telangiectasia signaling pathways. Cell. 2002 May 17;109(4):459-72.

Taylor AM. Ataxia telangiectasia genes and predisposition to leukaemia, lymphoma and breast cancer. Br J Cancer. 1992 Jul;66(1):5-9.

te Poele RH, Okorokov AL, Jardine L, Cummings J, Joel SP. DNA damage is able to induce senescence in tumor cells in vitro and in vivo. Cancer Res. 2002 Mar 15;62(6):1876-83.

Terskikh A, Fradkov A, Ermakova G, Zaraisky A, Tan P, Kajava AV, Zhao X, Lukyanov S, Matz M, Kim S, Weissman I, Siebert P. "Fluorescent timer": protein that changes color with time. Science. 2000 Nov 24;290(5496):1585-8.

Thompson D, Duedal S, Kirner J, McGuffog L, Last J, Reiman A, Byrd P, Taylor M, Easton DF. Cancer risks and mortality in heterozygous ATM mutation carriers. J Natl Cancer Inst. 2005 Jun 1;97(11):813-22.

Tibbetts RS, Cortez D, Brumbaugh KM, Scully R, Livingston D, Elledge SJ, Abraham RT. Functional interactions between BRCA1 and the checkpoint kinase ATR during genotoxic stress. Genes Dev. 2000 Dec 1;14(23):2989-3002.

Tong T, Ji J, Jin S, Li X, Fan W, Song Y, Wang M, Liu Z, Wu M, Zhan Q. Gadd45a expression induces Bim dissociation from the cytoskeleton and translocation to mitochondria. Mol Cell Biol. 2005 Jun;25(11):4488-500.

Truman JP, Gueven N, Lavin M, Leibel S, Kolesnick R, Fuks Z, Haimovitz-Friedman A. Down-regulation of ATM protein sensitizes human prostate cancer cells to radiation-induced apoptosis. J Biol Chem. 2005 Jun 17;280(24):23262-72. Epub 2005 Apr 18.

Tummala H, Ali M, Getty P, Hocking PM, Burt DW, Inglehearn CF, Lester DH. Mutation in the guanine nucleotide-binding protein beta-3 causes retinal degeneration and embryonic mortality in chickens. Invest Ophthalmol Vis Sci. 2006 Nov;47(11):4714-8.

Tummala H, Khalil HS, Zhelev N. Repair, abort, ignore? Strategies for dealing with UV damage. Biotechnol and Biotechnol Eq. 2011; 25:2443-2446.

Turchi JJ, Henkels K. Human Ku autoantigen binds cisplatin-damaged DNA but fails to stimulate human DNA-activated protein kinase. J Biol Chem. 1996 Jun 7;271(23):13861-7.

Turenne GA, Paul P, Laflair L, Price BD. Activation of P53 transcriptional activity requires ATM's kinase domain and multiple N-terminal serine residues of P53. Oncogene. 2001 Aug 23;20(37):5100-10.

Urist M, Tanaka T, Poyurovsky MV, Prives C. P73 induction after DNA damage is regulated by checkpoint kinases Chk1 and Chk2. Genes Dev. 2004 Dec 15;18(24):3041-54.

Uziel T, Savitsky K, Platzer M, Ziv Y, Helbitz T, Nehls M, Boehm T, Rosenthal A, Shiloh Y, Rotman G. Genomic Organization of the ATM gene. Genomics. 1996 Apr 15;33(2):317-20.

Valerie K, Povirk LF. Regulation and mechanisms of mammalian double-strand break repair. Oncogene. 2003 Sep 1;22(37):5792-812.

Van Dyck E, Stasiak AZ, Stasiak A, West SC. Binding of double-strand breaks in DNA by human Rad52 protein. Nature. 1999 Apr 22;398(6729):728-31.

Vinters HV, Gatti RA, Rakic P. Sequence of cellular events in cerebellar ontogeny relevant to expression of neuronal abnormalities in ataxia-telangiectasia. Kroc Found Ser. 1985;19:233-55.

Vlahos CJ, Matter WF, Hui KY, Brown RF. A specific inhibitor of phosphatidylinositol 3-kinase, 2-(4-morpholinyl)-8-phenyl-4H-1-benzopyran-4-one (LY294002). J Biol Chem. 1994 Feb 18;269(7):5241-8.

Nayak BK, Das GM. Stabilization of P53 and transactivation of its target genes in response to replication blockade. Oncogene. 2002 Oct 17;21(47):7226-9.

Walker JR, Corpina RA, Goldberg J. Structure of the Ku heterodimer bound to DNA and its implications for double-strand break repair. Nature. 2001 Aug 9;412(6847):607-14.

Wang H, Guan J, Wang H, Perrault AR, Wang Y, Iliakis G. Replication protein A2 phosphorylation after DNA damage by the coordinated action of ataxia telangiectasia-mutated and DNA-dependent protein kinase. Cancer Res. 2001 Dec 1;61(23):8554-63.

Wang JY. Regulation of cell death by the Abl tyrosine kinase. Oncogene. 2000 Nov 20;19(49):5643-50.

Wang Q, Zhang H, Fishel R, Greene MI. BRCA1 and cell signaling. Oncogene. 2000 Dec 11;19(53):6152-8.

Watanabe G, Albanese C, Lee RJ, Reutens A, Vairo G, Henglein B, Pestell RG. Inhibition of cyclin D1 kinase activity is associated with E2F-mediated inhibition of cyclin D1 promoter activity through E2F and Sp1. Mol Cell Biol. 1998 Jun;18(6):3212-22.

Watters D, Kedar P, Spring K, Bjorkman J, Chen P, Gatei M, Birrell G, Garrone B, Srinivasa P, Crane DI, Lavin MF. Localisation of a portion of extranuclear ATM to peroxisomes. J Biol Chem. 1999 Nov 26;274(48):34277-82.

Watters D, Khanna KK, Beamish H, Birrell G, Spring K, Kedar P, Gatei M, Stenzel D, Hobson K, Kozlov S, Zhang N, Farrell A, Ramsay J, Gatti R, Lavin M. Cellular localisation of the ataxia-telangiectasia (ATM) gene product and discrimination between mutated and normal forms. Oncogene. 1997 Apr 24;14(16):1911-21.

Westphal CH, Rowan S, Schmaltz C, Elson A, Fisher DE, Leder P. atm and P53 cooperate in apoptosis and suppression of tumorigenesis, but not in resistance to acute radiation toxicity. Nat Genet. 1997 Aug;16(4):397-401.

Williams RS, Williams JS, Tainer JA. Mre11-Rad50-Nbs1 is a keystone complex connecting DNA repair machinery, double-strand break signaling, and the chromatin template. Biochem Cell Biol. 2007 Aug;85(4):509-20.

Wu X, Levine AJ. P53 and E2F-1 cooperate to mediate apoptosis. Proc Natl Acad Sci U S A. 1994 Apr 26;91(9):3602-6.

Xu B, Kim St, Kastan MB. Involvement of BRCA1 in S-phase and G(2)-phase checkpoints after ionizing irradiation. Mol Cell Biol. 2001 May;21(10):3445-50. PubMed PMID: 11313470;

Xu B, O'Donnell AH, Kim ST, Kastan MB. Phosphorylation of serine 1387 in BRCA1 is specifically required for the Atm-mediated S-phase checkpoint after ionizing irradiation. Cancer Res. 2002 Aug 15;62(16):4588-91.

Xu Y, Baltimore D. Dual roles of ATM in the cellular response to radiation and in cell growth control. Genes Dev. 1996 Oct 1;10(19):2401-10.

Yang DQ, Kastan MB. Participation of ATM in insulin signalling through phosphorylation of eIF-4E-binding protein 1. Nat Cell Biol. 2000 Dec;2(12):893-8.

Yang H, Jeffrey PD, Miller J, Kinnucan E, Sun Y, Thoma NH, Zheng N, Chen PL, Lee WH, Pavletich NP. BRCA2 function in DNA binding and recombination from a BRCA2-DSS1-ssDNA structure. Science. 2002 Sep 13;297(5588):1837-48.

Yoo S, Dynan WS. Geometry of a complex formed by double strand break repair proteins at a single DNA end: recruitment of DNA-PKcs induces inward translocation of Ku protein. Nucleic Acids Res. 1999 Dec 15;27(24):4679-86.

Young DB, Jonnalagadda J, Gatei M, Jans DA, Meyn S, Khanna KK. Identification of domains of ataxia-telangiectasia mutated required for nuclear localisation and chromatin association. J Biol Chem. 2005 Jul 29;280(30):27587-94.

Zabludoff SD, Deng C, Grondine MR, Sheehy AM, Ashwell S, Caleb BL, Green S, Haye HR, Horn CL, Janetka JW, Liu D, Mouchet E, Ready S, Rosenthal JL, Queva C, Schwartz GK, Taylor KJ, Tse AN, Walker GE, White AM. AZD7762, a novel checkpoint kinase inhibitor, drives checkpoint abrogation and potentiates DNA-targeted therapies. Mol Cancer Ther. 2008 Sep;7(9):2955-66.

Zhang H, Somasundaram K, Peng Y, Tian H, Zhang H, Bi D, Weber BL, El-Deiry WS. BRCA1 physically associates with P53 and stimulates its transcriptional activity. Oncogene. 1998 Apr 2;16(13):1713-21.

Zhang L, Tie Y, Tian C, Xing G, Song Y, Zhu Y, Sun Z, He F. CKIP-1 recruits nuclear ATM partially to the plasma membrane through interaction with ATM. Cell Signal. 2006 Sep;18(9):1386-95.

Zhao Y, Chaiswing L, Velez JM, Batinic-Haberle I, Colburn NH, Oberley TD, St Clair DK. P53 translocation to mitochondria precedes its nuclear translocation and targets mitochondrial oxidative defense protein-manganese superoxide dismutase. Cancer Res. 2005 May 1;65(9):3745-50.

Zhao Y, Thomas HD, Batey MA, Cowell IG, Richardson CJ, Griffin RJ, Calvert AH, Newell DR, Smith GC, Curtin NJ. 2006. Preclinical evaluation of a potent novel DNA-dependent protein kinase inhibitor NU7441. Cancer Res. 15, 66(10):5354-62.

hu JW, DeRyckere D, Li FX, Wan YY, DeGregori J. A role for E2F1 in the induction of ARF, P53, and apoptosis during thymic negative selection. Cell Growth Differ. 1999 Dec;10(12):829-38.

Ziv Y, Bar-Shira A, Pecker I, Russell P, Jorgensen TJ, Tsarfati I, Shiloh Y. Recombinant ATM protein complements the cellular A-T phenotype. Oncogene. 1997 Jul 10;15(2):159-67.

**Online Resources:**

ATM Figure 1.9 [Online]. Accessed from: http://traditional4fun.blogspot.com/2008/07/ataxia-telangiectasia-information.html. Date accessed: 1st Jan, 2012.

BLAST [Online]. Accessed from: http://blast.ncbi.nlm.nih.gov/Blast.cgi. Date accessed: 23rd Nov, 2011.

DNA sequencing service [Online]. Accessed from: www.dnaseq.co.uk. Date accessed: 12th Aug, 2011.

EMBL [Online]. Accessed from: http://www.ebi.ac.uk/embl/. Date accessed: 17th Nov, 2011.

Ensembl [Online]. Accessed from: http://www.ensembl.org/index.html. Date accessed : 16th Nov, 2011.

Expasy [Online]. Accessed from: http://expasy.org/. Date accessed: 21st Dec, 2011.

IDT oligoanalyzer [Online]. Accessed from: http://eu.idtdna.com/analyzer/applications/oligoanalyzer/. Date accessed: 16th Nov, 2011.

ImajeJ [Online]. Accessed from: http://imagej.nih.gov/ij/. Date accessed: 29th Nov, 2011.

NCBI [Online]. Accessed from: http://www.ncbi.nlm.nih.gov/. Date accessed: 16th Nov, 2011.

NEB cutter [Online]. Accessed from: http://tools.neb.com/NEBcutter2/. Date accessed: 1st Nov, 2011.

Reverse and complementation [Online]. Accessed from: http://www.bioinformatics.org/sms/rev_comp.html. Date accessed: 22nd Dec, 2011.

Uniprot [Online]. Accessed from: http://www.uniprot.org/. Date accessed: 1st Dec, 2011.

# Chapter Nine

# Appendices

Someone's boring me. I think it's me.

Dylan Thomas, Poet, (1914 - 1953).

# APPENDIX-I Additional DATA

## A1. 1 ATM promoter cloning:

### A1.1.1 Isolation of Genomic DNA from Buccal swabs

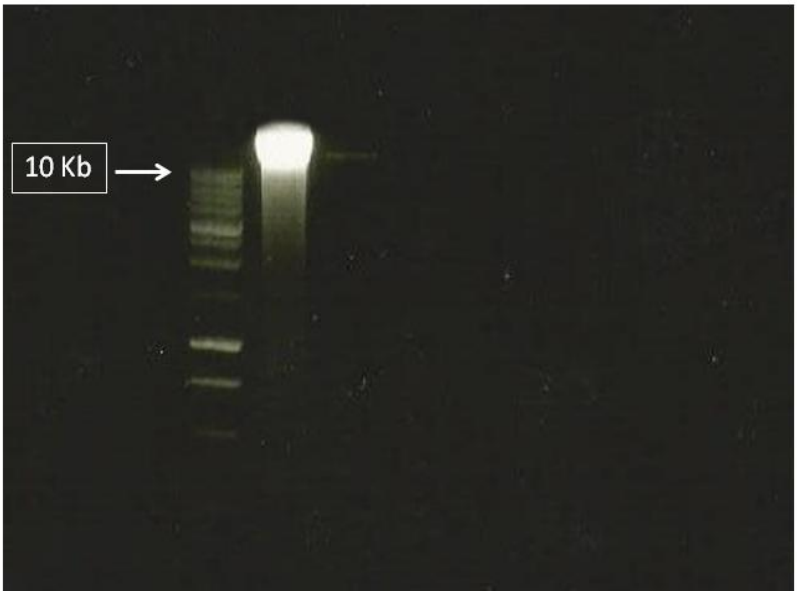


**Figure A1.1: Isolated Genomic DNA from buccal swabs**. 10µL of the isolated genomic DNA was run on 1% agarose gel along with 1Kb DNA ladder (Qiagen) to check for its integrity.

### A1.1.2 Quantification of isolated genomic DNA and determination of its purity.

Table A1: Absorbance of isolated DNA at 260 and 280nm.

| Absorbance at 260nm | Absorbance at 280nm |
|---|---|
| 0.012 | 0.008 |
| 0.011 | 0.011 |
| 0.025 | 0.006 |
| 0.016 | 0.008333 |
| 0.02 | 0.009 |
| **Mean= 0.0168** | **Mean = 0.00846** |

**0.0168 x 50µg/mL x 50 (dil. Factor) = 42µg/mL DNA. Purity: 0.0168/.00846 = 1.98**

### A1.1.3 Promoter sequence and *cis*-regulatory elements

5-
GCTTCCCTACCAAGGGAAAACCTTTGGCCTCAAAGGTCCTTCTGTCCAGCATAGCCGGGTCCAATAA
CCCTCCATCCCGCGTCCGCGCTTACCCAATACAAGCCGGGCTACGTCCGAGGGTAACAACATGATCA
AAACCACAGCAGGAACCACAATAAGGAACAAGACTCAGGTTAAAGCAAACACAGCGACAGCTCCTGC
GCCGCATCTCCTGGTTCCAGTGGCGGCACTGAACTCGCGGCAATTTGTCCCGCCTCTTTCGCTTCAC
GGCAGCCAATCGCTTCCGCCAGAGAAAGAAAGGCGCCGAAATGAAACCCGCCTCCGTTCGCCTTCGG
AACTGTCGTCACTTCCGTCCTCAGACTTGGAGGGGCGGGGATGAGGAGGGCGGGGAGGACGACGAGG
GCGAAGAGGGTGGGTGAGAGCC-3

SP1 sites

cAMP responsive element

CAAT boxes

Insulin responsive element

(Byrde JP et al., 1996)

### A1.1.4 Primer Sequences for promoter amplification:

**Forward primer: $F_X$**

5′-CCGCTCGAGCGG GCTTCCCTACCAAGGGAAAACC-3′(XhoI restriction site)

**Reverse primers: $R_N$**

5′-CATGCCAT GGCTCTCACCCACCCTCTTC-3′(Nco-I restriction site)

**Reverse primer: $R_H$**

5′-CCGAAGCTT GGCTCTCACCCACCCTCTTC-3′(HindIII restriction site)

### A1.1.5 PCR conditions for ATM promoter amplification

Initial Denaturation.....95°C for 2 min

Denaturation.....95°C for 0.5 min

Primer Annealing.....55°C for 0.5 min

Extension.....72°C for 1 min

35 Cycles

Final extension.....72°C for 5 min

### A1.1.6 PCR product of ATM promoter

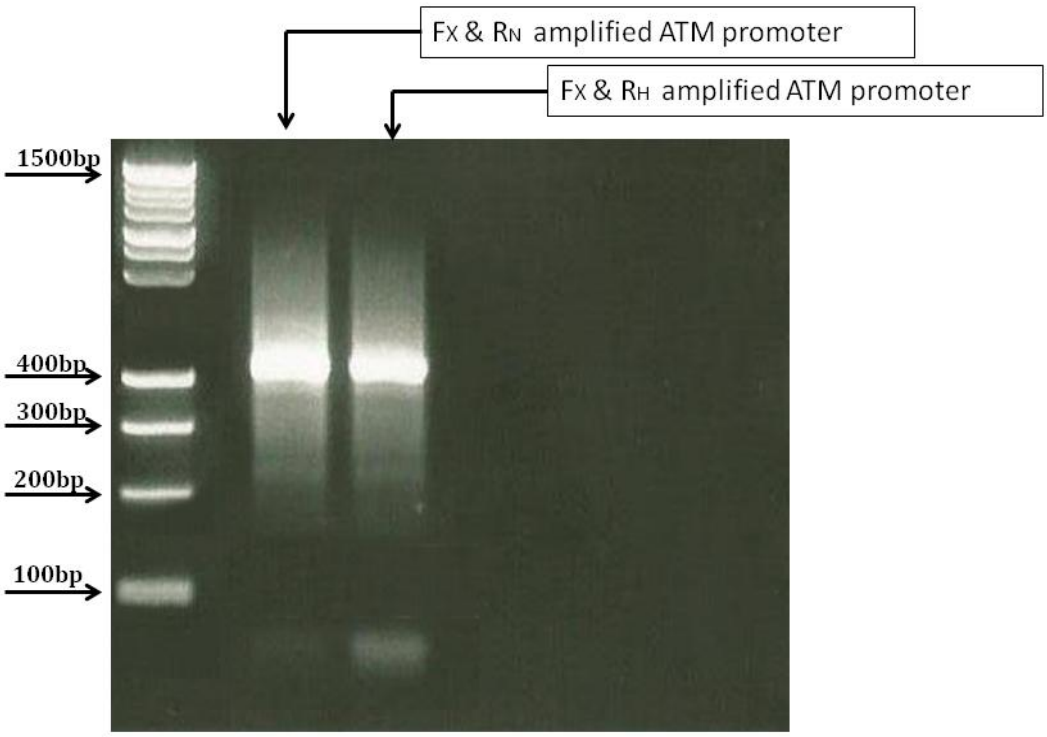


**Figure A1.2: PCR amplification of ATM promoter.** 10µL of PCR amplified products were run on 1% agarose gel along with 100bp plus DNA ladder (Qiagen).

### A1.1.7 Screening for ATMpr/PGL3 and ATMpr/PTimer constructs

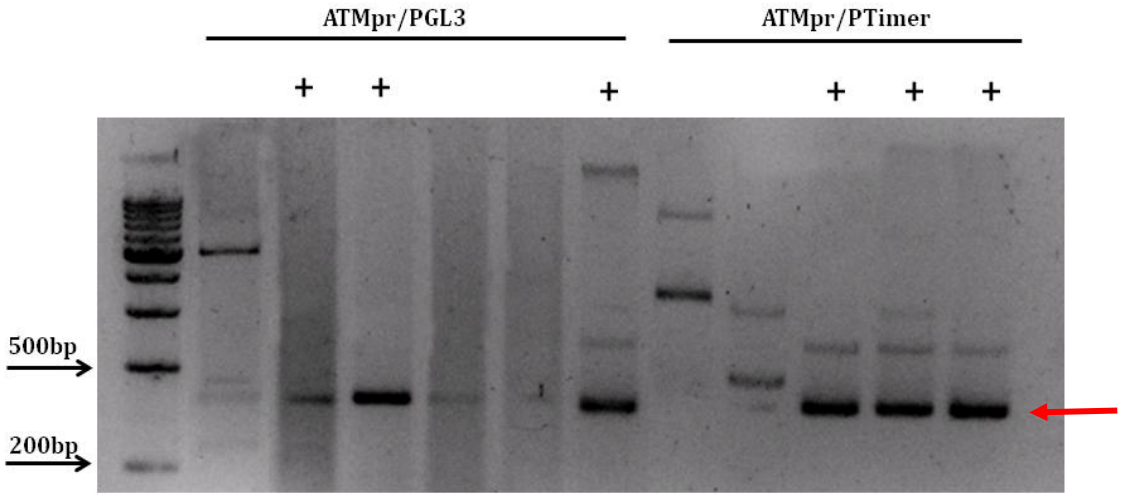


**Figure A1.3: Colony PCR of ATM promoter-reporter candidates**. PCR results from colonies grown on bacterial plates previously transformed with ATMpr/PGL3 and ATMpr/PTimer constructs. The products were run on 1% agarose gel along with a long range DNA ladder for size reference (Qiagen). Red arrow points towards bands of positive PCR results denoted by "+" on top. The expected positive clones were further subjected to Miniprep screening (Fig. A1.4).

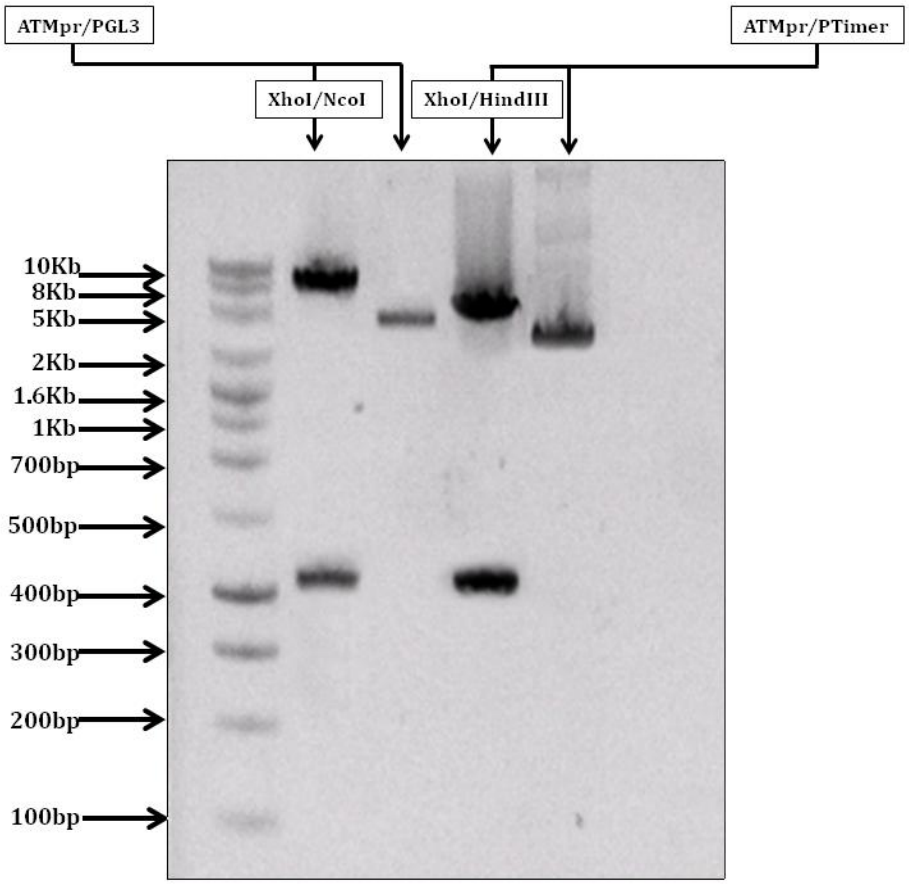


**Figure A1.4: Restriction digestion screening to identify positive clones of ATM promoter in Luciferase and Fluorescence reporter vectors.** Colonies that previously gave a positive Colony-PCR result, were picked up, grown overnight and their minipreps prepared. The Minipreps were subjected to restriction digestion to identify potential positive clones. XhoI and NcoI restriction digestion was used to screen for ATMpr/PGL3 while XhoI and HindIII digestion was used for ATMpr/PTimer screening. Size estimates of DNA bands were made by running a 1kb plus DNA ladder (Qiagen).

### A1. 1.8: DNA sequencing chromatogram of the positive clones of ATM promoter

The successful candidate clones from restriction digestion were sequenced using a commercial sequencing service (www.dnaseq.co.uk) to confirm the fidelity of cloned constructs.

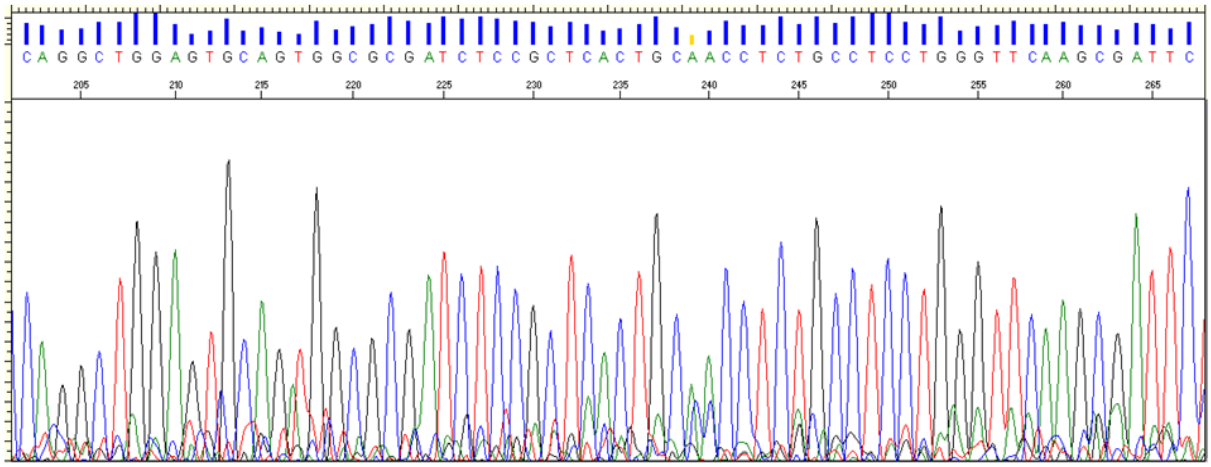


Sequences producing significant alignments:

| Accession | Description | Max score | Total score | Query coverage | E value | Max ident |
|---|---|---|---|---|---|---|
| NT_033899.8 | Homo sapiens chromosome 11 genomic contig, GRCh37.p5 Pri | 1264 | 1264 | 85% | 0.0 | 97% |
| NW_001838042.2 | Homo sapiens chromosome 11 genomic contig, alternate asse | 1264 | 1264 | 85% | 0.0 | 97% |

**Figure A1.5: DNA sequence chromatogram of ATMpr constructs.** Plasmid Minipreps of the clones giving positive result with restriction digestion screening were sent for DNA sequencing. The sequencing chromatogram using the promoter primers Fx and $R_N$/$R_H$ and the BLAST results confirmed the identity of the clones sequence.

## A1.2 Site Directed Mutagenesis of ATM

### A1.2.1: Examining the integrity and stability of RNA.

RNA was extracted for HaCaT cells in order to acquire cDNA for the subsequent cloning of human ATM and β-COPI.

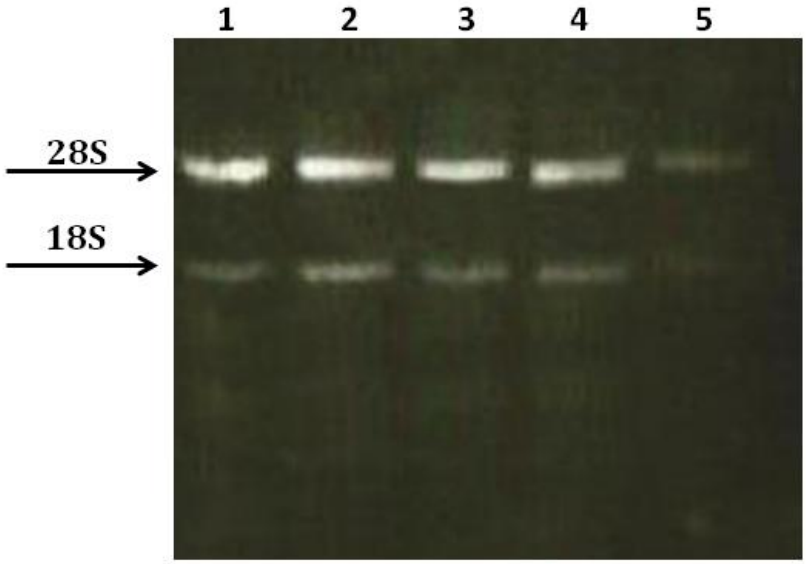


**Figure A1.6: Examining the integrity of extracted total RNA.** The RNA was extracted from 5 fully confluent HaCat cells and was run on 1% agarose gel to check for the appearance of two bands corresponding to the 28s and 18s subunits of ribosomal RNA.

### A1.2.2 Quantification of Extracted RNA and determination of its purity

**Table A2:** Absorbance of RNA at 260 and 280nm

| Absorbance at 260nm | Absorbance at 280nm |
|---|---|
| 0.302 | 0.147 |
| 0.250 | 0.133 |
| 0.293 | 0.136 |
| 0.311 | 0.156 |
| 0.290 | 0.144 |
| **Mean= 0.289** | **Mean=0.143** |

**0.289 x 44µg/mL x 50 (dil. Factor) = 635µg/mL. Purity = 0.289/0.143 = 2.02**

### A1.2.3 Primer sequences of YFP/GFP

Both the YFP and GFP containing plasmid vectors were previously obtained from Post Doc in my lab (Hemanth Tummala). The sequences of these tags were amplified by using specific primers that also introduced BamHI and NotI restriction sites at N-terminal and C-terminal sites respectively for their clonal manipulation. This allowed these tags to be cloned in PCDNA 3.1 vectors for the subsequent tagging of human genes. Primers used in these experiments were:

**Forward primer: FYFP:**

**5′ GGATCC ATGGTGAGCAAGGGCGAGGAGCTG 3′ (BamH1)**

**Reverse primer RYFP:**

**5′ CGCCGGCG CCTTGTACAGCTCGTCCATGCCGAG 3′ (Not I)**

### A1.2.4 PCR conditions for YFP/GFP amplification

Initial Denaturation.....95°C for 2 min

Denaturation.....95°C for 0.5 min

Primer Annealing.....58°C for 0.5 min

Extension.....72°C for 1 min

30 Cycles

Final extension.....72°C for 5 min

### A1.2.4 PCR product of YFP and GFP fluorescent tags

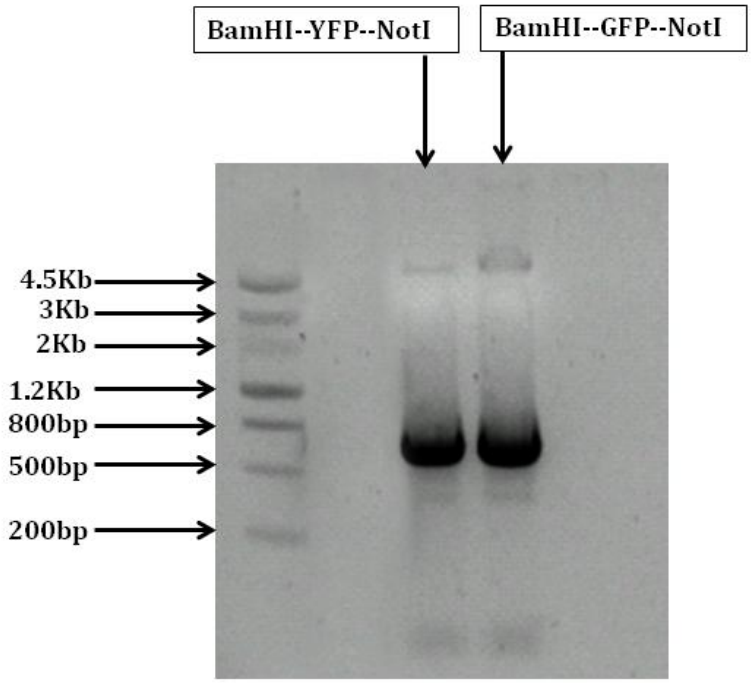


**Figure A1.7: PCR amplification of fluorescence genes.** YFP and GFP genes previously cloned in PCDNA 3.1 vector were amplified using primers with BamHI recognition sequence in forward primer and NotI recognition sequence in reverse primer for subsequent clonal manipulation. The products were run on 1% agarose gel along with Gelpilot Wide range DNA ladder (Qiagen) for size reference.

### A1.2.5 Screening for GFP-PCDNA3.1 and YFP PCDNA 3.1 constructs

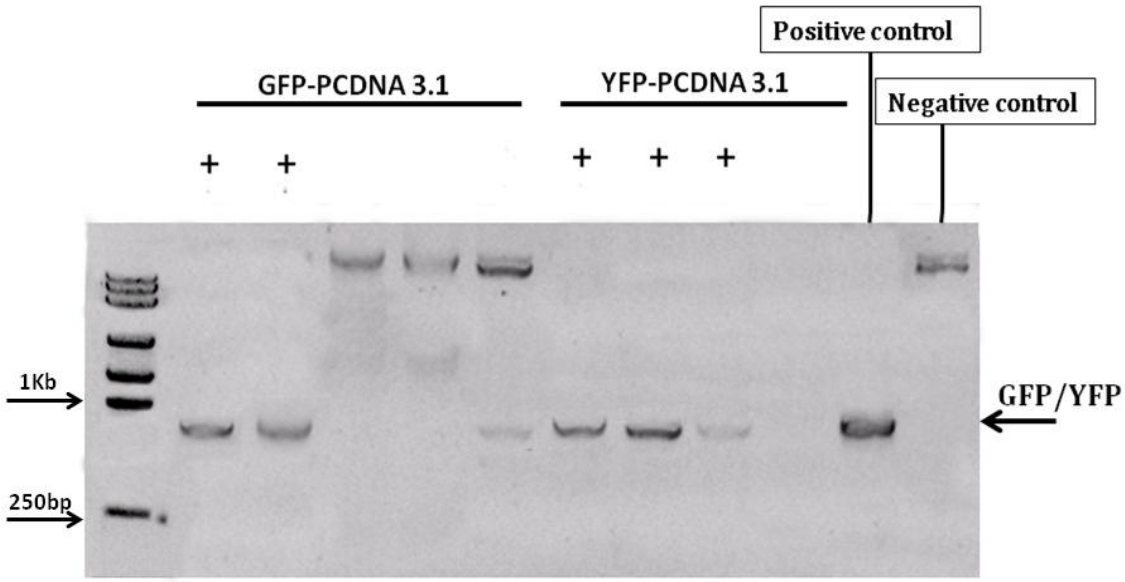

**Figure A1.8: Colony PCR of GFP and YFP-PCDNA3.1 candidate colonies**. PCR results from colonies grown on bacterial plates previously transformed with YFP-PCDNA 3.1 and GFP-PCDNA 3.1 constructs. The products were run on 1% agarose gel along with DNA ladder for size reference (Qiagen). A positive clone (previously transformed colony with YFP) and a negative control (empty PCDNA3.1 vector) were included for accurate interpretation of results. The "+" signs on top of each lane indicate positive clonal result.

### A1.2.6 N-terminally tagged YFP-ATM gene construct:

ATM was cloned into the PCDNA 3.1 vector carrying the above mentioned YFP gene, as generated above. The cloning procedure was performed by Post Doc in my lab (Dr. Hemanth Tummala). Briefly, the cDNA generated in the current research was subjected to amplification using ATM specific primers and was cloned C-terminal to the YFP tag demonstrated in sections A1.2.4-5 above, between Not1 and Xho1 sites. The maxipreps of the YFP-ATM constructs were used for further characterisation and experiments. For restriction screening of YFP-ATM constructs, XbaI digestion was carried out. XbaI digests Human ATM at 5 sites producing a particular banding pattern (0.5, 0.6, 0.8, 1.2, 4.4 and 6 kb bands) specific for ATM gene.

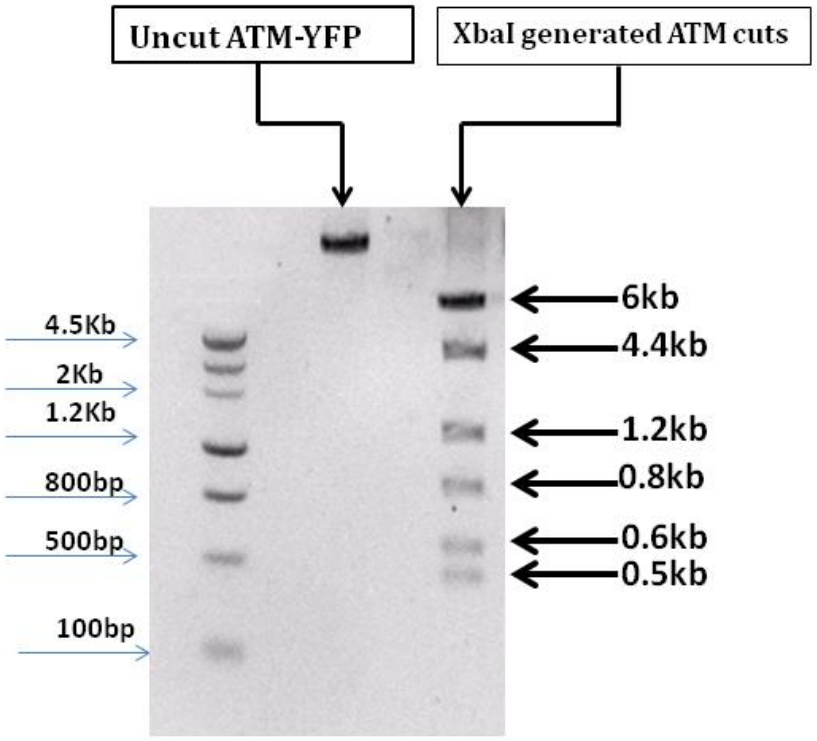


**Figure A1.9: XbaI screening of YFP-ATM**. The YFP-ATM construct was cloned, and the plasmid miniprep subjected to XbaI digestion and run on 0.5% agarose gel to reproduce the characteristic ATM banding pattern upon XbaI digestion. The black arrows indicate the digested ATM bands along with their expected sizes. A wide range DNA ladder (Qiagen) and uncut YFP-ATM (PCDNA3.1) was also run to provide reference.

It is noteworthy to mention that the restriction digestion screened YFP-ATM construct at this point was also transfected into cells and their lysates prepared and blotted using YFP antibody to confirm over expression of ATM (Fig. A1.7). Furthermore, YFP-ATM expressing cells were also observed under microscope to examine YFP-ATM fluorescence under DNA damaging and non damaging conditions (Fig. 5.30). Once the construct was confirmed to be fully functional, it was further used for the creation of mutated ATM kinase (385-KRKK→KRAA-388, $ATM_{MUT}$).

### A1.2.6 Sequences of primers for site directed mutagenesis (SDM) of ATM to generate $ATM_{mut.}$

To carryout site directed mutagenesis of ATM, specific primers were designed with set criteria. First of all, the primers were designed in such a way that both forward and reverse primers overlapped the same sequence on opposite stands. Secondly, apart from incorporating the desired mutated nucleotides (changing dilysines to dialanines), these primers were also made to incorporate a unique restriction endonuclease recognition site for the purpose of screening. The sequences of these primers are listed below.

**Forward primer $F_{MUT}$**

5′- GTC CCT TGC AAA AGG GGC GCC ATA GAA CTA GGC TGG G-‘3

**Reverse primer $R_{MUT}$**

5′- GTC CCT TGC AAA AGG GGC GCG ATC GAA CTA GGC TGG G-‘3

The highlighted nucleotides incorporated the desired mutation and a PvuI restriction endonuclease site.

### A1.2.7 PCR conditions for site directed mutagenesis of ATM to generate $ATM_{mut}$

Hot start.....98°C

Initial denaturation.....95°C, for 5 min

Denaturation.....95°C for 30 seconds

Annealing.....58°C for 30 seconds

Extension.....66°C for 15 min

18 cycles

Final Extension .....72°C for 15 min

### A1.2.8 Restriction digestion screening of site directed mutagenesis product of ATM.

After completing site directed mutagenesis for generating $ATM_{MUT}$ constructs, Minipreps from the emerging colonies (after Dpn 1 digestion and transformation) were first of all subjected to Xba-1 digestion. If PCR amplification during the process of site directed mutagenesis was successful, it would have amplified the full length ATM with its YFP tag and hence, the resulting banding pattern would be similar to the one generated after YFP-ATM digestion (Fig. A1.9). To find this out, XbaI digestion was performed on SDM product of ATM. Fig. A1.10 revealed that the banding pattern of one of the clones was similar to the characteristic ATM banding after digestion.

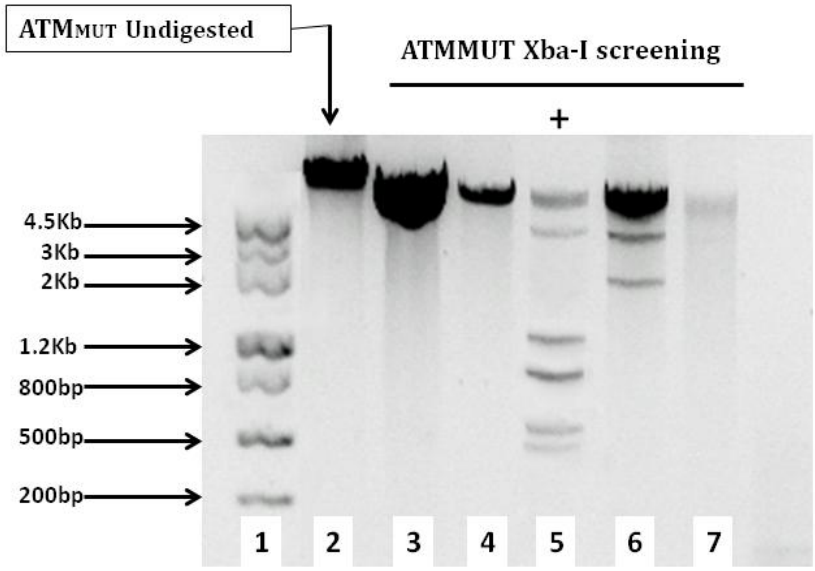


**Figure A1.10: XbaI screening of $ATM_{mut}$.** The product of SDM of ATM was transformed and the Minipreps of the grown colonies were subjected XbaI screening and the products run on 0.5% agarose gel. Lane 1 has a wide range DNA ladder (Qiagen), lane 2 has an uncut miniprep of $ATM_{MUT,}$ while lane 5 (with a "+" sign) produced the exact banding order with XbaI digestion that is characteristic of YFP-ATM cloned in PCDNA 3.1.

**A1. 2.7: DNA sequencing chromatogram of the $ATM_{MUT}$ containing construct.**

After completing site directed mutagenesis for generating $ATM_{MUT}$ construct, Minipreps from the emerging colonies (after Dpn 1 digestion and transformation) were sent to commercial DNA sequencing service (www.DNAseq.co.uk) to confirm the identity and fidelity of the successfully cloned and mutated ATM construct.

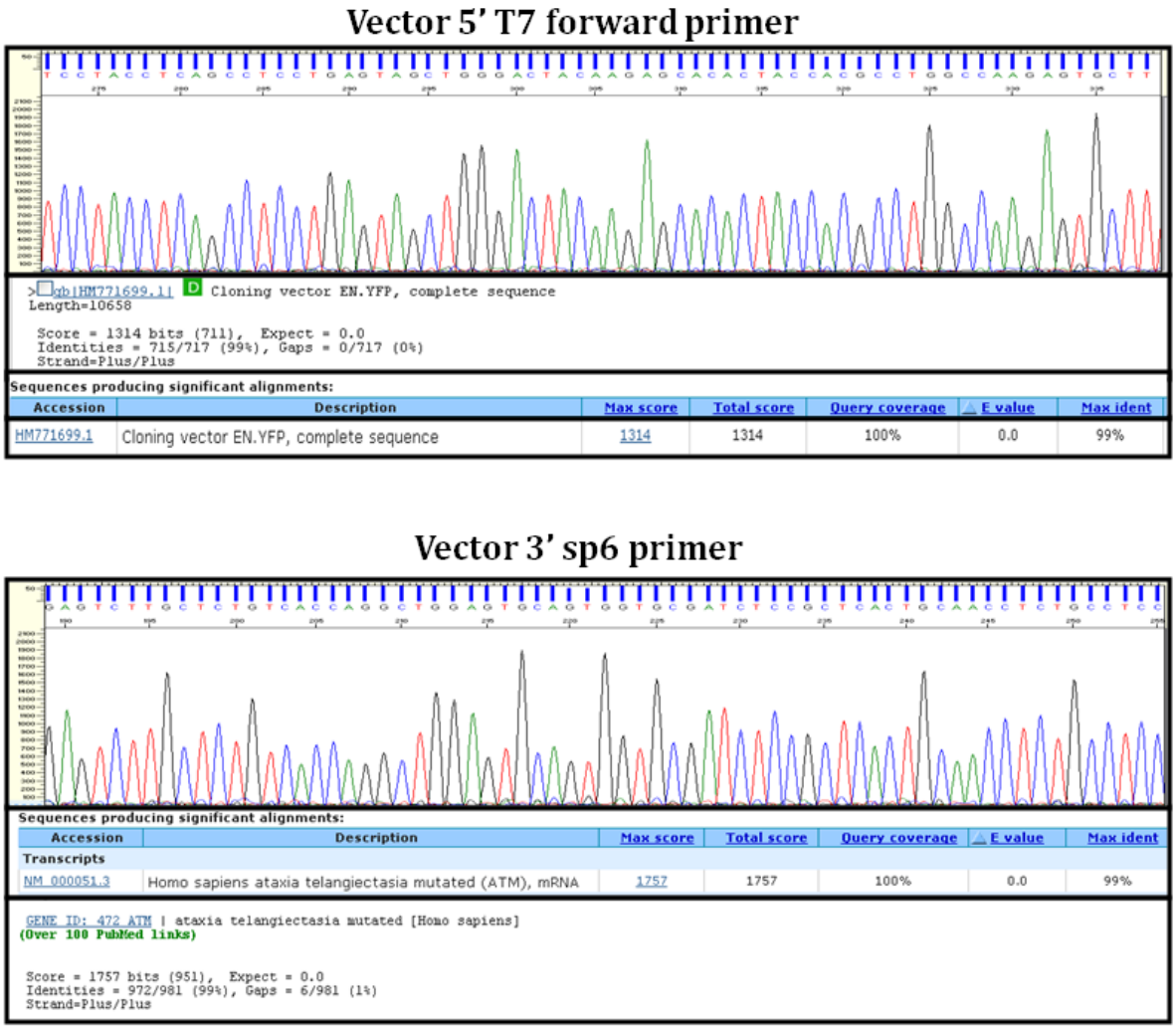


**Figure A1.11: DNA sequencing chromatogram of ATMmut construct.** Plasmid Minipreps of the clones that gave positive results for restriction digestion were sent for DNA sequencing using the vector based $T_7$ and sp6 primers. The DNA sequence chromatogram and the BLAST results confirmed the identity of the SDM construct as YFP-ATM in PCDNA3.1.

### A1.2.8 SDM specific restriction screening of $ATM_{mut}$ constructs

While Figures A1.10 and A1.11 illustrated the successful amplification of YFP-ATM during the process of SDM, which should have resulted in the generation of the mutant ATM, I next wanted to confirm whether the desired mutation within the ATM sequence had been incorporated. To answer this, ATM mutation specific restriction digestion was carried out by employing Pvu-I endonuclease digestion. Figure A1.11 demonstrated the successfully incorporation of mutation within ATM sequence as Pvu-I digestion gave an additional band of expected size in the mutated ATM while the non-mutated did not.

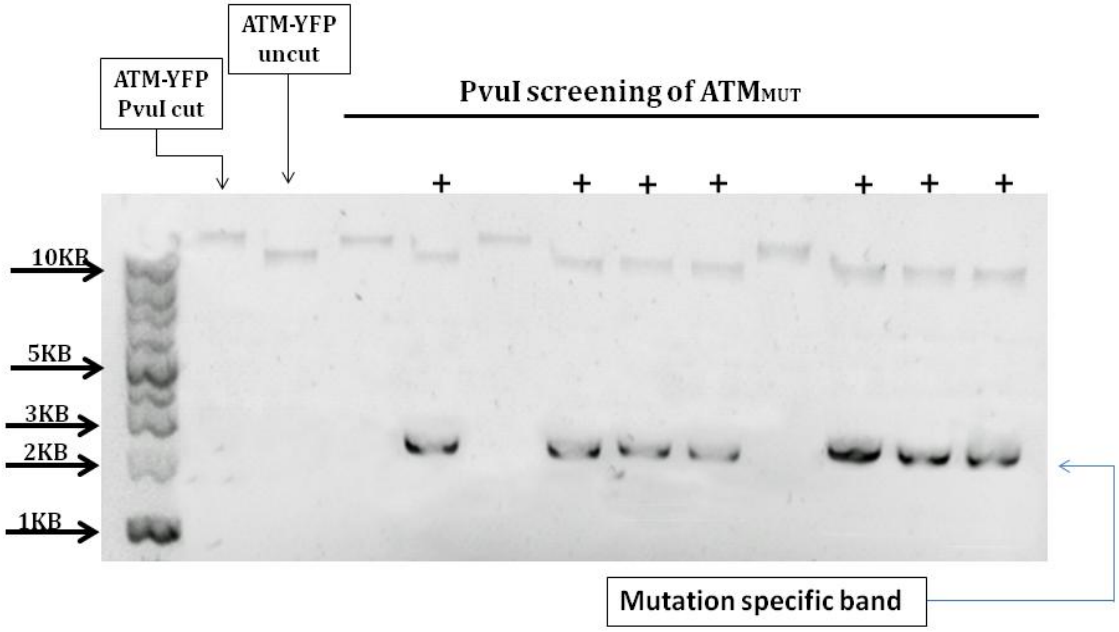


**Figure A1.12: Restriction digestion screening of $ATM_{MUT}$.** The product of site directed mutagenesis was subjected to PvuI restriction digestion and run on 0.5% agarose gel to examine if the ATM had been mutated and hence incorporated additional restriction site. The "+" signs indicate positive clonal results which produced an additional band at 2.5Kb while the negative clones, which did not undergo mutation, and hence did not incorporate the PvuI site were only linearized without producing the characteristic 2.5Kb band. Wild type ATM tagged with YFP was also subjected to PvuI digestion and run on agarose gel along with the other samples. As expected, wild type YFP-ATM vector only linearized after digestion without producing the digestion specific band. For size reference, 1Kb DNA ladder (Qiagen) was also run.

### A1.3 Cloning of β-COPI and tagging it with GFP

In order to perform ATM trafficking studies, β-COP subunit of COPI coatomer protein was cloned and tagged with YFP in PCDNA 3.1 vector (Invitrogen). The RNA extracted earlier in the current research (A1.2.1) was used to create cDNA and using β-COPI specific primers, β-COPI was amplified with the incorporation of Not-I restriction site on N-terminal while XhoI restriction site on C-terminal for clonal manipulation.

#### A1.3.1 Primer sequences for β-COPI

**Forward primer $F_N$**

**5′-GCGCGGCCGC ATGACGGCGGCTGAGAACG-‘3 (NotI restriction site)**

**Reverse primer $R_X$**

**5′-CCGCTCGAGCGG CTATTATATACTAGTTTTCTTCTGTGAC-‘3**

**(XhoI restriction site)**

#### A1.3.2 PCR conditions for β-COPI amplification:

Initial denaturation.....95°C, for 2 min

Denaturation.....95°C for 30 seconds

Annealing (Gradient).....50-58°C for 30 seconds

Extention.....72°C for 3 min

30 cycles

Final Extention .....72°C for 10 min

### A1.3.3 PCR product of β-COPI:

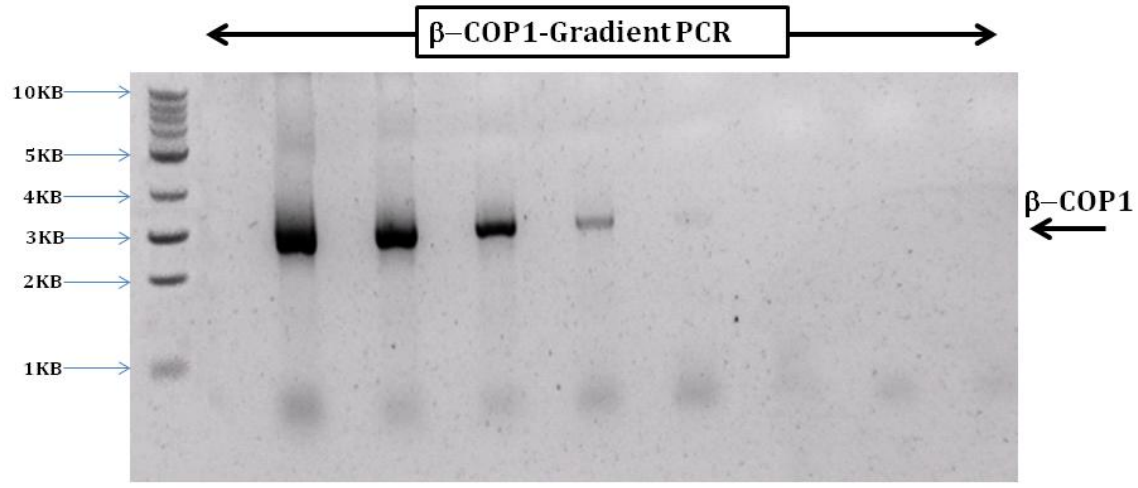


**Figure A1.13: Gradient PCR of β-COPI gene.** The β-COPI gene was amplified by primers listed in A1.3.1 that also incorporated the restriction sites for its clonal manipulation. The products were run on 1% agarose gel. A 1Kb DNA ladder (Qiagen) was also run to provide a size reference.

### A1.3.4 N-terminal GFP tagging of human β-COPI gene

The PCR product of β-COPI (Fig. A.1.13) was subjected to restriction digestion (Not-I and XhoI) for its clonal manipulation. The vector PCDNA3.1 carrying the GFP tag between BamHI and Not-I sites (established in section A1.2.4-A1.2.5) was linearized with Not-I and XhoI restriction endonucleases and the digested PCR product of β-COPI (Not-I and XhoI) was cloned into it. Screening of the successfully cloned constructs was performed by both colony PCR and restriction digestion.

### A1.3.5 Colony PCR of β-COPI to screen for successfully cloned GFP-βCOPI (PCDNA3.1) constructs.

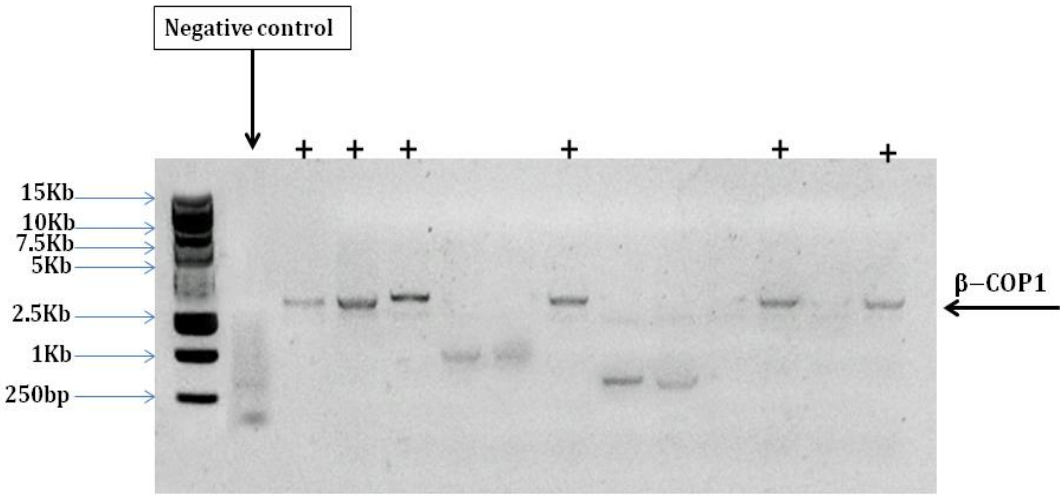


**Figure A1.14: Colony PCR to screen for successfully cloned β-COPI constructs.** PCR results from colonies grown on bacterial plates previously transformed with GFP-β-COPI (PCDNA 3.1) candidate constructs to screen for positive hits. The products were run on 1% agarose gel and a negative control (PCNDNA 3.1) was also included. A high range DNA ladder (Qiagen) was also run for providing size reference for DNA bands. The "+" signs indicate positive clonal results.

### A1.3.6 Restriction digestion screening for GFP-β-COPI constructs

The successful clones from the colony PCR were then subjected to restriction endonuclease digestion with Not-I and XhoI to confirm that the cloned β-COPI bands are reproduced from the GFP-βCOPI (PCDNA 3.1) constructs.

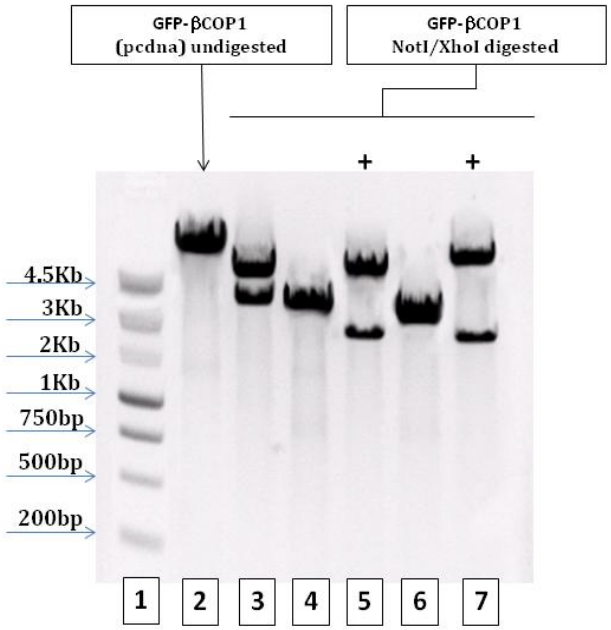


**Figure A1.15: Restriction screening for GFP-βCOPI (PCDNA 3.1) constructs.** Minipreps of bacterial colonies that gave positive colony PCR result for β-COPI cloning were further verified by restriction digestion screening with NotI and XhoI. Samples were run on 1% agarose gel with a wide range DNA ladder (Qiagen) in lane 1. An undigested GFP-βCOPI (PCDNA 3.1) was also included (lane 2). The "+" signs in lanes 5 and 7 indicate positive restriction screening results for β-COPI cloning.

### A1.3.6 DNA sequencing chromatogram of the GFP-βCOPI containing construct.

After the successful colony PCR and restriction screening result for GFP tagged βCOPI gene cloned in PCDNA 3.1, Minipreps from the successful clones were sent to commercial DNA sequencing service (www.DNAseq.co.uk) to confirm the identity and fidelity of the cloned construct.

Vector 5' T7 forward primer

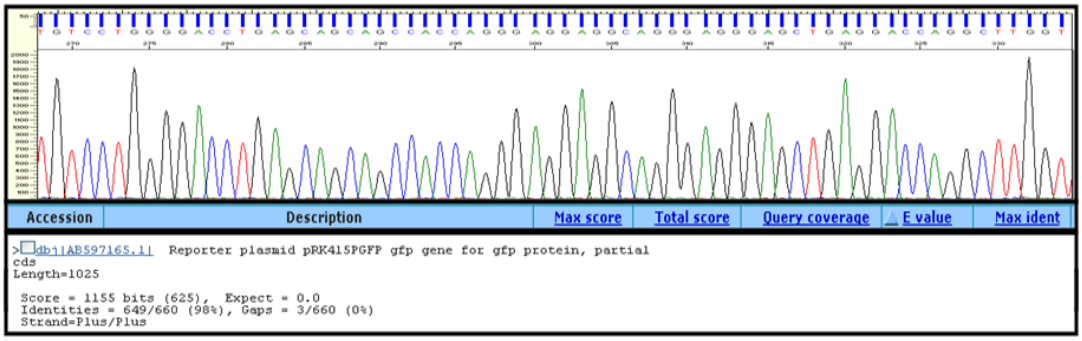


Vector 3' SP6 forward primer

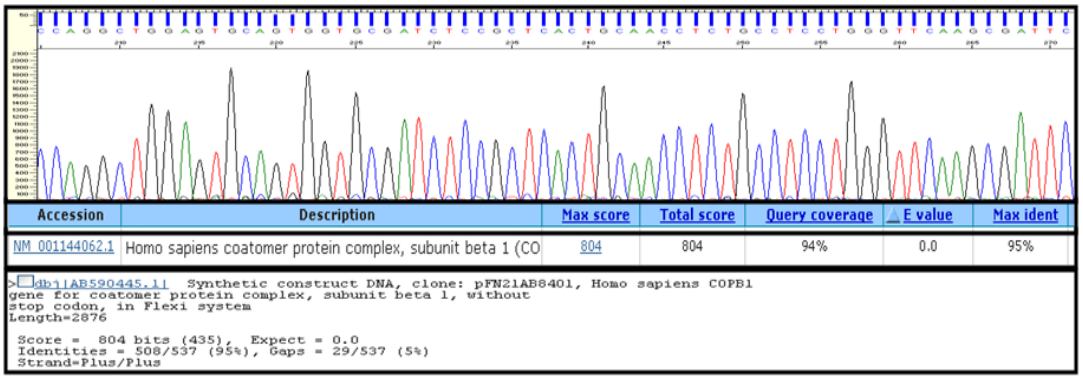


**Figure A1.16: β-COPI DNA sequencing chromatogram.** Plasmid Minipreps of the clones that gave positive results for restriction digestion were sent for DNA sequencing using the vector based $T_7$ and sp6 primers. The DNA sequence chromatogram and the BLAST results confirmed the identity of the construct as β-COPI tagged N-terminally with GFP in PCDNA3.1 vector.

## A1.4 Optimization of fluorescence detection based WesternDot$^{TM}$ kit for Immuno Blotting

In the current research study, WesternDot$^{TM}$ kit was used for immuno blotting analysis of proteins of interest. This new protein detection system of western blotting employs fluorescence based detection via the use of streptavidine. Since this system was introduced for the first time in my lab, I sought to optimize this technique first, prior to performing experiments. While optimization was performed with a number of primary antibodies, data only acquired for difficult to detect, ATM protein is presented. Table A1.3 lists the different conditions employed to find the best combination of different variables in immuno blotting via WesternDot$^{TM}$.

**Table A3:** Different conditions and reagents tested for optimization of WesternDot$^{TM}$ kit.

| Code | Primary antibody (dilution 1 in 1000) | Primary antibody diluting agent | Primary antibody incubation | Membrane Blocking agent | Blocking incubation |
|---|---|---|---|---|---|
| **1** | Total ATM | BSA | 1 hour | BSA | Overnight |
| **2** | Total ATM | Milk | 1 hour | BSA | Overnght |
| **3** | Total ATM | Commercially available | 1 hour | BSA | Overnight |
| **4** | Total ATM | PBS | 1 hour | BSA | Overnight |
| **5** | Reused total ATM | BSA | 1 hour | BSA | Overnight |
| **6** | Total ATM | BSA | 1 hour | Milk | Overnight |
| **7** | Total ATM | Milk | 1 hour | Milk | Overnight |
| **8** | Total ATM | BSA | Overnight | Milk | 1 hour |
| **9** | Total ATM | Milk | Overnight | BSA | 1 hour |
| **10** | Total ATM | Commercially available | Overnight | BSA | 1 hour |
| **11** | Total ATM | PBS | Overnight | BSA | 1 hour |
| **12** | Reused Total ATM | BSA | Overnight | BSA | 1 hour |
| **13** | Total ATM | BSA | Overnight | BSA | 1 hour |
| **14** | Total ATM | Milk | Overnight | Milk | 1hour |

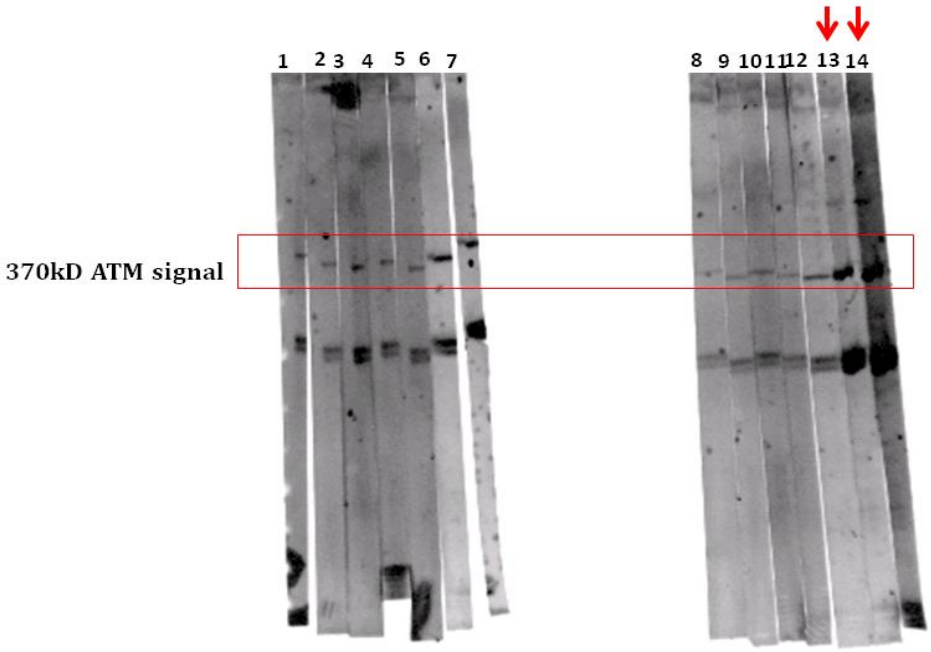


**Figure A1.17: Optimization of conditions and reagents for WesternDot™ kit.** Numbers on top of nitrocellulose membrane strips indicate codes as set out in table A1.3. Red square corresponds to a region of 370kD where ATM detection is expected while red arrows on top of the strips indicate optimum signals. 20µg of protein lysates collected from HaCat cells were loaded into 4-12% precast gels (Novex® Nupage, Invitrogen) and blotted on nitrocellulose membrane, the protein lanes visualized by ponceau stain, individual lanes cut out and separately blotted for total ATM using different conditions and reagents as set out in table A1.3. Test conditions corresponding to code 13 and 14 gave an ATM band and hence were used during experiments.

Once the optimal detection conditions for WesternDot™ kit were found, I next set out to determine the optimum dilutions for the primary antibodies employed in the current study. Table A1.4 lists the dilutions while Fig. A1.16 shows the resulting western blot signal of total ATM.

**Table A4 Antibody dilutions:**

| S no. | Primary antibody | Blocking agent | Dilution |
|---|---|---|---|
| **1** | Total ATM | BSA | 1 in 250 |
| **2** | Total ATM | BSA | 1 in 500 |
| **3** | Total ATM | BSA | 1 in 2500 |
| **4** | Total ATM | BSA | 1 in 5000 |
| **5** | Total ATM | BSA | 1 in 10,000 |

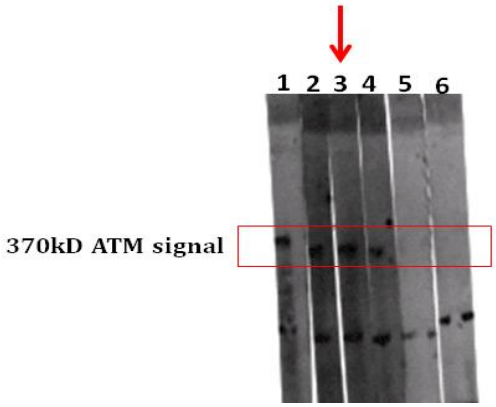


**Figure A1.18: Optimization of total ATM antibody dilution for WesternDot™ kit.** Numbers on top of nitrocellulose membrane strips indicate codes as set out in table A1.4. Red square corresponds to a region of 370kD where ATM detection is expected while red arrow on top of the strips indicates the optimum condition for signal. 20µg of protein lysates collected from HaCat cells were loaded into 4-12% precast gels (Novex® Nupage, Invitrogen) and blotted on nitrocellulose membrane, the protein lanes visualized by ponceau stain, individual lanes cut out and separately blotted for total ATM using different dilutions as set out in table A1.4. Test conditions corresponding to code 3gave an ATM band and hence were used during experiments.

## A1.5 Optimization of Electroporation programs and over-expressing YFP-ATM in HaCat cells

To carryout electroporation, the electroporation parameters were first optimized to achieve maximum transfection. The electroporator in my lab (Easyject, Equibio, Kent, UK) had a number of predefined electroporation programs. However, to examine the optimum parameters for transfection into HaCat cells, which are generally thought to be difficult to transfect, I first set out to do series of transfections with each program. The N-terminally tagged YFP-ATM construct cloned in PCDNA 3.1 was used (10µg) to transfect HaCat cells with different electroporation parameters.

The transfected cells were grown in 100mm tissue culture plates, allowed 48 hrs to express and lysates prepared as mentioned in materials and methods. 10µg of the lysates were run 4.-12% precast gels for SDS PAGE, transferred to nitrocellulose membrane and blotted using YFP antibody.

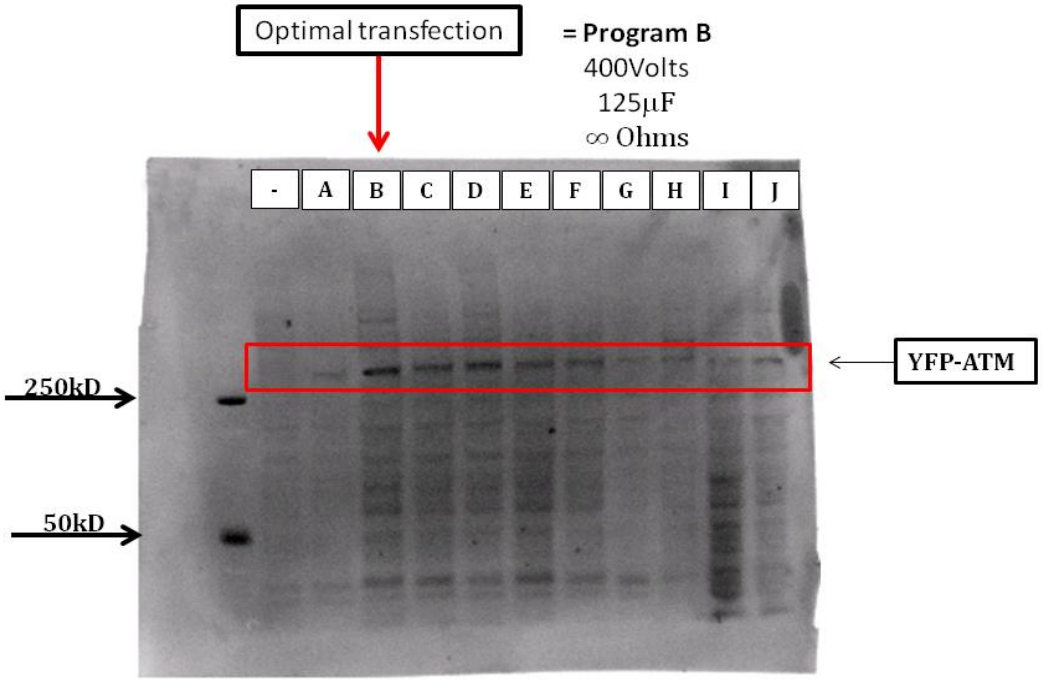


**Figure A1.19: Optimization of parameters for electroporation protocol via YFP-ATM (PCDNA 3.1) transfection**. A-J denote the inbuilt transfection programs each with different parameter sets for electroporation. 10µg of protein lysate, derived from HaCat cells transfected previously with 10µg of YFP-ATM 48 hr before, were loaded in each well of precast SDS PAGE gels, transferred onto nitrocellulose and blotted for YFP expression. The YFP signal, obtained above the 250kD protein ladder is enclosed in red triangle and is shown to be maximum with program B of electroporation, whose parameters are listed in the figure. All the subsequent mammalian cell electroporations were performed with program B.

### A1.6 HPLC data

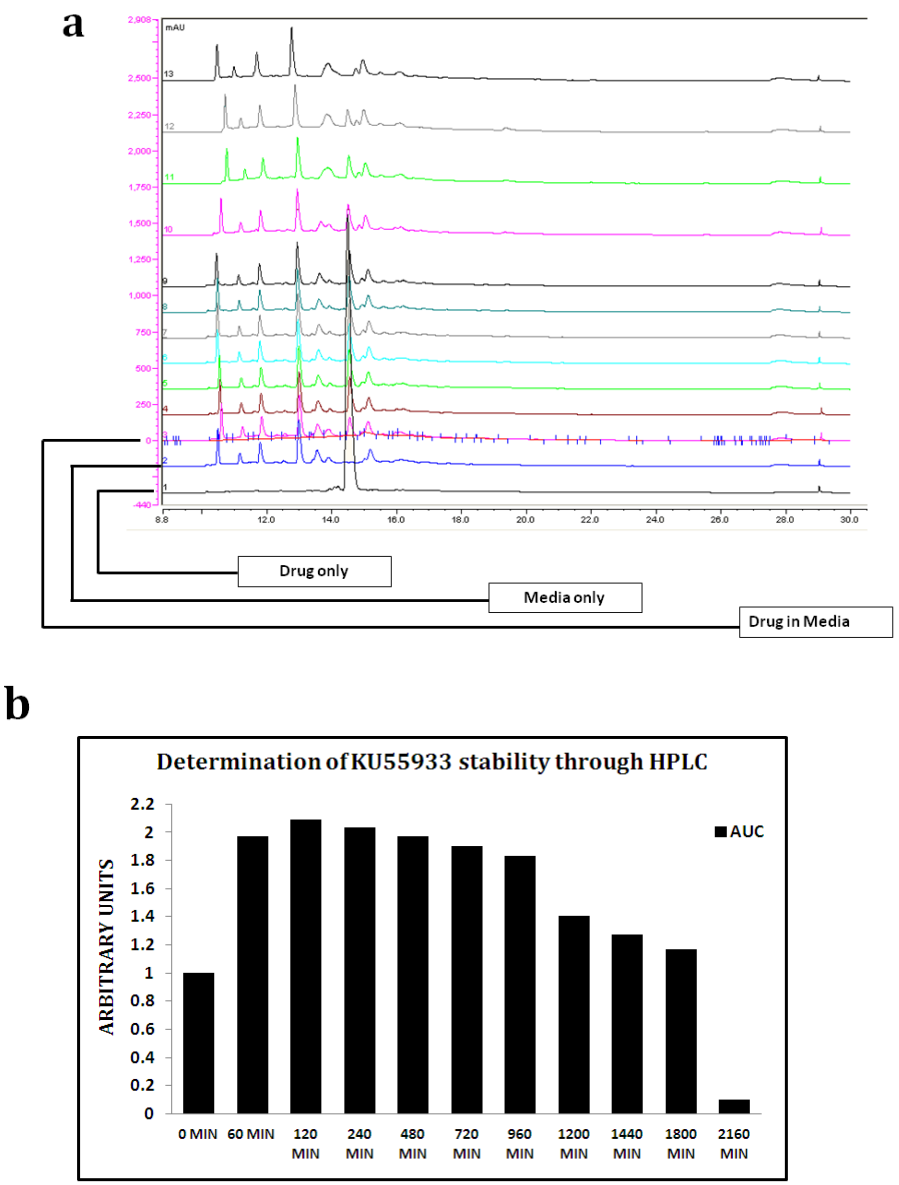


**Figure A1.20: HPLC data for determining KU stability in cell culture media.** **(a)** shows the KU peak at different time points ranging from time 0 to 2160min covering the entire range of time for which this drug was used in the current study. Peaks from the drug only sample and the media only sample were compared to identify the drug peak. **(B)** Stability of the drug was determined by quantifying Area under curve (AUC) for the identified drug peak at different time points.

### A1.7 Bradford assay

The standard protein concentration curve for Bradford assay was established by using a standard protein Bovine Serum Albumin (BSA). The stock was at a concentration of 2mg/mL and was diluted to produce varying concentrations, carrying out Bradford assay and plotting the standard graph. The dilutions were made as shown in the Table 9.1.

**Table A6:** Dilution of the standard protein.

| 2mg/mL BSA (µL) | Water (µL) | Final concentration (mg/mL) |
|---|---|---|
| 0 | 20 | 0 |
| 1 | 19 | 0.1 |
| 2.5 | 17.5 | 0.25 |
| 5 | 15 | 0.5 |
| 7.5 | 12.5 | 0.75 |
| 10 | 10 | 1.0 |

Each of the 20µL mix was transferred to wells in 96-well plate and 180µL of 1x Bradford reagent was introduced and the contents mixed together. After 10min of incubation, absorbance from each well was measured at 595nm shown in table 9.2.

**Table A7:** Absorbance of standard protein

| BSA (mg/mL) | Absorbance @ 595nm |
|---|---|
| **0** | 0.214 |
| **0.1** | 0.401 |
| **0.25** | 0.780 |
| **0.5** | 1.371 |
| **0.75** | 1.834 |
| **1.0** | 2.309 |

The absorbance value of the blank (0mg/mL) was subtracted from the absorbance values of the samples and the resulting values were plotted on a graph to establish a concentration curve.

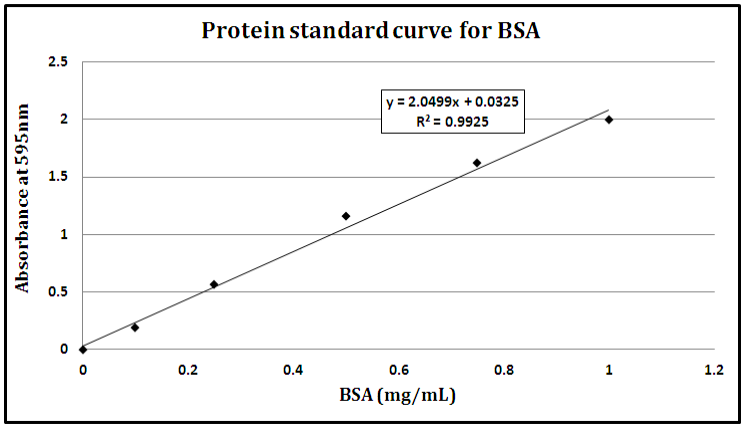


**Figure A1.21: Protein standard curve for Bradford assay.** To provide a protein standard curve for Bradford assay different dilutions of a known standard (2mg/mL BSA) were made as set out in table A1.6 and their absorbance measured at 595nm. The data was plotted in a graph using the x,y scatter and its trend line shown. Using the equation shown in the figure, protein concentrations of the experimental protein lysates were determined and used as mentioned.

### A1.8: Verification of the quality of nuclear (Nuc) and cytoplasmic (Cyt) fractions.

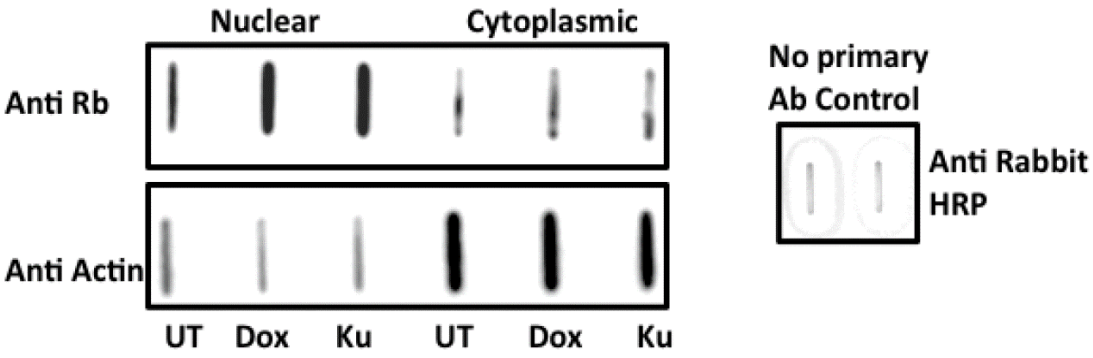


**Figure A1.22: Verification of the quality of nuclear (Nuc) and cytoplasmic (Cyt) fractions.** MCF10 cells were either left untreated, or treated with 10μM KU alone or 0.5μM Dox plus 10μM KU for 0.5 hr. Protein lysates were prepared as Nuc and Cyt fractions and slot blotted against nuclear antigen primary anti rabbit retinoblastoma and cytoplasmic antigen anti-rabbit beta actin in blocking reagent. No primary control was included. The slot blot methodology was performed according to Tummala H et al., 2006.

# APPENDIX-II: Buffers and chemicals

## A2.1 50x TAE buffer

121gm Tris Base

28.5mL Glacial acetic acid

100mL 0.25M EDTA

Contents mixed together and water added to the final volume of 500mL. The pH of the buffer is around 8.5.

To make 0.25M EDTA stock, 46.5 gm of EDTA disodium salt was added to 400mL of water, pH adjusted to 8 with NaOH, and the contents dissolved until clear. The final volume was taken up to 500mL with water.

## A2.2 Poly L-lysine coating

For immunostaining procedures, cells were seeded on sterile cover-slips which were first coated with Poly L-lysine. All the procedure was performed in tissue culture hood under sterile condition in the following way:

Cover-slips to be coated were first autoclaved and placed in tissue culture hood. 1% Poly L-lysine solution was made in sterile water by taking 9.9mL of sterile water and 100µL of Poly L-lysine solution. The cover-slips to be coated were then put in 50mL eppendorf tube and the solution was poured in it so that all the cover-slips are covered in the liquid. The eppendorf was capped tightly and the tube was placed on a gyro shaker and shaken gently at 30rpm for 2 hr. After that, the tube was placed back into the hood, the solution poured off and the coverslips washed three times with sterile water in the same tube. After the last wash, the water was decanted, the coated cover-slips placed flat on a sterile paper towel placed in the hood for to dry them for 30min. Cover-slips were stored in a sterile jar ready to use.

## A2.3 3% Paraformaldehyde (PFA)

3gm Paraformaldehyde

100mL Phosphate buffered saline

100µL 0.1M NaOH

Heated to 70°C and dissolved. Allowed to cool to room temperature and pH adjusted to 7.2 with concentrated HCL.

To make 0.1M NaOH, 40mg of NaOH was dissolved in 10mL of water.

**A2.4 Terrific Broth (TB)**

12 gm Tryptone

24gm Yeast extract

4mL Glycerol

Distilled water added to 900mL

Next, salts for TB made in another bottle as:

1.85gm $KH_2PO_4$

10gm $K_2HPO_4$

Distilled water added to 100mL

Both bottles autoclaved and the contents of each mixed together in a sterile environment to make a litre of TB.

**A2.5 Permeabilization buffer**

0.5% solution of Triton X-100 in PBS by adding 500µL of Triton X-100 added in 100mL of PBS, and mixed well.

**A2.6 Quenching buffer**

50mM $NH_4CL$ solution in water was made by transferring 2.65gm $NH_4CL$in a bottle and adding water to the final volume of 1 litre and dissolving until clear.

**A2.7 Blocking buffer for Immunocytochemistry and ELISA**

2.5gm Bovine serum albumin (BSA)

5mL Foetal bovine serum (FBS)

5µL Triton X-100

PBS added to the final volume of 50mL in a 50mL falcon tube and mixed well until all contents dissolved.

**A2.8 10x Phosphate Buffered Saline (PBS)**

80gm NaCL

2gm KCL

14.4gm $Na_2HPO_4$

2.4gm $KH_2PO_4$

Water was added to the volume of 800mL. pH was set at 7.4 and again water was added until the final volume of 1 L. 1x PBS was made from the stock with water and usually autoclaved before using.

**A2.9 Preparation of Luciferase Assay Reagent II (LAR-II):**

All the reagents used were provided in the Dual Luciferase Assay kit (Promega, UK). The lyophilized Luciferase Assay Substrate was resuspended in the 10ml of the supplied Luciferase Assay Buffer II. Once the substrates and buffer were mixed, the vial was labelled "LAR II" and stored at -80°C. At the time of use, the frozen LAR-II was thawed in water bath set at 37°C.

**A2.10 Preparation of Passive Lysis buffer**:

The passive lysis buffer was provided as 5x concentrate (Dual Luciferase Assay kit, Promega, UK). 5mL of this concentrate was mixed with 20mL of distilled water to make a working stock of passive lysis buffer.

**A2.11 Preparation of Stop and Glo® reagent:**

The Stop and Glo® reagent was provided as 50x concentrate (Dual Luciferase Assay kit, Promega, UK). It was always prepared on the day of use by transferring 10µL of this reagent with 490µL of distilled water. The working stock was protected from light and stored at -80°C until used. At the time of use, the frozen stock was thawed in water bath set at 37°C.

**A2.12 Running buffer for immunoblotting**:

50mL 20x Nupage® MOPS SDS running buffer (Invitrogen, UK)

1mL Nupage® Sample reducing agent (Invitrogen, UK)

Distilled water was added to the final volume of 1 Litre. Mixed and stored at 4°C until used.

**A2.13 Transfer Buffer for immunoblotting:**

50mL 20x Nupage® Transfer buffer (Invitrogen, UK)

100mL Methanol

1mL Nupage® Sample reducing agent (Invitrogen, UK)

Distilled water was added to the final volume of 1 Litre. Mixed and stored at 4°C until used.

**A2.14 Washing buffer for Immunoblotting:**

A 10x concentrated washing buffer provided with WesternDOT$^{TM}$625 Goat anti rabbit/mouse western blot kit (Invitrogen, UK) was diluted to 1x with distilled water. Alternatively, a 0.1% solution of Tween20 in PBS was used in the same manner.

**A2.15 Blocking buffer for Immunoblotting:**

For antibodies purchased from Abcam (Table 2.4), BSA based blocking buffer was used as:

2.5gm BSA

50µL Tween20

PBS added to 50mL and mixed well until all contents were dissolved.

For antibodies purchased from Abcam (Table 2.4), milk based blocking buffer was used by replacing BSA above with 2.5gm milk keeping everything else the same.

**A2.16 Washing buffer for ELISA:**

To prepare washing buffer for ELISA, a 0.01% solution of Tween20 was made with PBS.

**A2.17 SDS sample buffer for western blot:**

A 4x concentrated Nupage® LDS sample buffer was used by diluting it to 1x with the RIPA extracted protein lysates.

**A2.18 Super Optimal Broth (SOB) media:**

20gm Tryptone

5gm Yeast Extract

0.5gm NaCl

Dissolved in 800mL distilled water.

10mL 0.25M KCl

pH adjusted to 7. Water added to the final volume of 1 Litre. The media was autoclaved. Before use, 5mL of sterile 2M $MgCl_2$ added.0.25M KCl made by dissolving 0.93gm of KCl in water to the final volume of 50mL. 2M $MgCl_2$ made by dissolving 9.52gm of $MgCl_2$ in water to the final volume of 50mL.

**A2.19 RF1 media:**

2.457mL $MnCl_2.4H_2O$

3gm RbCl

0.74gm $CH_3COOK$

0.38gm $CaCl_2.2H_2O$

37.5gm Glycerol

Dissolved in 175mL nanopure water, pH adjusted to 5.8 using dilute acetic acid and total volume brought to 240mL with nanopure water and filter sterilized and stored in -20°C until used.

**A2.20 RF2 media:**

4mL 0.5M MOPS (pH 6.8)

0.24gm RbCl

2.2gm $CaCl_2.2H_2O$

30gm Glycerol

Dissolved in 160mL of nanopure water, pH adjusted to 6.8 with NaOH and water added to the final volume of 200mL. The media was filter sterilized and stored at -20°C.

0.5M MOPS was made by dissolving 4.18gm in 28mL of nanopure water, pH adjusted to 6.8 using NaOH and nanopure water added further to the final volume of 40mL. The MOPS buffer was filter sterilized and stored in -20°C until used.

**A2.21 Luria Bertani (LB) media:**

10gm Tryptone

5gm Yeast Extract

10gm NaCl

Dissolved in 800mL of distilled water and pH adjusted to 7.5 by NaOH. Distilled water was further added to the final volume of 1litre and autoclaved. The medium was stored at 4°C.

To make LB-Agar plates, 1.5% of technical Agar was added to LB and then autoclaved. The media was allowed to cool to 40°C and previously made stock of 100mg/mL ampicillin antibody was added to the final concentration of 100µg/mL.

**A2.22 Freezing Medium for mammalian cell storage:**

Freezing medium was made in tissue culture hood using sterile reagents. 10mL of freezing medium was made in a 15mL falcon tube in the following way:

7mL Cell culture media

2mL Foetal bovine serum

1mL DMSO

These contents were mixed together and stored at -20°C. During use, the freezing medium was thawed in water bath set at 37°C. 1mL of the medium was usually used to store 100% confluent cells from a T75 flask in cryotubes.

**A2.23 Hypotonic buffer for cytosolic protein extraction**

37.25gm KCL

1.9mg EGTA

1.46mg EDTA

119.15mg HEPES

7.71mg DTT

4.35PMSF

500µL Protease and phosphatase inhibitor cocktail

All of the above dissolved in sterile distilled water to the final volume of 50mL.

**A2.24 Hypertonic buffer for nuclear fractions:**

19mg EGTA

14.6mg EDTA

239mg HEPES

1.901mg EGTA

7.71mg DTT

1.17gm.NaCl

500µL Protease and phosphatase inhibitor cocktail

All of the above dissolved in sterile distilled water to the final volume of 50mL and was stored at 4°C until used.

**A2.25 Neutral Red (NR) stock solution:**

0.33gm of Neutral red powder was dissolved in 100mL water, filter sterilized (pore size 0.2µm) and stored in dark at room temperature until further used. On the day of the cytotoxicity assay, the neutral red solution was placed in sterile tissue culture hood, 1mL of the stock solution was mixed with 99mL of cell culture media. The final NR concentration in media was 33µg/mL. It was warmed to 37°C and used within 30min of diluting it in media.

**A2.26 NR desorb:**

1mL Glacial acetic acid

50mL Ethanol

50mL $H_2O$

All contents mixed together and stored at 4°C for future use.

**A2.27 Drug solutions:**

All solutions were filter sterilised before using.

**A2.27.1** DOXORUBICIN:

1mM stock solution of Doxorubicin was prepared by dissolving 10mg Doxorubicin powder in sterile distilled water to a final volume of 17.24mL. The vial was protected from light and stored at 4°C. The final concentration of the drug (usually 0.5µM) was obtained by diluting it in the cell culture media.

**A2.27.2** KU55933:

10mM stock of KU55933 was prepared by dissolving 2mg KU55933 powder in DMSO to a final volume of 505µL. The vial was protected from light and stored at -80°C. The final concentration of 10µM was obtained by diluting the stock in cell culture media during treatment.

**A2.27.3** HYDROXYUREA:

100mM stock of Hydroxyurea was prepared by dissolving 7.6mg Hydroxyurea powder in sterile distilled water to a final volume of 1mL. The vial was stored at 4°C. The final concentration of 1mM was obtained by diluting the stock in cell culture media during treatment.

**A2.27.4** BLEOMYCIN:

5mM stock of Bleomycin was prepared by dissolving 7mg powder in sterile distilled water to a final volume of 1mL. The vial was stored at 4°C. The final concentration of 5μM was obtained by diluting the stock in cell culture media during treatment.

**A2.27.5** CISPLATIN:

1mM stock of Cisplatin was prepared by dissolving 3mg cisplatin in sterile distilled water to a final volume of 10mL. The vial was protected from light and stored at 4°C. The final concentration of 4.8μM was obtained by diluting it in cell culture media during treatment.

**A2.27.6** CYCLOHEXIMIDE:

50mM stock of Cycloheximide prepared by dissolving 14gm of Cycloheximide powder in sterile distilled water to a final volume of 1ml. The vial was protected from light and stored at 4°C. The final concentration of 50μM was obtained by diluting it in cell culture media during drug treatment. The Cycloheximide treatment was always performed 1 hr prior to any other drug treatment.

**A2.28 Stripping Buffer for reprobing immunoblot:**

20% SDS

67.5μM Tris-HCl of a pH 6.7

100μm β-Marcaptoethanol

The solution was applied to the immunoblot and incubated usually for 1 hr at 37°C.

**A2.29 Amplex® red reagent:**

10μL of Amplex® red reagent was mixed with 10mL of $NaH_2PO_4$ and 1μL of $H_2O_2$ was added. 100μl of this mixture was used per well of 96-well plate and incubation was performed for 1 hr.

# Appendix-III

## Purchased reagents, chemicals and kits

**Table A8: Chemicals, reagents and kits used in the current research, their catalogue numbers and manufacturers**

| Chemical/Reagent/Kits | Company and catalogue number |
|---|---|
| Agar | A5306-250G Sigma-Aldrich |
| Agarose | BIO-41025 Bioline |
| Alexa fluor 568 goat anti rabbit | A11011 Invitrogen |
| Alexa fluor 568 goat anti mouse | A11004 Invitrogen |
| Alexa fluor488 goat anti rabbit | A11008 Invitrogen |
| Alexa fluor488 goat antimouse | A11001 Invitrogen |
| Amplex® Red reagent | A22188 Invitrogen |
| Bleomycin | 15361-10MG Sigma Aldrich |
| Bovine serum albumin | A2153-100G Sigma Aldrich |
| Bradford reagent | 23200 Pierce Biotechnology |
| Cisplatin | P4394-100MG Sigma Aldrich |
| Cycloheximide | C7698-5G Sigma Aldrich |
| DMEM cell culture media | 12491-015 Invitrogen |
| DMEM/F-12 cell culture media | 11320-033 Invitrogen |
| DNAfectin™ | G2100 Abm |
| Doxorubicin | 25316-40-9 Sigma Aldrich |
| Dual luciferase assay reagent | E1910 Promega |
| Electroporation cuvettes | 5540 Molecular bioproducts |
| Gel pilot DNA loading dye | 239901 Qiagen |

| | |
|---|---|
| Gel pilot DNA loading ladders | 239045 Qiagen |
| Glass cover slips | CB00080RA1 Menzel Glaser |
| Glycerol | G5516 Sigma Aldrich |
| GoTaq® Flexi DNA polymerase | M8305 Promega |
| HaltTM Protease phosphatase Inhibitor Cocktail | 78440 Pierce Biotechnology |
| HRP linked anti mouse antibody | 7076 Cell signalling |
| HRP linked anti rabbit antibody | 7074 Cell signalling |
| Hybond ECL nitrocellulose membrane | RPN3032D GE Healthcare |
| Hydroxyurea | H8627-10G Sigma Aldrich |
| KU55933 | 118500 Calbiochem |
| Neutral Red powder | N4638-5G Sigma Aldrich |
| Novex®Nupage® bis tris SDS PAGE gels | NP0322BOX Invitrogen |
| Novex®sharp prestained protein standard | LC5800 Invitrogen |
| Nupage® LDS sample buffer | NP0007 Invitrogen |
| Nupage® MOPS SDS running buffer | NP0001 Invitrogen |
| Nupage® Sample reducing agent | NP0009 Invitrogen |
| Nupage® Transfer buffer | NP0006 Invitrogen |
| Omni swab pack | WHA-WB100035 Whatman |
| OPTIMEM serum reduced media | 31985070 Invitrogen |
| PBS | 20012-027 Invitrogen |
| Poly L lysine solution | P4707-50ML Cell signalling |
| QIAprep spin miniprep kit | 27104 Qiagen |
| QIAquick gel extraction kit | 28704 Qiagen |
| plasmid plus Maxi kit | 12963 Qiagen |

| | |
|---|---|
| QuikChangeII site directed mutagenesis kit | 200521 Agilent genomics |
| Restriction endonucleases | R6161 Promega |
| RIPA buffer | 89901 Pierce biotechnology |
| Safeview DNA stain | NBS-SV NBs biological |
| Sodium chloride | S3014-1KG Sigma Aldrich |
| T4 DNA ligase | M1801 Promega |
| Trypsin | 25300054 Invitrogen |
| Tryptone | T7293-1KG Sigma Aldrich |
| TSAP Alkaline phosphatase | M9910 |
| Vectashield mounting medium with DAPI | H-1200 Vectashield |
| WesternDot$^{TM}$625 western detection kit | W10142 Invitrogen |
| Xcell Surelock® mincell system | E10007 Invitrogen |
| Yeast Extract | Y1625 Sigma Aldrich |
| 18 Gauge Needles | Fisher scientific |

**Table A9: Scientific Equipment used in the current research.**

| **Equipment** | **Makers** |
|---|---|
| Ultra violet transillumation box | UVP Upland USA |
| Gel documentation machine | Alpha-innotech, USA |
| PCR amplification machine | Techgene, UK |
| Eukaryotic electroporator | Easyject, Equibio UK. |
| 96 well plate reader for absorption | Rosys anthos HTIII |
| 96 well Luminometer and fluorometer | Modulus microplate, Turner biosystems, UK. |
| HPLC | Dionex |
| Autoclave machine | Priorclave, UK |
| Nanopure water | Barnsted Nanopure Diamond$^{TM}$, USA |
| Microscope | Lieca DM-IRE2 inverted fluorescence microscope |
| Capturing system | iXonEM + 867 EMCCD, Andor technologies, USA. |
| Bacterial cell electroporator | Biorad gene pulser, UK. |
| Spectrophotometer | Thermospectronic, USA |
| Thermomixer comfort | Eppendorf, UK |